DEFORMATION CHARACTERISTICS OF SOIL(Dissertation_全文)

AUTHOR(S):

Matsuoka, Hajime

DEFORMATION CHARACTERISTICS OF SOIL

AUGUST 1973

HAJIME MATSUOKA

DEFORMATION CHARACTERISTICS OF SOIL

AUGUST 1973

HAJIME MATSUOKA

CONTENTS

PART I

STRESS-STRAIN RELATIONSHIPS OF SOIL

CHAPTER 1

INTRODUCTION

Soil mechanics is concerned fundamentally with granular materials. Take sand, for example. Unmistakably it is an assembly of grains and is believed to manifest its macroscopic mechanical properties by reflecting the behavior of its individual constituent grains. Not merely in sand but equally in clay which is made up of very fine particles, phenomena are observed which are indicative of dilatancy and other particle properties. In the field of soil mechanics, many studies seem to have phenomenalistically dealt with macroscopic responses of soil mass to applied external force without shedding light on properties inherent to soil. Many of the reported theoretical analyses are noted to be based on continuum mechanics such as of elasticity, plasticity and viscoelasticity.

Some hold the view that properties of all materials are determined by their micro-structure. From their point of view, the microscopic approach which seeks the correlation between the micro-structure and the macro-property of soil is as an extremely interesting and ambitious way of pursuing the study of soil mechanics which belongs in the realm of materials science. In the case of metallic, vitreous and macromolecular materials, studies are made with respect to their structures at atomic, molecular or crystalline level. It is believed that in the case of soil materials the relationship between structure and macroscopic mechanical properties will be clarified more definitely by studying the granular sturcture of soil as an assembly of soil particles rather than by investigating the crystalline nature of constituent substances themselves which compose soil particles. From such a point of view, the approach of "*Mechanics of Granular Materials*[1]" which has come to find increasing advocates in recent years appears to represent an effort which is made toward establishing a system of mechanics inherent to soils as granular materials. The general theories of elasticity, plasticity and viscoelasticity have been developed by considering idealized materials; they have not been established by considering materials as an assemblage of particles. Attempts[2),3)] to resort to these general theories in dealing with granular materials as multiphase mixtures comprising particles and surrounding voids have not yet brought about any definite results. In the circumstances, the aforesaid concept of "*Mechanics of Granular Materials*" appears to be quite interesting.

In the present paper, the author seeks to comprehend the granular structure of soil from the microscopic point of view and elucidate thoroughgoingly the macroscopic mechanical properties of soil, particularly the stress-strain properties in shear, in relation to the granular structure, with the hope of finally deriving general stress-strain formulas.

The chapters of this part may be outlined as follows:

With a view to clarifying, from the microscopic standpoint, the internal mechanism of the shearing phenomenon of sandy soil, Chapter 2 describes the direct shear box test and the simple shear test conducted by using not only real soil samples but also piles of aluminum rods of various diameters and rods of photoelastic materials as two-dimensional models of sandy soil. Piles of these rods have never been utilized in the past as test samples for such shear tests. The microscopic factors directly governing the shear resistance are the interparticle force "f" on the potential sliding plane (called "*mobilized plane*"), the angle of interparticle friction "ϕ_μ" and the angle of contact plane between particles "θ" (called "*angle of interparticle contact*") on the mobilized plane. By the use of these factors, the shear resistance (τ/σ_N) and the dilatancy (ϵ_N) are rated from the microscopic viewpoint. From the results of the rating, there are derived equations expressing the correlations between them, viz. the relation between the shear stress-normal stress ratio (τ/σ_N) and the normal strain-shear strain increment ratio ($d\epsilon_N/d\gamma$), etc. In the course of the derivation of these equations, the concept of the frequency distribution of the angle of interparticle contact "θ" is introduced in order to express, in terms of the variation in the pattern of the distribution, the irregular change that occurs in the angles of interparticle contacts on the mobilized plane in consequence of shear. The frequency distribution of the angle of interparticle contact "θ" is regarded as one of the indices involved in the rating of the granular structure of soil. It is demonstrated that this frequency distribution is closely related to the stress-strain-dilatancy relation of soil. Further, the repeated shear property is discussed in terms of change in granular structure.

In Chapter 3, the various stress-strain relationships of soil derived from the microscopic viewpoint in Chapter 2 are verified on the basis of the data from various shear tests using real sands and glass beads. The aforementioned discussion is further expanded to derive basic equations which are indicative of stress-strain relations on the mobilized plane. Based on the basic equation concerning the stress-strain relations on the mobilized plane, general constitutive equations under three different principal stresses are derived by introducing a new concept of compounded mobilized planes. By use of the data from various tests, it is verified that these equations can simultaneously explain the results of triaxial compression test, triaxial extension test, plane strain test and universal triaxial test under three different principal stresses. In addition, it is described that the aforementioned equations on the stress-strain relation can similarly explain the results of repeated shear test and undrained shear test.

Chapter 4 shows that the various equations involving the stress-strain relation which have been verified in Chapter 3 with respect to sands and other granular materials are similarly applicable to clayey soils. The underlying mechanism in this case is also discussed.

In Chapter 5, the author proposes his view as to the Rowe et al's stress-dilatancy theory, Roscoe et al's energy theory centering around the stress ratio-strain increment ratio relation and Hvorslev's strength constant which are considered to be closely related with the important basic equation in the author's own study on the relation between the shear stress-normal stress ratio (τ/σ_N) and the normal strain-shear strain increment ratio ($d\epsilon_N/d\gamma$).

At this point, the author wishes to clarify the position which the aforementioned study of the author's occupies in the world's trend of studies on soil mechanics. The author's study has been built up by incorporating the concept of the probability distribution of angle of interparticle contact introduced by Murayama[4] into the concept of the angle of interparticle contact and the friction angle between particles adopted for the first time in Newland and Allely's study [5] and in Rowe's study [6] and further evaluating the condition of the transmission of force between particles. If the various studies so far performed in the field of soil mechanics throughout the world with respect to the stress-strain relations of soil are to be classified at all, they will broadly be divided into two major types; those of Rowe's kind and those of Roscoe's kind. The studies of the first kind are based on a concept that the shear resistance is determined by the overall balance of forces exerted by individual particles on the sliding plane. In this case, the mechanical properties of soil are rated by the stress ratio τ/σ_N on the potential sliding plane (or the principal stress ratio σ_1/σ_3). This concept, therefore, may be regarded as being subject to Coulomb's law of friction. Although the author's study is believed to belong in this branch, it may well be characterized in that the change of granular structure resulting from the shear phenomenon is rated and analyzed in full observance of the particulate nature of soil taken as a random assembly[7] of particles having a great range of grain size. By contrast, the studies of Roscoe's kind are based on the energy theory and the plasticity theory. In this case, the underlying concept is that the state of soil is determined by the void ratio e, mean effective principal stress p and deviator stress q. This suggests that these studies are based on von Mises' view that the shear resistance of soil is mainly caused by the interparticle combining force. Thus, studies of Rowe's kind and those of Roscoe's kind are based on the apparently different concepts. The author's study reveals, as described afterward, that the these two kinds of studies have a common point.

In recent years, increasingly more emphasis has come to be attached to the significance of the concept of granular structure[8] of soil. Yet, no specific parameter seems to have been proposed for accurate interpretation of the said structure. In this respect, the frequency distribution of angle of interparticle contact "θ" on the potential sliding plane or the mobilized plane which the author discusses in this paper is one of the first of the specific parameters governing at least the granular structure of soil. The author's equations concerning the stress-strain relations which embrace the concept of such granular structure of soil seem to hold good under various stress

conditions and strain conditions mentioned above probably because they are derived fundamentally from the microscopic consideration of the shearing mechanism of soil. All these things point to the universality of the proposed equations.

References

1) Mogami, T.: Soil Mechanics, Chap. 8, Mechanics of Granular Materials, Gihōdō, 1969, pp.893–1036, (in Japanese).

2) Adachi, N.: Consideration of Constitutive Equation for Soil Materials as Multiphase Body, Proc., Annual Meeting of J.S.C.E. (25th), *III*–24, 1970, pp.73–76, (in Japanese).

3) Adachi, N.: A Consideration of Constitutive Equation for Soil Materials, Proc., Annual Meeting of J.S.C.E. (27th), *III*–187, 1972, pp.589–592, (in Japanese).

4) Murayama, S.: A Theoretical Consideration on a Behaviour of Sand, Proc. of I.U.T.A.M. Symposium on Rheology and Soil Mechanics, Grenoble, 1964, Springer-Verlag, 1966, pp.146–159.

5) Newland, P. L. and Allely, B. H.: Volume Change in Drained Triaxial Tests on Granular Materials, Géotechnique, Vol.7, No.17, 1957, pp.17–34.

6) Rowe, P. W.: The Stress-dilatancy Relation for Static Equilibrium of an Assembly of Particles in Contact, Proc. Roy. Soc. London, Ser. A, Vol.269, 1962, pp.500–527.

7) Murayama, S.: A Constitutive Equation of Soils, Annuals, Disaster Prevention Research Institute, Kyoto University, No.14B, 1971, pp.17–29, (in Japanese).

8) Mikasa, M.: On the Significance of Concept of Structure in Soil Mechanics, Proc., Annual Meeting of J.S.C.E. (17th), *III*–14, 1962, pp.35–38, (in Japanese).

CHAPTER 2

MICROSCOPIC STUDY ON SHEAR MECHANISM OF SANDY SOIL[1),2)]

2.1 GENERAL DESCRIPTION

In the field of the soil mechanics, various test data on the mechanical properties of soil have been accumulated for the past ten years or so, with popularization of the triaxial test apparatus as one contributory factor. Even the shear test of soil alone covers static shear, repeated shear, vibratory shear, etc. It is otherwise classified by stress conditions and drainage conditions. Frequently in these tests, magnitudes of macroscopic responses offered by the soil element to external stimuli are measured to make some evaluation or other with respect to mechanical properties of the soil. But the fundamental question concerning the attribute of soil in which such macroscopic responses originate has been pursued very rarely.

For thorough elucidation of the fundamental mechanism that underlies the mechanical properties of such granular materials as sand and gravel, it is essential to regard them in their inherent form as an assemblage of grains, comprehend their behaviors from the microscopic point of view and investigate the correlation between the microscopic properties and macroscopic properties observed in the test. To make such an approach to the shear phenomenon in the sandy soil, a pile of round rods of aluminum and those of photoelastic material were used as two-dimensional models of sandy soil for the present study. The author decided to use this model with a belief that such model could sufficiently simulate the fundamental behavior of sandy soil in shear, i.e., the behavior in which some grains rise over other grains and eventually slide beyond them. The pile of the rods of the photoelastic material was also used because the photoelastic experiment was thought to lead to comprehension of the condition in which the exerted force is conveyed from grains to grains in shear.

To begin with, an attempt was made to estimate the arrangement (structure) of grains prior to shearing as a two-dimensional problem with respect to a given granular material having a known grain size distribution. Then, what variation the shearing would bring forth in the structure of grains and the condition of transmission of interparticle force was analyzed by the shear test performed with respect to a pile composed of rods of aluminum and rods of photoelastic material. As microscopic factors directly governing the shear resistance, there were introduced interparticle force, angle of interparticle friction and angle of interparticle contact. In particular, the magnitudes of shear resistance and dilatancy were evaluated from the microscopic point of view by expressing, in terms of the change of frequency distribution, the irregular change of angle of interparticle contact due to shearing. Based on the results, the fundamental nature

of stress-strain-dilatancy properties inherent to such granular bodies as sand was investigated, with the distribution of angles of interparticle contact taken as one index for the evaluation of grain structure under shearing. At the same time, the properties observed in repeated shear were also covered.

2.2 STUDIES IN THE PAST

To date, researches have been made to elucidate the macroscopic mechanical properties of sandy soil on the basis of microscopic observations of the behavior of grains which go to make up the sandy soil. Some typical researches are cited below.

P. L. Newland and B. H. Allely[3] took interest in the phenomenon of slippage which would occur between individual grains in a given mass of grains in shear. Taking the angle of interparticle friction (ϕ_μ) and the angle of interparticle contact (θ) as microscopic factors, they tried to explain the difference of the peak strength (τ_{max}) and the residual strength (τ_R) by the following expressions.

$$\frac{\tau_{max}}{\sigma_N} = \tan(\phi_\mu + \theta) \qquad (1.2.1)$$

$$\frac{\tau_R}{\sigma_N} = \tan\phi_\mu \qquad (1.2.2)$$

$$\left(\frac{\delta v}{\delta \triangle}\right)_{max} = \tan\theta \qquad (1.2.3)$$

where, σ_N represents the effective normal stress exerted on the shear plane and ($\delta v/\delta\triangle$) the quantity relative to the dilatancy in consequence of shear. Throughout this report, the stress σ is used to mean the effective stress invariably, although it is not expressed as σ'. However, the value of τ_R calculated from the foregoing equation does not agree to the residual strength to be found by the actual test. Thus, it is proposed to make necessary compensation by ascribing the cause for this disagreement to the difference in the microscopic mode of failure of grains. This research is quite interesting as a pioneering work in this field. Yet, it fails to evaluate the variation in the structure of grains due to shearing because the value of θ is assumed to be constant at all the points of grain contact. The researchers seem to have been compelled to use the expression "*difference in mode of failure*" to fill the gap found in their theory.

P. W. Rowe[4] similarly took notice of the phenomenon of slippage occurring between grains in shear. He made an analysis with respect to the regular arrangement of

rod and spheres of an equal diameter by considering interparticle force, the angle of interparticle friction (ϕ_μ), the angle of interparticle contact (β) and angle (α) showing the geometric magnitude of grain arrangement as governing factors. From the results of this analysis, he derived the following equation as indicating the stress-strain-dilatancy relationship.

$$\frac{\sigma_1}{\sigma_3} = \tan\alpha \cdot \tan(\phi_\mu + \beta) \qquad (1.2.4)$$

$$\frac{\sigma_1 \dot{\epsilon}_1}{2\sigma_3 \dot{\epsilon}_3} = \frac{\sigma_1}{\sigma_3\left(1 - \frac{\dot{dV}}{V\dot{\epsilon}_1}\right)} = \frac{\tan(\phi_\mu + \beta)}{\tan\beta} \qquad (1.2.5)$$

To expand this relationship so as to be applicable to the general grain arrangement, Rowe postulated that the value of β would be such as to minimize the amount of work to be done internally and, based on this postulation, derived the equation $\beta = (45^\circ - \phi_\mu/2)$ from the condition $d\dot{E}/d\beta = 0$ as $\sigma_1\dot{\epsilon}_1/2\sigma_3\epsilon_3 = \dot{E}$. The following expression is obtained by substituting the value of β in the equation (1.2.5).

$$\frac{\sigma_1}{\sigma_3\left(1 - \frac{\dot{dV}}{V\dot{\epsilon}_1}\right)} = \tan^2\left(45^\circ + \frac{\phi_\mu}{2}\right) \qquad (1.2.6)$$

His conclusion is that an increase in volume during shear occurs when there exists a small partial slippage, that the preceding equations hold throughout the entire course of deformation prior to the failure and that they are the fundamental equations indicating the stress-dilatancy relationship. In the case of a regular arrangement, the relationship between stress and interparticle force and that among strain, dispacement and volumetric change are determined based on the geometric nature. Therefore, the stress-strain-dilatancy relationship can easily be defined. The condition that the angle of interparticle contact, $\beta = (45^\circ - \phi_\mu/2)$, be constant should be obtained by the condition for minimizing the energy ratio. As will be described afterward, the author's test confirmed that the angle of interparticle contact would vary with shearing. The author's view on this study will be described in detail in Chapter 5.

Mogami[5] advocated a view that the mechanical properties of a granular body as an assembly of irregular grains would be governed by the average void ratio and its deviation. He conducted a test on the behavior of spheres having a uniform radius and arranged on a flat plate and, on the basis of the observation made in the test, derived the following equation by introducing a method of statistics.

$$\sin \phi = \frac{k}{1 + e} \qquad (1.2.7)$$

where, ϕ represents the angle of internal friction, e the average void ratio for the whole assembly, and k the coefficient relative to the deviation of the void ratio. He also showed that the coefficient k found in the foregoing expression (1.2.7) satisfied the following equation regarding the relationship with the grain size distribution[6].

$$k = -a \cdot \log_{10} U + b \qquad (1.2.8)$$

where, U denotes the uniformity coefficient (D_{60}/D_{10}) and a, b are constants. In addition, he proposed the following equations with respect to the case of triaxial compression (axial symmetry) condition and the case of plane strain condition respectively[7].

$$\sin \phi = \frac{3 k_t}{2(1+e) + k_t} \qquad (1.2.9)$$

$$\sin \phi = \frac{3 k_p}{2(1+e)} \qquad (1.2.10)$$

where, k_t and k_p represent the coefficients corresponding to k respectively in the case of the triaxial compression condition and in the case of the plane strain condition. It should be noted that the above four equations have been verified by various test data.

Murayama[8),9),10),11)] focussed his attention upon the fact that soil is a random assembly of soil particles. He assumed that the angle β with which the interparticle force being transmitted by the applied stress is inclined with reference to one particle and the angle of interparticle contact θ which is formed in opposition to the said force would show Gaussian distribution in the soil. On the basis of this assumption, he sought the probability with which soil particles would be mobilized, while taking into account the angle of interparticle friction δ. From this probability, Murayama derived the following equations indicating the stress-strain relationship which would exist where the stress ratio z ($=(\sigma_1 - \sigma_3)/\sigma_m$) was smaller than the elastic limit z_{el}.

$$\tau_e = A_e \cdot \frac{(P - P_o)}{\cos \beta} = A_e \cdot W_e \cdot z \qquad (1.2.11)$$

where,

$$A_e = \frac{c \cdot \lambda_e \cdot N}{d} \quad , \quad W_e = \frac{1}{4} \cos \frac{\theta + \delta}{2} \quad , \quad z = \frac{\sigma_1 - \sigma_3}{\sigma_m}$$

Referring to the equations (1.2.11), z denotes the applied stress ratio, γ_e the maximum shear strain in the elastic state. P the probability of mobilization of particles under the condition of triaxial compression stresses exposed to the principal stress σ_1 and σ_3, and P_0 the probability of mobilization of particles under the condition of isotropic stresses. c and γ_e are constants, σ_m is the mean principal stress, and A_e is provisionally designated as displacement factor and W_e as structural factor respectively.

Where $z > z_{el}$, the sand undergoes plastic deformation and the particle structure of sand is deformed and, at the same time, disintegrated. Let γ_p stand for the maximum shear strain of sand exceeding the elastic limit and $z^*(= z - z_{el})$ for the stress ratio, then the plastic deformation which occurs before failure will be expressed by the following equation.

$$\gamma_p = A_p \cdot W_p \cdot z^* \qquad (1.2.12)$$

where, $W_p = W_e \cdot z^*_\infty (z^*_\infty - z^*)$, and $A_p > A_e$.

In the preceding equation, A_p represents the displacement factor in the plastic condition and $z^*_\infty (= z_\infty - z_{el})$ is a constant.

Murayama further pursued a theoretical study on the problem of residual strain after repeated application of load and of initial compression of loose sand. He also proposed a new failure criterion of sand from the standpoint of the theory of probability. For application to the random assembly of such viscous, elastic, plastic particles as those of clay, he made the necessary analysis by introducing the generalized Voigt model (or generalized Maxwell's model), substituting the physicochemical interparticle force with its equivalent binding pressure σ_b and extracting only the viscous, elastic effect in addition to following the procedure applicable to the sand. By this incorporation of the model, he analyzed the soil on the same principle without reference to discrimination between sand and clay.

2.3 SIMULATION OF TWO-DIMENSIONAL PARTICLE ARRANGEMENT IN SANDY SOIL

It is frequently observed that, when a given mass of sand having a fixed grain size distribution is poured into a box a number of times by the same method, the

void ratio is practically the same in each occasion of pouring, though dispersed to a slight extent. This observation suggests that the particle arrangement (structure) is substantially the same for a given grain size distribution. This paragraph gives an account of the author's attempt to simulate the particle arrangement before shearing as a two-dimensional problem relative to a granular body of a fixed grain size distribution.[12),13)]

When a granular body is poured into a box, individual particles are believed to settle stably in position close to points of their impingement and, in this manner, to be piled up gradually. To simulate this condition of piling, the first step of particle extraction was carried out as indicated below, by following the method which Matsuo, Komada and Takahashi[14)] developed for applying Monte Carlo method to sands of general grain size distribution. In most cases, the author performed the experiment by using two piles of aluminum rods; one pile of rods of two different diameters (1.6 mm and 3 mm) and the other pile of rods of four different diameters (1.6 mm, 3 mm, 5 mm and 9 mm). The results were found to be similar to those obtained by using rods of more numerous diameters. Here, the explanation is limited to the test using the said two piles of aluminum rods. Referring first to the pile of two diameters, the mixed weight ratio of two diameters (60:40) was converted to the ratio of particle numbers (84:16) and randomized by consulting the uniform random number. Particles 1.6 mm in diameter were taken out where there were obtained numerals 01 – 84 and those 3 mm in diameter were taken out where there were obtained numerals 85 – 00 (00 denoting 100). The sampling was made by repeating this step. Similarly in the pile of four diameters, the mixed weight ratio of the four diameters (10:40:40:10) was converted to the ratio of particle numbers (39:44:16:1) and randomized by consulting the uniform random number. Particles 1.6 mm in diameter were taken out for numerals 01 – 39, those 3 mm in diameter for numerals 40 – 83, those 5 mm in diameter for numerals 84 – 99 and those 9 mm in diameter for numeral 00. This procedure amounts to random sampling of particles in accordance with the given particle size distribution.

The next question was how the particles thus taken out should be arranged in order to meet the natural law. The particles, subsequent to impingement, were allowed to settle stably in position and, in this manner, to pile up gradually. It is so easy to describe the phenomenon but it is difficult to simulate the same phenomenon with accuracy. Even if particles are arranged at apparently stabilized positions, there is a possibility that the completed arrangement of particles will be destroyed by the weight of particles to be piled up on top of them, by an externally applied force or by stirring. The study on this mechanism necessitates introduction of mechanical rules governing the stability of particle arrangement under interparticle force. The mechanism itself does not seem to be governed solely by statistic rules such as of Monte Carlo Method. As a first trial, the author arranged the sampled particles gradually in accord-

ance with rules which were simplified as described below.

The lowermost layer was formed by arranging sampled particles laterally side by side from the left edge to the right in the direction of the width of the container to be simulated. The layer immediately above was formed by having other sampled particles arranged again from the left edge so as to settle stably by their own weight in the clefts formed between the particles already arranged in the lowermost layer. The desired simulation was effected by repeating this procedure so as to pile layers of particles gradually upward from the bottom. Here, the designation "*from left to right*" constituted one of the rules for determining the sequence of particle arrangement. Since the sampling of particles was made in accordance with the random number, it is improbable that any appreciable difference would occur if the sampled particles were arranged from the right edge to the left. In the pile of four diameters, the lowermost layer was formed by arranging sampled particles from left to right, the layer immediately above by arranging sampled particles from right to left, the next above layer by arranging sampled particles again from left to right, and so on. Thus, the particles were arranged as though they were discharged from a swinging aperture.

A mixture of particles of two diameters (1.6 mm and 3 mm) was introduced into a box 2 cm X 1.5 cm in area in accordance with the aforementioned rule. The simulated two-dimensional particle arrangement thus obtained is illustrated by Fig. 1.2.1. The serial numbers found in this drawing denote the sequence of particle arrangement. Calculation shows the void ratio in this particle arrangement to be 0.23, a value which closely agrees with the void ratio actually found in the test using aluminum rods. It is consequently concluded that Fig.1.2.1 satisfactorily serves the purpose of simulating the arrangement of granular particles having two diameters.

To evaluate the stability which the particles arranged in the condition of Fig. 1.2.1 enjoyed owing to their own weight, the force transmitted between particles because of own weight was calculated from the balance of forces at points of contact. For the convenience of calculation, the particles were regarded as rigid bodies and possible interparticle friction was disregarded on the assumption that no relative displacement could occur between particles under such condition. It was additionally assumed that where the number of unknown points of contact available for transmission of force exceeded 3, the force would be transmitted in the two directions closer to the direction of resultant force. In the drawing, therefore, the six points of contact indicated by mark "x" were where possible transmission of force was disregarded in the calculation. The weight of each aluminum rod (5 cm in length) was 0.27 gr. for the diameter of 1.6 mm and 0.95 gr. for the diameter of 3 mm respectively. The magnitude of force transmitted between particles was expressed by the unit of "gr." and placed in the parentheses of the drawing. From the drawing, it is seen that the magnitude of force transmitted at the point of contact between the particles of Serial Nos. 14 and 24, at the point of contact between the particles of Serial Nos. 51 and

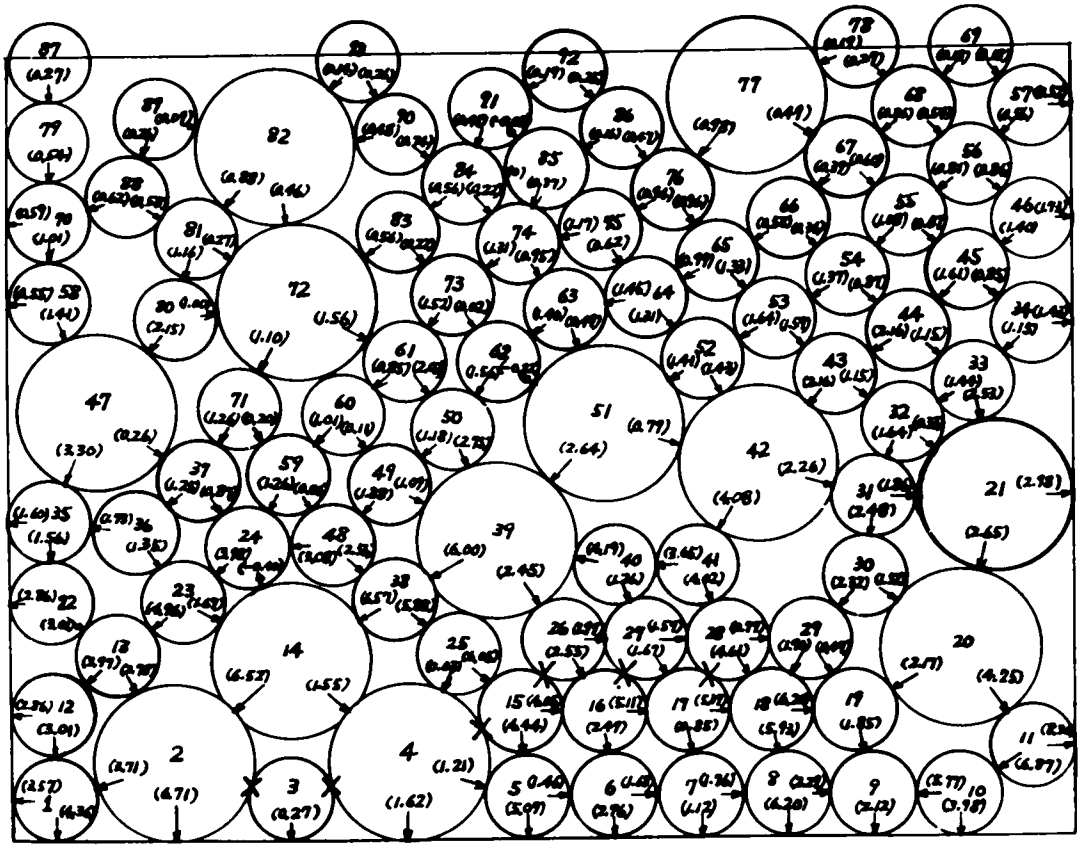

Fig.1.2.1 Simulation of two-dimensional particle arrangement obtained by applying Monte Carlo method and transmission of interparticle force due to own weight of particles (in the case of two diameters).

62 and at the point of contact between the particles of Serial Nos. 85 and 91 had a negative value, suggesting that the particle arrangement involving these particular particles would result in broken equilibrium. However, the negative values in question were invariably so small that the interparticle friction, if manifested at all, would enable the particles to remain in their stabilized state. Fig.1.2.1, therefore, may safely be concluded to simulate an essentially practicable particle arrangement also from the standpoint of stability of particles due to their own weight. The calculation based on this simulation showed the resultant force exerted on the bottom plane to be 34.23 gr., the resultant force exerted on the left side to be 11.37 gr. and on the right side to be 14.96 gr.. By contrast, the macroscopic calculation based on the weight of particles per unit volume, 2.18 g/cm^3, fixed the resultant force exerted on the bottom plane at 32.7 g (= 2.18 X 1.5 X 2 X 5)* and the resultant force exerted on the lateral side at K_0 X 12.26 (= K_0 X 2.18 X 1.5^2 X 5/2), wherein K_0 stands for the coefficient of lateral

*) Width of box = 2 cm, height of box = 1.5 cm and length of rods = 5 cm.

stress at rest. Comparison of this value with the resultant force exerted on the left or right side as calculated from the interparticle force justifies $K_0 \cong 1$. A logical explanation of this postulates that the interparticle friction was totally disregarded while, in actuality, a slight relative displacement occurred locally between particles.

By the same procedure, a mixture of particles having four different diameters (1.6 mm, 3 mm, 5 mm and 9 mm) was placed in a box 6 cm × 2 cm in area. The simulated particle arrangement thus obtained is illustrated in Fig.1.2.2. The serial numbers found in this drawing are to denote the sequence of particle arrangement as

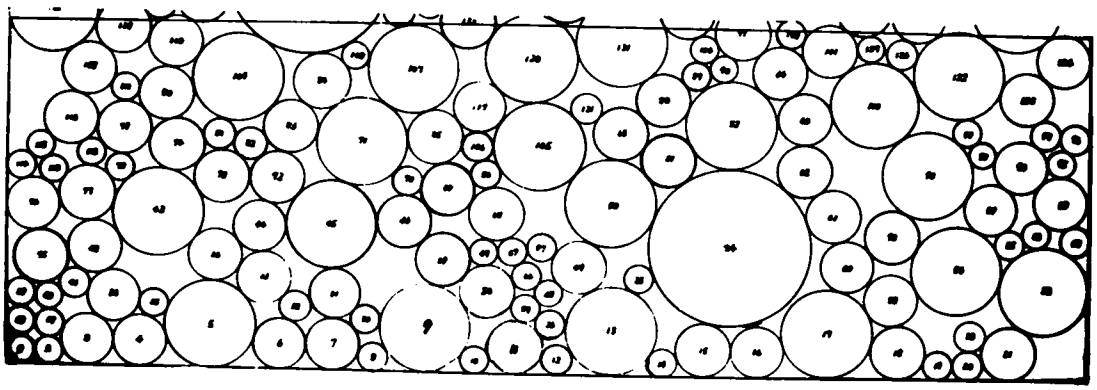

Fig.1.2.2 Simulation of two-dimensional particle arrangement obtained by applying Monte Carlo method (in the case of four diameters).

described previously. Calculation shows the void ratio in this particle arrangement to be about 0.31, a value which is slightly greater than the void ratio found actually in the test using aluminum rods. This difference implies that, owing to the weight of particles, externally applied force or stirring, the particle arrangement obtained in the actual test had an increased compactness compared with the particle arrangement to be found by simulation. As is clear from the comparison of Fig.1.2.1 with Fig.1.2.2, the mixture of particles having four diameters formed a less dense structure than the mixture of particles having two diameters and this smaller denseness of structure was responsible for the higher susceptibility to structural change. As already described, the rules of particle arrangement employed here do not presume any mechanical consideration other than what would be involved in arranging additional particles so as to settle stably by virtue of their own weight on a completed layer of particles. The rules presume the condition in which any force producible by the weight of particles or the load supported would not be transmitted downward. It is quite likely that these rules would apply to the loosest structure that a granular body of a given grain size distribution could assume. How accurately the mechanical consideration discussed above should be incorporated into the present method of simulation of particle arrangement so as to obey the natural law as faithfully as possible is a problem yet to be tackled.

2.4 SPECIMENS AND APPARATUS USED IN TESTS

The shear phenomenon in the sandy soil was studied from the microscopic point of view as described previously. For this purpose, the shear test was performed by using round rods of aluminum and round rods made of a photoelastic substance respectively as two-dimensional models of sandy soil. The aluminum rods were used in the form of a mixed mass of rods having two diameters 1.6 and 3 mm (mixing ratio by weight 60:40), a mixed mass of rods having three diameters 3, 5 and 9 mm (mixing ratio by weight 40:35:25) and a mixed mass of rods having four diameters 1.6, 3, 5 and 9 mm (mixing ratio by weight 10:40:40:10). The aluminum rods were in two lengths 5 cm and 3 cm. The smaller length was used in consideration of ease in the observation of points of contact. The rods of photoelastic substance (Araldite B, 10.7 kg/cm in photoelastic sensitivity) used in the photoelastic shear test had a uniform length of 2 cm. They were used in the form of a mixed mass of rods having two diameters (6.2 mm and 10 mm) (mixing ratio by weight 60:40). These round rods of photoelastic material were obtained from an Araldite plate 2 cm in thickness by using punch cutters with hollows of predetermined inside diameters (6.2 mm and 10 mm).

For the present test were used two kinds of shear test apparatus: One was of the direct shear box type shown in Photo.1.2.1 and the other was of the simple shear type shown in Photo.1.2.2. In the apparatus of direct shear box type, the shear force (horizontal) was determined by the probing ring. In some instances, the vertical load was exerted by means of a weight of iron in the shape of a cube. In other instances, it was applied by a load lever on a load plate. The horizontal displacement and the vertical displacement were measured by means of a dial gauge. The specimens for the shear test were prepared in two different widths 20 cm and 15 cm so that, in the case of a pile of aluminum rods, about 100 points of contact would be obtained on the shear plane to permit a statistical analysis. The specimens had heights 10 cm to 13 cm. The change in the granular structure due to shear could be obtained by photographing the end planes of rods. In the case of the photoelastic test, the condition of interparticle transmission of force could be analyzed by photographing the aspect of photoelastic fringes. Further, the behavior of steel balls or gravels of large diameters in the course of shear could be observed by fastening transparent plates one each on the front and rear sides.

The apparatus of the simple shear type was used for the purpose of investigating the change in the angle of contact at points of contact of individual particles as formed on the horizontal plane and on the vertical plane when the particles were exposed to a uniform shear strain. Thus, it was not fitted with a device designed for the measurement of shear force. The specimens used in this case measured 20 cm in width and about 20 cm in height. The applied shear strain was determined by

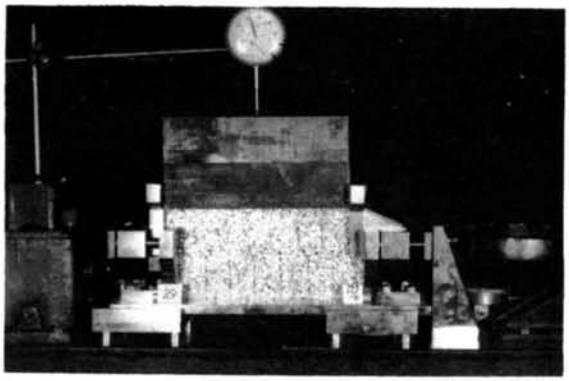

(a) Complete view (width of specimen: 20 cm)

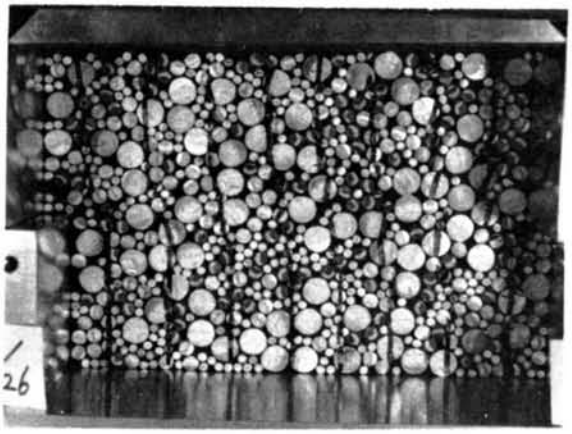

(b) Enlarged photograph during shear (width of specimen: 15 cm)

Photo.1.2.1 Direct shear box apparatus for rod mass.

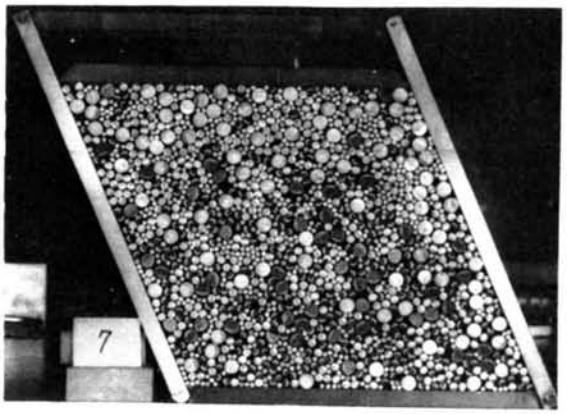

Photo.1.2.2 Simple shear apparatus for rod mass.

measuring the angle of rotation of the parallelogrammic frame illustrated in Photo.1.2.2.

2.5 MICROSCOPIC FACTORS GOVERNING SHEAR RESISTANCE IN TWO-DIMENSIONAL SANDY SOIL MODEL

2.5.1 Rod-shaped Model of a Uniform Diameter

The case of rods of a uniform diameter was considered first as representing the simplest form of the rod-shaped model. As illustrated in Fig.1.2.3, aluminum rods of a

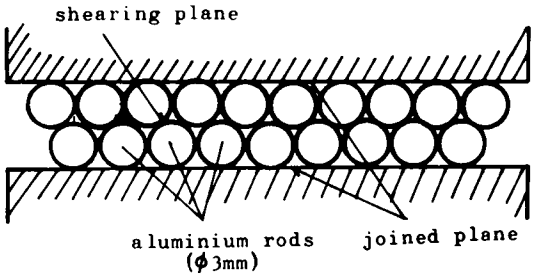

Fig.1.2.3 Aluminum rods of a uniform diameter prior to shear.

uniform diameter (3 mm) were arranged in the compactest state in two layers, with the particles in the upper layer brought into contact with the upper plate and those in the lower layer into contact with the lower plate. By this arrangement, the shear test could be performed while relative displacement was allowed to occur only between the particles in the upper layer and those in the lower layer. The relationslhip between the shear-normal force ratio (S/N) and the horizontal displacement x (mm) and that between the vertical displacement y (mm) and the horizontal displacement x (mm) as actually determined by the present test are represented by plots of circles (o) and solid circles (●) respectively in Fig.1.2.4.[15] In this graph, each solid line represents a curve obtained by calculation according to the following equations on the basis of equilibrium of force and geometric relation.

$$\frac{S}{N} = \tan (\theta + \phi_{\mu}) \qquad (1.2.13)$$

$$(x - \frac{d}{2})^2 + (y + \frac{\sqrt{3}}{2} d)^2 = d^2 \qquad (1.2.14)$$

$$\tan \theta = \frac{dy}{dx} \qquad (1.2.15)$$

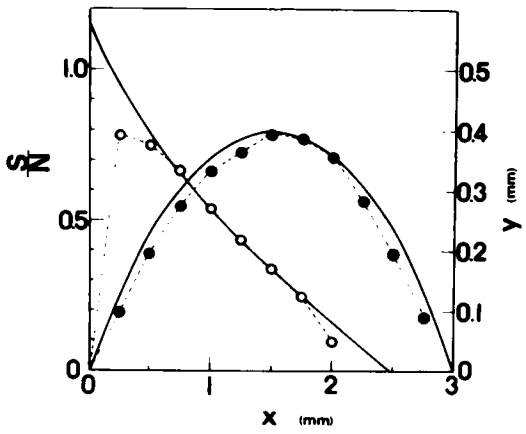

Fig.1.2.4 Relationship among shear-normal force ratio, horizontal displacement and vertical displacement on aluminum rods of a uniform diameter

where, θ denotes the angle formed between the tangential plane containing the point of contact of two mutually engaging particles and the shear plane (horizontal), the said angle called the angle of interparticle contact. The term ϕ_μ denotes the angle of interparticle friction. In the case of aluminum rods placed side by side, the actual measurement gives $\phi_\mu = 19^\circ$ ($\tan \phi_\mu = 0.35$). The sign "d" denotes the diameter of rods and it has a value of 3 mm in the present case.

From Fig.1.2.4, it is seen that the data from actual measurement closely agree with the curve of calculation. It is noted that the plot of circles (○) slightly deviates from the curve of calculation in the area in which x has smaller values. This deviation may be explained by taking into account the fact that some displacement is required for the mobilization of ϕ_μ or that the round rods are not furnished with sufficient dimensional accuracy for precluding possible deviation of the actual particle arrangement from what is obtained by calculation. Where the particles in use have a uniform diameter and are arranged regularly, however, the force to be transmitted between particles can be estimated and the relationship between the displacement and the angle of interparticle contact can be determined by calculation. Consequently, the relationship between the force and the displacement displayed by particles as an assembled body, viz. the stress-strain relation can be easily found by calculation. Where the upper and lower planes of mobilized particles arranged in the side-by-side engagement are kept in contact respectly with the upper and lower plates so that the shear force is directly transmitted immediately after its application to the particles on the shear plane as shown in Fig. 1.2.3, the phenomenon popularly known as "*play*" and ascribable to the discreteness of particles inherent to all granular materials does not occur. As a consequence, close agreement with the curve of calculation is believed to begin where the magnitude of horizontal displacement is relatively small.

Photo.1.2.3 shows the state in which a pile formed solely of aluminum rods of

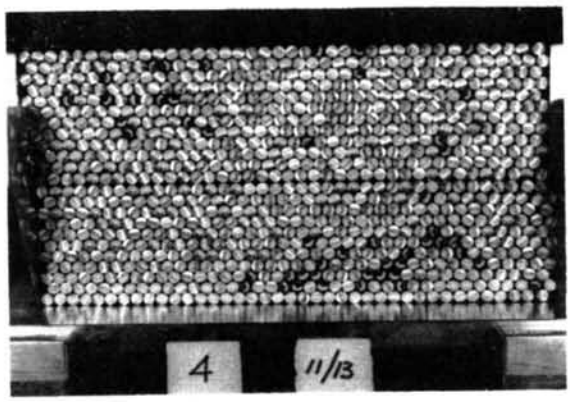

Photo.1.2.3 Particle arrangement of aluminum rods of a uniform diameter (5 mm) during shear.

a uniform diameter 5 mm has been subjected to shear displacement. It is observed that the particles on the shear plane are caused to rise simultaneously in one plane. In the case of such regular arrangement of particles as this, the play between particles rarely occurs as already stated and the interparticle force is believed to be transmitted virtually equally to all the particles on the shear plane. Since the angle of interparticle contact "θ" is determined by the shear displacement because of its geometric relationship, the magnitude of the mobilized ϕ (to be expressed as ϕ_{mo}; $\tan\phi_{mo} = S/N = \tau/\sigma_N$) as a macroscopic quantity resulting from the shear displacement can easily be calculated if the angle of interparticle friction "ϕ_μ" of aluminum rods is known. Assume a case in which the interparticle force due to shear force is transmitted to the particles arranged in the shape of an equilateral triangle in the initial stage of shear, for example. In this case, $\theta = 30^\circ$ exists and $\phi_\mu = 19^\circ$ is already known through actual measurement. Consequently, the value of ϕ_{mo} is found to be 49°, which closely agrees with the value found by the actual measurement. When particles in one layer are caused to rise directly above the corresponding particles in the layer immediately below, $\theta = 0^\circ$ is obtained and ϕ_{mo} becomes nearly equal to the angle of interparticle friction "ϕ_μ" and assumes the value of 19°. This also agrees closely with the value found by the actual measurement. The angle of interparticle friction "ϕ_μ" is that which has been determined by measuring the friction angle occurring between aluminum rods and the aluminum plate or the friction angle between aluminum rods positioned in a mutually intersecting relationship. The stress-strain relation can easily be defined where the particles are arranged regularly as mentioned above. As previously pointed out, Rowe proposed a solution fundamentally with respect to such case. Fig.1.2.5 is a diagram illustrating the relationship between the principal stress ratio and the displacement as observed by Rowe[4] with respect to steel rods of a uniform diameter. The plot of circles (o) represents the values of actual measurement. It is seen that the plot begins to agree closely with the curve (solid line) of calculation as the displacement reaches a certain value.

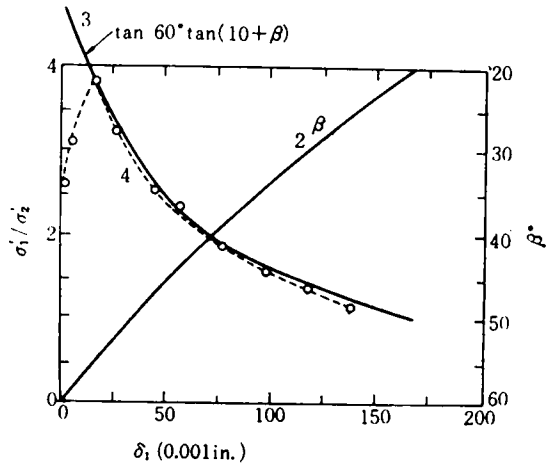

Fig.1.2.5 Relationship between principal stress ratio and displacement on steel rods of a uniform diameter (after Rowe[4]).

A contemplation of Fig.1.2.4 and Fig.1.2.5 results in conception of some image in the author's mind. On his mental screen, he sees the stress-strain curve obtained of densely packed sand particles falling completely on the stress ratio vs. displacement curve indicated by the dotted lines in the two diagrams. Since a granular body like sand is an assembly of particles, it involves the pheonmenon "*play*" between its constituent particles. It can be readily presumed, therefore, that appropriate strain (displacement) would be required for the applied external force to be sufficiently transmitted to the particles on the shear plane. The peak strength would be attained if the force was sufficiently transmitted to the particles on the shear plane and the angle of interparticle contact was such as to offer resistance most advantageously on the average. In this sense, it is imagined that the curves (solid lines) of calculation given in Fig.1.2.4 and Fig.1.2.5 would begin to show close agreement after the peak strength.

With the foregoing inference in mind, the author sought to choose the interparticle force "f", the angle of interparticle friction "ϕ_μ" and the angle of interparticle contact "θ" as microscopic factors directly governing the shear resistance. Here, the angle of interparticle contact "θ" is that which is formed between the tangential plane containing the relevant point of contact of the two particles and the shear plane. The angle θ of which particles slide over on the lower particles is regarded as positive, the angle of which particles are just above the lower particles as 0, and the angle θ of which particles slide down on the lower particles as negative. Theoretically, therefore, the angle "θ" can assume any value from $-90°$ to $+90°$.

2.5.2 On the Angle of Interparticle Contact "θ"

Photo.1.2.4 shows the appearance of a pile of aluminum rods having four different diameters (1.6 mm, 3 mm, 5 mm and 9 mm) during shear. The angles of interparticle contact "θ" on the shear plane are variable and the interparticle forces "f" do

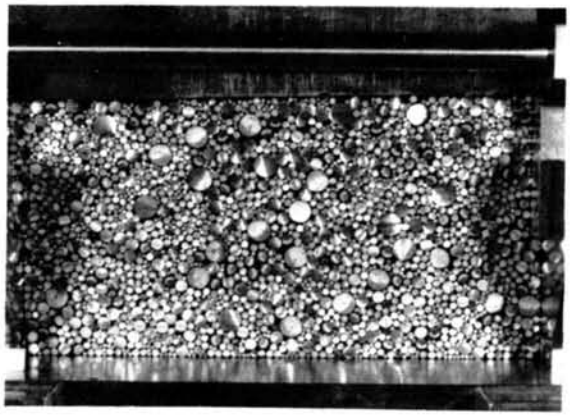

Photo.1.2.4 Particle arrangement of aluminum rods having four different diameters (1.6mm, 3mm, 5mm and 9mm) during shear.

not seem to be constant. The first question, therefore, is how the angles of interparticle contact "θ" on the shear plane should be analyzed and evaluated comprehensively in the case of usual irregular arrangement of particles. For the present analysis, the whole range of "θ" from -90° to $+90^\circ$ was divided into 18 equal zones each of 10°. From the photograph, angles of interparticle contact "θ" on the shear plane were read out and separated by their magnitude into the 18 zones to find the frequency distribution[13] of θ. The angles of interparticle contact on the shear plane selected for the purpose of this analysis were those which were thought to govern the shear resistance in due consideration of the equilibrium of force between the upper half portion and the lower half portion divided by the shear plane as the border line (See Fig.1.2.11). Fig.1.2.6 illustrates how the frequency distribution of θ thus determined would be changed with the magnitude of shear. In the diagram, (a) corresponds to the initial condition prior to shear, (b) to the neighborhood of peak strength and (c) to the neighborhood of residual strength. Now, the characteristic nature of this sort of frequency distribution of θ is described. As shown in (a), the frequency distribution of θ tends to show random left-to-right symmetry substantially uniformly with the exception of the edge portions. This implies that in the case of particles the majority of which enjoy ready engagement, these particles can come into contact with one another while forming various values of angle "θ" with the same degree of probability. Then, the peak appears on the right portion (positive zone of θ) as the shear displacement makes progress thereafter. The angle changes in such way as to give resistance more effectively in proportion as the peak shifts to the right. The frequency distribution of θ shown in (b), therefore, corresponds to the neighborhood of peak strength concerning the stress-strain relationship. Since particles are forced to slide off position as the shear displacement advanced further, the peak of frequency distribution returns towards the center from the right and there consequently appears a trend that the shear resis-

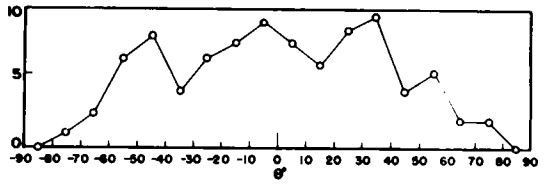

(a) Initial state prior to shear

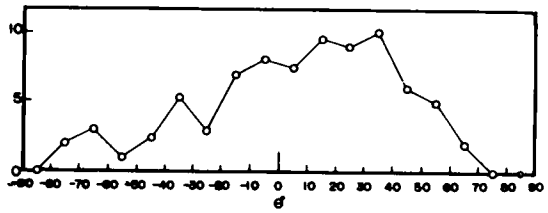

(b) At the peak strength

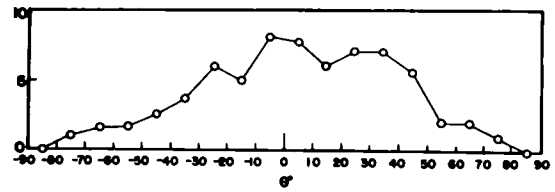

(c) At the residual strength

Fig.1.2.6 Frequency distribution of θ of aluminum rod mass.

tance weakens and eventually equals the residual strength (See Fig.1.2.6 (c)). The observation that particles held in mutual engagement on the shear plane would not slide over one another repetitively in shear but the major portion of particles would slide over one another at the most once seems to be an extremely interesting thing suggestive of the underlying principle of the stress-strain relation in such granular body as sand.

2.5.3 On the Interparticle Force "f"

Photo.1.2.5 is a photograph illustrating the result of a direct shear test with the photoelastic experiment conducted on a pile of rods (having two diameters 6.2 mm and 10 mm) of a photoelastic material. This photograph illustrates the condition close to the residual strength. The magnitude of the interparticle force "f" at the points of interparticle contact can be found by reading out the fringe values at the said points of contact on the shear plane from such photograph. In consideration of

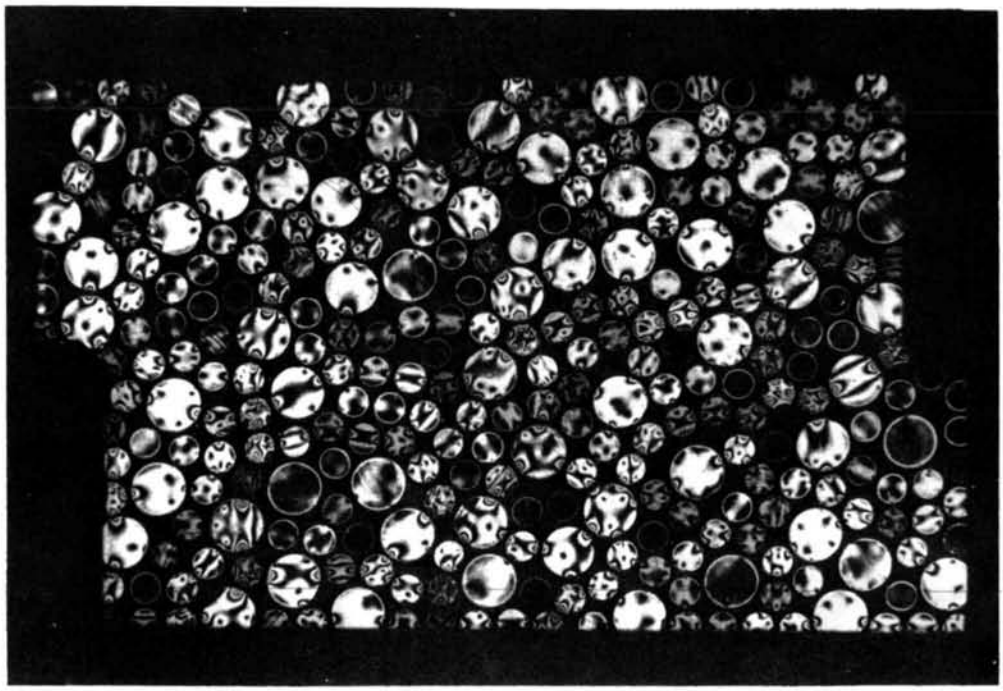

Photo.1.2.5 Isochromatic lines of photoelastic rod mass at the residual strength state.

the trend that the fringe values under an unchanged force vary with the diameter of the particles involved, the fringe values based on particle diameters are to be adequately compensated. The question at this stage is how the various magnitudes of interparticle force "f" transmitted in directions forming various angles with the shear plane should be analyzed and evaluated comprehensively. For the present study, the author sought to determine the sum of interparticle force "f" (named as F_j) within each of variable zones divided by a uniform width of θ (20° in this particular case) and investigate the correlation between this sum and the frequency of θ (named as N_j) occurring within the same variable zone.

Fig.1.2.7 illustrates the relationship between the frequency, N_j, of θ within each of the nine variable zones divided by a uniform angle of 20° and the magnitude, F_j (per unit depth of rod), of the interparticle force within the same zone. This relationship shown in Fig.1.2.7 has been corrected appropriately in consideration of the fact that the absolute quantity of interparticle force to be transmitted through the shear plane increases owing to the increase in shear force and the fact that the number of points of interparticle contact on the shear plane decreases in proportion to the advancement of shear. In the diagram, the plots are noted to be dispersed to a considerable extent. It may be permissible, however, to assume that the magnitude, F_j, of the interparticle force is proportional to the frequency, N_j, of θ by way of primary approximation.

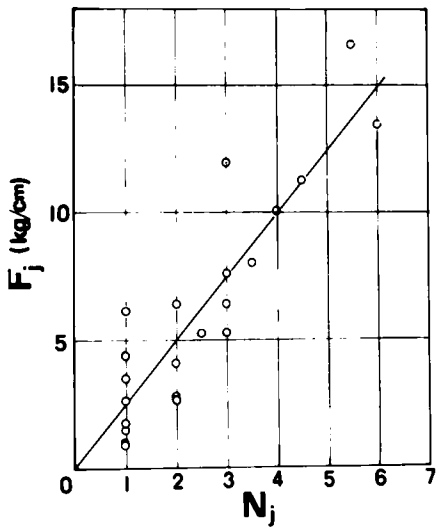

Fig.1.2.7 Relationship between F_j and N_j.

2.6 FREQUENCY DISTRIBUTION OF THE ANGLE OF INTERPARTICLE CONTACT

The author proposes to give further consideration to the frequency distribution of the angle of interparticle contact "θ" to some extent. The concept of the probability distribution of the angle of interparticle contact in soil was first made public by Murayama.[8] To be more specific, Murayama assumed that the angles of interparticle contact would be normally distributed and, on this assumption, analyzed the mechanism of mobilization occurring for sand particles and consequently derived a general stress-strain relationship of soil. As already described, the author conducted numerous shear tests on various specimens such as piles of aluminum rods and rods of photoelastic material having different diameters, assemblies of steel balls of different diameters and naturally occurring gravels having large diameters with the aid of direct shear box test apparatus, to determine the change in the angles of interparticle contact "θ" on the shear plane due to shearing. With a simple shear type test apparatus, he also determined the condition of the change of θ in consequence of the increase in the shear strain. In addition, he investigated the mechanism of dilatancy.

The typical determination of the distribution of θ with respect to a pile of aluminum rods has already been dealt with in Fig.1.2.6. Here, the result of the determination of θ distribution on the shear plane as carried out for the case of a pile of rods (having diameters 6.2 mm and 10 mm) made of a photoelastic material is discussed. The result is depicted in Fig.1.2.8. In the drawing, (a) illustrates the initial condition prior to shear, (b) the neighborhood of peak strength and (c) the distribution of θ

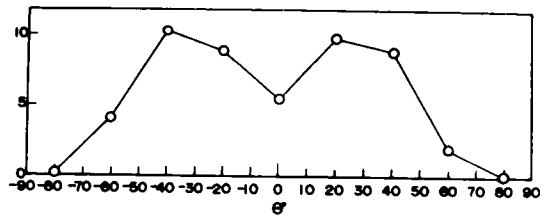

(a) Initial state prior to shear.

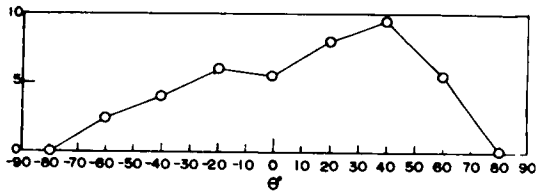

(b) At the peak strength.

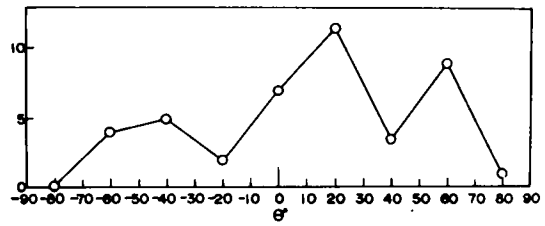

(c) After the peak strength.

Fig.1.2.8 Frequency distribution of θ of photoelastic rod mass (ϕ6.2, 10mm).

after the peak strength respectively. Use of the rods made of a photoelastic material provides an advantage that, of the points of interparticle contact in the neighborhood of shear plane, those which actually contribute to the shear resistance can be easily discriminated in view of photoelastic fringes. As a natural consequence, the points of contact at which photoelastic fringes appeared to indicate presence of interparticle force, namely only the points of contact that involved mobilization were selected for the determination of the frequency distribution of θ. The diagram of Fig.1.2.8 is also noted to indicate practically the same trend as that of Fig.1.2.6 representing the case using a pile of aluminum rods.

Fig.1.2.9 and Fig.1.2.10 illustrate the conditions of the change in θ distribution on the shear plane due to shearing as determined with respect to a mixture of steel balls (having three different diameters 4 mm, 6.3 mm and 8 mm) and to naturally

occurring gravels having diameters large enough to permit ready measurement of angle of interparticle contact. In the test using steel balls and the test using gravels, the angles of interparticle contact directly observed to occur close to the transparent side plates of a shear box were considered as approximately representing the whole trend (See Photo.1.2.6 and Photo.1.2.7).

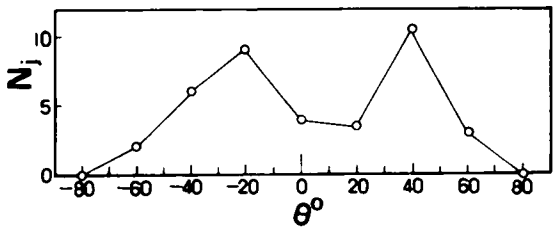

(a) Initial state prior to shear.

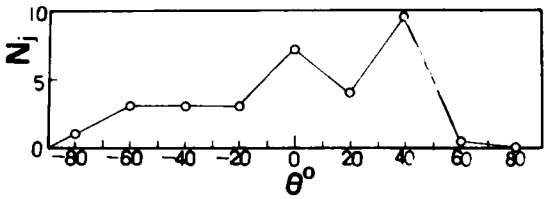

(b) At the peak strength.

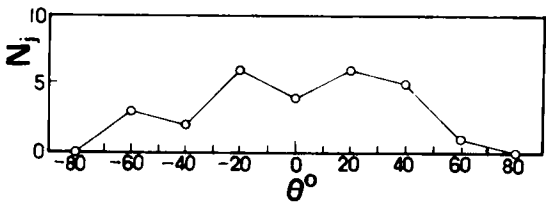

(c) At the residual strength.

Fig.1.2.9 Frequency distribution of θ of steel ball mass (ϕ4, 6.3, 8mm).

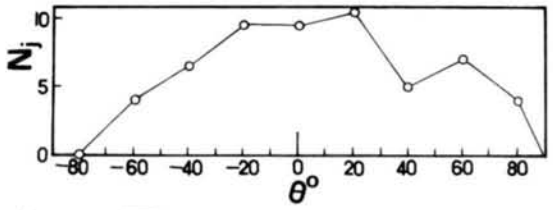

(a) Initial state prior to shear.

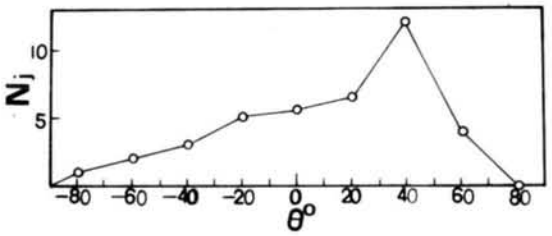

(b) At the peak strength.

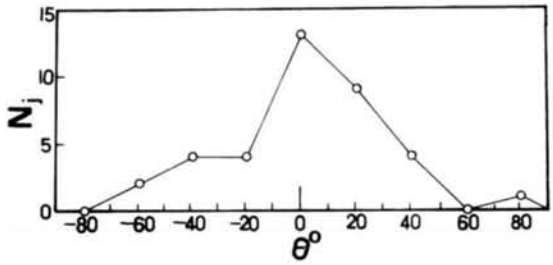

(c) At the residual strength.

Fig.1.2.10 Frequency distribution of θ of gravels.

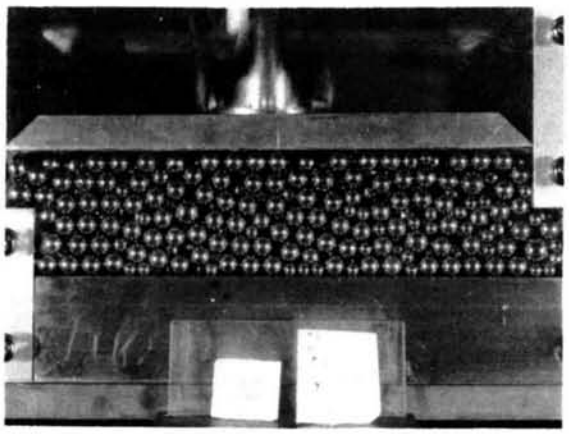

Photo.1.2.6 Particle arrangement of steel balls (ϕ4, 6.3, 8mm) during shear.

Photo.1.2.7 Particle arrangement of gravels during shear.

A study of Fig.1.2.6, Fig.1.2.8, Fig.1.2.9 and Fig.1.2.10 reveals a consistent trend with respect to the change in the distribution of angles of interparticle contact "θ" on the shear plane due to shearing. Specifically, the substantially symmetrical distribution existing prior to shear shifts to the distribution which shows the peak on the right portion (positive zone of θ) and eventually returns to the former symmetrical distribution. This brings forth a question regarding the physical significance which gives birth to such a peculiar change of distribution. First, the principal mechanism responsible for the change from the symmetrical distribution to the distribution having the peak on the right portion may be logically explained by postulating that the particles supported in position by the equilibrium combination of positive angles of contact and negative angles of contact would be deprived of the support by negative angles of contact as they set out to slide over in the shear direction. In the photoelastic test, it is frequently observed that the particles showing fringes at positive and negative points of contact prior to shear gradually cease to show the fringes at the negative points of contact as the shear advances. The observation that the distribution of θ shifts to the rightmost protion (positive direction of θ) is an indication that the proportion of particles which are about to slide over has reached its maximum. In this state, the angle of interparticle contact provides the most effective resistance to the shear. It seems quite natural that the peak strength should be reached at this time. A logical interpretation of the shift of the right-sided distribution back to the symmetrical distribution assumes that the movement of particles to slide over on the shear plane is activated and the proportion of particles which gradually come to occupy a position directly above particles in the layer immediately below ($\theta = 0^\circ$ at this time) is increased on the average. At this point, the ratio of particles which slide over the lower particles to particles which slide down becomes nearly consistent on the average and the form of symmetrical distribution is not changed appreciably even if the shear displacement is increased further, probably because the particles are less sufficiently

interlocked and, namely, have a looser structure than in the initial stage of shear. This stage is believed to correspond to the neighborhood of residual strength. As is evident from the foregoing explanation, the interpretation of the internal mechanism in review here is believed to be applicable to a structure of densely packed particles -- it should be noted that a pile of rods inevitably gives rise to a densely packed structure. The interpretation of the mechanism with respect to a loosely packed structure will be explained afterward in Paragraph 2.8.

Oda [16),17)] subjected samples of sand to the shear test on a triaxial apparatus while using a cementing agent having low viscosity as a fluid to fill the void. At various stages of shear, sand particles were left to stand for a long time enough to be cemented. From various cut faces formed in the cemented specimens, he obtained thin sections and observed them under a microscope to determine the change taking place in the granular structure. Based on the results of this test, he made efforts to comprehend the three-dimensional behavior of sand particles in triaxial specimens. Ochiai et al [18)] conducted a biaxial shear test in which a pile of aluminum rods similar to that of the author's was used as test specimen and the external force was applied in the axial direction and in the lateral direction, to investigate the moving property of particles during shear. In the two studies mentioned above, all the angles of interparticle contact detected under the condition of undefined sliding plane were evaluated as identical. Therefore, their results do not seem to have thoroughly elucidated the relationship with mechanical properties. As will be described afterward, the author based his investigation on the test using a direct shear test apparatus and obtained satisfactory results by applying the findings to the simple shear test. He further succeeded in appropriately interpreting the results of the triaxial test by comprehensively analyzing them with respect to the $(\tau/\sigma_N)_{max}$ plane, viz. the mobilized plane (potential sliding plane) which was the plane forming an angle $(45^\circ + \phi_{mo}/2)$ with the maximum principal stress plane (where, $\tau/\sigma_N = \tan\sigma_{mo}$). In reading out the angles of interparticle contact, Oda and Ochiai et al took all the angles to be identical without taking into account mechanical properties dealt with in the preceding Sub-paragraph 2.5.2. When their results of measurement are reanalyzed on the basis of the mobilized plane, however, there is observed a trend qualitatively similar to that of the peculiar nature of the change in the distribution of angles of interparticle contact due to shear as proposed by the author.

2.7 MICROSCOPIC ANALYSIS OF SHEAR RESISTANCE AND DILATANCY[19),20),21)]

In this paragraph, the author proposes to evaluate the magnitudes of shear resistance and dilatancy offered by the sandy soil from the microscopic point of view, with emphasis focussed on the granularity of the soil. Let us now pay attention to the points of contact of

the individual particles which are sliding against each other on the potential sliding plane as illustrated in Fig.1.2.11. Then, let "f_i" stand for the interparticle force at the i'th point of contact "θ_i" for the angle of interparticle contact and further assume that the angles of

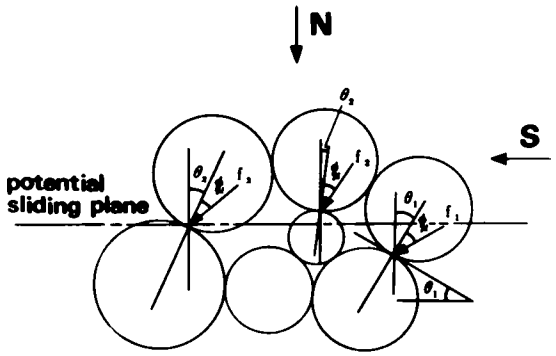

Fig.1.2.11 The angle of interparticle contact θ_i, the interparticle force f_i and the angle of interparticle friction ϕ_μ.

interparticle friction are completely mobilized at the points of interparticle contact so as to take up a fixed value "ϕ_μ". Then, the shear resistance (τ/σ_N) will be represented generally as follows:

$$\frac{\tau}{\sigma_N}=\frac{S}{N}=\frac{\sum_{i=1}^{n} f_i \cdot \sin(\theta_i+\phi_\mu)}{\sum_{i=1}^{n} f_i \cdot \cos(\theta_i+\phi_\mu)} \qquad (1.2.16)$$

where, n denotes the number of points of contact between particles sliding on the shear plane, S the shear force and N the normal force. Then the entire range of the angle of interparticle contact (-90° to +90°) is divided into variable zones (the medium value denoted as θ_j) each of a fixed interval $\triangle\theta$ and the sum of the interparticle force "f_i" within the variable zone θ_j is denoted as F_j [$=\sum f_i\,(\theta_j-\triangle\theta/2<\theta<\theta_j+\triangle\theta/2)$] The formula (1.2.16) can, then, be converted as follows:

$$\frac{\tau}{\sigma_N}=\frac{\sum_{j=1}^{m} F_j \cdot \sin(\theta_j+\phi_\mu)}{\sum_{j=1}^{m} F_j \cdot \cos(\theta_j+\phi_\mu)} \qquad (1.2.17)$$

where, m denotes the number of the divided variable zones. Let N_j stand for the number of points of interparticle contact (generally referred to as "*frequency of* θ")

within each variable zone θ_j (j = 1 to m), then there will result the following equation.

$$F_j = \Sigma f_i \left(\theta_j - \Delta\theta/2 < \theta < \theta_j + \Delta\theta/2 \right) = \frac{\Sigma f_i}{N_j} \cdot N_j = \bar{f}_j \cdot N_j \qquad (1.2.18)$$

Thus, F_j is expressed in the form of the product of the average interparticle force "$\bar{f}_j$" within the variable zone θ_j multiplied by the number, N_j, of points of interparticle contact. In this connection, a direct shear test combined with the photoelastic experiment was conducted by using a pile of round rods (having diameters 6.2 mm and 10 mm) made of a photoelastic material to determine the relationslhip between F_j and N_j. Consequently, the following expression was assumed for the primary approximation of the F_j vs. N_j relationship prior to and during shear, as already described in Sub-paragraph 2.5.3.

$$F_j \cong c \cdot N_j \qquad (\text{where, } c \text{ is a constant}) \qquad (1.2.19)$$

This implies that, as is evident from the comparison of the formula (1.2.18) and the formula (1.2.19), the magnitude of the average interparticle force "f_j" of each variable zone is substantially constant irrespectively of the value of θ_j. By substituting the equation of (1.2.19) in the formula (1.2.17), one obtains the following equation.

$$\frac{\tau}{\sigma_N} = \frac{\sum_{j=1}^{m} N_j \cdot \sin\left(\theta_j + \phi_\mu\right)}{\sum_{j=1}^{m} N_j \cdot \sin\left(\theta_j + \phi_\mu\right)} \qquad (1.2.20)$$

By approximating the discrete function N_j to the continuous function $N(\theta)$ and expressing the formula (1.2.5) in the integrated form, one obtains the following equation.

$$\frac{\tau}{\sigma_N} = \frac{\int_{-\frac{\pi}{2}}^{\frac{\pi}{2}} N(\theta) \cdot \sin\left(\theta + \phi_\mu\right) \cdot d\theta}{\int_{-\frac{\pi}{2}}^{\frac{\pi}{2}} N(\theta) \cdot \cos\left(\theta + \phi_\mu\right) \cdot d\theta} \qquad (1.2.21)$$

Only if $N(\theta)$ is given in its functional form in the equation (1.2.21), then the shear resistance (τ/σ_N) can be calculated by carrying out the operation of integration.

In regards to the condition of the change in the frequency distribution, $N(\theta)$, of θ due to shear, the author performed various forms of shear test using, as test speci-

mens, piles of aluminum rods of different diameters and round rods of photoelastic material, assemblies of steel balls having different diameters, and samples of naturally occurring gravels having large diameters to determine the angle of interparticle contact on the shear plane. The results thus obtained suggest a possibility that a trend substantially similar to that which is illustrated in Fig.1.2.6 (described previously) is invariably manifested. The shear resistance (τ/σ_N) can be calculated as follows if the trapezoidal distribution and the triangular distribution shown in Fig.1.2.12 are approxi-

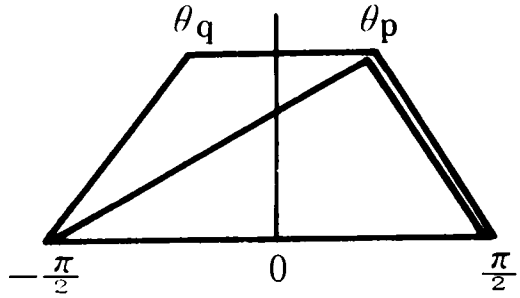

Fig.1.2.12 Trapezoidal and triangular frequency distribution of θ.

mately assumed for $N(\theta)$ in view of the observations made in the aforementioned test. The change in the form of distribution due to shear is expressed in this case, with θ_p and θ_q at the two shoulders in the case of the trapezoidal distribution or θ_p at the vertex in the case of the triangular distribution taken each as a variable. Thus, the following equation is derived in the case of the trapezoidal distribution.

$$\frac{\tau}{\sigma_N}=\frac{(\pi/2-\theta_p)\sin(\theta_q+\phi_\mu)+(\pi/2+\theta_q)\sin(\theta_p+\phi_\mu)-(\theta_p+\theta_q)\cos\phi_\mu}{(\pi/2-\theta_p)\cos(\theta_q+\phi_\mu)+(\pi/2+\theta_q)\cos(\theta_p+\phi_\mu)+(\theta_p+\theta_q)\sin\phi_\mu} \qquad (1.2.22)$$

In the case of the triangular distribution ($\theta_p=\theta_q$), the following equation is obtained.

$$\frac{\tau}{\sigma_N}=\frac{\pi\cdot\sin(\theta_p+\phi_\mu)-2\theta_p\cdot\cos\phi_\mu}{\pi\cdot\cos(\theta_p+\phi_\mu)+2\theta_p\cdot\sin\phi_\mu} \qquad (1.2.23)$$

If, in this case, the value of θ_q is not very close to $-\pi/2$, neither the trapezoidal distribution nor the triangular distribution is reflected very sensitively on the value of τ/σ_N. In such case, there is adopted a simpler triangular distribution. Since θ which is the average value of θ is obtained by the following formula,

$$\bar{\theta} = \int_{-\frac{\pi}{2}}^{\frac{\pi}{2}} N(\theta) \cdot \theta \cdot d\theta / \int_{-\frac{\pi}{2}}^{\frac{\pi}{2}} N(\theta) \cdot d\theta = \theta_p / 3 \qquad (1.2.24)$$

τ/σ_N is calculated with respect to $\bar{\theta}$ in accordance with the equation (1.2.23). The result of this calculation is shown in Fig.1.2.13. Form this diagram, it is seen that in a limited range of $\bar{\theta}$, τ/σ_N has a substantially linear relationslhip against θ, with ϕ_μ as a parameter.

$$\frac{\tau}{\sigma_N} = \lambda \cdot \bar{\theta} + \mu \qquad (1.2.25)$$

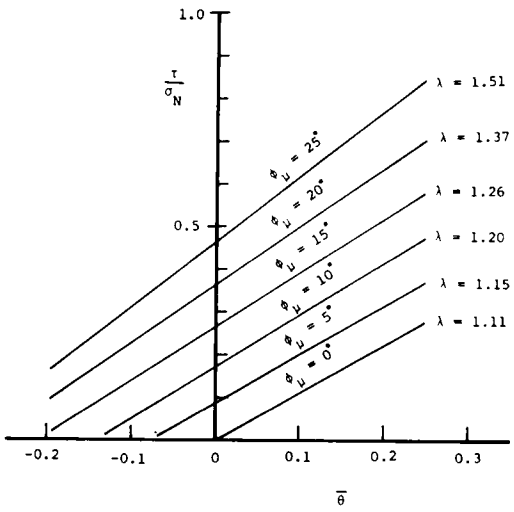

Fig.1.2.13 Relationship between τ/σ_N and $\bar{\theta}$ with paremeter ϕ_μ.

where, μ denotes a physical constant which equals the interparticle friction, tan ϕ_μ. And, λ denotes a constant decided by the value of μ and it takes an approximate value (1.1 to 1.5) obtained from the linear gradient of Fig.1.2.13.

Fig.1.2.14 is a model representation of the mechanism for the development of dilatancy in the granular soil as viewed from the microscopic standpoint. Assuming that there exist n' particles in the vertical direction relative to the shear plane, the total length L in the vertical direction and the increment $\triangle L$ of length due to the change $\triangle\theta_i$ ($i = 1$ to $n' - 1$) in angle can be expressed as shown below, if the particles are regarded as a rigid body.

$$L = \sum_{i=1}^{n'-1} (r_i + r_{i+1}) \cdot \cos\theta_i + (r_1 + r_{n'}) \qquad (1.2.26)$$

$$\Delta L = \sum_{i=1}^{n'-1} \Delta l_i = \sum_{i=1}^{n'-1} (r_i + r_{i+1}) \cdot \sin\theta_i \, (-\Delta\theta_i) \qquad (1.2.27)$$

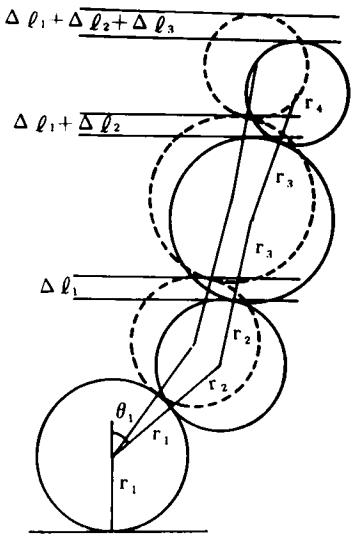

Fig.1.2.14 Microscopic mechanism of dilatancy.

where, r_i denotes the radius of the i'th particle and Δl_i denotes the amount of change in height produced when the angle θ_i of interparticle contact formed by the (i + 1)'th particle relative to the i'th particle is changed by an increment of $\Delta\theta_i$. Let us now consider the case in which there is a uniform shear strain γ of simple shear. In this case, the frequency distribution $N(\theta)$ of θ with respect to the vertical (height) direction is believed to show a variation characteristic similar to that which is depicted in Fig.1.2.6. In the equations (1.1.26) and (1.1.27), r_i and θ_i are completely independent of each other and have no functional relationship. Therefore the operation of averaging is performed here by representing the average value of $(r_i + r_{i+1})$ as $\bar{d}$, the average value of θ_i as $\bar{\theta}$ and the average value of $\Delta\theta_i$ as $\Delta\bar{\theta}$ respectively as follows.

$$L = (n'-1) \cdot \bar{d} \cdot \cos\bar{\theta} + \bar{d} \cong (n'-1) \cdot \bar{d} \cdot \cos\bar{\theta} \qquad (1.2.28)$$

$$\triangle L = (n' - 1) \cdot \bar{d} \cdot \sin \bar{\theta} \ (-\triangle \bar{\theta}) \qquad (1.2.29)$$

And the following equation will be derived from the expressions (1.2.28) and (1.2.29).

$$\frac{\triangle L/L}{\triangle \bar{\theta}} = \tan \bar{\theta} \qquad (1.2.30)$$

Since $\bar{\theta}$ increases and L decreases (contacts) in proportion as γ increases before τ/σ_N reaches its peak strength, L shows a positive compression against an increse in γ. Here, since it is considered that ($\Delta L/L$) equals the increment $d\epsilon_N$ (ϵ_N: compression in a positive value) in the normal strain and $\triangle\bar{\theta}$ substantially equals the increment $d\gamma$ in the shear strain (indicated by data obtained from actual measurement), the equation (1.2.30) can be converted as follows.

$$\frac{\triangle L/L}{\triangle \bar{\theta}} \cong \frac{d\epsilon_N}{d\tau} \cong \frac{d\epsilon_N}{d\bar{\theta}} = - \tan \bar{\theta} \qquad (1.2.31)$$

By subjecting the expression (1.2.31) to integration and granting that $\epsilon_N = 0$ when $\theta = -\theta_0$, the following equation is obtained as indicating the value ϵ_N prior to the peak strength.

$$\epsilon_N = \log_e \left| \frac{\cos \bar{\theta}}{\cos \bar{\theta}_0} \right| \qquad (1.2.32)$$

where, $\bar{\theta}_0$ denotes $\bar{\theta}$ immediately after the start of shear. Assume that $\bar{\theta}$ has a value $\bar{\theta}_p$ at the peak strength, then the normal strain ϵ_{NP} at the peak strength will be expressed as follows.

$$\epsilon_{Np} = \log_e \left| \frac{\cos \bar{\theta}_p}{\cos \bar{\theta}_0} \right| \qquad (1.2.33)$$

The length L shows a positive expansion against an increase in γ since $\bar{\theta}$ decreases and L increases (expands) in proportion with the increase of γ after the peak strength. By taking note of this relationship and assuming that the relation $d\bar{\theta} = - d\gamma$ exists after

the peak strength, the expression (1.2.31) will be converted as shown below.

$$\frac{\triangle L/L}{\triangle \bar{\theta}} \cong \frac{-d\epsilon_N}{-d\tau} \cong \frac{-d\epsilon_N}{d\bar{\theta}} = -\tan\bar{\theta} \qquad (1.2.34)$$

The following expression indicating the value of ϵ_N (compression as positive) after the peak strength can be obtained by subjecting the preceding equation (1.2.34) to integration and granting that $\epsilon_N = \epsilon_{NP}$ where $\bar{\theta} = \bar{\theta}_P$.

$$\epsilon_N = \log_e \left| \frac{\cos^2 \bar{\theta}_p}{\cos\bar{\theta} \cdot \cos\bar{\theta}_0} \right| \qquad (1.2.35)$$

The relationship between ϵ_N and $\bar{\theta}$ as depicted from the expressions (1.2.32) and (1.2.35) is illustrated in the form of model in Fig.1.2.15.

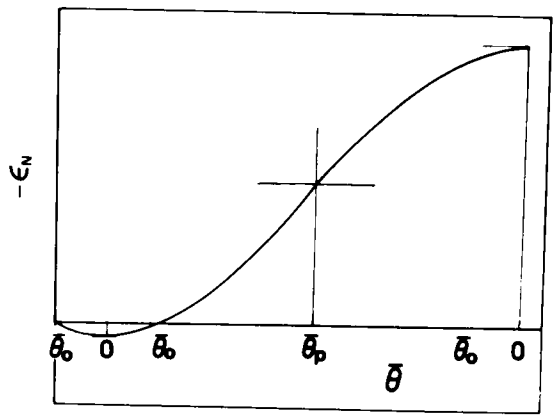

Fig.1.2.15 Relationship between ϵ_N and $\bar{\theta}$.

Now, the following expression showing the relationship between the stress ratio (τ/σ_N) and the strain increment ratio $(d\epsilon_N/d\gamma)$ is derived by substituting the equations (1.2.31) and (1.2.34) in the expression (1.2.25).

$$\frac{\tau}{\sigma_N} = \lambda \cdot \arctan\left(-\frac{d\epsilon_N}{d\tau}\right) + \mu \cong \lambda \cdot \left(-\frac{d\epsilon_N}{d\tau}\right) + \mu \qquad (1.2.36)$$

By substituting the equations (1.2.32) and (1.2.35) in the expression (1.2.25), there are obtained the following expressions which show the relationship between the stress ratio (τ/σ_N) and the normal strain (ϵ_N) prior to and subsequent to the peak

strength respectively.

$$\frac{\tau}{\sigma_N} = \lambda \cdot \arccos\{\cos\bar{\theta}_o \cdot \exp(\epsilon_N)\} + \mu \qquad (1.2.37)$$

$$\frac{\tau}{\sigma_N} = \lambda \cdot \arccos\{\cos^2\bar{\theta}_p \cdot \cos^{-1}\bar{\theta}_o \cdot \exp(-\epsilon_N)\} + \mu \qquad (1.2.38)$$

The following equation is derived by assuming that the principal stress and the principal strain increment coincide in direction.

$$\frac{d\epsilon_N}{d\gamma} = \frac{(d\epsilon_1 + d\epsilon_3) - (d\epsilon_1 - d\epsilon_3)\sin\phi_{mo}}{2(d\epsilon_1 - d\epsilon_3)\cos\phi_{mo}} \qquad (1.2.39)$$

Because of the following relationships,

$$\frac{\tau}{\sigma_N} = \tan\phi_{mo} = \frac{\sigma_1 - \sigma_3}{2\sqrt{\sigma_1\sigma_3}} \qquad (1.2.40)$$

$$\sin\phi_{mo} = \frac{\sigma_1 - \sigma_3}{\sigma_1 + \sigma_3} \qquad (1.2.41)$$

$$\cos\phi_{mo} = \frac{2\sqrt{\sigma_1\sigma_3}}{\sigma_1 + \sigma_3} \qquad (1.2.42)$$

the following expression is obtained as a formula indicative of the relationship between the principal stress ratio (σ_1/σ_3) and the principal strain increment ratio ($d\epsilon_3/d\epsilon_1$) by substituting the foregoing four equations in the expression (1.2.36).

$$\frac{d\epsilon_3}{d\epsilon_1} = \frac{\sigma_1/\sigma_3 - 2\mu\cdot\sqrt{\sigma_1/\sigma_3} + (\lambda - 1)}{(1-\lambda)\cdot\sigma_1/\sigma_3 - 2\mu\cdot\sqrt{\sigma_1/\sigma_3} - 1} \qquad (1.2.43)$$

The verification of the expressions (1.2.36) and (1.2.43) on the basis of data obtained in actual measurements will be described with respect to sand in Chapter 3 and with respect to clay in Chapter 4 respectively.

2.8 MICROSCOPIC CONSIDERATION OF STRESS RATIO-STRAIN-DILATANCY CHARACTERISTICS[22)]

Pursuing the origin of the stress-strain curve of soil forms one of the basic subjects on soil mechanics. As things stand now, however, there has hardly been made any lucid explanation of this particular problem. It is observed that densely packed sand has a peaked stress-strain characteristic and loosely packed sand has a stress-strain characteristic of the type of monotonous increase. This paragraph aims to consider the physical significance of such characteristics from the microscopic point of view attaching special interest to the change in the frequency distribution of the angle of interparticle contact "θ".

For the stated purpose, the author performed a test by using an apparatus incorporating hinges one each at the four corners as shown in Photo.1.2.2. The condition of the change in the frequency distribution of θ on a given horizontal shear plane due to the increase in shear strain was investigated by giving a uniform simple shear deformation to a pile of aluminum rods (having three diameters 3 mm, 5 mm and 9 mm). To be more specific, the end view of the pile of aluminum rods was photographed and the photographs showing the changing end view were enlarged so as to permit measurement of θ on a given horizontal shear plane. The shear strain γ produced in the pile was determined by measuring the angle of rotation of the parallelogramic frame. The change in the distribution of θ due to the increase of shear strain γ thus determined is illustrated in Fig.1.2.16 (1) through (8). Similarly to the case of shear test of the direct shear box type described previously, it is seen from these diagrams that the symmetric distribution gradually shifts to the triangular distribution having a peak on the righthand portion with the progress of shear and that the peak of distribution moves back to the center from the right portion as the shear strain further increases. In Fig.1.2.17, the change in the form of θ distribution as rated in terms of the average value $\bar{\theta}$ is presented aginst various values of shear strain γ. The eight plots found in this graph correspond to the diagrams (1) through (8) of Fig.1.2.16. Generally speaking, the fact that $\bar{\theta}$ has a large value proves advantageous with respect to the shear resistance. The aspect of the change of $\bar{\theta}$ relative to γ as depicted in Fig.1.2.17. reminds us of the peak-containing stress-strain curve for the densely packed sand.

As already pointed out, the shear-normal stress ratio τ/σ_N on the potential sliding plane can be expressed relative to $\bar{\theta}$ by the equation (1.2.25), which is reproduced here for the convenience of reference.

$$\tau/\sigma_N = \lambda \cdot \bar{\theta} + \mu \qquad (1.2.44)$$

where, $\lambda = 1.1$ to 1.5 (constant) and $\mu = \tan\phi_\mu$ (interparticle friction). Through the review

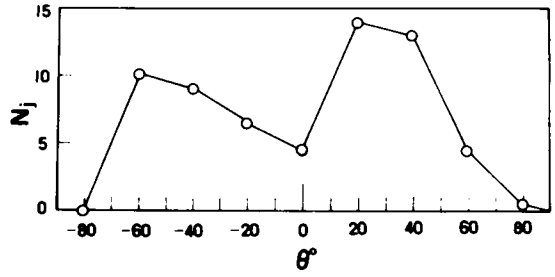

(1)

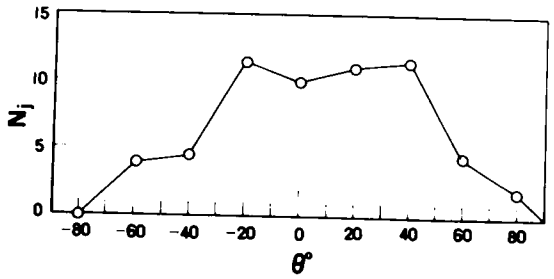

(5)

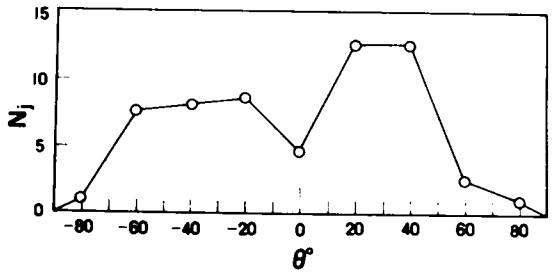

(2)

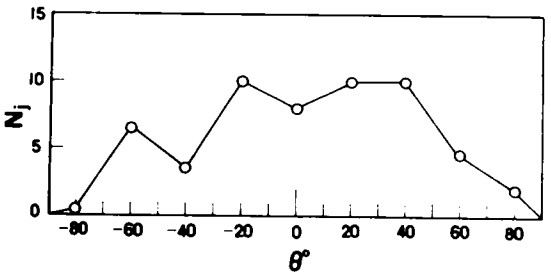

(6)

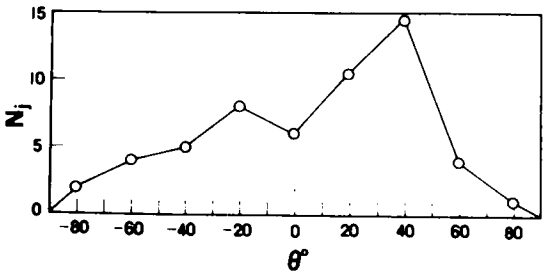

(3)

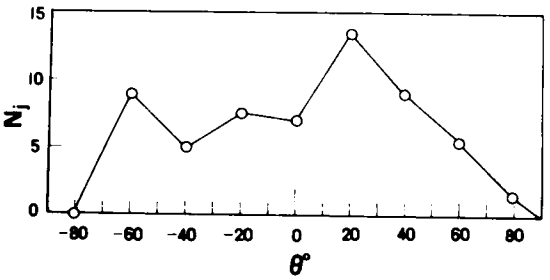

(7)

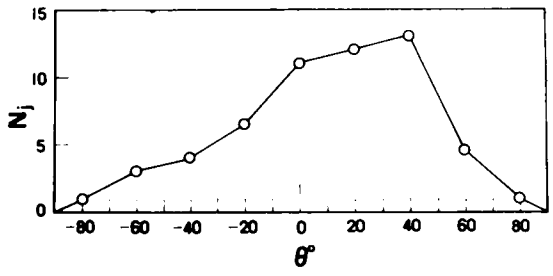

(4)

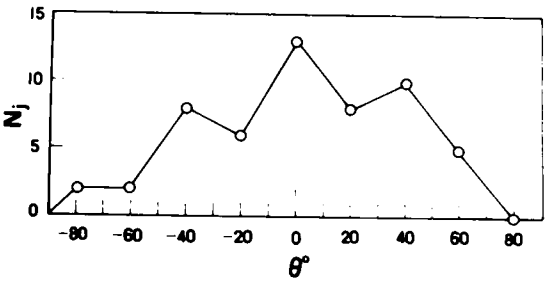

(8)

Fig.1.2.16 Change of frequency distribution of θ of aluminum rod mass (ϕ3, 5, 9mm) during shear.

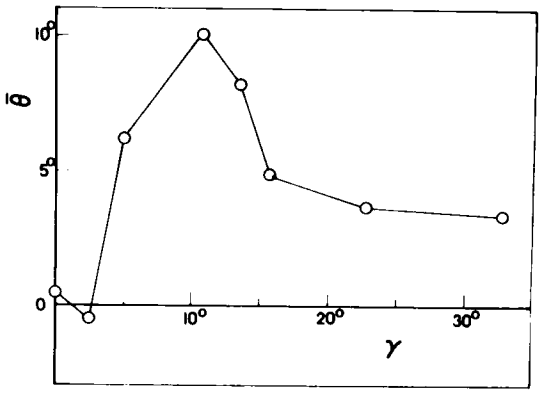

Fig.1.2.17 Relationship between $\bar{\theta}$ and γ.

of the mechanism for the generation of dilatancy, one can express the normal strain ϵ_N (compression as positive) on the aforementioned plane prior to and subsequent to the peak strength respectively by the formulas (1.2.32) and (1.2.35), which are also reproduced here.

$$\epsilon_N = \log_e \left| \frac{\cos\bar{\theta}}{\cos\bar{\theta}_0} \right| \qquad (1.2.45)$$

$$\epsilon_N = \log_e \left| \frac{\cos^2\bar{\theta}_p}{\cos\bar{\theta} \cdot \cos\bar{\theta}_0} \right| \qquad (1.2.46)$$

where, $-\bar{\theta}_0$ and $\bar{\theta}_p$ denote the values which $\bar{\theta}$ has immediately after the start of shear and at the time the shear resistance reaches its peak strength respectively. Since the plots of $\bar{\theta}$ against γ are available from Fig.1.2.17, the relationship of $\tau/\sigma_N \sim \gamma \sim \epsilon_N$ can be calculated in view of the formulas (1.2.44), (1.2.45) and (1.2.46). The result of the calculation is given in Fig.1.2.18. For this calculation, $\gamma = 1.4$, $\mu = 0.35$ based on the actually measured frictional coefficient between alminum rods (providing $\mu = 0$ in case of $\gamma = 0$), $\bar{\theta}_p = 10.1°$ derived from the fourth plot of Fig.1.2.17 and $-\bar{\theta}_0 \cong -7°$ derived from the intersections of the elongations of the second and third plots with the vertical axis are used. No comparison can be made with τ/σ_N of Fig.1.2.18 because the present test apparatus does not permit measurement of the shear stress. From the photograph, however, the final value of the normal strain, ϵ_N, is found to be -2.0% which closely corresponds to the final value of ϵ_N found in Fig.1.2.18. The sandy soil model using aluminum rods corresponds to a densely packed structure under all conditions. The graph of Fig.1.2.18 is noted to bear striking resemblance in form to the stress ratio-strain-dilatancy curve of densely packed sand.

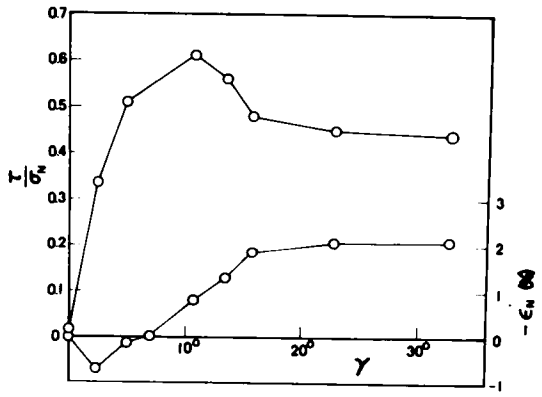

Fig.1.2.18 Relationship among τ/σ_N, γ and ϵ_N.

Fig.1.2.19 (a) and (b) are two-dimensional representations of the arrangement of densely packed and loosely packed particles as observed in the test. Fig.1.2.20 (a) and (b) represent, in the form of model, the change in the distribution of θ due to the

(a) (b)

Fig.1.2.19 View of two-dimensional arrangement of densely packed particles (a) and loosely packed particles (b).

corresponding variation of shear.[19] The circled numerals ① , ② and ③ are to show qualitatively the sequence in which the distribution changes in consequence of shear. When large sand grains are placed in a transparent box to make measurement of the angle of interparticle contact θ on the horizontal plane, there is observed a fixed trend: In the case of densely packed sand grains, the distribution of θ in the state prior to shear is obtained in a substantially symmetrical trapezoidal shape indicated by ① in Fig.1.2.20 (a). In the case of loosely packed sand grains, the distribution is obtained in a triangular shape having concentration in the neighborhood of $\theta = 0°$ as indicated by ① in Fig.1.2.10 (b). (Please see Fig.1.2.21 (a) and (b).)[23] This trend is also understandable from Fig.1.2.19 (a) and (b). In the distribution obtained in the trapezoidal shape, it is logical to conclude that the efficiency of interlocking between sand grains increases in proportion as the width of the shoulder (upper edge) is increased. This seems to have some bearing on the observation that the peak strength increases as the step shifts from ① to ② in Fig.1.2.20 (a). A fairly detailed des-

cription has already been made with respect to densely packed particles. The description here is, therefore, limited to loosely packed particles. Let us imagine a mass of very loosely packed particles. In this case, the majority of particles are hold in an instable arrangement in the neighborhood of $\theta = 0^\circ$ as illustrated in Fig.1.2.19 (b). On exposure to shear, such particles tend to slide down in the direction of shear and the distribution of θ is thought to occur as illustrated in Fig.1.2.20 (b) ②. As the shear further progresses, however, the proportion of particles which begin to slide over on the lower particles increases and, consequently, the distribution of θ is thought to returned to the state of ③ . Since the distribution ③ corresponds to a slightly denser condition than that of ① , it is inferred that the concentration tends to reduce in the neighborhood of 0°. From the foregoing discussion, it may really be understood that a mass of very loosely packed sand grains shows a stress-strain characteristic of the type of simple increase which lacks a clear peak. The resemblance in form between the distribution of (a) ③ and that of (b) ③ in Fig.1.2.20 is not inconsistent with the observation that both densely packed sand grains and loosely packed sand grains eventually take up substantially the same structure when exposed to large deformation. Thus, the distribution of θ is believed to constitute itself as one index for the evaluation of granular structure.

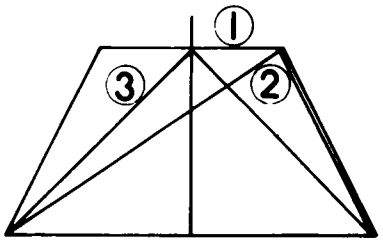

(a) Very dense packing.

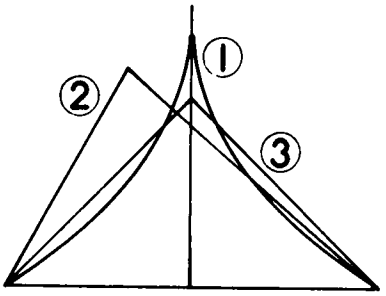

(b) Very loose packing.

Fig.1.2.20 Patterns of frequency distribution of θ during shear.

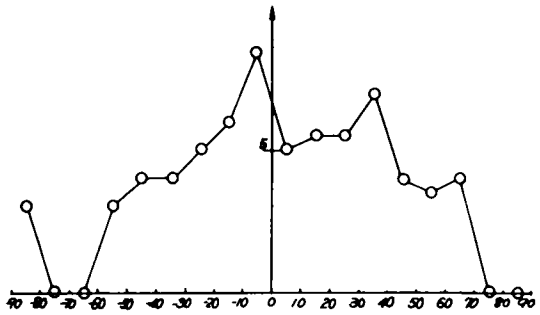

(a) Dense packing

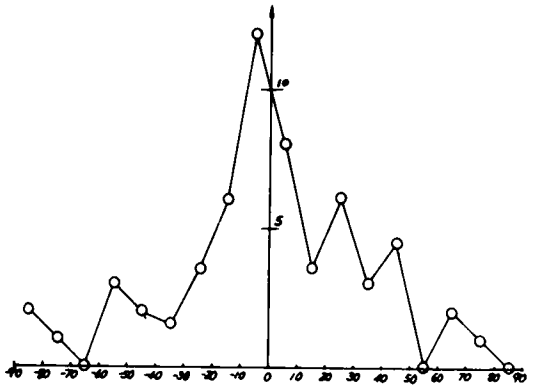

(b) Loose packing

Fig.1.2.21 Frequency distribution of θ of grains prior to shear.

2.9 MICROSCOPIC CONSIDERATION OF REPEATED SHEAR CHARACTERISTICS

2.9.1 Change in Granular Structure under Positively Repeated Shear[1)]

The repeated shear test is popularly employed in the sense that it would represent mechanical properties intermediate between those obtained by the ordinary static shear test and those by the vibratory shear test as well as for the purpose of investigation of the possible effect of stress hysteresis. The mechanical properties obtained by the repeated shear test are frequently compared with those diplayed by the ordinary static shear test, with the differences subjected to discussion. In many cases, such differences are likely to be ascribed eventually to differences in granular structure. It is, therefore, proposed to consider from the microscopic point of view the essential significance of the mechanical properties disclosed by the repeated shear test while in strict observance of the aforesaid frequency distribution of the angle of interparticle contact

"θ" which is thought, as previously described, to constitute one guidepost for the evaluation of granular structure. Of the various differences found between the mechanical properties displayed by the ordinary static shear and those by the repeated shear, those pointed out below are taken up as subjects for the present study. One problem resides in the fact that the stress-strain relationship obtained in the case of the repeated shear has a greater gradient than that obtained in the case of ordinary shear even when the void ratio is increased. As pointed out previously, in the case of the ordinary shear, there seems to exist a trend that the practically random form of θ frequency distribution in the initial state shifts gradually with the increase of shear strain to the peak-containing form of distribution having concentration in the positive zone advantageous for shear resistance and eventually reaches the peak strength. It is concluded, therefore, that in proportion to the increase in shear strain, the granular structure is changed and the shear resistance is manifested until the peak strength is reached. In that case, the shear resistance to be manifested per unit shear strain will consequently correspond to the gradient of the stess-strain relationship.

Fig.1.2.22 shows, in terms of stress ratio-shear displacement relationship, the result

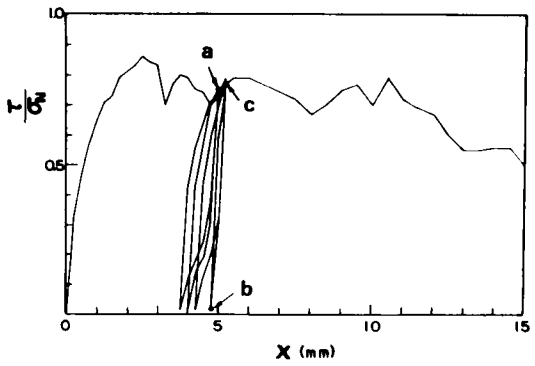

Fig.1.2.22 Relationship between stress ratio and shear displacement of aluminum rod mass (ϕ1.6, 3, 5, 9mm) in repeated shear.

of the positively repeated shear test conducted by using a mixed pile of aluminum rods having four diameters (1.6 mm, 3 mm, 5 mm and 9 mm). Fig.1.2.23 (a) shows the frequency distribution of θ at the point a at which the repetition was started, Fig.1.2.23 (b) the frequency distribution of θ at the point b at which the stress fell in the 5th repetition and Fig.1.2.23 (c) the frequency distribution of θ at the point c at which the stress returned to its former magnitude in the 5th repetition. In this particular test, the shear was exerted a total of five times.

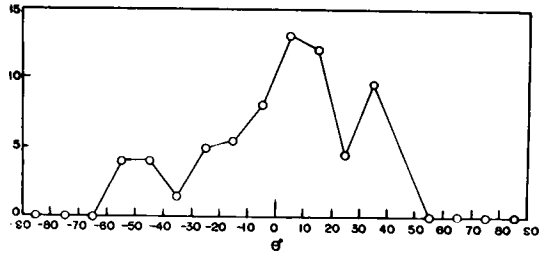

(a) At point a in Fig.1.2.22.

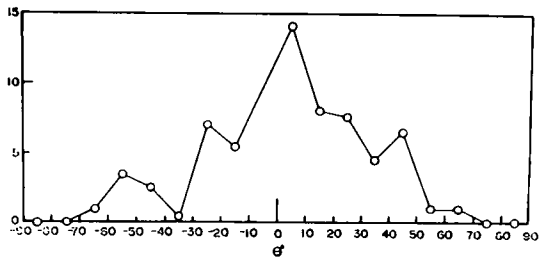

(b) At point b in Fig.1.2.23.

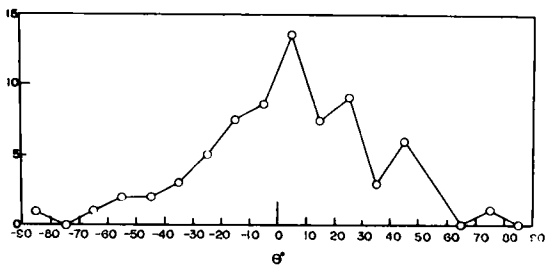

(c) At point c in Fig.1.2.22

Fig.1.2.23 Frequency distribution of θ in repeated shear.

The repeated shear is effected with respect to a granular material which has been sheared to the point **a** of Fig.1.2.22 and consequently acquired a granular structure corresponding to the frequency distribution of θ as shown in Fig.1.2.23 (a), for example, by giving shear displacement in the opposite direction so as to lower the stress and thereafter giving the shear displacement again in the former direction so as to heighten the stress to the former level. The frequency distribution of θ at the point **b** after five repetitional shear applications (Fig.1.2.23 (b)) bears resemblance to the frequency distribution of θ at the point **a** (Fig.1.2.23 (a)). It is also observed that the frequ-

ency distribution of θ at the point c to which the stress was elevated from the point b (Fig.1.2.23 (c)) bears striking resemblance to the frequency distribution of θ at the point b. From this, it is concluded that the granular structure is compacted barely appreciable and is not substantially changed even after five repeated shear applications and that the granular structure is changed very little while the shift is taking place from the point b to the point c. A review of the photoelastic fringe photographs showing the progress of the repeated shear test conducted on a pile of rods (6.2 mm and 10 mm in diameter) made of a photoelastic material reveals that under the conditions such as of the point b and the point c of Fig.1.2.22, the granular structure does not undergo any conspicuous change on exposure to the repeated shear and, depending on the direction in which the shear displacement is given, the interparticle force is produced effectively, dissipated altogether or transmitted in a different direction.

It is evident from the foregoing discussion that repeated shear amounts to having the stress reciprocate between the magnitude at which the granular body in question acquires a structure permitting full manifestation of stress and 0. Therefore, the repeated stress condition can be satisfied by allowing the interparticle force to be transmitted or dissipated without having to fundamentally change the granular structure. This means that a required magnitude of stress can be acquired with a small amount of strain enough to permit transmission of the interparticle force. The gradient of the stress-strain relationship is increased even when the void ratio has been increased because of the change given previously to the garnular structure. In contrast, for the case of ordinary shear, the granular structure is required to be changed in order to permit generation of a required magnitude of stress as already pointed out. This necessitates a comparatively large strain. It is inferred that in such a case, the gradient of the stress-strain relationship is smaller than that of the repeated shear even when the void ratio is small. Accordingly, the magnitude of the shear resistance provided by the granular body is not necessarily governed by the void ratio alone and, in this connection, the concept of the frequency distribution of the angle of interparticle contact "θ" employed for the evaluation of "*granular structure*" on the shear plane acquires an increased significance.

2.9.2 Change in Granular Structure under Alternately Repeated Shear[24)]

Here the author seeks to explain from the microscopic point of view the significance of the hysteresis loop which such a granular body as sand describes in alternetely repeated shear, with special interest attached to the change in granular structure. For this purpose, the author performed the repeated shear test by using mixed piles of aluminum rods having different diameters as well as samples of sand. In the test, the frequency distribution of θ on the shear plane was measured at various points on the hysteresis loop and the result was investigated as the stress ratio-strain-

dilatancy characteristic corresponding to the change in the direction of shear.

Fig.1.2.24 shows, in terms of model, the hysteresis loop described in alternately repeated shear and the form of the frequency distribution of θ at the various points on that loop. In many cases, the distribution at the point ① prior to shear has a symmetric trapezoidal shape. At the point ② representing the time of peak strength, the distribution tends to acquire a practically triangular shape having the vertex deviated in the positive zone of θ. In the case of the point ③ representing the time past the peak, the vertex shifts slightly in the direction of the center. The stress ratio (τ/σ_N) would immediately reduced to 0 (point ④) if the direction of shear was reversed from the point ③ . As described in 2.9.1, the granular structure does not

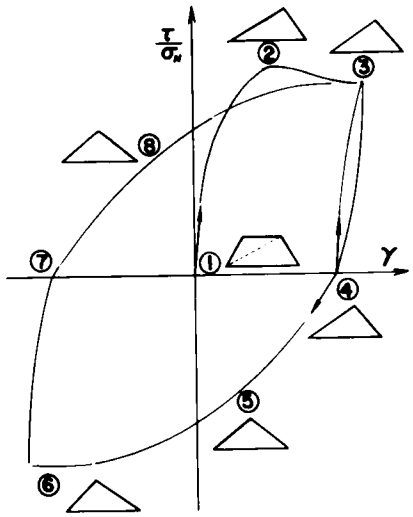

Fig.1.2.24 Patterns of frequency distribution of θ at points on hysterisis loop in repeated shear.

undergo any appreciable change at this time and the form of the frequency distribution of θ is considered to remain substantially unaltered from that at the point ③ . From Fig.1.2.24, it is seen that the hysteresis loop is essentially symmetrical with respect to the origin. The thought of this fact leads one to infer that the frequency distribution of θ at the point ⑥ which is symmetrical relative to the point ③ will form, with respect to $\theta = 0°$, a shape practically symmetrical against that at the point ③ . If so, then it is also imagined that similarly symmetrical frequency distribution forms of θ will exist in the neighborhood of the points ⑤ and ⑧ falling between the points ③ and ⑥ . Fig.1.2.25 (a) through (e) represent the frequency distributions of θ actually measured at the points corresponding to ① , ② , ③ , ⑤ and ⑥ in the repeated shear test performed on a mixed pile of aluminum rods (having diameters of 1.6, 3, 5 and 9 mm). It is noted that these frequency distribution forms of θ substantially indicate the aforementioned trend.

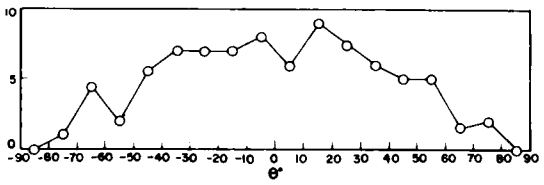

(a) At point ① in Fig.1.2.24.

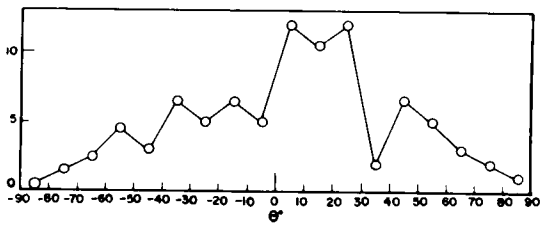

(b) At point ② in Fig.1.2.24.

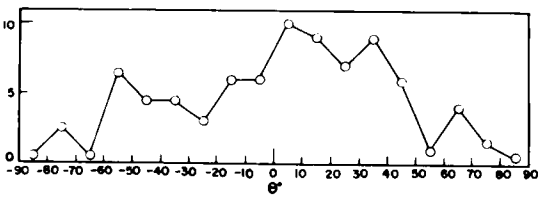

(c) At point ③ in Fig.1.2.24.

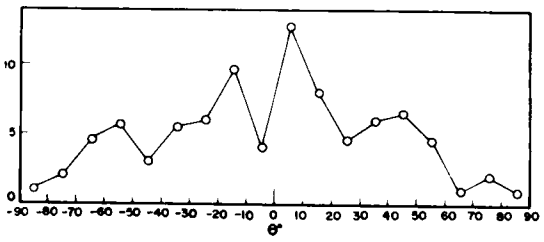

(d) At point ⑤ in Fig.1.2.24.

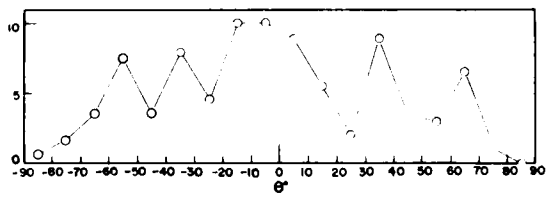

(e) At point ⑥ in Fig.1.2.24.

Fig.1.2.25 Measured frequency distribution of θ of aluminum rod mass at points on hysterisis loop.

In the hysteresis loop shown in Fig.1.2.24, the gradients indicated by the arrow marks ① → ② , ④ → ③ and ④ → ⑤ are compared. It is seen that generally the gradient of ④ → ③ has the largest value, the gradient of ④ → ⑤ the smallest value and the gradient of ① → ② the intermediary value. As already described, of all the gradients involved here, particularly the gradient of ④ → ③ under the repeated application of load in repeated shear has a larger value than the gradient of ① → ② representing the initial stage despite an increase in the void ratio. This has posed a subject for frequent discussion. This can be explained clearly by resorting to the concept of the frequency distribution of θ. The distribution forms of θ at the point and the point ④ shown in Fig.1.2.24 are compared. Since the distribution form at the point ④ is such that the distribution is deviated in the positive zone of θ, it provides more advantageous resistance to the shear exerted in the right direction than

the distribution of the left-right symmetric form at the point ① . In this distribution form, it is believed that the resistance can immediately be manifested at least up to the level of the shear resistance offered at the point ③ having substantially the same form of distribution. As a consequence, the gradient of ④ → ③ rises more sharply than the gradient of ① → ② even when the void ratio is increased. When the shear is exerted toward the left at the point ④ , however, the form of distribution is still less advantageous for the purpose of resistance than the distribution at the point ① . This provides a logical interpretation to the fact that the gradient of ④ → ⑤ has the smallest value. It is interesting to note that this is suggestive of the directivity of the granular structure at the point ④ .

Through the microscopic analysis of the shear resistance and dilatancy as described in 2.7, it is learnt that where the frequency distribution of θ is completely symmetric with respect to $\theta = 0^\circ$ (and consequently $\bar{\theta} = 0$), the gradient of the dilatancy-shear strain curve ($d\epsilon_N/d\gamma$) is found to be 0 from the equation (1.2.31) and the shear resistance (τ/σ_N) is found to equal the interparticle friction μ (= $\tan\phi_\mu$) in accordance with the equation (1.2.36) respectively. In alternately repeated shear, points which satisfy $d\epsilon_N/d\gamma = 0$ appear frequently. It has been demonstrated at these points, that the magnitude equals the interparticle friction of the material of test specimen, no matter whether the specimen in use is actual sand or rod-shaped model. To cover these and other similar observations, Chapter 3 deals also with the data of actual measurements made in the repeated shear test performed on sand.

2.10 CONCLUSIONS

A few points which have some bearing on the essential nature of the logic underlying the discussions in the present chapter will be summarized. First, the author confirmed, with the aid of a direct shear box type test apparatus, the presence of a shear zone having a width. He ascertained that the characteristic property displayed on the plane (not necessarily on flat plane in the microscopic sense) on which the relative displacement is largest within that zone governs the shear properties of the entire test specimen in use. In each case the author's study started from the consideration of the equilibrium of soil particles on such *mobilized plane* (potential sliding plane), keeping in mind the equilibrium of soil partilces changing moment by moment. It may, therefore, be safe to conclude that the same equation can invariably be applied even if soil particles should rotate around their center, only so far as there is produced a slight relative displacement enough for manifestation of interparticle friction. The author made detailed observation of the behavior of particles on the shear plane by using a rod-shaped model. Consequently, he has learnt that particles placed in mutual contact position on the shear plane would not slide over one another so often even

when there was exerted a shear displacement of the size of 20 to 30 mm and that the majority of particles excepting those located close to the right and left edges of the shear box would slide over one another barely once unexpectedly. The same trend was also observed in the test using large grains. It is, therefore, a reasonable inference that the same trend may be observed with finer sand particles. The reason is that the possible change in the angle between adjoining particles is not appreciably large even in the presence of a large displacement because there exists a shear zone having a width as mentioned above. This is an interesting fact which has some bearing upon the change in the distribution of the angle of interparticle contact due to shear and consequently on the very origin of the stress-strain property of the soil. With this fact in mind, the author introduced the concept of the frequency distribution of the angle of interparticle contact on the shear plane and took into consideration the property of interparticle force in order to drive various formulas governing the relationship between the stress ratio and the strain increment ratio, the relationship between the stress ratio and the dilatancy, and so on. All these formulas are based on the thought that, first of all, the stress ratio (τ/σ_N) equals to the interparticle friction (μ) when the normal strain reaches the maximum compression point ($d\epsilon_N/d\gamma = 0$) and that the stress ratio is closely related with the dilatancy characteristics.

The results which have been obtained in the present chapter may be summarized as follows.

(1) Assuming that the sandy soil had a known grain size distribution, the author sought to sample particles randomly in accordance with Monte Carlo Method and simulate the particle arrangement two-dimensionally. When the void ratio determined consequently was compared with the void ratio actually found by measurement with the rod-shaped model, they seemed to be in close agreement with each other. The author feels that the future study may necessitate appropriate introduction of laws of mechanics on the stability of particle arrangement against the weight of particles and possible external force.

(2) As microscopic factors directly governing the shear resistance of soil, the author introduced the interparticle force "f", the angle of interparticle friction "ϕ_μ" and the angle of interparticle contact "θ".

(3) The author expressed the angle of interparticle contact "θ" on the shear plane, which can assume various values, in terms of the frequency distribution of θ and consequently came to be interested in the observation that the form of this distribution would vary with shearing. This distribution of θ is thought to be one index for the evaluation of the granular structure during shear which has posed itself as a subject of serious discussion in the recent years.

(4) The author derived a formula expressing the equilibrium of soil particles on the shear plane by taking into consideration the aforementioned microscopic factors. Then, he introduced the concept of the distribution of θ and also took into consideration the

peculiar nature of the interparticle force transmission so as to derive formulas expressing the relationship between the stress ratio and the strain increment ratio, the relationship between the stress ratio and dilatancy, and the like. In the course of the derivation of these formulas, it was shown that the average value $\bar{\theta}$ of the distribution of θ was approximately equal to the normal-shear strain increment ratio ($d\epsilon_N/d\gamma$) on the shear plane. This means that the macroscopic evaluation of the distribution of θ could be effected on the basis of the said ratio $d\epsilon_N/d\gamma$.

(5) The author furnished a far-reaching explanation on the stress ratio-strain-dilatancy characteristics of the soil from the microscopic point of view while using the aforementioned formulas and the concept of the distribution of θ.

(6) The author discussed the hysteresis loop which the soil describes during shear by resorting to the concept of the distribution of θ, with special emphasis focussed on the change in the granular structure.

References

1) Murayama, S. and Matsuoka, H.: A Microscopic Consideration on the Shearing Behavior of Granular Materials using the Two-dimensional Models, Annuals, Disaster Prevention Research Institute, Kyoto University, No.13B, 1970, pp.505–523, (in Japanese).
2) Murayama, S. and Matsuoka, H.: The Mechanism of Shearing and its Similarity for Sands and Clays, Annuals, Disaster Prevention Research Institute, Kyoto University, No.14B, 1971, pp.551–563, (in Japanese).
3) Newland, P. L. and Allely, B. H.: Volume Change in Drained Triaxial Tests on Granular Materials, Géotechnique, Vol.7, No.17, 1957, pp.17–34.
4) Rowe, P. W.: The Stress-dilatancy Relation for Static Equilibrium of an Assembly of Particles in Contact, Proc. Roy. Soc. London, Ser. A. Vol.269, 1962, pp.500–527.
5) Mogami, T.: A Statistical Theory of Mechanics of Granular Materials, Journ. Faculty of Eng., Univ. of Tokyo, Ser. B, Vol.28, No.2, 1965, pp.65–79.
6) Mogami, T. and Yoshikoshi, H.: Angle of Internal Friction of Sands and Gravels, Proc., Annual Meeting of J.S.C.E. (23rd), III-17, 1968, pp.51–52, (in Japanese).
7) Mogami, T.: Angle of Internal Friction of the Granular Material and a Simple Transient Phenomenon, Trans. of J.S.C.E., No.128, 1966, pp.53–62.
8) Murayama, S.: A Theoretical Consideration on a Behaviour of Sand, Proc. of I.U.T.A.M. Symposium of Rheology and Soil Mechanics, Grenoble, 1964, Springer-Verlag, 1966, pp.146–159.
9) Murayama, S.: Stress Strain-Time Behavior of Soils Subjected to Deviatoric Stress, Proc. of 7th Int. Conf. on S.M.F.E., Vol.1, 1969, pp.297–306.

10) Murayama, S.: A Constitutive Equation of Soils, Annuals, Disaster Prevention Research Institute, Kyoto University, No.14B, 1971, pp.17–29, (in Japanese).
11) Murayama, S. (chief of the minor study group for deformation and failure of soft ground): Deformation and Failure of Soft Ground, Annuals, Disaster Prevention Research Institute, Kyoto University, No.15A, 1972, pp.43–59, (in Japanese).
12) Murayama, S. and Matsuoka, H.: Transmission of Interparticle Force in Two-dimensional Granular Models, Proc., Annual Meeting of Kansai Br., J.S.C.E., III-17, 1969, (in Japanese).
13) Murayama, S. and Matsuoka, H.: Microscopic Consideration on Shear Phenomenon of Granular Materials, Proc., Annual Meeting of J.S.C.E. (24th), III-8, 1969, pp.25–26, (in Japanese).
14) Matsuo, M., Komada, T. and Takahashi, M.: A Study on Deformation of Sand Layer by Monte Carlo Method, Proc., Annual Meeting of J.S.C.E. (21st), III-52, 1966, (in Japanese).
15) Matsuoka, H.: Fundamental Study of Earth Pressure on Tunnel in Sandy Soil, Master Thesis, Department of Civil Engineering, Kyoto University, No.368, 1968, (in Japanese).
16) Oda, M.: Fabric Changes during Deformation of Sand, Proc., Annual Meeting of J.S.C.E. (26th), III-14, 1971, pp.45–48, (in Japanese).
17) Oda, M.: The Mechanism of Fabric Changes during Compressional Deformation of Sand, Soils and Foundations, Vol.12, No.2, 1972, pp.1–18.
18) Ochiai, H., Yamanouchi, T. and Tanahashi, Y.: Moving Properties of Particles during Shear using Two-demensional Rod Model, Proc., Annual Meeting of J.S.C.E. (26th), III-13, 1971, pp.41–44, (in Japanese).
19) Murayama, S. and Matsuoka, H.: Shear Resistance and Particle Structure of Granular Soils, Proc., Annual Meeting of J.S.C.E. (25th), III-36, 1970, pp.105–108, (in Japanese).
20) Matsuoka, H.: The Stress-Strain Relation of Soils under Shearing drived from a Microscopic Consideration, Annuals, Disaster Prevention Research Institute, Kyoto University, No.15B, 1972, pp.499–511, (in Japanese).
21) Murayama, S. and Matsuoka, H.: A Microscopic Study on Shearing Mechanism of Soils, Proc. 8th Int. Conf. S.M.F.E., 1973, (to be published).
22) Matsuoka, H.: A Microscopic Study on Stress-Strain Relation of Soils, Proc., Annual Meeting of Kansai Br., J.S.C.E., III-7, 1972, (in Japanese).
23) Murayama, S., Matsuoka, H., Bandō, H. and Maeda, K.: Microscopic Consideration on Shear Mechanism of Granular Soils, Proc., Annual Meeting of J.S.S.M.F.E. (5th), IV-25, 1970, pp.469–472, (in Japanese).
24) Murayama, S., Matsuoka, H. and Bandō, H.: Some Considerations on Hysteresis Loop of Granular Materials, Proc., Annual Meeting of Kansai Br., J.S.C.E., III-25, 1970, (in Japanese).

CHAPTER 3

STRESS-STRAIN RELATIONSHIP OF SANDY SOIL[1),2),3)]

3.1 GENERAL DESCRIPTION

In Chapter 2, the author studied the shear mechanism of such granular materials as sand from the microscopic point of view by chiefly using two-dimensional models of sandy soil composed of aluminum rods or photoelastic rods, steel balls, gravel and so on as test specimens in an effort to offer a fundamental explanation to the stress-strain characteristics of soil. Here, he proposes to derive expressions of stress ratio-strain relationship of soil applicable to the mobilized plane from the various relationships which were confirmed through the microscopic study of Chapter 2. He then proceeds to derive from these expressions general stress ratio-strain formulas under three different principal stess conditions, with emphasis focussed on the mobilized planes involved. The general stress-strain relationships will be verified on the basis of data obtained by the conventional triaxial compression test, conventional triaxial extension test, plane strain test and universal triaxial test involving the actions of three different principal stresses. Then the relationships will be reviewed for their unversality. A description will be given of a method for applying the aforementioned expressions to the undrained shear test. The results of the application will be compared with data of measurements. At the same time, it will be substantiated that the results of the repeated shear test can be explained by the same principle.

In Chapter 2, the shear characteristics during the direct shear were ascertained from the microscopic point of view and then reviewed in connection with the dilatancy characteristics exhibited during the simple shear deformation in which a given test specimen is wholly subject to uniform shear strain. In this case, the stress plane under review is considered as a plane in which soil particles are mobilized most heavily. Therefore, the basic expressions of the stress-strain relationship derived as mentioned above should be taken as applicable to the plane of $(\tau/\sigma_N)_{max}$ or *the mobilized plane*. In the case of a model using rods, a single mobilized plane under two-dimensional stress may well be presumed. In dealing with the behaviors of soil particles under three principal stresses which are naturally of three-dimensional nature, however, the idea of three compounded mobilized planes is introduced as a new concept. On the basis of this idea of compounded mobilized planes, the stress-strain expressions under such three principal stresses will be derived from the basic expressions of the stress-strain relationship on the single mobilized plane. The reason for the author's attachment of special attention to these mobilized planes is that even in a triaxial test in which no shear plane is defined in advance, a mobilized plane makes its appearance as the deformation pro-

ceeds to the extent of peak strength and residual strength and, therefore, that it is possible to assume a plane in which soil particles are most actively mobilized even before the peak strength. In assuming field conditions, it is only logical to consider that the ground does not offer uniform resistance but there exists a zone governing the shear resistance or there occurs the weakest palne (generally referred to as "*slip surface*") within such a zone.

Fig..1.3.1 and Fig.1.3.2 illustrate the results of the direct shear test and the triaxial test conducted on a densely packed sand and a loosely packed sand[4]. These drawings are indicative of a trend that, at least qualitatively, a fixed stress ratio (believed to correspond to the interparticle friction) is assumed at the point of the maximum volume compaction, irrespectively of denseness or looseness of sand packing and that the stress ratio reaches its peak at the point of the highest gradient of the volume change curve[5),6)] and soon decreases as the gradient begins to decline past the peak of gradient. In this chapter, the author proposes to express these interesting characteristics quantitatively on the basis of the formulas derived in Chapter 2 in an effort to define the general stress-strain relationships.

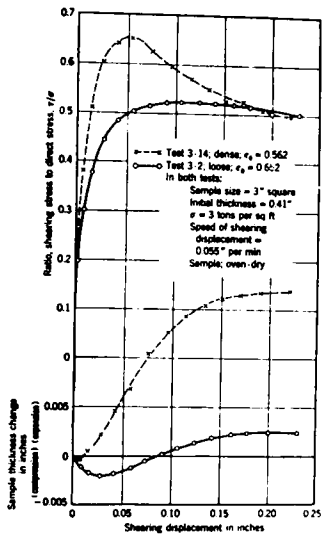

Fig.1.3.1 Plots of typical direct shear tests on loose and dense sand (after Taylor[4]).

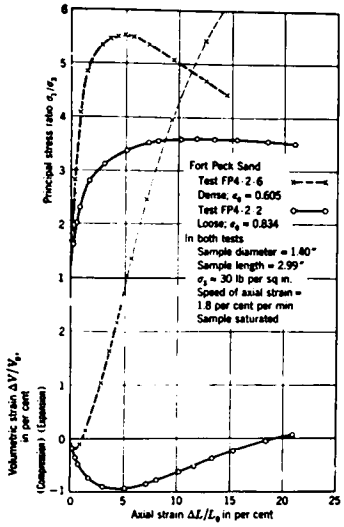

Fig.1.3.2 Plots of typical triaxial compression tests on loose and dense sand (after Taylor[4]).

3.2 SPECIMENS AND APPARATUS USED IN TESTS

To enrich the variety of test specimens in terms of grain size, shape, surface condition and grain-size distribution, the author used Toyoura standard sand (Yamaguchi). Ishii River sand (Kobe), Sagami River sand (Kanagawa), glass beads, etc. in the test.

Toyoura standard sand had an average grain size of 0.19 mm, a uniformity coefficient of 1.6, a specific gravity of 2.65 and a maximum and a minimum void ratio of 0.95 and 0.58 respectively. The grain size distribution curve of this sand is shown in Fig.1.3.3 and the photomicrograph of the sand is shown in Photo.1.3.1.

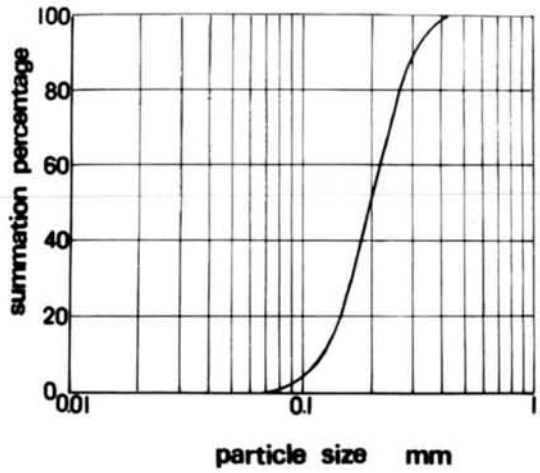

Fig.1.3.3 Grain size distribution curve of Toyoura standard sand.

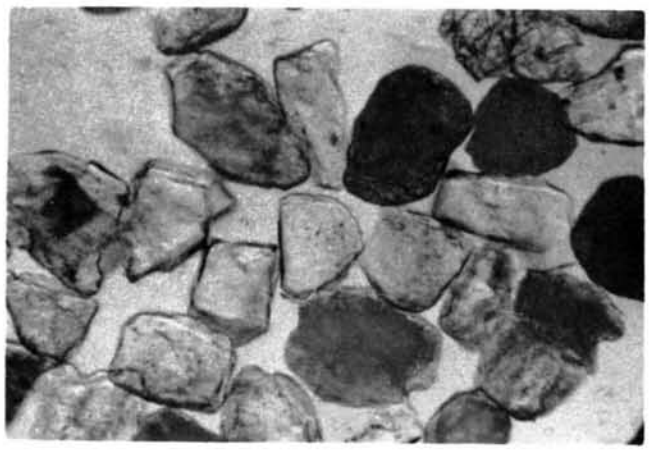

Photo.1.3.1 Photomicrograph of Toyoura standard sand.

Ishii River sand had an average grain size of 0.95 mm, a uniformity coefficient of 5.2, a specific gravity of 2.67, and a maximum and a minimum void ratio of 0.94 and 0.56 respectively. The grain size distribution curve of this sand is shown in Fig.1.3.4

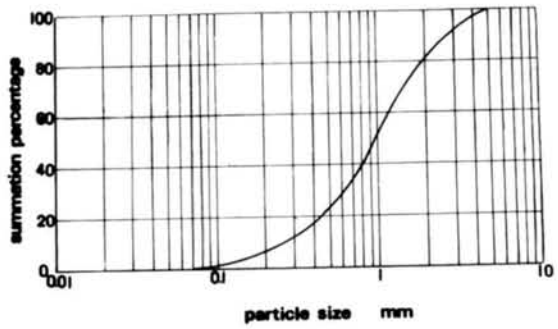

Fig.1.3.4 Grain size distribution curve of Ishii River sand.

and the photograph of the sand is shown in Photo.1.3.2.

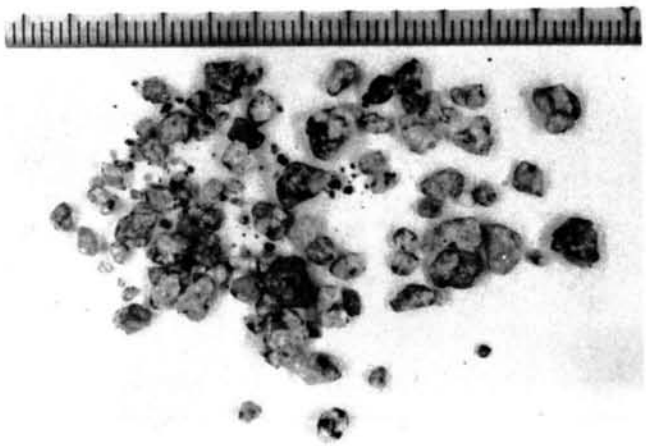

Photo.1.3.2 Photograph of Ishii River sand.

Sagami River sand had an average grain size of 0.42 mm, a uniformity coefficient of 2.2, a specific gravity of 2.68 and a maximum and a minimum void ratio of 1.08 and 0.53 respectively. The photomicrograph of this sand is shown in Photo.1.3.3. From this photograph, it is observed that the individual particles of this sand are somewhat angular.

The glass beads had a grain size falling within the range of sand's grain size (0.074 mm - 4.76 mm). The average grain size was 0.15 mm, the uniform coefficient was 1.2, the specific gravity was 2.48 and the maximum and the minimum void ratio was 0.71

and 0.50 respectively. The photomicrograph of the glass beads is shown in Photo.1.3.4.

Photo.1.3.3 Photomicrograph of Sagami River sand.

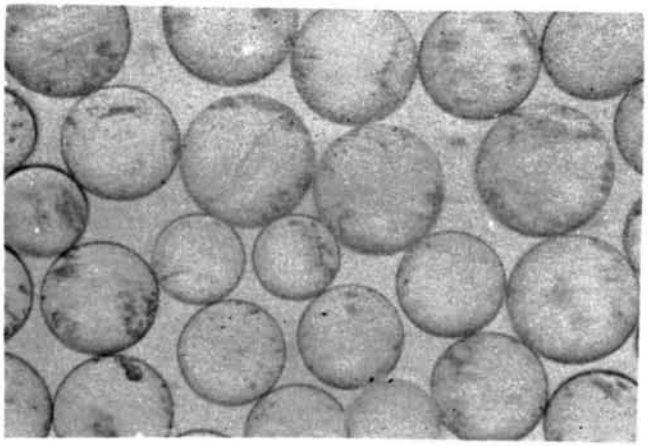

Photo.1.3.4 Photomicrograph of glass beads.

For the present tests were used an ordinary triaxial apparatus (N.G.I. type made by Geonor), a simple shear apparatus (N.G.I. type made by Geonor) and a newly trial-manufactured universal triaxial apparatus[7] capable of application of three mutually different principal stresses. The photographs of these apparatuses and the schematic diagram of the universal triaxial apparatus are shown in Photos.1.3.5, 1.3.6 and 1.3.7 and in Fig.1.3.5 respectively. In the case of the triaxial apparatus test specimens were prepared in two sizes – 3.5 cm in diameter and 7 cm in height and 5 cm in diameter and 5 cm in height (for Ishii River sand). To reduce possible friction on the upper and lower end surfaces, a rubber membrane coated with silicone grease was inserted each between the specimen and the cap and between the specimen and the pedestal. In the case of

the simple shear apparatus, test specimens measured 7.98 cm in diameter (50 cm^2 in cross sectional area) and about 2 cm in height. In the universal triaxial apparatus, test specimens were cubes of about 7 cm in edge length as illustrated in Fig.1.3.5 and the load was applied to the specimens via the loading plates. One pair of opposite loading plates (disposed in the direction of the minor principal stress) were so designed that a built-in board was pushed out of each end face in proportion to the displacement of the loading plate (disposed in the direction of the intermediate principal stress) by virtue of the resilience of a spring, so as to fill up any possible gap between loading plates. To minimize possible friction between each loading plate and the specimen, a thin rubber membrane or polyethylene membrane coated with grease was inserted. By actual measurement, the frictional coefficient existing between the loading plates and the specimen under the conditions was found to be about 0.02, a value which does not seem to have any appreciable effect upon test results. It is added that all test specimens used for the triaxial test were in saturated conditions and those for the simple shear test and the universal triaxial test were invariably in dry conditions.

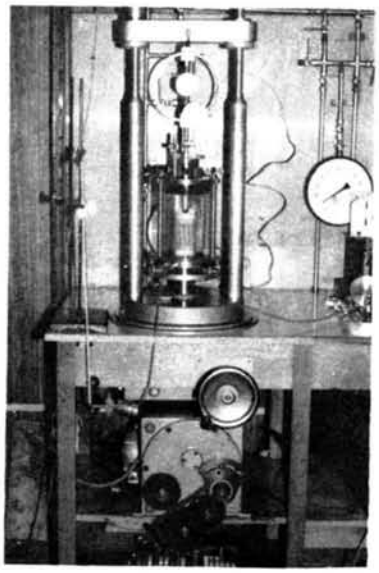

Photo.1.3.5 Triaxial apparatus (N.G.I. type made by Geonor).

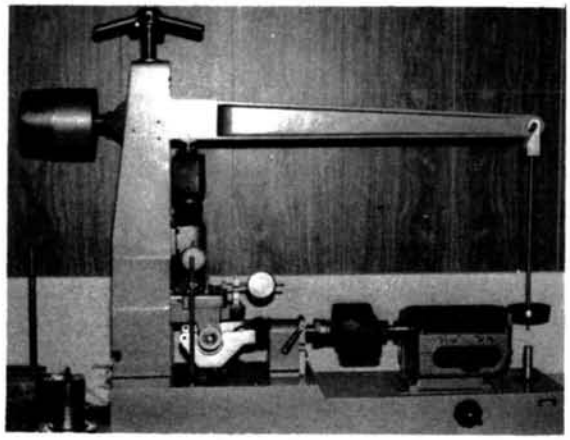

(a) Complete view.

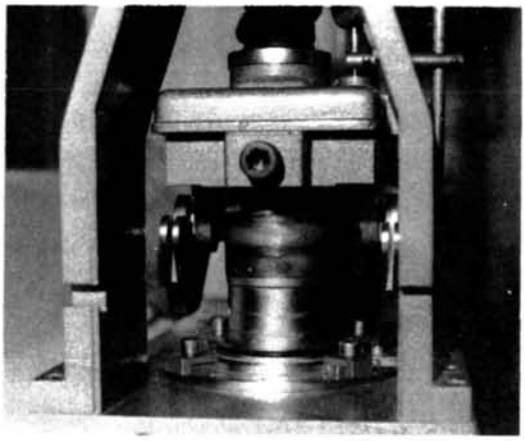

(b) Part of specimen.

Photo.1.3.6 Simple shear apparatus (N.G.I. type made by Geonor).

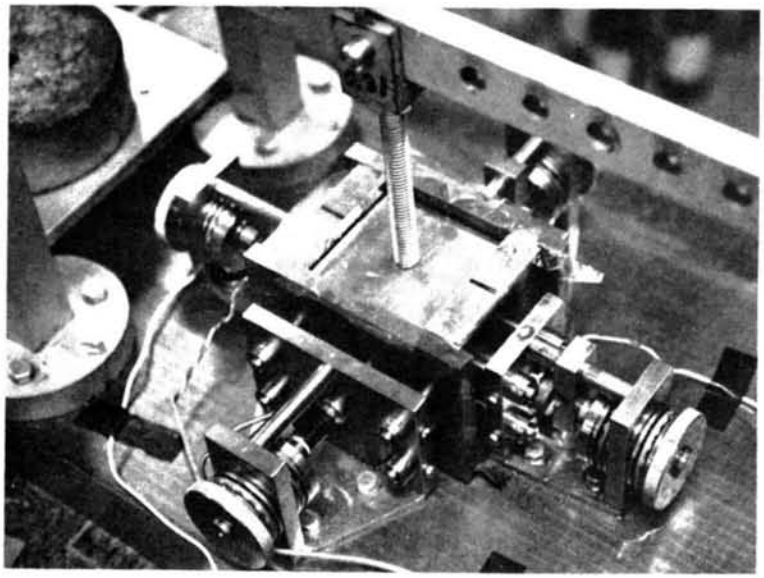

Photo.1.3.7 Universal triaxial apparatus (newly trial-manufactured in D.P.R.I. Kyoto Univ.)

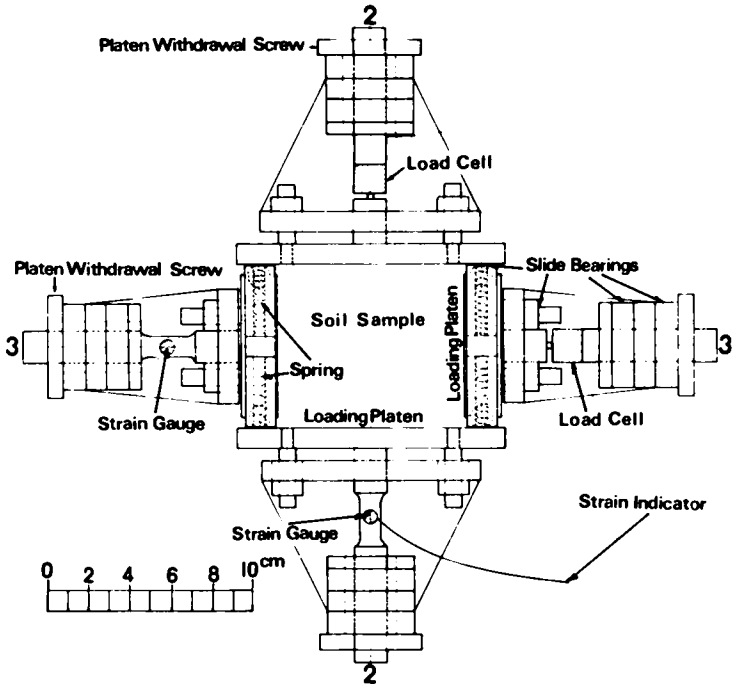

Fig.1.3.5 Plan view of universal triaxial apparatus.

3.3 STRESS-STRAIN RELATIONSHIPS ON MOBILIZED PLANE

In Paragraph 2.7 of Chapter 2, the author drew out the relationship existing between the shear-normal stress ratio (τ/σ_N) and the normal-shear strain increment ratio ($d\epsilon_N/d\gamma$) on the mobilized palne. The expression of this relationship is shown once again below.

$$\frac{\tau}{\sigma_N} = \lambda \cdot \left(-\frac{d\epsilon_N}{d\gamma}\right) + \mu \qquad (1.3.1)$$

Here, ϵ_N presumes compression as positive, μ is an interparticle frictional coefficient of soil particles and λ is a constant of an approximate value of $1.1 - 1.5$ to be determined by the value of μ. Now, the author proposes to derive a practical expression of stress-strain relationship by incorporating a new equation to the equation of (1.3.1) given above. When the ratio τ/σ_N is still on the way to the peak strength, the normal strain ϵ_N on the mobilized plane can be approximated as shown below by developing power series of $\log_e\cos\bar{\theta}$ $(= -\bar{\theta}^2/2 - \bar{\theta}^4/12 - \cdots\cdots)$ from the equation (1.2.32). of Paragraph 2.7 and disregarding terms of high order.

$$\epsilon_N = \log_e \left| \frac{\cos\bar{\theta}}{\cos\bar{\theta}_0} \right| \cong -\frac{1}{2}\bar{\theta}^2 - \left(-\frac{1}{2}\bar{\theta}_0^2\right)$$

$$= \frac{1}{2}(\bar{\theta}_0^2 - \bar{\theta}^2) = \frac{1}{2}(\bar{\theta}_0 + \bar{\theta}) \cdot (\bar{\theta}_0 - \bar{\theta}) \qquad (1.3.2)$$

Assuming that there exists the approximation of $d\gamma = d\bar{\theta}$ in this case, one can appromixate $\gamma \cong (\theta_0 + \theta)/2$ for the neighborhood where $\bar{\theta} = \bar{\theta}_0$ or $\epsilon_N = 0$. Since this gives rise to $\bar{\theta} \cong -\epsilon_N/\gamma + \bar{\theta}_0$, one can derive the following equation from the expression (1.2.25) of Paragraph 2.7, Chapter 2.

$$\frac{\tau}{\sigma_N} = \lambda \cdot \bar{\theta} + \mu \cong \lambda \cdot \left(-\frac{\epsilon_N}{\gamma}\right) + \lambda \cdot \bar{\theta}_0 + \mu$$

$$= \lambda \cdot \left(-\frac{\epsilon_N}{\gamma}\right) + \mu' \qquad (1.3.3)$$

Here, $\mu' = \lambda\bar{\theta}_0 + \mu$. By combining the equations (1.3.3) and (1.3.1) and solving the differential equation, one obtains the following equations:

$$\frac{\tau}{\sigma_N} = (\mu' - \mu) \cdot \log_e \frac{\gamma}{\gamma_0} + \mu$$

$$= 2.3\,(\mu' - \mu) \cdot \log_{10} \frac{\gamma}{\gamma_0} + \mu \qquad (1.3.4)$$

$$\epsilon_N = \frac{\mu - \mu'}{\lambda} \cdot \gamma \cdot \left\{ \log_e \frac{\gamma}{\gamma_0} - 1 \right\}$$

$$= \frac{\mu - \mu'}{\lambda} \cdot \gamma \cdot \left\{ 2.3 \log_{10} \frac{\gamma}{\gamma_0} - 1 \right\} \qquad (1.3.5)$$

where, γ_0 represents γ at the maximum compression point of ϵ_N. In this connection, the expression (1.3.4) evaluates this point as the value inherent to the material "*soil*" by taking into account the fact that the ratio τ/σ_N amounts to the interparticle frictional coefficient μ where $\gamma = \gamma_0$. Further by dividing both members of the equation (1.3.4) by μ, one obtains the following equation which means that $\tau/\mu\cdot\sigma_N$ and γ/γ_0 are straight lines passing the point (1,1) on the semi-logarithmic graph paper.

$$\frac{\tau}{\mu \cdot \sigma_N} = \left(\frac{\mu'}{\mu} - 1\right) \cdot \log_e \frac{\gamma}{\gamma_0} + 1$$

$$= 2.3\left(\frac{\mu'}{\mu} - 1\right) \cdot \log_{10} \frac{\gamma}{\gamma_0} + 1 \qquad (1.3.6)$$

This equation can be interpreted to represent the outcome of the normalization performed by assuming that $\mu\cdot\sigma_N$ equals the standard value τ_0 of shear stress ($\tau_0 = \mu\cdot\sigma_N$) and

the standard value of shear strain is γ_0 respectively. Then by assuming that the direction of the principal stress and that of the principal strain increment are the same with reference to the equations (1.3.4) and (1.3.5) which apply to this mobilized plane, the said equations can be converted into the following equations which govern the relationship between the principal stress ratio and the principal strain (cf. Appendix A). It should be noted that an approximation is involved in the course of integral computation. For the convenience of expression, X is taken to denote $\sqrt{\sigma_1/\sigma_3} - \sqrt{\sigma_3/\sigma_1}$.

$$\varepsilon_1 = \frac{\gamma_0 \cdot \exp\left(-\frac{\mu}{\mu'-\mu}\right)}{2} \cdot \exp\left\{\frac{X}{2(\mu'-\mu)}\right\} \cdot \left\{\frac{X^2}{8} + \left(\frac{1}{2} - \frac{1}{\lambda} - \frac{\mu'-\mu}{2}\right) \cdot X + (\mu'-\mu)^2 - (\mu'-\mu) + \frac{2\mu'}{\lambda} + 1\right\} \equiv f\left(\frac{\sigma_1}{\sigma_3}\right) \qquad (1.3.7)$$

$$\varepsilon_3 = \frac{\gamma_0 \cdot \exp\left(-\frac{\mu}{\mu'-\mu}\right)}{2} \cdot \exp\left\{\frac{X}{2(\mu'-\mu)}\right\} \cdot \left\{-\frac{X^2}{8} + \left(\frac{1}{2} - \frac{1}{\lambda} + \frac{\mu'-\mu}{2}\right) \cdot X - (\mu'-\mu)^2 - (\mu'-\mu) + \frac{2\mu'}{\lambda} - 1\right\} \equiv g\left(\frac{\sigma_1}{\sigma_3}\right) \qquad (1.3.8)$$

These are the expressions of the relationships which occur between the principal stress ratio and the principal strains on one mobilized plane.

3.4 STRESS-STRAIN RELATIONSHIP UNDER THREE PRINCIPAL STRESSES

In the preceding paragraph, the expression of the relationship between the stress ratio and the strain on the mobilized plane of soil and the expression of the principal stress ratio and the principal strain relationship as converted for application to the principal stress plane were derived. Here, the term "*mobilized plane*" refers to the plane of $(\tau/\sigma_N)_{max}$ which touches on Mohr's stress circle which changes from time to time and this plane, as is evident from Fig.1.3.6 (a), forms an angle of $(45^\circ + \phi_{mo}/2)$ with the major principal stress plane. The condition in which the stress is exerted on this mobilized plane may be depicted in terms of two dimensions as shown in Fig.1.3.6 (b). Murayama[8] theoretically derived an equation of the stress-strain relationship of soil by attaching his attention to the plane having soil particles mobilized to the highest extent. Karube[9] studied the stress-strain relation of soil by focussing his attention on the soil element running in parallel with the direction of the intermediate principal

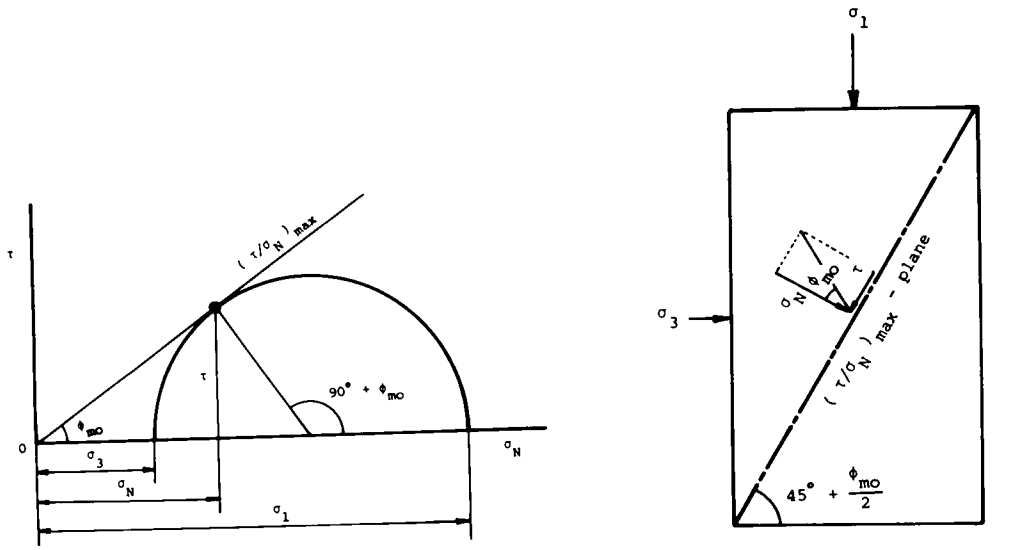

(a) Mobilized plane on which (τ/σ_N) is maximum (after Murayama[7]).

(b) Stress condition on mobilized plane (after Murayama[7]).

Fig.1.3.6 A single mobilized plane for two-dimensional models.

stress σ_2 and forming a certain angle with the plane of the major principal stress. The behavior of soil particles under three principal stresses is generally three-dimensional. So, the author introduces the new concept of three mobilized planes which are compounded as illustrated in Fig.1.3.7. This concept presumes that, under three different principal stresses, a mobilized plane touching upon its corresponding Mohr's stress circle exists, as shown in Fig.1.3.6 (a), in the stress planes governed by σ_1 and σ_2 on the one part and σ_2 and σ_3 on the other part as well as in the stress plane governed by σ_1 and σ_3. From this, it follows that there generally exist three mobilized planes as shown in Fig.1.3.7 (b). It is assumed that these mobilized planes are parallel to their corresponding third principal stress axes in the same way that the mobilized plane governed by σ_1 and σ_2 is parallel to the σ_3 axis. Here, the following expressions can be derived on the basis of Fig.1.3.7 (b) if it is assumed that the equations (1.3.7) and (1.3.8) hold true for the principal stress ratios σ_1/σ_3, σ_1/σ_2 and σ_2/σ_3 of the three principal stresses $(\sigma_1 \geqq \sigma_2 \geqq \sigma_3)$, and strains can be superposed.

$$\left.\begin{aligned} \varepsilon_1 &= f\left(\frac{\sigma_1}{\sigma_3}\right) + f\left(\frac{\sigma_1}{\sigma_2}\right) \\ \varepsilon_2 &= f\left(\frac{\sigma_2}{\sigma_3}\right) + g\left(\frac{\sigma_1}{\sigma_2}\right) \\ \varepsilon_3 &= g\left(\frac{\sigma_1}{\sigma_3}\right) + g\left(\frac{\sigma_2}{\sigma_3}\right) \end{aligned}\right\} \qquad (1.3.9)$$

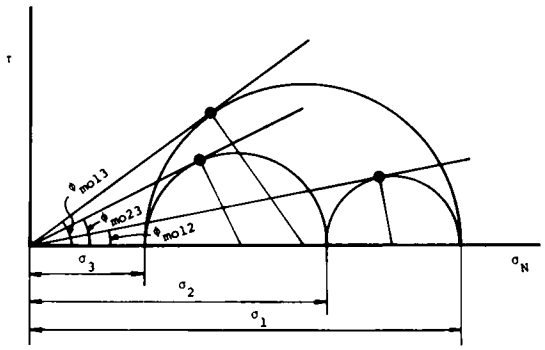

(a) Three mobilized planes on which (τ/σ_N) is maximum under three different principal stresses.

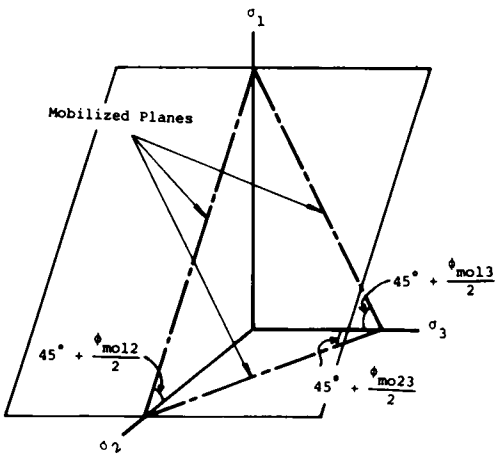

(b) Three mobilized planes under three different principal stresses.

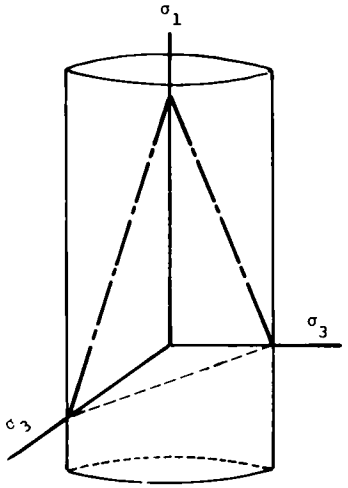

(c) Mobilized planes in triaxial compression test.

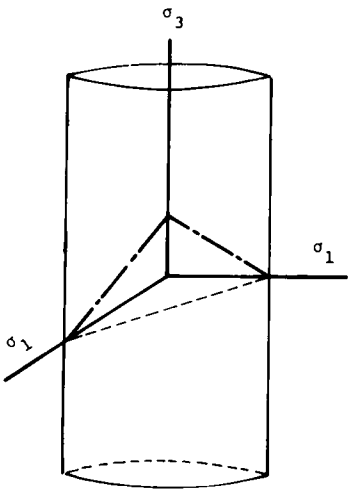

(d) Mobilized planes in triaxial extension test.

Fig.1.3.7 Three compounded mobilized planes for three-dimensional behavior of particles.

where, the following equations are assumed to hold good for $X \equiv \sqrt{\sigma_i/\sigma_j} - \sqrt{\sigma_j/\sigma_i}$ $(i, j = 1, 2, 3,\ i \leqq j)$

$$f\left(\frac{\sigma_i}{\sigma_j}\right) = \frac{\tau_0 \cdot \exp\left(-\frac{\mu}{\mu'-\mu}\right)}{2} \cdot \exp\left\{\frac{X}{2(\mu'-\mu)}\right\}$$

$$\cdot \left\{\frac{X^2}{8} + \left(\frac{1}{2} - \frac{1}{\lambda} - \frac{\mu'-\mu}{2}\right) \cdot X + (\mu'-\mu)^2 - (\mu'-\mu) + \frac{2\mu'}{\lambda} + 1\right\} \quad (i<j)$$

$$g\left(\frac{\sigma_i}{\sigma_j}\right) = \frac{\tau_0 \cdot \exp\left(-\frac{\mu}{\mu'-\mu}\right)}{2} \cdot \exp\left\{\frac{X}{2(\mu'-\mu)}\right\}$$

$$\cdot \left\{-\frac{X^2}{8} + \left(\frac{1}{2} - \frac{1}{\lambda} + \frac{\mu'-\mu}{2}\right) \cdot X - (\mu'-\mu)^2 - (\mu'-\mu) + \frac{2\mu'}{\lambda} - 1\right\} \quad (i<j)$$

$$f\left(\frac{\sigma_i}{\sigma_i}\right) = g\left(\frac{\sigma_i}{\sigma_i}\right) = 0 \qquad (i=j)$$

According to the equation (1.3.9), the principal strains (ϵ_1, ϵ_2 and ϵ_3) and the volumetric strain ($\Delta V/V$) for application to the triaxial compression test ($\sigma_1 \geqq \sigma_2 = \sigma_3$) can be expressed as follows:

$$\epsilon_1 = 2f\left(\frac{\sigma_1}{\sigma_3}\right), \quad \epsilon_2 = \epsilon_3 = g\left(\frac{\sigma_1}{\sigma_3}\right) \qquad (1.3.10)$$

$$\frac{\Delta V}{V} = \epsilon_1 + 2\epsilon_3 = 2f\left(\frac{\sigma_1}{\sigma_3}\right) + 2g\left(\frac{\sigma_1}{\sigma_3}\right) \qquad (1.3.11)$$

The mobilized plane in the case of triaxial compression is illustrated in Fig. 1.3.7 (c).

In the case of the triaxial extension test ($\sigma_1 = \sigma_2 \geqq \sigma_3$), the principal strains and the volumetric strain are to be expressed as follows.

$$\epsilon_1 = \epsilon_2 = f\left(\frac{\sigma_1}{\sigma_3}\right), \quad \epsilon_3 = 2g\left(\frac{\sigma_1}{\sigma_3}\right) \qquad (1.3.12)$$

$$\frac{\Delta V}{V} = 2\,\epsilon_1 + \epsilon_3 = 2\,f\left(\frac{\sigma_1}{\sigma_3}\right) + 2\,g\left(\frac{\sigma_1}{\sigma_3}\right) \qquad (1.3.13)$$

The mobilized plane in the case of triaxial extension is illustrated in Fig.1.3.7 (d).

In the case of the plane strain conditions ($\epsilon_2 = 0$), the principal strains is to be expressed as follows:

$$\epsilon_1 = f\left(\frac{\sigma_1}{\sigma_3}\right) + f\left(\frac{\sigma_1}{\sigma_2}\right) \cong f\left(\frac{\sigma_1}{\sigma_3}\right)$$

$$\epsilon_3 = g\left(\frac{\sigma_1}{\sigma_3}\right) + g\left(\frac{\sigma_2}{\sigma_3}\right) \cong g\left(\frac{\sigma_1}{\sigma_3}\right) \qquad (1.3.14)$$

In most cases, the ratios σ_1/σ_2 and σ_2/σ_3 in the equation (1.3.14) have values which are at most on the order of 2. Thus, it is believed that the approximate equality sign of this equation is true in most cases. In this connection, comparison of the equation (1.3.10) and the equation (1.3.12) reveals that, in the case of test specimens having the same initial granular structure, ϵ_1 of triaxial compression is twice ϵ_1 in triaxial extension and ϵ_3 in triaxial extension is conversely twice ϵ_3 in triaxial compression. In order to obtain the relationships relating to one mobilized plane from measured data, it is clear, from the equation (1.3.10), (1.3.12) and (1.3.14), that the found value of ϵ_1 must be multiplied by 1/2 in the case of triaxial compression test, the found value of ϵ_3 multiplied by 1/2 in the case of triaxial extension test and the found value used in its unaltered form in the case of plane strain test respectively prior to proceeding to the required computations. It is predicted from the equations (1.3.11) and (1.3.13) that the inclination of the volumetric strain $\Delta V/V$, if computed by using the principal stress ratio σ_1/σ_3 or the shear-normal stress ratio τ/σ_N on the mobilized plane as a parameter, will correspond with either of triaxial compression and triaxial extension. These relationships will be verified afterward by the use of measured data.

3.5 VERIFICATION BY TEST DATA

3.5.1 Verification of Relationship between Shear-normal Stress Ratio (τ/σ_N) and Normal-shear Strain Increment Ratio ($d\epsilon_N/d\gamma$)[10),11)]

In this paragraph, the expressions of the relationship existing between stress and strain on one mobilized plane and the expressions of the relationship existing between stress and strain under three principal stress conditions will be verified in accordance with various test data. First, the equation (1.3.1) indicating the relationship between

τ/σ_N and $d\epsilon_N/d\gamma$ on the mobilized plane will be reviewed. For example, computation of the values of stress and strain on one mobilized plane from the test data of triaxial compression can be accomplished by using in the equation (1.3.10) the found value of ϵ_1 multiplied by 1/2 and the found value of ϵ_3 in its unaltered form and, on assumption of the condition that the direction of the principal stress and that of the principal strain increment are in agreement, converting the resulting equation so as to indicate the stress-strain relationship on the mobilized plane. Fig.1.3.8 represents the results of triaxial compression test on Toyoura sand as rearranged in terms of relationship between

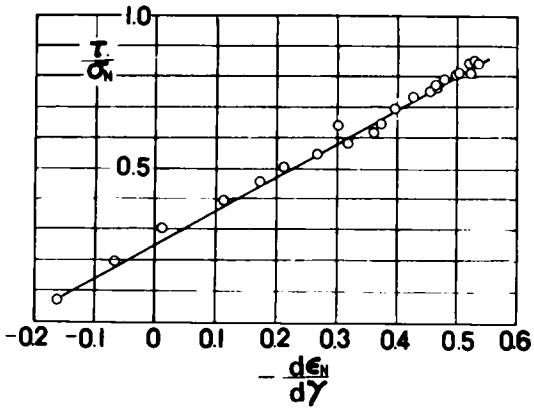

Fig.1.3.8 Relationship between τ/σ_N and $d\epsilon_N/d\gamma$ on one mobilized plane in triaxial compression test on Toyoura sand.

τ/σ_N and $d\epsilon_N/d\gamma$ on the mobilized plane. As for test conditions, the mean effective principal stress $\sigma_m = 1.0$ kg/cm^2 and the initial void ratio $e_i = 0.889$. This diagram indicates that the found values, if plotted graphically, depict a linear relationship as is implied by the equation (1.3.1). The ordinate intersection 0.25, therefore, represents the interparticle friction μ and the linear gradient 1.1 - 1.2 is found in view of Fig. 1.2.13 to be practically reasonable value for λ relative to this value of μ. Since the relationship of $\tau/\sigma_N \sim d\epsilon_N/d\gamma$ should exist invariably under various stress conditions only so far as there are used the same test specimens, the data of the triaxial extension test have been rearranged in the same manner. The results are indicated below. In the case of the triaxial extension test, the relationship on the mobilized plane may be derived by using the found value of ϵ_3 as a product of its multiplication by 1/2 and the found value of ϵ_1 in its unaltered form on reference to the equation (1.3.12). Fig.1.3.9 shows, in a rearranged form, the results of the triaxial extension test carried out on Toyoura sand. The test was performed under conditions of $\sigma_m = 3.0$ kg/cm^2 and $e_i = 0.641$. From this diagram, it is observed that the ordinate intersection 0.23 and the linear gradient 1.2 practically correspond to those of Fig.1.3.8. In the case of

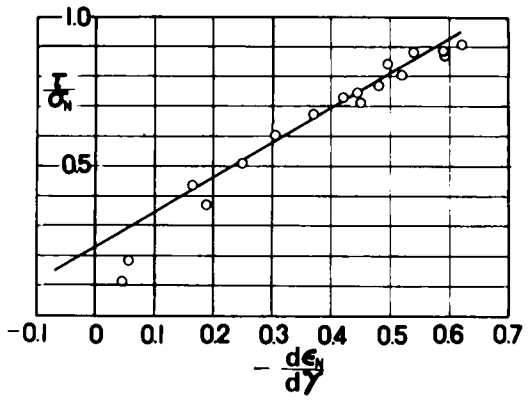

Fig.1.3.9 Relationship between τ/σ_N and $d\epsilon_N/d\gamma$ on one mobilized plane in triaxial extension test on Toyoura sand.

plane strain conditions, the relationship on the mobilized plane may be derived approximately by using the found values of ϵ_1 and ϵ_3 in their unaltered form on reference to the equation (1.3.14). Fig.1.3.10 shows, in the same rearranged form, the results of the plane strain test conducted on Toyoura sand with the manufactured universal triaxial apparatus, with the test performed under conditions of $\sigma_1 \cong 1.6$ kg/cm^2 and $e_i = 0.878$. The plot falls on the right upper portion, because this apparatus has such a structure that the state of K_0-compression forms the starting point. It is observed from this diagram that the ordinate intersection 0.23 and the linear gradient 1.2 substantially agree with those of Fig.1.3.8. Fig.1.3.11 shows, similarly in a form, the results of the plane strain test conducted on Toyoura sand by Ichihara and Matsuzawa[12]. The test conditions were $\sigma_3 = 2.0$ kg/cm^2 and $e_i = 0.663$. Again in this diagram, the ordinate intersection is found to be 0.24 and the linear gradient to be 1.2 respectively. In all these four diagrams, both λ and μ are found to assume substantially the same values. In the case of Toyoura sand, direct measurement of the frictional coefficient was impossible because of unavailability of its mother rock. As an alternative, glass beads for which frictional coefficients were easy to measure were used as a test specimen to carry out triaxial compression test, triaxial extension test and plane strain test. Fig.1.3.12 shows, in terms of $\tau/\sigma_N \sim d\epsilon_N/d\gamma$ relationship on the mobilized plane, the results of triaxial compression test, (indicated by o marks; $\sigma_m = 3.0$ kg/cm^2), triaxial extension test (indicated by • marks; $\sigma_m = 3.0$ kg/cm^2) and plane strain test (indicated by $\triangle$ marks; $\sigma_1 \cong 1.6$ kg/cm^2) conducted on glass beads. From this diagram, it is seen that the plots of the values found in the three tests give virtually equal gradient ($\lambda = 1.2$) and equal ordinate intersection ($\mu \cong 0.10$). It is interesting to note that the value of this ordinate intersection is in sufficient agreement with the

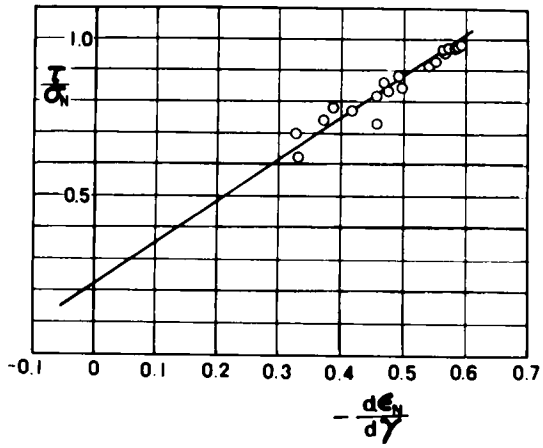

Fig.1.3.10 Relationship between τ/σ_N and $d\epsilon_N/d\gamma$ on one mobilized plane in plane strain test after K_0-compression on Toyoura sand.

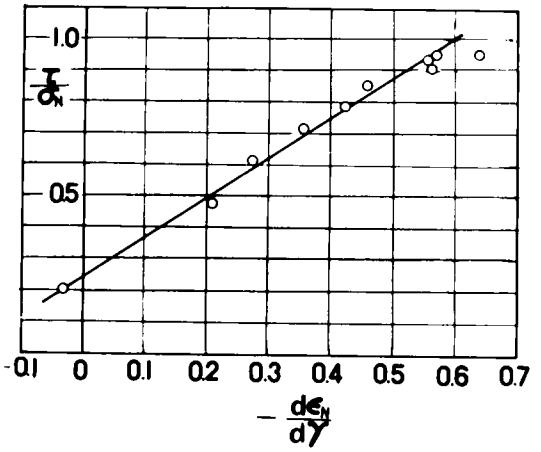

Fig.1.3.11 Relationship between τ/σ_N and $d\epsilon_N/d\gamma$ on one mobilized plane in plane strain test on Toyoura sand.

value 0.10 – 0.13 of frictional coefficient found between glass plates or between a glass plate and glass beads placed on the glass plate. Fig.1.3.13 similarly shows the results[13] of the triaxial compression test ($\sigma_3 = 1.0$ kg/cm^2 and $e_i = 0.706$) conducted on Ishii River sand. From this diagram, it is seen that μ is about 0.40 and λ is 1.1 to 1.2. Fig.1.3.14 shows, in terms of $\tau/\sigma_N \sim d\epsilon_N/d\gamma$ relationship on the mobilized plane, the results[14),15),16)] of triaxial compression test (indicated by ● marks; $\sigma_m = 1.0$ kg/cm^2, loose) and triaxial extension test (indicated by o marks; $\sigma_m = 3.0$ kg/cm^2, loose) conducted on Sagami River sand. It is observed from this diagram that the linear gradient

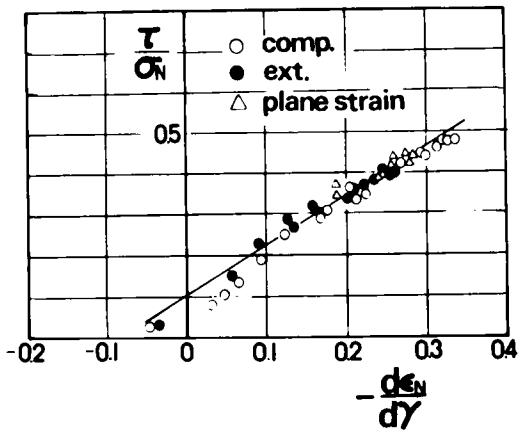

Fig.1.3.12 Relationship between τ/σ_N and $d\epsilon_N/d\gamma$ on one mobilized plane in triaxial compression test, triaxial extension test and plane strain test on glass beads.

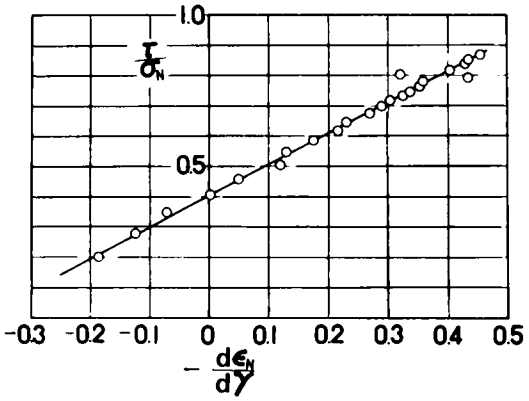

Fig.1.3.13 Relationship beween τ/σ_N and $d\epsilon_N/d\gamma$ on one mobilized plane in triaxial compression on Ishii River sand.

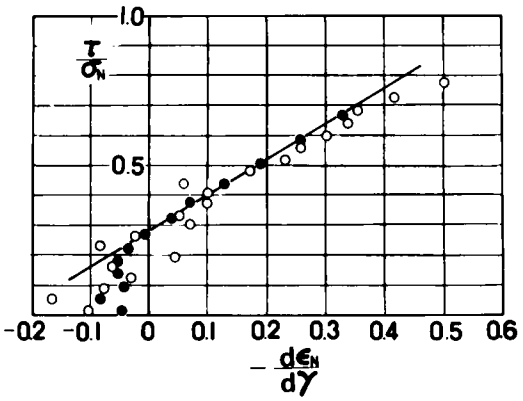

Fig.1.3.14 Relationship between τ/σ_N and $d\epsilon_N/d\gamma$ on one mobilized plane in triaxial compression test and triaxial extension test on Sagami River sand.

($\lambda = 1.2$) and the ordinate intersection ($\mu \cong 0.28$) are practically the same for both triaxial compression and triaxial extension. All the data dicussed above verify that the formula (1.3.1) practically holds good under various stress conditions and satisfies the physical significance of coefficients. In view of the basic idea which underlies the process of deriving the strain of the formula (1.3.1), this strain is believed to be ascribable to dilatancy, i.e. the phenomenon of particles' movement to ride one over another due to shear. Strictly speaking, therefore, the verification should be made by a test conducted at a constant mean effective principal stress σ_m. It is possibly because of the relatively small compressibility of sand that the said formula practically holds good as mentioned above even if σ_m is not constant.

3.5.2 Verification of Relationship between Principal Stess Ratio (σ_1/σ_3) and Principal Strain Increment Ratio ($d\epsilon_3/d\epsilon_1$)

In Paragraph 2.7 of Chapter 2, the relationship between the principal stress ratio (σ_1/σ_3) and the principal strain increment ratio ($d\epsilon_3/d\epsilon_1$) was derived by assuming a precondition that the principal stess and the principal strain increment would agree in direction. The derived formula representing this relationship is shown again below.

$$\frac{d\varepsilon_3}{d\varepsilon_1} = \frac{\sigma_1/\sigma_3 - 2\mu \cdot \sqrt{\sigma_1/\sigma_3} + (\lambda - 1)}{(1-\lambda) \cdot \sigma_1/\sigma_3 - 2\mu \cdot \sqrt{\sigma_1/\sigma_3} - 1} \qquad (1.3.15)$$

In the formula, μ denotes an interparticle frictional coefficient and λ is a constant which is determined by μ. The formula of (1.3.15) represents a relationship which is established in the case of a single mobilized plane. It is, therefore, considered to be such that, under plane strain conditions, measured values may approximately be applied, in their unaltered form, to this formula. In the case of triaxial compression test, it is seen from the formula of (1.3.10) that the measured value of $d\epsilon_1$ should be multiplied by 1/2. If the measured values are to be plotted in their unaltered form, then the formula (1.3.15) is required to be modified as shown below.

$$\frac{d\varepsilon_3}{d\varepsilon_1} = \frac{1}{2} \cdot \frac{\sigma_1/\sigma_3 - 2\mu \cdot \sqrt{\sigma_1/\sigma_3} + (\lambda - 1)}{(1-\lambda) \cdot \sigma_1/\sigma_3 - 2\mu \cdot \sqrt{\sigma_1/\sigma_3} - 1} \qquad (1.3.16)$$

In respect of the triaxial extension test, the formula (1.3.12) indicates a necessity that the measured value of $d\epsilon_3$ should be multiplied by 1/2. Where measured values are to be plotted in their unaltered form, therefore, this formula must be modified as shown below.

$$\frac{d\varepsilon_3}{d\varepsilon_1} = 2 \cdot \frac{\sigma_1/\sigma_3 - 2\mu \cdot \sqrt{\sigma_1/\sigma_3} + (\lambda - 1)}{(1-\lambda) \cdot \sigma_1/\sigma_3 - 2\mu \cdot \sqrt{\sigma_1/\sigma_3} - 1} \qquad (1.3.17)$$

With a view to verifying these expressions, the results of the triaxial compression test ($\sigma_m = 1.0$ kg/cm^2 and $e_i = 0.889$), the plane strain test (by Ichihara and Matsuzawa 12) $\sigma_3 = 2.0$ kg/cm^2 and $e_i = 0.663$) and the triaxial extension test ($\sigma_m = 3.0$ kg/cm^2 and $e_i = 0.641$) conducted on Toyoura sand have been plotted as shown in Fig.1.3.15. In the diagram, the solid line represents a calculated curve based on the formulas of (1.3.15) through (1.3.17). In the related calculations, the constants $\mu \cong 0.24$ and $\lambda = 1.2$ proper to Toyoura sand were used. It is seen from this diagram that theoretical curves and measured values obtained of the three tests show relatively satisfactory agreement with each other. Fig.1.3.16 represents a graph of the results[13] of the triaxial compression test (indicated by o marks, $\sigma_3 = 1.0$ kg/cm^2 and $e_i = 0.706$; indicated by ● marks, $\sigma_3 = 2.0$ kg/cm^2 and $e_i = 0.723$) conducted on Ishii River sand.

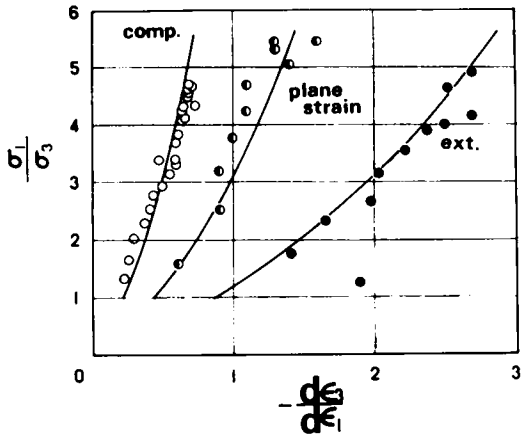

Fig.1.3.15 Relationship between σ_1/σ_3 and $d\epsilon_3/d\epsilon_1$ in triaxial compression test, plane strain test and triaxial extension test on Toyoura sand.

The solid line of this graph represents a calculated curve based on the formula (1.3.16). In the calculations, the constants $\mu = 0.40$ and $\lambda = 1.2$ proper to Ishii River sand were used. Fig.1.3.17 represents a graph of the results of the triaxial compression test ($\sigma_m = 3.0$ kg/cm^2), the triaxial extension test ($\sigma_m = 3.0$ kg/cm^2) and the plane strain test ($\sigma_1 \cong 1.6$ kg/cm^2) using the universal triaxial apparatus conducted on glass beads. In the calculations involved in this case, the coefficients, $\mu \cong 0.10$ which was actually measured and $\lambda = 1.2$, were used. It is observed that the measured values are approximately in agreement with those in the theoretical curve. Fig.1.3.18 represents a

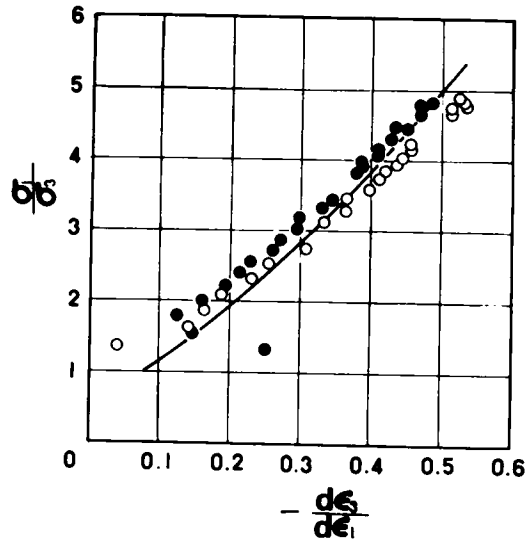

Fig.1.3.16 Relationship between σ_1/σ_3 and $d\epsilon_3/d\epsilon_1$ in triaxial compression test on Ishii River sand.

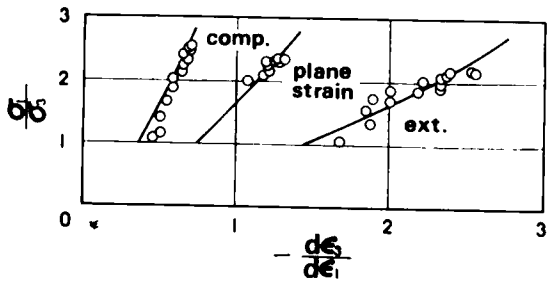

Fig.1.3.17 Relationship between σ_1/σ_3 and $d\epsilon_3/d\epsilon_1$ in triaxial compression test, plane strain test and triaxial extension test on glass beads.

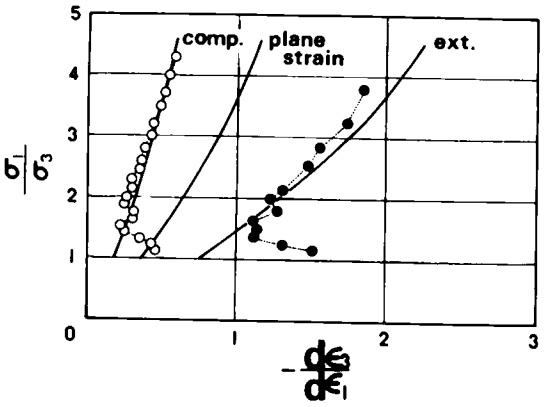

Fig.1.3.18 Relationship between σ_1/σ_3 and $d\epsilon_3/d\epsilon_1$ in triaxial compression test and triaxial extension test on Sagami River sand.

graph obtained by plotting the data[14),15)16)] of the triaxial compression test (σ_m = 2.0 kg/cm^2, loose) and the triaxial extension test (σ_m = 1.0 kg/cm^2, loose) conducted on Sagami River sand. The theoretical curve represents the values calculated by using the coefficients $\lambda = 1.2$ and $\mu = 0.28$ (see Fig.1.3.14). Since the axial strain ϵ_1 at the point at which the plot of the data of triaxial compression test begins to overlap the theoretical curve is about 0.4%, it seems that the principal portion up to the peak strength can be explained by the expressions (1.3.15), (1.3.16) and (1.3.17). According to Rowe's stress-dilatancy theory[17)], the theoreticl values are supposed to describe a straight line passing the origin of these coordinates. The problem of comparison with Rowe's theory will be reserved for detailed discussion in Chapter 5.

3.5.3 Verification of Relationship between Shear-Normal Stress Ratio (τ/σ_N) and Normal-Shear Strain Ratio (ϵ_N/γ)

Some data obtained by actual measurement are cited here with a view to investigating the extent to which the formula (1.3.3) holds true with respect to the relationship of $\tau/\sigma_N \sim \epsilon_N/\gamma$ on the mobilized plane. Fig.1.3.19 represents the results of the

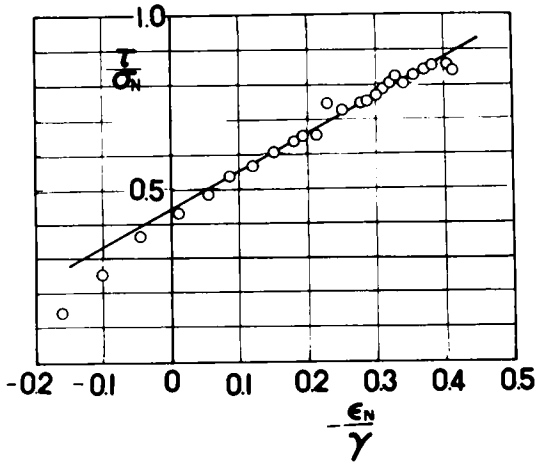

Fig.1.3.19 Relationship between τ/σ_N and ϵ_N/γ on one mobilized plane in triaxial compression test on Toyoura sand.

conversion of the data in triaxial compression test on Toyoura sand (σ_m = 1.0 kg/cm^2, $e_i = 0.889$) to $\tau/\sigma_N \sim \epsilon_N/\gamma$ relationship on a single mobilized plane. It is observed that the plot approximately overlaps the straight line described by the gradient coefficient $\lambda = 1.1$ to 1.2 as implied by the formula (1.3.3). Fig.1.3.20 represents the results obtained by converting the data of triaxial compression test on Ishii River sand (σ_3 = 1.0 kg/cm^2 and $e_i = 0.706$) into the similar relationship on a single mobilized plane. It seems that the plot is in fair agreement with the expression of (1.3.3).

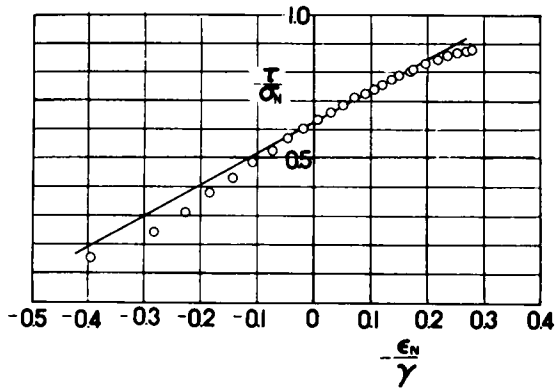

Fig.1.3.20 Relationship between τ/σ_N and ϵ_N/γ on one mobilized plane in triaxial compression test on Ishii River sand.

3.5.4 Verification of Relationship among Shear-Normal Stress Ratio (τ/σ_N), Shear Strain (γ) and Normal Strain (ϵ_N)

The data obtained by actual measurement with respect to the expressions (1.3.4) and (1.3.5) are plotted in Fig.1.3.21 to Fig.1.3.26. Fig.1.3.21 represents the results of

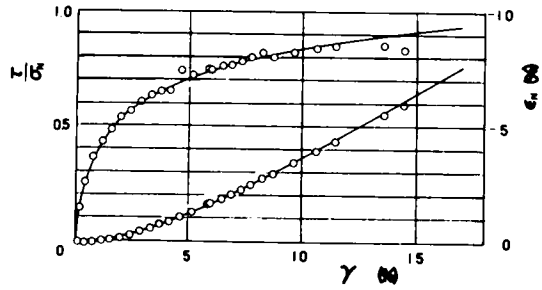

Fig.1.3.21 Relationship among τ/σ_N, γ and ϵ_N on one mobilized plane in triaxial compression test on Toyoura sand.

the conversion of the data of triaxial compression test on Toyoura sand (σ_m = 1.0 kg/cm^2 and e_i = 0.889) to the relationship of the mobilized plane, in conjunction with the curve of values found by the calculation based on the expressions (1.3.4) and (1.3.5). For the related calculations, the coefficients λ = 1.2, μ = 0.25, μ' = 0.44 proper to Toyoura sand and γ_0 = 0.45% were used. Fig.1.3.22 shows the results[13] of the conversion of the data of triaxial compression test on Ishii River sand (σ_3 = 1.0 kg/cm^2 and e_i = 0.706) into the relationship on the mobilized plane and the curve of the values calculated on the basis of the expressions (1.3.4) and (1.3.5). For the purpose of these calculations were used the coefficients λ = 1.2, μ = 0.40, μ' = 0.62 proper to Ishii River sand and γ_0 = 1.3%. Fig.1.3.23 and Fig.1.3.24 represent the results of the conversion of the data

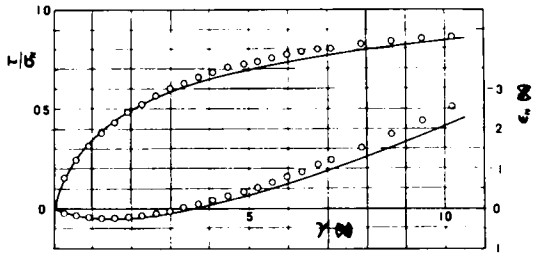

Fig.1.3.22 Relationship among τ/σ_N, γ and ϵ_N on one mobilized plane in triaxial compression test on Ishii River sand.

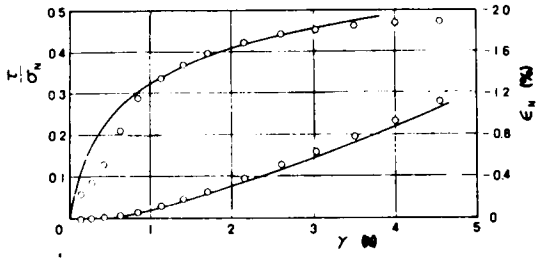

Fig.1.3.23 Relationship among τ/σ_N, γ and ϵ_N on one mobilized plane in triaxial compression test on glass beads.

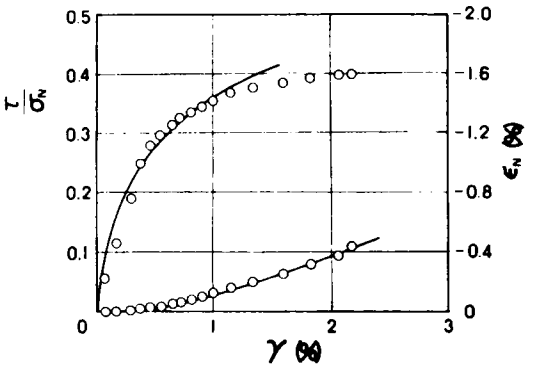

Fig.1.3.24 Relationship among τ/σ_N, γ and ϵ_N on one mobilized plane in triaxial extension test on glass beads.

of triaxial compression test ($\sigma_m = 3.0$ kg/cm^2) and triaxial extension test ($\sigma_m = 3.0$ kg/cm^2) on glass beads to their respective relationships of $\tau/\sigma_N \sim \gamma \sim \epsilon_N$ on the mobilized plane. The solid lines are curves of calculated values. In the related calculations, the coefficients $\lambda = 1.2$, $\mu = 0.10$, $\mu' = 0.22$ and $\gamma_0 = 0.15\%$ (Fig.1.3.23) and $\gamma_0 = 0.11\%$ (Fig.1.3.24) were used. Fig.1.3.25 and Fig.1.3.26 represent the results of the conversion of the data[14),15),16)] of triaxial compression test ($\sigma_m = 2.0$ kg/cm^2, loose) and triaxial extension test ($\sigma_m = 1.0$ kg/cm^2, loose) on Sagami River sand into their respective

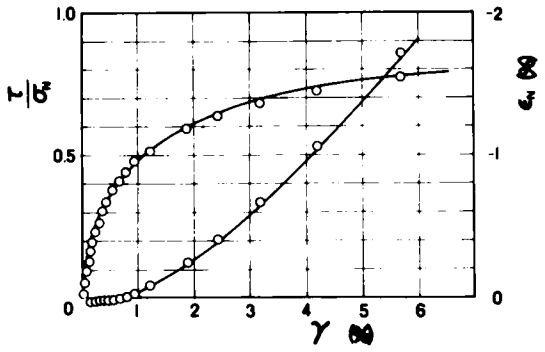

Fig.1.3.25 Relationship among τ/σ_N, γ and ϵ_N on one mobilized plane in triaxial compression test on Sagami River sand.

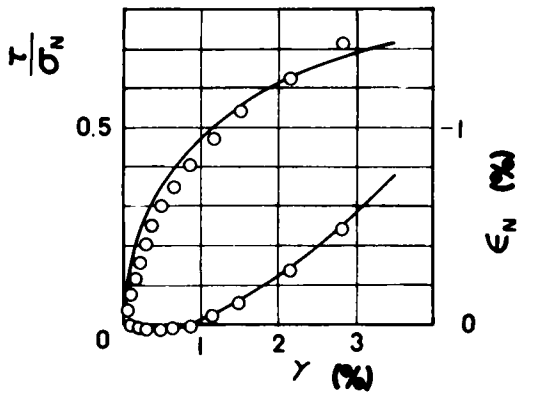

Fig.1.3.26 Relationship among τ/σ_N, γ and ϵ_N on one mobilized plane in triaxial extension test on Sagami River sand.

$\tau/\sigma_N \sim \gamma \sim \epsilon_N$ relationships on the mobilized plane. The solid lines are curves of calculated values. In the related calculations, there were used the coefficients $\lambda = 1.2$, $\mu = 0.28$, $\mu' = 0.46$ and $\gamma_0 = 0.3\%$. Thus, the results of both triaxial compression and triaxial extension tests can be interpreted by using entirely the same values of coefficients. This implies that the initial granular structure of test specimens used for the tests was identical.

What is worthy of special attention about the preceding plotting of data is the fact that the relationship between stress and strain on the mobilized plane could be interpreted by entirely the same coefficients (λ, μ and μ') of each given test specimen, no matter whether it was triaxial compression test or triaxial extension test, whether the test specimen was packed loosely or densely, or whether the confined stress was large or small. As one exception, the coefficient γ_0 is a parameter for the evaluation of the initial granular structure and, therefore, varied with the initial void ratio and the confined stress. The fact that the stress-strain relationships under various conditions

could be calculated by values of coefficients definitely identical on the basis of relationships existing on the mobilized plane constitutes one of the targets to which the present dissertation is aimed. And this explains why the $\tau/\sigma_N \sim \gamma \sim \epsilon_N$ relationship existing on the mobilized plane is referred to as the basic expression of the stress-strain relationship of soil.

3.5.5 Verification of $\tau/\mu\cdot\sigma_N \sim \gamma/\gamma_0$ Relationship

Now the author proposes to verify the expression (1.3.6) which indicates that the ratios $\tau/\mu\cdot\sigma_N$ and γ/γ_0 give coordinates describing a straight line drawn through the point (1, 1) on a semi-logarithmic section paper. The data of actual measurement obtained in the drained triaxial test with respect to the expression are plotted in Fig. 1.3.27 to Fig.1.3.29. The data of Fig.1.3.27 were obtained by using Toyoura sand as

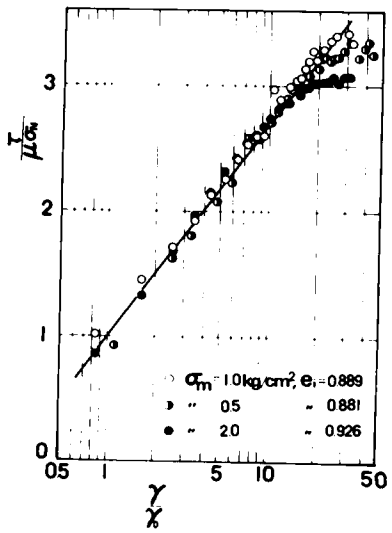

Fig.1.3.27 Relationship between $\tau/\mu\cdot\sigma_N$ and γ/γ_0 on Toyoura sand.

the test specimen. Three sets of test conditions were used, involving different mean effective principal stresses in the range of from 0.5 to 2.0 kg/cm^2 as indicated in the graph. The data[13] of Fig.1.3.28 were obtained of Ishii River sand under two sets of test conditions, involving σ_m = 2.0 kg/cm^2 and σ_3 = 1.0 kg/cm^2. Fig.1.3.29 represents the plotted data[14),15),16] of triaxial compression and triaxial extension tests conducted on Sagami River sand. It is observed from these graphs that the expression of (1.3.6) is established almost similarly on the mobilized plane, no matter whether the confined stress may vary or whether there is performed triaxial compression test or triaxial extension test. The linear gradients in these graphs are concluded to be such that they should be specified by such factors as interparticle friction and granular structure of test specimens in view of the coefficients of the

formula (1.3.6). A review of Fig.1.3.27 through Fig.1.3.29 leads to a concludion that the void ratio has no marked effect. From this, it may be inferred that, so far as the test specimen is fixed, the gradient of the said linear relationship under the condition of the normal initial granular structure is practically definite in terms of primary approximation.

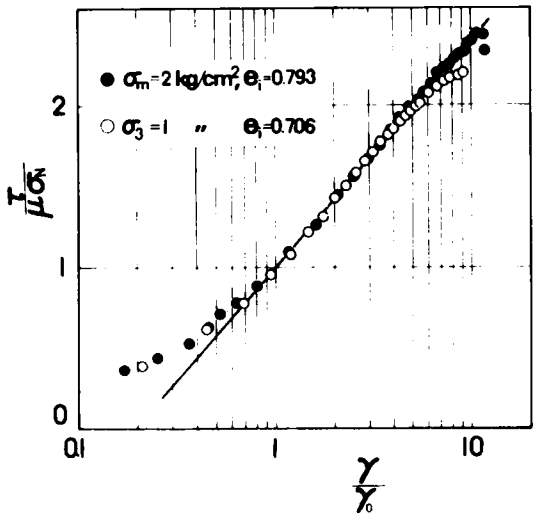

Fig.1.3.28 Relationship between $\tau/\mu\cdot\sigma_N$ and γ/γ_0 on Ishii River sand.

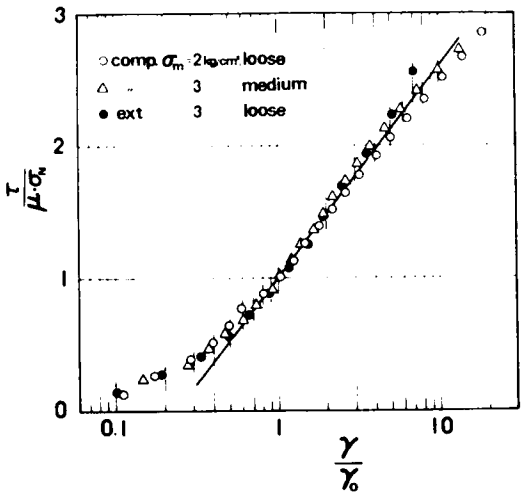

Fig.1.3.29 Relationship between $\tau/\mu\cdot\sigma_N$ and γ/γ_0 on Sagami River sand.

3.5.6 Verification of Relationships between Principal Stress Ratio (σ_1/σ_3) and Principal Strains (ϵ_1 and ϵ_3) under Triaxial Compression and Triaxial Extension Stress Conditions

In 3.5.5, it has been verified that, so far as the test specimen is fixed, the formula of the relationship between stress and strain on the mobilized plane is established with respect to equal coefficients (λ, μ and μ'). Here, the author proceeds to verify the principal stress ratio – principal strain relationship under triaxial compression and triaxial extension conditions derived on the basis of the fundamental relationship between stress and strain on the mobilized plane. First, Fig.1.3.30 represents the data

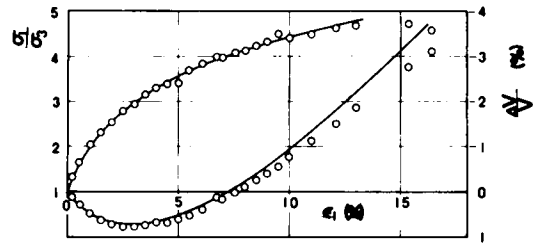

Fig.1.3.30 Relationship among σ_1/σ_3, ϵ_1 and $\Delta V/V$ in triaxial compression test on Toyoura sand.

of triaxial compression test ($\sigma_m = 1.0$ kg/cm^2 and $e_i = 0.889$) on Toyoura sand as plotted in terms of the relationship of $\sigma_1/\sigma_3 \sim \epsilon_1 \sim \Delta V/V$ ($= \epsilon_1 + 2\epsilon_3$) and the curves of values calculated from the expression of (1.3.10). In the related calculations, there were used the coefficients $\lambda = 1.2$, $\mu = 0.25$, $\mu' = 0.44$ proper to Toyoura sand similarly to the previous case and $\gamma_0 = 0.45\%$. The method for determination of these coefficients will be described in detail in a latter paragraph. Then, Fig.1.3.31 represents the data[13] of

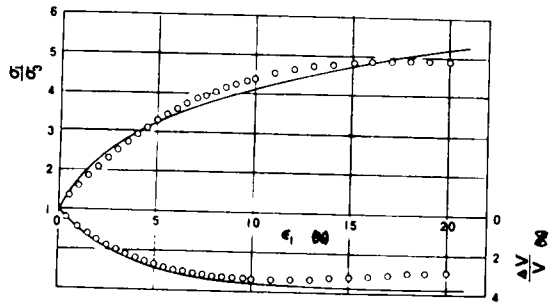

Fig.1.3.31 Relationship among σ_1/σ_3, ϵ_1 and $\Delta V/V$ in triaxial compression test on Ishii River sand.

triaxial compression test ($\sigma_3 = 1.0$ kg/cm^2 and $e_i = 0.706$) on Ishii River sand as plotted similarly in terms of the relationship of $\sigma_1/\sigma_3 \sim \epsilon_1 \sim \Delta V/V$ and the curves of values calculated according to the expression of (1.3.10). In the related calculations, the coefficients $\lambda = 1.2$, $\mu = 0.40$, $\mu' = 0.62$ proper to Ishii River sand and $\gamma_0 = 1.3\%$ were used.

Fig.1.3.32 represents the data of triaxial compression test (o marks; $\sigma_m = 3.0$ kg/cm^2)

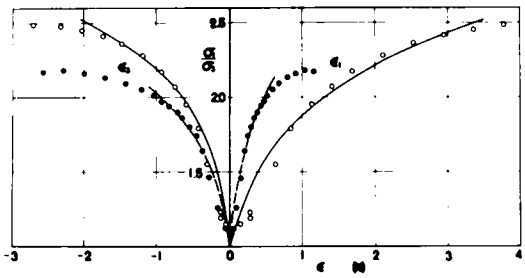

Fig.1.3.32 Relationship among σ_1/σ_3, ϵ_1 and ϵ_3 in triaxial compression and extension tests on glass beads.

and triaxial extension test (● marks; $\sigma_m = 3.0$ kg/cm^2) on glass beads as plotted in terms of the relationship of $\sigma_1/\sigma_3 \sim \epsilon_1$ (right half) and the relationship of $\sigma_1/\sigma_3 \sim \epsilon_3$ (left half) and the curves of values calculated in accordance with the expressions (1.3.10) and (1.3.12). In the related calculations, the coefficients $\lambda = 1.2$, $\mu = 0.10$, $\mu' = 0.22$ proper to glass beads and $\gamma_0 = 0.15\%$ (triaxial compression) and $\gamma_0 = 0.11\%$ (triaxial extension) were used. Fig.1.3.33 represents the data[14),15),16)] of triaxial compression test (○ marks; $\sigma_m = 2.0$ kg/cm^2, loose) and triaxial extension test (● marks; $\sigma_m = 1.0$ kg/cm^2, loose) on Sagami River sand as plotted in terms of the $\sigma_1/\sigma_3 \sim \epsilon_1$ relationship and the $\sigma_1/\sigma_3 \sim \epsilon_3$ relationship and the curves of values calculated in accordance with the expressions (1.3.10) and (1.3.12). In the related calculations, entirely the same coefficients $\lambda = 1.2$, $\mu = 0.28$, $\mu' = 0.46$ and $\gamma_0 = 0.3\%$ were used for the results of both triaxial compression and triaxial extension tests. This implied that the initial

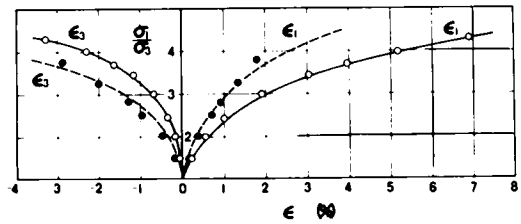

Fig.1.3.33 Relationship among σ_1/σ_3, ϵ_1 and ϵ_3 in triaxial compression and extension tests on Sagami River sand.

granular structures in both tests were same. It is, therefore, observed that, as described in the preceding paragraph, the relationship that the value of ϵ_1 of triaxial compression is twice as large as that of ϵ_1 of triaxial extension and the vaule of ϵ_3 of triaxial extension is twice as large as that of ϵ_3 of triaxial compression is also satisfied.

Fig.1.3.34 represents the data[16)] of triaxial compression test (o and Δ marks; loose and medium; σ_m = const.) and triaxial extension test (● marks; loose; σ_m = const.)

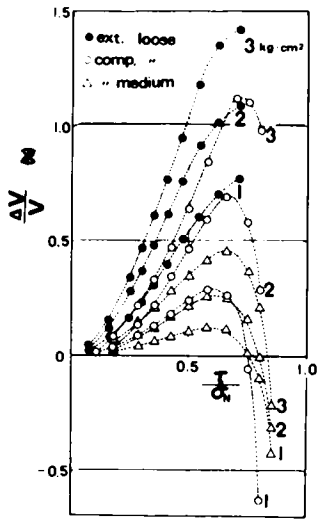

Fig.1.3.34 Relationship between $\Delta V/V$ and τ/σ_N in triaxial compression and extension tests on Sagami River sand.

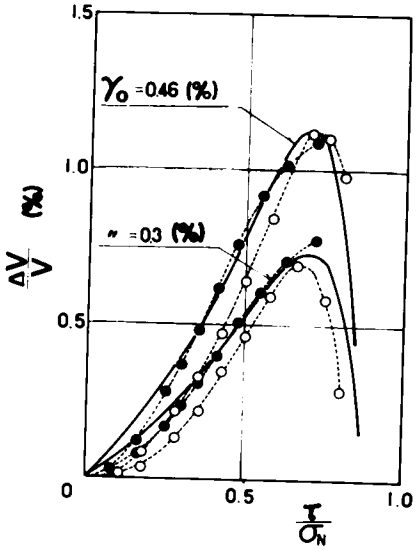

Fig. 1.3.35 Teheoretical and experimental relationship between $\Delta V/V$ and τ/σ_N.

on Sagami River sand as plotted in terms of the relationship between $\Delta V/V$ and τ/σ_N (corresponding to σ_1/σ_3). The numbers in the diagram denote the values of σ_m (kg/cm^2). In this diagram, it is observed that the curve of dilatancy $\Delta V/V$ is inverted from the compression direction to the expansion direction at practically the same value of τ/σ_N. Further, the curve in which the maximum compression value of $\Delta V/V$ is virtually the same is believed to represent a test specimen with an equal value of γ_0. It is interesting to note that, in such a case, both triaxial compression and triaxial extension describe practically the same curves, supporting the appropriateness of the expressions (1.3.11) and (1.3.13). In Fig.1.3.35, representative data of compression (σ_m = 3.0 kg/cm^2) and extension (σ_m = 2.0 kg/cm^2) and those of compression (σ_m = 2.0 kg/cm^2) and extension (σ_m = 1.0 kg/cm^2) respectively selected from the data of Fig.1.3.34 are compared with the curves of values (indicated by solid lines) calculated in accordance with the expressions (1.3.11) and (1.3.13). In these calculations, the coefficients $\lambda = 1.2$, $\mu = 0.28$, $\mu' = 0.46$ proper to Sagami River sand and $\gamma_0 = 0.3\%$ and $\gamma_0 = 0.46\%$ were used.

Here, the author tries to calculate the value of τ/σ_N (or σ_1/σ_3) at the maximum compression point (minimum point) of dilatancy. At the minimum point of dilatancy, the equation $d(\Delta V/V) = d\epsilon_1 + 2d\epsilon_3 = 0$ is established for triaxial compression and the equation $d(\Delta V/V) = 2d\epsilon_1 + d\epsilon_3 = 0$ is established for triaxial extension respectively. Therefore, the following expression can be derived from the formulas of (1.3.16) and (1.3.17).

$$\frac{\sigma_1}{\sigma_3} + \frac{4\mu}{\lambda - 2} \cdot \sqrt{\frac{\sigma_1}{\sigma_3}} - 1 = 0 \qquad (1.3.18)$$

Since Sagami River sand has the coefficients $\lambda = 1.2$ and $\mu \cong 0.28$, $\sigma_1/\sigma_3 = 3.69$ and consequently $\tau/\sigma_N = 0.70$ are obtained from the formula of (1.3.18) for the minimum point of dilatancy. It is observed that these values naturally correspond to Fig.1.3.35.

Fig.1.3.36 and Fig.1.3.37 represent the results obtained by replotting the volu-

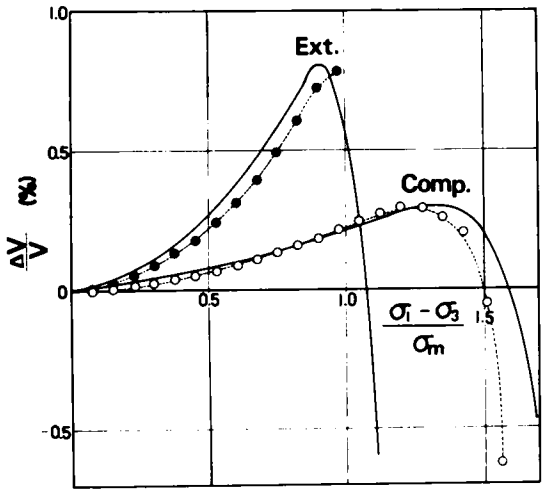

Fig.1.3.36 Relationship between $\Delta V/V$ and $(\sigma_1 - \sigma_3)/\sigma_m$ in triaxial compression and extension tests on Sagami River sand ($\sigma_m = 1.0$ kg/cm^2).

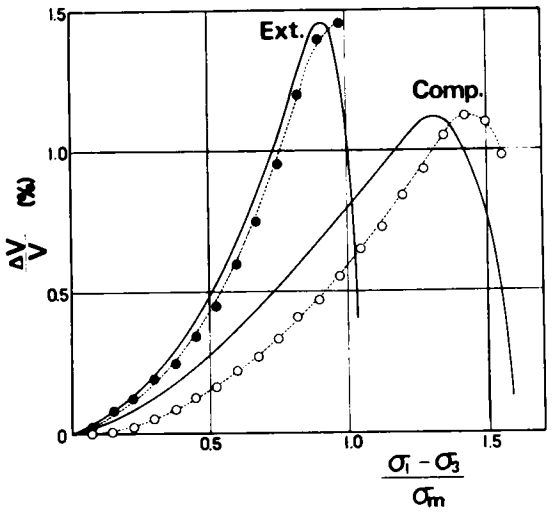

Fig.1.3.37 Relationship between $\Delta V/V$ and $(\sigma_1 - \sigma_3)/\sigma_m$ in triaxial compression and extension tests on Sagami River sand ($\sigma_m = 3.0$ kg/cm^2).

metric strain $\Delta V/V$ against the abscissa of the ratio between principal stress difference and mean effective principal stress, $(\sigma_1 - \sigma_3)/\sigma_m$ $(\equiv q/p)$ in place of τ/σ_N (or σ_1/σ_3) respectively. The variable $(\sigma_1 - \sigma_3)/\sigma_m$ has been proposed by Shibata[18], Shibata and Karube[19),20),21)], Karube and Kurihara[22)] as a parameter governing the dilatancy of clay and has also been established by Murayama and Yagi[23),24)], Yagi[25),26)], Tatsuoka and Shiba[16)], and other workers with respect to sand. Besides, Hata and Ohta[27)], and Ohta[28)] have independently derived relationships between stress and strain of soil by presuming that the dilatancy of soil is expressed in a linear relationship with respect to this variable. Fig.1.3.36 represents the results of triaxial compression and triaxial extension tests using $\sigma_m = 1.0\ kg/cm^2$ of Fig.1.3.34. In the diagram, the solid lines represent the curves of values found by the calculations according to Eqs. (1.3.11) and (1.3.13). In the realted calculations, there were used the coefficients $\lambda = 1.2$, $\mu = 0.28$, $\mu' = 0.46$ and $\gamma_0 = 0.13\%$ for triaxial compression and $\gamma_0 = 0.3\%$ for triaxial extension which are proper to Sagami River sand. Fig.1.3.37 represents the results of triaxial compression and triaxial extension tests using $\sigma_m = 3.0\ kg/cm^2$ of Fig.1.3.34. In the diagram, the curves of values found by calculation were obtained by presuming $\gamma_0 = 0.46\%$ for triaxial compression and $\gamma_0 = 0.59\%$ for triaxial extension respectively. Comparison of these two diagrams with Fig. 1.3.35 clearly indicates that the dilatancy of soil is uniquely controlled not by $(\sigma_1 - \sigma_3)/\sigma_m (\equiv q/p)$ but by the ratio of τ/σ_N (or σ_1/σ_3). This relationship is predicted also from the equations of (1.3.11) and (1.3.13).

3.5.7 Verification of Relationships between Principal Stress Ratios (σ_1/σ_3, σ_1/σ_2 and σ_2/σ_3) and Principal Strains (ϵ_1, ϵ_2 and ϵ_3) under Multiaxial Stress Conditions

Here, the author proposes to verify, by the use of experimental data, the formulas (1.3.9) and (1.3.14) for the relationships between principal stress ratio and principal strain under three different principal stresses as derived from the formulas of the stress ratio – strain relationship on the mobilized plane. First, the formula (1.3.14) which is established under plane strain conditions is verified in terms of the plane strain test. In the diagram of Fig.1.3.38 which represents the results of the plane

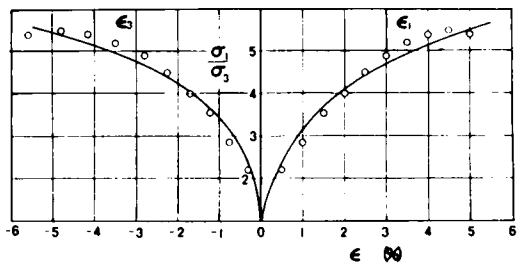

Fig.1.3.38 Relationship among σ_1/σ_3, ϵ_1 and ϵ_3 in plane strain test on Toyoura sand.

strain test[12] ($\sigma_3 = 2.0$ kg/cm^2 and $e_i = 0.663$) and the curves of values calculated in accordance with the formula of (1.3.14), there is observed a satisfactory agreement between the said data. In the related calculations, the same coefficients $\lambda = 1.2$, $\mu = 0.25$, $\mu' = 0.44$ proper to Toyoura sand and $\gamma_0 = 0.2\%$ as described above were used. Fig. 1.3.39 shows the results of plane strain test ($\sigma_1 \cong 1.4$ kg/cm^2 and $e_i = 0.660$) conducted

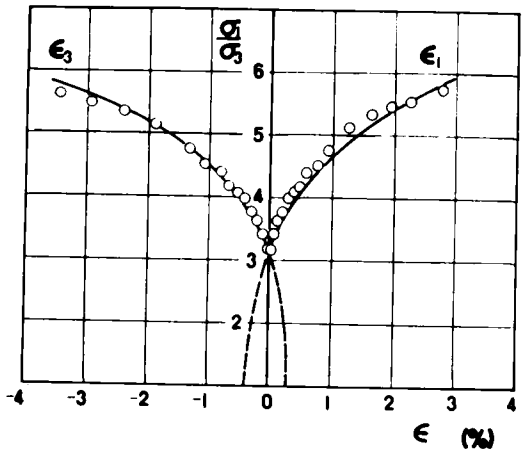

Fig.1.3.39 Relationship among σ_1/σ_3, ϵ_1 and ϵ_3 in plane strain test after K_0-compression on Toyoura sand.

on Toyoura sand by the use of the manufactured universal triaxial apparatus in comparison with the curves of values calculated in accordance with the expression of (1.3.14). Since, in the case of this apparatus, the shear phenomenon usually starts from the K_0-compression state, the curves of the calculated values are parallelly translated to compare them with actually measured values as shown in the diagram. This parallel translation of the curves is supported by a concept that the K_0-compression had already caused an amount of shear corresponding to the initial principal stess ratio ($1/K_0$). From the diagram, it is observed that the curves of calculated values give a generally satisfactory explanation to the values found by test. In the related calculations, the coefficients $\lambda = 1.2$, $\mu = 0.25$, $\mu' = 0.44$ proper to Toyoura sand and $\gamma_0 = 0.1\%$ were used. Fig.1.3.40 shows the results of plane strain test ($\sigma_1 \cong 1.5$ kg/cm^2) conducted on glass beads by the universal triaxial apparatus and the curves of values calculated accordingly. In the related calculations, the coefficients $\lambda = 1.2$, $\mu = 0.10$, $\mu' = 0.22$ proper to glass beads and $\gamma_0 = 0.2\%$ were used. The preceding comparative study has verified that the expression of (1.3.14) is established for the plane strain test, suggesting that this expression may similarly be applied to the shear test after anisotropic consolidation.

Then, the author proceeds to verify, with the aid of universal triaxial test results, the general formula (1.3.9) governing the principal stress ratio – principal strain relationship under different principal stress conditions. Ko and Scott[29),30),31)] trially manufactured an apparatus designed to permit three principal stresses applied independently via rubber membrances to a test specimen in the shape of a cube. With this apparatus,

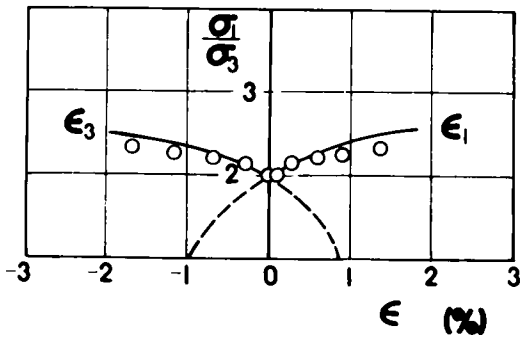

Fig.1.3.40 Relationship among σ_1/σ_3, ϵ_1 and ϵ_3 in plane strain test after K_0-compression on glass beads.

they performed triaxial compression and triaxial extension tests under conditions having the mean effective principal stress σ_m kept constant. They also carried out the shear test under three principal stresses exerted along stress paths linearly variable in the radial directions on the octahedral plane (with the magnitude of σ_m automatically fixed). Figs.1.3.41 through 1.3.43 show the results of triaxial compression and triaxial extension

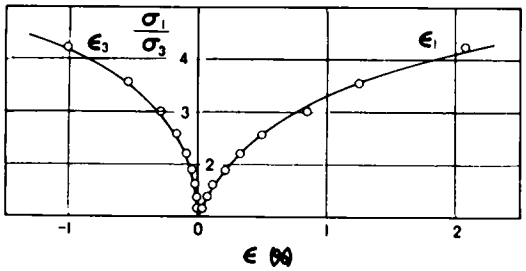

Fig.1.3.41 Relationship among σ_1/σ_3, ϵ_1 and ϵ_3 in triaxial compression test on Ottawa sand.

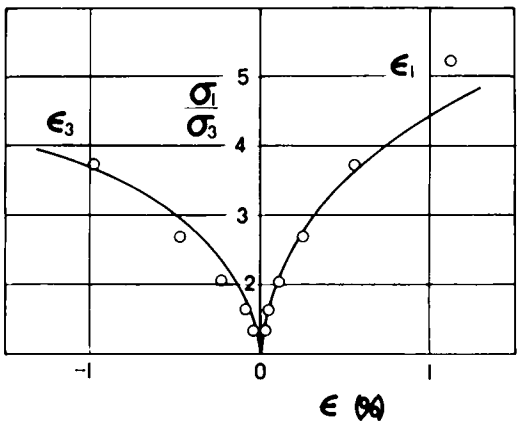

Fig.1.3.42 Relationship among σ_1/σ_3, ϵ_1 and ϵ_3 in triaxial extension test on Ottawa sand.

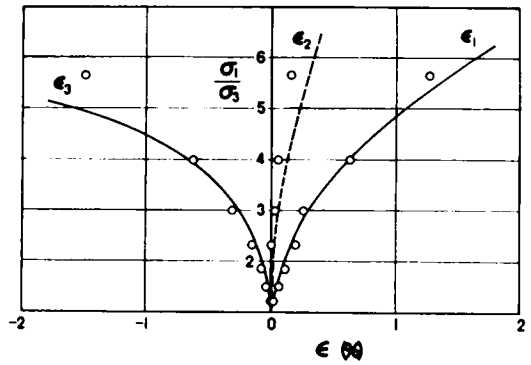

Fig.1.3.43 Relationship among σ_1/σ_3, ϵ_1, ϵ_2 and ϵ_3 in universal triaxial test on Ottawa sand.

tests and those of test under three different principal stresses referred to as RS 60° (RS standing for radial shear) conducted with respect to relatively loosely packed Ottawa sand, in comparison with the curves (solid and dotted lines) of values calculated in accordance with the expression (1.3.9). In the related calcualtions, the coefficients $\lambda = 1.2$, $\mu = 0.25$ and $\mu' = 0.45$ proper to Ottawa sand determined by rearranging the various relationships existing on the mobilized plane with respect to the results of triaxial compression test shown in Fig.1.3.41 were used in conjunction with $\gamma_0 = 0.12\%$ (for Fig.1.3.41), $\gamma_0 = 0.10\%$ (for Fig.1.3.42) and $\gamma_0 = 0.08\%$ (for Fig.1.3.43) which were a little different owing to the difference in granular structure at the outset. Fig.1.3.44 represents the results of shear test performed under three different principal stresses determined by Miyamori and Shiraishi[32] on Toyoura sand, in comparison with the curves of values calculated in

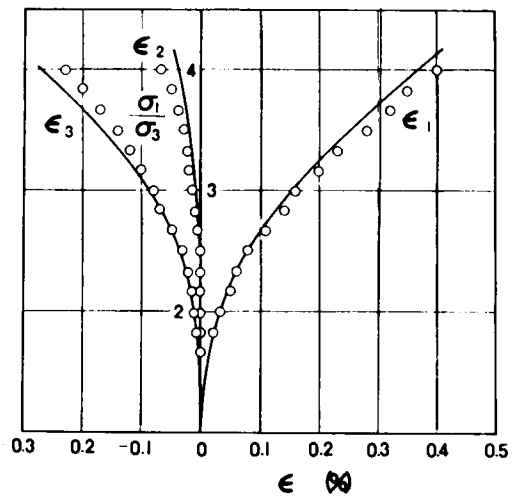

Fig.1.3.44 Relationship among σ_1/σ_3, ϵ_1 and ϵ_3 in universal triaxial test on Toyoura sand.

accordance with the expression of (1.3.9). Under the test conditions, the initial void ratio $e_i = 0.661$ was used and the value of σ_1 was increased where $\sigma_2 = 1.0$ kg/cm^2 and $\sigma_3 = 0.6$ kg/cm^2. This means that the value of σ_m for this test was not constant. In the related calculations, the coefficients of $\lambda = 1.2$, $\mu = 0.25$, $\mu' = 0.44$ proper to Toyoura sand and $\gamma_0 = 0.04\%$ were used. A possible reason for the small value of γ_0 in this case may be that there was assumed a dense granular structure due to anisotropic compression prior to shear. Fig.1.3.45 represents the results of test conducted on Toyoura sand by the use of manufactured universal triaxial apparatus ($\sigma_1 \cong 1.5$ kg/cm^2 and $e_i = 0.698$), in comparison with the curves of values calculated in accordance with the expression of (1.3.9). In the related calculations, there were used the coefficients $\lambda = 1.2$, $\mu = 0.25$, $\mu' = 0.44$ proper to Toyoura sand and $\gamma_0 = 0.1\%$. In the diagram, the data are observed to be roughly in agreement with each other. For the same reason as mentioned above, the curves of calculated values are parallelly translated to eliminate possible effect of the initial shear.

From the foregoing comparative study, it may safely be concluded that the expression of (1.3.9) provides a generally appropriate explanation to the relationship between principal stress ratio and principal strain under different principal stresses, cover-

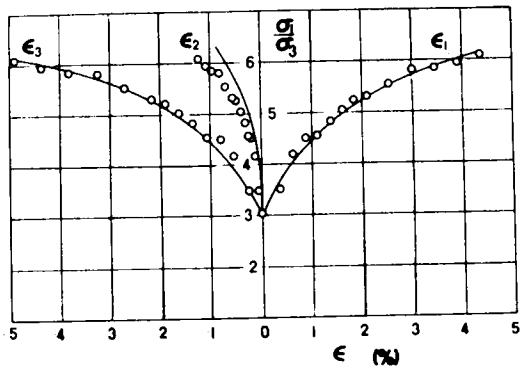

Fig.1.3.45 Relationship among σ_1/σ_3, ϵ_1, ϵ_2 and ϵ_3 in universal triaxial test after K_0-compression on Toyoura sand.

ing triaxial compression and triaxial extension tests as well as plane strain test. An effort to formularize general stress – strain relationships under such three mutually different principal stresses in terms of basic parameters which are appropriate even from the microscopic point of view is considered to form one of the most important tasks for the present-day soil mechanics. The author is convinced that he has given one possible solution to this task.

3.5.8 Review of Results of Simple Shear Test

The simple shear apparatus (N.G.I. type made by Geonor) is considered to be an apparatus which is designed to permit direct measurement of shear stress τ, normal

stress σ_N and shear strain γ, and normal strain ϵ_N on the mobilized plane under a plane strain condition. By way of illustration, the results of simple shear test conducted on Toyoura sand ($\sigma_N = 2.0$ kg/cm^2 and $e_i = 0.748$) have been rearranged in terms of τ/σ_N and $d\epsilon_N/d\gamma$ relationship to obtain a plot of o marks given in Fig.1.3.46. The

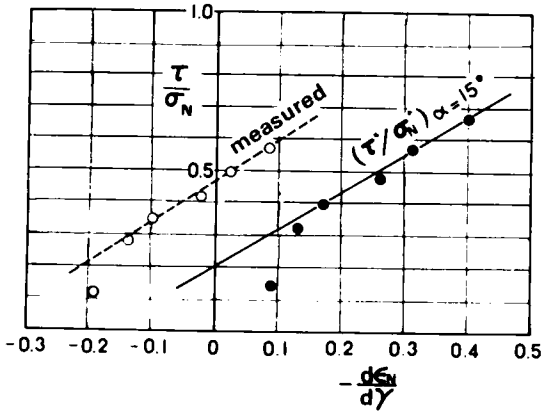

Fig.1.3.46 Relationship between τ/σ_N and $d\epsilon_N/d\gamma$ in simple shear test on Toyoura sand.

expression of (1.3.1) leads one to conclude that, in this plot, the ordinate intersection represents the interparticle frictional coefficient μ and tne gradient of the linear relationship represents λ. It is noted, however, that the value of the ordinate intersection (about 0.45) in this case is fairly large compared with the value (0.20 – 0.25) of the interparticle frictional coefficient so far described to be proper to Toyoura sand. With a view to determining the cause for this difference, the author used a piled mass of aluminum rods serving as the two-dimensional model of sandy soil and gave it a deformation of simple shear to observe the condition in which particles would be mobilized. To facilitate the observation, vertical lines were drawn in ink on the end faces of aluminum rods prior to shear so that the process of deformation in the rod mass could be observed by taking notice of relative change of the lines drawn on the end surfaces (Photo.1.3.8). From this observation, the author nas learnt that, so far as the height of the test specimen is not very high (less than about one half the width), the plane in which soil particles are mobilized to the greatest extent does not fall horizontally but falls on a diagonal plane indicated in Fig.1.3.47 by a dotted line. This conclusion is consistent with the observations that slip planes appeared on a diagonal plane in the simple shear test and the slice shear test conducted respectively by Sugiuchi[33] and Ōmaki[34].

The angle α which the diagonal line forms with the horizontal plane varies with the height of the test specimen. In the case of the simple shear apparatus (N.G.I. type made by Geonor), the angle mostly occurs in the range of from 11° to 15°. When the $\tau/\sigma_N \sim d\epsilon_N/d\gamma$ relationship on the true mobilized plane is to be calculated from the values found by assuming $\alpha = 15°$, for example, there is obtained a plot

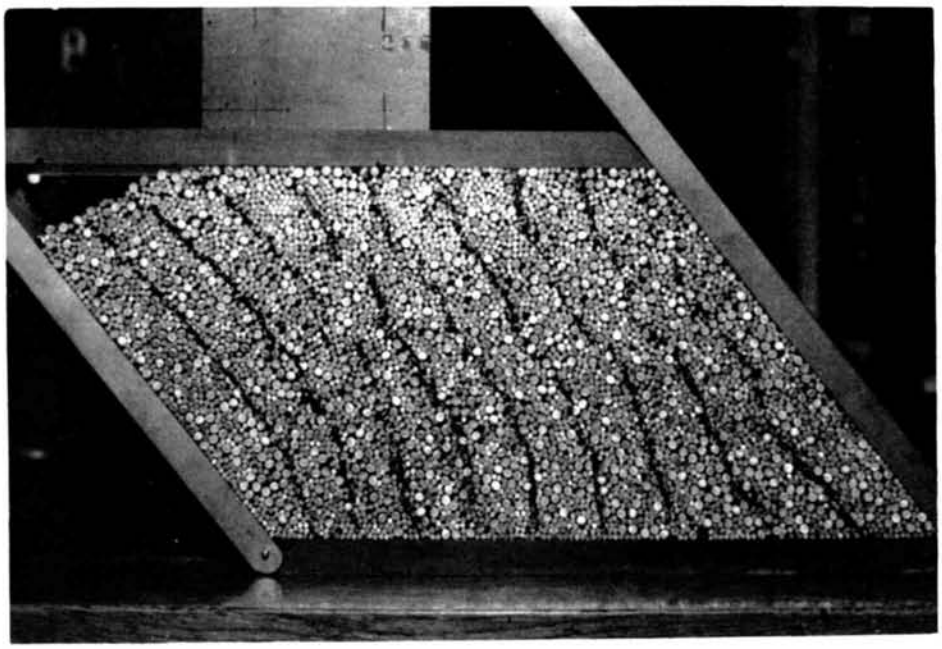

Photo.1.3.8 Relative displacement of particles in aluminum rod mass due to deformation of simple shear.

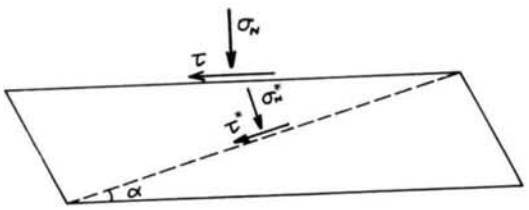

Fig.1.3.47 Diagonal mobilized plane in the specimen of simple shear test.

indicated by the • marks in Fig.1.3.46. In this case, the ordinate intersection (0.20) and the linear gradient (1.2) both prove to be generally appropriate values for μ and λ of Toyoura sand. If the preceding discussions with respect to the mobilized plane are judged to be correct, then the data on the simple shear test do not prove to be inconsistent with the results of triaxial compression test, triaxial extension test, plane strain test and multiaxial test which have been discussed to this point. Since the present study is based on a hypotehsis that the true mobilized plane falls on the diagonal line, it leaves out the treatment of the data on simple shear test except the following 3.5.9.

3.5.9. Review of Results of Repeated Shear Test

In Paragraph 2.9, Chapter 2, the author discussed the change of granular structure during the repeated shear in terms of the change in distribution of angles of inter-particle contact "θ". In consideration of the fact that the change in granular structure during shear is particularly conspicuous in the case of the alternately repeated shear, it is interesting to verify, on the basis of actually measured data, the applicability of the various stress-strain relationships discussed so far. Here, the author proposes to verify the relationship between stress ratio (τ/σ_N) and strain increment ratio ($d\epsilon_N/d\gamma$), the relationship between stress ratio (τ/σ_N) and shear strain (γ), the relationship between dilatancy (ϵ_N) and shear strain (γ), etc. on the basis of the results of repeated shear test conducted on Toyoura sand by means of a simple shear apparatus, in an effort to judge as to whether or not the mechanical properties of soil during repeated shear which have so far proved to be difficult of treatment can be interpreted by the preceding theory.

Fig.1.3.48 shows the results of repeated shear test (σ_N = 2.0 kg/cm^2 constant and e_i = 0.668) conducted on Toyoura sand by a simple shear apparatus, in terms of the

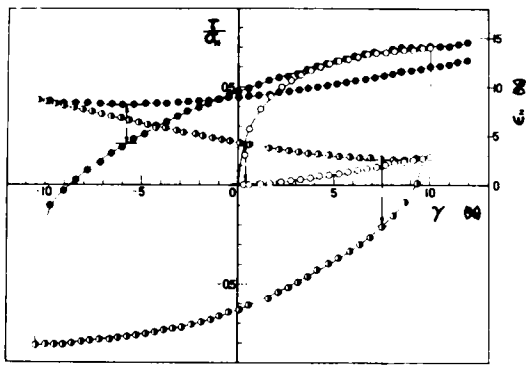

Fig.1.3.48 Relationship among τ/σ_N, γ and ϵ_N in repeated simple shear test on Toyoura sand.

relationship between shear-normal stress ratio τ/σ_N and shear strain γ and the relationship between normal strain ϵ_N and shear strain γ existing on the true mobilized plane (see 3.5.8.). The angle α which the diagonal line is believed to constitute the true mobilized plane forms with the horizontal plane was fixed at 12° in consideration of the height of test specimen. The portion indicated by o marks is referred to as "*1st loading*", the portion indicated by ◑ markes as "*2nd loading*" and the portion indicated by ● marks as "*3rd loading*" respectively. In the diagram, each arrow mark shows the minimum point of ϵ_N and the value of stress ratio τ/σ_N existing at that point. It is seen that absolute values of τ/σ_N as indicated by arrow marks are invariably in the neighborhood of 0.21. Here, the terminating point of 1st loading and that of 2nd

loading were assumed to constitute starting points of 2nd loading and 3rd loading respectively and also serve as origins for shear strain γ and normal strain ϵ_N. Under this assumption, the granular structure broadly varies at the starting point of 1st loading and that of 2nd loading. The author, regarding this difference as that of initial structures, tried to apply the aforementioned stress-strain relationships. The plot of the relationship between τ/σ_N and $d\epsilon_N/d\gamma$ to be drawn on the basis of this concept is shown in Fig.1.3.49. The ○, ◑ and ● marks found in the diagram represent 1st, 2nd

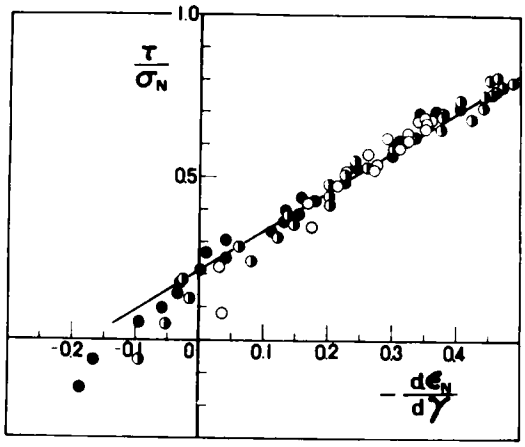

Fig.1.3.49 Relationship between τ/σ_N and $d\epsilon_N/d\gamma$ in repeated simple shear test on Toyoura sand.

and 3rd loading respectively. From this diagram, it is observed that nearly all plots fall on an essentially straight line and that the linear gradient 1.2 and the ordinate intersection 0.21 are appropriate values for λ and μ of Toyoura sand from a broad standpoint. It is, accordingly, verified that the $\tau/\sigma_N \sim d\epsilon_N/d\gamma$ relationship on the mobilized plane which is proposed in the present study holds good even for repeated shear.

When $\tau/\mu\cdot\sigma_N$ and γ/γ_0 are plotted in accordance with the expression of (1.3.6) on a semi-logarithmic section paper, the results are as shown in Fig.1.3.50. In the diagram, the ○, ● and ● marks similarly represent 1st, 2nd and 3rd loading respectively. From this diagram, it may be concluded that the linearity which the coordinates from the expression of (1.3.6) exhibit on the semi-logarithmic section paper is established nearly satisfactorily on each loading. The gradient of 1st loading is observed to differ significantly from that of 2nd or 3rd loading. This marked difference may be explained in view of the broad difference in initial structures. To be more specific, the distribution of θ in the initial condition of 1st loading is considered to be substantially symmetrical as shown by a model in Fig.1.2.24 of Paragraph 2.9, Chapter 2, whereas the distribution is of an asymmetrical form abounding in negative angles of interparticle contact with reference to the direction of shear in the case of the initial condition of 2nd and 3rd loading. The absolute value of $\bar{\theta}_0$ in 2nd and 3rd loading, therefore, is considered to

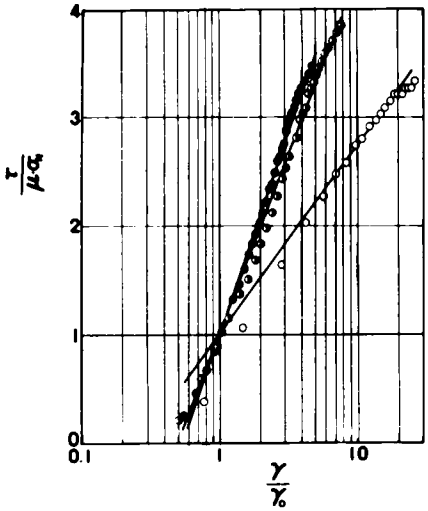

Fig.1.3.50 Relationship between $\tau/\mu\cdot\sigma_N$ and γ/γ_0 in repeated simple shear test on Toyoura sand.

be greater than that in 1st loading, making the value of μ' in the former loading proportionally greater than in the latter loading (for, $\mu' = \lambda\cdot\bar{\theta}_0 + \mu$). Consequently, the expression of (1.3.6) provides an explanation why the gradient, 2.3 ($\mu'/\mu - 1$), of the relationship of $\tau/\mu\cdot\sigma_N$ to $\log_{10}\ \gamma/\gamma_0$ assumes a large value.

When μ' is obtained from the linear gradient on the semi-logarithmic graph of Fig.1.3.50 by assuming $\lambda = 1.2$ (constant) and $\mu = 0.21$ (constant) from Fig.1.3.49, there are derived $\mu' = 0.38$ (1st loading), $\mu' = 0.52$ (2nd loading) and $\mu' = 0.56$ (3rd loading) respectively. From the actually measured values of Fig.1.3.48, there are derived $\gamma_0 =$ 0.39% (1st loading), $\gamma_0 = 2.56\%$ (2nd loading) and $\gamma_0 = 4.73\%$ (3rd loading) respectively. When the $\tau/\sigma_N \sim \gamma$ relationship and the $\epsilon_N \sim \gamma$ relationship during repeated shear are calculated by applying these values to the expressions of (1.3.4) and (1.3.5), there are obtained the results shown in Fig.1.3.51. This diagram shows a rather satisfactory correspondence with the measured values of hysteresis loop and dilatancy curve shown in Fig. 1.3.48.

The foregoing discussion has verified that the alternately repeated shear can similarly be treated fundamentally as a shear phenomenon. Only the necessity for quantitative estimation of the values of μ' and γ_0 for 2nd and subsequent loading remains yet to be elucidated. Finally, in the case of reloading curve of the hysteresis loop of positively repeated shear (see Fig.1.2.22, Paragraph 2.9 of Chapter 2), since the shear occurs while the distribution of θ of asymmetrical form abounding in positive angles of interparticle contact is assumed as the initial distribution, the value of γ_0 is extremely small in contrast to the case of the said alternately repeated shear. The author wishes to add that a satisfactory explanation is also found

in this analysis which is made from such point of view.

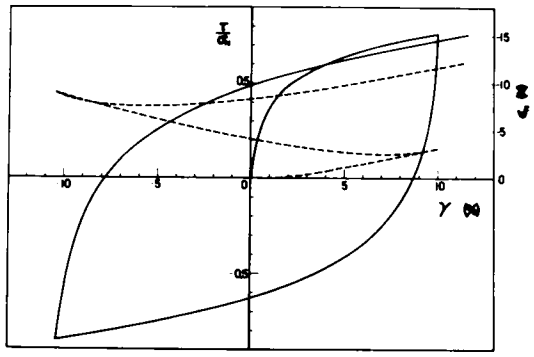

Fig.1.3.51 Calculated relationship among τ/σ_N, γ and ϵ_N in repeated simple shear test on Toyoura sand.

3.6 APPLICATION TO UNDRAINED SHEAR TEST

In the field of soil mechanics, it has been customary for the convenience of treatment to regard the volumetric strain of soil as comprising volumetric strain due to isotropic consolidation and volumetric strain due to shear (dilatancy). The principal strains ϵ_1 and ϵ_3 expressed by the formulas of (1.3.7) and (1.3.8) in Paragraph 3.3 are judged to be principal strains $(\epsilon_1)_d$ and $(\epsilon_3)_d$ due to dilatancy in view of the basic concept underlying the derivation of the said formulas. It is, therefore, proposed here to consider that volumetric strains calculated from these formulas are those ascribable to dilatancy, viz. $(\Delta V/V)_d$. In the case of triaxial compression and triaxial extension test, therefore, the following equation can be derived. In the equation, X is used to stand for $\sqrt{\sigma_1/\sigma_3} - \sqrt{\sigma_3/\sigma_1}$.

$$\left(\frac{\Delta V}{V}\right)_d = 2\,f\left(\frac{\sigma_1}{\sigma_3}\right) + 2\,g\left(\frac{\sigma_1}{\sigma_3}\right)$$

$$= \gamma_0 \cdot \exp\left(-\frac{\mu}{\mu' - \mu}\right) \cdot \exp\left\{\frac{\mu}{2(\mu' - \mu)}\right\}$$

$$\cdot \left\{\left(1 - \frac{2}{\lambda}\right) \cdot X - 2(\mu' - \mu) + \frac{4\mu'}{\lambda}\right\} \qquad (1.3.19)$$

Where three different principal stesses are exerted as generally experienced, then the following equation is derived from the formula of (1.3.9).

$$\left(\frac{\Delta V}{V}\right)_d = f\left(\frac{\sigma_1}{\sigma_3}\right)+f\left(\frac{\sigma_1}{\sigma_2}\right)+f\left(\frac{\sigma_2}{\sigma_3}\right)+g\left(\frac{\sigma_1}{\sigma_3}\right)+g\left(\frac{\sigma_1}{\sigma_2}\right)+g\left(\frac{\sigma_2}{\sigma_3}\right) \qquad (1.3.20)$$

wherein, the following equations are assumed to hold good.

$$X \equiv \sqrt{\sigma_i/\sigma_j} - \sqrt{\sigma_j/\sigma_i} \quad (i, j = 1, 2, 3,\ i \leqq j)$$

$$f\left(\frac{\sigma_i}{\sigma_j}\right) = \frac{\tau_0 \cdot \exp\left(-\frac{\mu}{\mu'-\mu}\right)}{2} \cdot \exp\left\{\frac{X}{2(\mu'-\mu)}\right\}$$

$$\cdot \left\{\frac{X^2}{8}+\left(\frac{1}{2}-\frac{1}{\lambda}-\frac{\mu'-\mu}{2}\right)\cdot X+(\mu'-\mu)^2-(\mu'-\mu)+\frac{2\mu'}{\lambda}+1\right\} \quad (i<j)$$

$$g\left(\frac{\sigma_i}{\sigma_j}\right) = \frac{\tau_0 \cdot \exp\left(-\frac{\mu}{\mu'-\mu}\right)}{2} \cdot \exp\left\{\frac{X}{2(\mu'-\mu)}\right\}$$

$$\cdot \left\{-\frac{X^2}{8}+\left(\frac{1}{2}-\frac{1}{\lambda}+\frac{\mu'-\mu}{2}\right)\cdot X-(\mu'-\mu)^2-(\mu'-\mu)+\frac{2\mu'}{\lambda}-1\right\} \quad (i<j)$$

$$f\left(\frac{\sigma_i}{\sigma_i}\right) = g\left(\frac{\sigma_i}{\sigma_i}\right) = 0 \quad (i=j)$$

The preceding expressions indicate that the volumetric strain due to dilatancy can be calculated as a function of the principal stress ratio.

On the other hand, the volumetric strain $(\Delta V/V)_c$ ascribable to consolidation is given, as is widely known, by the following equation.

$$\left(\frac{\Delta V}{V}\right)_c = \frac{C_c}{1+e_i} \cdot \log_{10}\frac{\sigma_m}{\sigma_{mi}} \qquad (1.3.21)$$

In this expression, C_c stands for compression index and e_i and σ_{mi} stand respectively for initial void ratio and initial mean effective principal stress existing prior to consolidation. Where σ_m decreases in shear, the coefficient C_s of swelling should be used in place of C_c. For the present purpose, C_c is used as its substitute.

For the convenience of further discussion, it is assumed that the volumetric strain produced in the soil element can be expressed in the form of a superposition of the volumetric strain $(\Delta V/V)_c$ due to consolidation and the volumetric strain $(\Delta V/V)_d$ due to dilatancy. Then, the following equation is derived consequently[18),28)].

$$\frac{\Delta V}{V} = \left(\frac{\Delta V}{V}\right)_c + \left(\frac{\Delta V}{V}\right)_d \qquad (1.3.22)$$

For a fixed soil specimen, the right hand side of the equation (1.3.22) can be calculated for stress condition in accordance with the formulas of (1.3.19) through (1.3.21). This means that the volumetric strain of this soil can be found by calculation.
The volumetric strain and the principal strains as well, the values of $(\epsilon_1)_d$, $(\epsilon_2)_d$ and $(\epsilon_3)_d$ for existing stress conditions can be found in accordance with the formulas of (1.3.9) through (1.3.14). Further, the principal strain due to consolidation is expressed as shown below.

$$(\epsilon_1)_c = (\epsilon_2)_c = (\epsilon_3)_c = \frac{1}{3}\left(\frac{\Delta V}{V}\right)_c = \frac{1}{3} \cdot \frac{C_c}{1+e_i} \cdot \log_{10}\frac{\sigma_m}{\sigma_{mi}} \qquad (1.3.23)$$

It follows as a consequence that the stress-strain relationship under a given stress condition involving simultaneous exertion of consolidation and shear can be found by calculation so far as the superposition of strain due to consolidation and that due to dilatancy is found acceptable.

Since the compressibility is generally small (C_c being small) in the case of sand, it is inferred that the difference between the test using a constant mean principal stress σ_m and the test using a constant lateral pressure σ_3 is not too conspicuous as pointed out previously. The difference in the stress-strain curves ascribable to such difference in stress conditions will be discussed by citing a concrete example in the paragraph dealing with clayey soil in Chapter 4. In the present paragraph, the author limits his discussion to the behavior of soil under undrained conditions, viz. conditions which do not permit drainage to occur during shear. Since undrained conditions are such that the soil specimen as a whole is not permitted to undergo any volumetric change, it is only natural to interpret that if the volume tends to contract because of negative dilatancy, the effective confining pressure decreases so as to induce a proportional volumetric expansion and if the volume tends to expand because of positive dilatancy, then the effective confining pressure increases to induce a proportional volumetric contraction. According to the formula of (1.3.22), therefore, this relationship may be expressed as follows:

$$\left(\frac{\Delta V}{V}\right)_c + \left(\frac{\Delta V}{V}\right)_d = 0 \qquad (1.3.24)$$

When the equations of (1.3.19) and (1.3.21) are substituted in the equation of (1.3.24) on the basis of the concept mentioned above, the formulated relationship of effective stress during shear in triaxial compression test and triaxial extension test, namely, the formula indicative of effective stress path, can be calculated. In the case of triaxial compression test, for example, since $\sigma_m = (\sigma_1 + 2\sigma_3)/3$, the following equation can be derived from the equation of (1.3.24).

$$2\left\{ f\left(\frac{\sigma_1}{\sigma_3}\right) + g\left(\frac{\sigma_1}{\sigma_3}\right)\right\} + \frac{C_c}{1+e_i}\left\{ \log_{10}\frac{\sigma_1/\sigma_3 + 2}{3\,\sigma_{mi}} + \log_{10}\sigma_3 \right\} = 0$$

From this equation, the value of σ_3 and consequently the value of σ_1 are determined for a given value of σ_1/σ_3. In the preceding formula, σ_1, σ_3 and σ_{mi} stand for effective stresses. Fig.1.3.52 compares the results of calculation performed in the manner

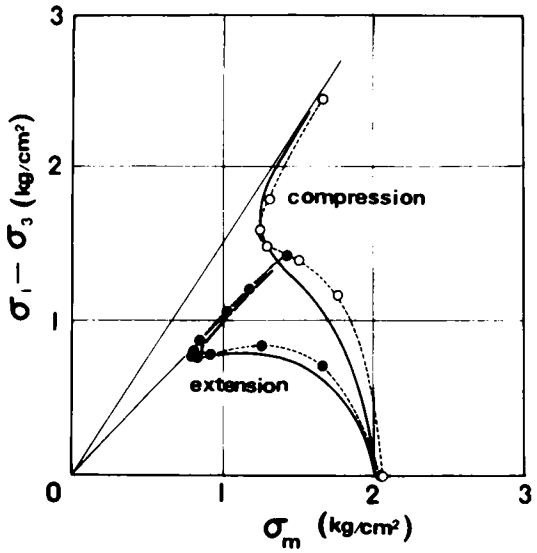

Fig.1.3.52 Relationship between $(\sigma_1 - \sigma_3)$ and σ_m in undrained triaxial compression and extension tests on Sagami River sand.

just mentioned with the actually found values. By "*actually found values*" are meant the data[16] of triaxial compression and triaxial extension test on Sagami River sand. In the related calcualtions, the constants $\lambda = 1.2$, $\mu = 0.26$, $\mu' = 0.44$, $\gamma_0 = 0.35\%$ (for triaxial compression) or 0.6% (for triaxial extension), $C_c = 0.06$ and $e_i = 0.74$ were used. It should be noted that all these coefficients were determined from the data of test conducted on Sagami River sand. It is observed from the diagram that, for both triaxial compression and triaxial extension, curves of calculated values and those of observed values are in satisfactory agreement. It is interesting to note that these curves are inverted from left to right under the influence of dilatancy[35]. The minimum point of

σ_m on this stress path is believed to correspond to the minimum point of volumetric strain $(\Delta V/V)_d$ ascribable to dilatancy. Therefore, the principal stress ratio at this point can be determined in accordance with the formula of (1.3.18).

In the graph of the $(\sigma_1 - \sigma_3) \sim \sigma_m$ relationship represented in Fig.1.3.52, the curves of measured values for triaxial compression and those for triaxial extension are fairly separated from each other. When these values are rearranged in terms of $\tau \sim \sigma_N$ relationship on the mobilized plane, the results are as shown in Fig.1.3.53. It appears from this diagram that the curves representing the values for triaxial compression and triaxial extension are both inverted from left to right at an equal value of τ/σ_N and they have the same maximum value of τ/σ_N (peak strength). Here, the conversion of the curves from left to right at the same value of τ/σ_N is evident from the formula of (1.3.18) and the acquisition of the same maximum value of τ/σ_N is considered to indicate faithful accordance with Mohr-Coulomb's failure criterion. It is also observed that the curves of calculated values (indicated by solid lines) obtained by using the same coefficients as those for Fig.1.3.52 show the same trend. These observations may support the hypothesis that the mechanical properties of soil are governed by τ/σ_N on the mobilized plane and not by the ratio of $(\sigma_1 - \sigma_3)/\sigma_m$ ($\equiv q/p$).

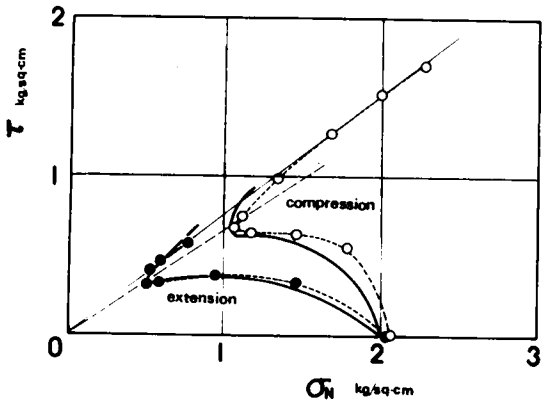

Fig.1.3.53 Relationship between τ and σ_N in undrained triaxial compression and extension tests on Sagami River sand.

3.7 METHOD FOR CALCULATION OF STRESS-STRAIN RELATIONSHIP

The author has continued his efforts to express general stress-strain relationships of soil by using the smallest possible number of basic parameters. As to such parameters, those indicative of properties proper to soil particles such as, for example, inter-particle friction μ and those serving to evaluate properties of soil as an assemblage of particles such as, for example, initial void ratio are not sufficient for the purpose. Parameters which permit evaluation of initial structure such as, for example, γ_0 (or $\bar{\theta}_0$)

are indispensable at least for the present purpose. Of the four coefficients (λ, μ, μ' and γ_0) which are involved here in dealing with the shear phenomenon, μ is a physical constant proper to soil which is believed to constitute a frictional coefficient ($= \tan \phi_\mu$) existing between soil particles. When the $\tau/\sigma_N \sim d\epsilon_N/d\gamma$ relationship is actually rearranged and the ordinate intersection is taken from the resultant graph, then the coefficient μ appears to assume a substantially constant value, irrespectively of the values of void ratio and confining pressure. Then, λ is a constant (see Fig.1.2.13) which is determined by the value of μ of the soil. When this is calculated from the linear gradient of the said $\tau/\sigma_N \sim d\epsilon_N/d\gamma$ relationship, it frequently assumes a value in the neighborhood of 1.2. And, μ' is a coefficient which, according to the defining formula $\mu' = \lambda \cdot \bar{\theta}_0 + \mu$, is related to the initial granular structure and the interparticle friction.
Finally, γ_0 means γ at the maximum compression point of the normal strain ϵ_N on the mobilized plane and, therefore, is considered to serve as a parameter for evaluation of the granular structure of soil. Under the normal soil structure, it is believed to constitute a coefficient governed by the initial void ratio (e_i) and confining pressure (σ_m) and the like (see Fig.1.3.54).

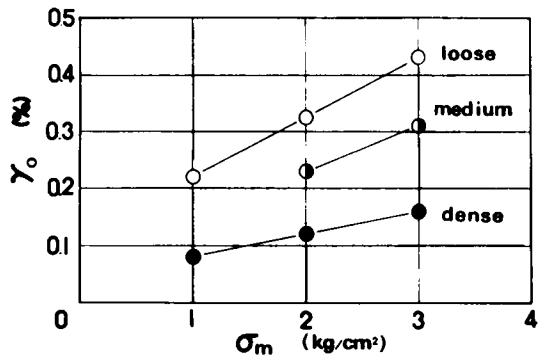

Fig.1.3.54 Relationship among γ_0, confining stress σ_m and density of sample in the case of Sagami River sand.

Among these coefficients, the following relationships exist. From the definition, there is derived:

$$\mu' = \lambda \cdot \bar{\theta}_0 + \mu \qquad (1.3.25)$$

Since the maximum compression value ϵ_{NO} of ϵ_N is produced where $\bar{\theta} = 0$, the following equation is derived from the equation of (1.2.32) of Paragraph 2.7 of Chapter 2.

$$\epsilon_{NO} = -\log_e |\cos \bar{\theta}_0| \qquad (1.3.26)$$

In consideration of the equation $\epsilon_N = \epsilon_{NO}$ which is established where $\gamma = \gamma_0$, the following relationship can be drawn from the formula of (1.3.5).

$$\epsilon_{NO} = \frac{\mu' - \mu}{\lambda} \cdot \gamma_0 \qquad (1.3.27)$$

By substituting the formula of (1.3.25) in the expression of (1.3.27) and then equalizing the resultant expression with the formula of (1.3.26), the following equation is obtained which indicates the relationship between γ_0 and $\bar{\theta}_0$.

$$\gamma_0 = -\frac{1}{\bar{\theta}_0} \cdot \log_e |\cos\bar{\theta}_0| \qquad (1.3.28)$$

This means that the value of μ' can be calculated in accordance with the equations (1.3.28) and (1.3.25) so far as the value of γ_0 can be estimated. Then, all the coefficients can be determined, since λ and μ are considered to be constants which are proper to the soil under review. However, the formula (1.3.28) is deficient of accuracy because of the fact that a hypothesis is involved in the process of the derivation of the formula (1.3.5) in which the said formula originates. In the circumstances, a highly reliable method capable of taking its place is required. So the author proceeds to discuss a possible method for determining a practical stress-strain relationship.

According to formua (1.3.6), the linear gradients of Fig.1.3.27 through Fig. 1.3.29 are found to correspond to 2.3 ($\mu'/\mu - 1$). An inspection of these diagrams leads one to infer that the values of the gradients are not appreciably affected by the confining pressure and the void ratio. In consideration of the constancy of the value of μ, therefore, the value of μ' by primary approximation under the normal granular structure is believed to be roughly constant. If the values of the coefficients (λ, μ and μ') are approximately fixed for a given test specimen, then the value of the remaining coefficient γ_0, it is considered, may roughly be estimated by applying to such a diagram as Fig.1.3.54 the confining pressure and the soil density (void ratio) at the present position in the field. Now, the method for the determination of each coefficient will specifically be discussed. To begin with, drained triaxial compression tests, for example, are performed on test specimens from the field under investigation under conditions involving a number of confining pressures including the confining pressure prevalent at the present position and having the density adjusted as much as permissible. The results of this test are analyzed for the $\tau/\sigma_N \sim d\epsilon_N/d\gamma$ relationship and the $\tau/\sigma_N \sim \log_{10}\gamma$ relationship on the mobilized plane in accordance with the method described in Paragraph 3.5. Since the equation, $\tau/\sigma_N = \lambda \cdot (-d\epsilon_N/d\gamma) + \mu$, is derived from the formula of (1.3.1),

the value of λ is determined from the linear gradient and the value of μ from the ordinate intersection respectively of the plot of the $\tau/\sigma_N \sim d\varepsilon_N/d\gamma$ relationship. These values ought to be approximately constant in spite of the variability of confining pressure and void ratio. Because of the equation, $\tau/\sigma_N = 2.3 \cdot (\mu' - \mu) \{ \log_{10}\gamma - \log_{10}\gamma_0 \} + \mu$, which is derived from the formula (1.3.4), the value of μ' is determined from the gradient in the $\tau/\sigma_N \sim \log_{10}\gamma$ relationship and the value of γ_0 from the ordinate for $\gamma = 1$. Where the value of μ' is dispersed, then an average value is adopted. Since the value of γ_0 is affected by σ_m and e_i, the value at the present position is estimated by carrying out a rearrangement of relevant data after the manner of Fig.1.3.54. Once the coefficients (λ, μ, μ' and γ_0) are thus determined, then it becomes possible to calculate stress-strain relationships prevailing basically under various conditions as previously described. What is important seems to be the question of generality and applicability of stress-strain relationships to be derived consequently. In all the calculations treated of in the preceding paragraphs, the values $\lambda = 1.2$, $\mu = 0.25$ and $\mu' = 0.44$ were used in the case of Toyoura sand, the values $\lambda = 1.2$, $\mu = 0.40$ and $\mu' = 0.62$ in the case of Ishii River sand, the values $\lambda = 1.2$, $\mu = 0.10$ and $\mu' = 0.22$ in the case of glass beads and the values $\lambda = 1.2$, $\mu = 0.26$ to 0.28 and $\mu' = 0.44$ in the case of Sagami River sand respectively as coefficients for relevant test specimens. The generality and applicability of the proposed formulas in that the stress-strain relationships obtained by triaxial compression test, triaxial extension test, plane strain test and universal triaxial test on the respective test specimens can be explained by these substantially constant coefficients deserves special attention. Accurate determination of the remaining coefficient γ_0 is an extremely difficult task. In the elucidation of the stress-strain relationships of soil, such parameters as are involved in the evaluation of granular structure are by all means necessary in some sense or other. Any stress-strain relationships derived in the absence of such parameters should be ruled out as lacking sufficient reliability. The coefficient γ_0 is the very parameter that should be estimated by making the most advanced data available under the circumstances as by resorting to the aforementioned method.

3.8 CONCLUSIONS

In the present chapter, the author derived stress-strain relationships of soil existing on the mobilized plane from the various relatonships drawn out in Chapter 2 from the microscopic point of view. Based on these basic relationships on the mobilized plane, general stress-strain relationships of soil under three mutually different principal stresses were formulated. The formulas of these stress-strain relationships were verified with respect to measured data of triaxial compression test, triaxial extension test, plane strain test and universal triaxial test involving exertion of three different principal stresses conducted on various kinds of sand and glass beads. Specific methods for determination

of the values of coefficients involved in these formulas were also explained.

The formulas of stress-strain relationships of soil proposed here have been introduced in terms of changes in the granular structure in the process of shear on the basis of a theory that the mechanical properties of soil are governed by the shear-normal stress ratio (τ/σ_N) on the mobilized plane (referred to tentatively as τ/σ_N theory). This is believed to correspond to Coulomb's law of friction. In the present-day soil mechanics, there prevails the concept[36),37)] of von Mises' view (referred to provisionally as q/p theory or τ_{oct}/σ_{oct} theory) that the behavior of soil is regulated by the ratio of the shear stress τ_{oct} ($=\sqrt{(\sigma_1-\sigma_2)^2+(\sigma_2-\sigma_3)^2+(\sigma_3-\sigma_1)^2}/3$) to the normal stress σ_{oct} ($=\sigma_m=(\sigma_1+\sigma_2+\sigma_3)/3$) on the octahedral plane or, in the case of triaxial tests, by the ratio of q ($=\sigma_1-\sigma_3$) to p ($=\sigma_m$). As pointed out in the present chapter with reference to some experimental facts, it appears that the mechanical properties of soil are uniquely explained more easily by resorting to the τ/σ_N theory. The τ_{oct}/σ_{oct} theory has an advantage that both τ_{oct} and σ_{oct} can be expressed in terms of invariants of stress and, at the same time, admits of a possibility that it fails to evaluate the direction of shear stress or the rotation of principal stress. Through the study introduced so far, the author has come to be convinced that the behavior of soil under normal density fundamentally follows the law of friction. For example, the equation $\tau/\sigma_N=\lambda(-d\epsilon_N/d\gamma)+\mu$, which is one of the basic formulas existing on the mobilized plane, is such that it corresponds to the law of friction which holds good when the surface is rugged[38)].

The results which have been drawn out in this chapter may be summarized as follows:

(1) The formulas of various stress-strain relationships on the mobilized plane introduced in the preceding chapter from the microscopic point of view were further developed to derive relationships among shear-normal stress ratio (τ/σ_N), shear strain (γ) and normal strain (ϵ_N) on the mobilized plane. These formulas of relationships on the mobilized plane constitute basic expressions of general stress-strain relationships under various kinds of stresses. Further, relationships between principal stress ratio (σ_1/σ_3) and principal strains (ϵ_1 and ϵ_3) were introduced by converting the said relationships into those on the principal stress plane.

(2) Under three principal stresses, the behavior of soil particles is three dimensional. So, the author introduced the new concept of three compounded mobilized planes. On the basis of this concept of compounded mobilized planes, general stress-strain relationships under three mutually different principal stresses were derived from the formulas of basic stress-strain relationships on the single mobilized plane. The formula on the general stress-strain relationship under three principal stresses can be used for expressing triaxial compression, triaxial extension, plane strain and other conditions as special cases.

(3) The formulas for the various relationships mentioned above were verified by the use of various test data. First, the relationship between shear-normal stress ratio (τ/σ_N) and normal-shear strain increment ratio ($d\epsilon_N/d\gamma$) on the single mobilized plane was verified by triaxial compression test, triaxial extension test and plane strain test conducted on Toyoura standard sand, Ishii River sand, Sagami River sand and glass beads. It was established that the linear gradient (λ) and the interparticle friction (μ) of ordinate intersection as found in all of these tests showed satisfactory agreement with the theoretical formulas. For a given test specimen, they were found to fall on the same straight line, irrespectively of method of tests, magnitude of confining stress and void ratio of test specimen.

(4) The relationship between principal stress ratio (σ_1/σ_3) and principal strain increment ratio ($d\epsilon_3/d\epsilon_1$) derived by converting the $\tau/\sigma_N \sim d\epsilon_N/d\gamma$ relationship on the mobilized plane into those on the principal stress plane were examined by triaxial compression test, triaxial extension test and plane strain test using Toyoura standard sand, Ishii River sand, Sagami River sand and glass beads. Consequently, it was proved that theoretical values were satisfactorily in agreement with measured values of the tests.

(5) When the shear-normal stress ratio (τ/σ_N)$\sim$ normal-shear strain ratio (ϵ_N/γ) relationship on the mobilized plane was examined in comparison with the results of triaxial compression test conducted on Toyoura sand and Ishii River sand, a satisfactory agreement was found between the theoretical values and the measured values.

(6) The shear-normal stress ratio (τ/σ_N)$\sim$shear strain (γ)$\sim$normal strain (ϵ_N) relationship was examined in comparison with the results of triaxial compression and triaxial extension test conducted on Toyoura sand, Ishii River sand, Sagami River sand and glass beads. The comparison showed a satisfactory agreement. In this respect, the author wishes to emphasize that the stress-strain relationship on the mobilized plane can be explained by the same values of coefficients (λ, μ and μ') proper to a given test specimen, no matter whether there is involved a triaxial compression test or triaxial extension test, whether the test specimen is packed loosely or densely, or whether the confining stress is high or low. The coefficient γ_0 is a parameter for the evaluation of the initial granular structure and, therefore, is variable with the initial void ratio and the confining stress.

(7) The formula obtained by dividing the two members of the equation of the said shear-normal stress ratio (τ/σ_N)$\sim$shear strain (γ) relationship on the mobilized plane by the interparticle friction (μ) represents straight lines which $\tau/\mu\cdot\sigma_N$ and γ/γ_0 describe past the point (1,1) on a semi-logarithmic section paper. They may be interpreted to be those obtained by normalizing $\mu\cdot\sigma_N(\equiv\tau_0)$ and γ_0 as standard values of shear stress and shear strain respectively. When the measured values corresponding to the formula of this relationship were plotted on a semi-logarithmic section paper, it was found that the data for Toyoura sand, Ishii River sand and

Sagami River sand would show substantially linear relationships. There are indications that data obtained for a fixed test specimen approximately fall on the same straight line under normal initial structure, no matter what confining stress and void ratio of the specimen may assume.

(8) When the principal stress ratio–principal strain relationship derived from the basic relationship of stress and strain on the mobilized ρlane was examined with respect to the results of triaxial compression and triaxial extension test conducted on Toyoura sand, Ishii River sand, Sagami River sand and glass beads, there was found a satisfactory agreement. A unique definition of soil dilatancy ($\Delta V/V$) for both triaxial compression and triaxial extension, it is judged, may be obtained more satisfactory by using τ/σ_N (or σ_1/σ_3) as the variable than by using $(\sigma_1 - \sigma_3)/\sigma_m$ ($\equiv q/p$) which has long been advocated. This conclusion finds support in the experimental facts as well as in the formulas proposed here by the author.

(9) The formula of the principal stress ratio–principal strain relationship introduced from the stress ratio–strain relationship on the mobilized plane was similarly examined with reference to the results of plane strain test and universal triaxial test conducted on Toyoura sand, glass beads and Ottawa sand. Consequently, a satisfactory agreement was found between the theoretical values and the measured values. It was additionally ascertained that the stress-strain characteristics found by the shear test conducted subsequent to K_0-consolidation could similarly be explained.

(10) It was confirmed that the stress ratio–strain–dilatancy charactersistics during the repeated shear of sand could likewise be expressed by the proposed formulas mentioned above, only so far as the change in the granular structure could appropriately be evaluated.

(11) The formula for the calculation of volumetric strain due to dilatancy was introduced from the aforementioned principal stress ratio – principal strain relationship. The stress path in the undrained shear test was calculated by assuming the sum of the volumetric strain due to dilatancy and that due to consolidation to be 0. When the results of this calculation were compared with the results of undrained triaxial compression test and undrained triaxial extension test on Sagami River sand, a satisfactory agreement was found. Experimental facts show that unique definition of the stress path could be obtained more satisfactorily by using τ/σ_N than by q/p.

(12) Specific methods for calculating the proposed formulas of stress ratio – strain relationships viz. a method for determining the values of the coefficients (λ, μ and μ') and also a method for estimating the coefficient γ_0 involved in the evaluation of possible effect of the initial soil structure, were discussed in detail.

(13) From the foregoing discussion, it is judged proper even from the standpoint of the microscopic discussion of shear mechanism to conclude that the mechanical properties of soil are governed by the value of τ/σ_N on the mobilized plane

(or principal stress ratio). In other words, it is concluded that the soil substance is a material which basically satisfies the law of friction (Coulomb's) under normal density.

References

1) Matsuoka, H.: The Stress-Strain Relation of Soils under Shearing derived from a Microscopic Consideration, Annuals, Disaster Prevention Research Institute, Kyoto University, No.15B, 1972, pp.499–511, (in Japanese).
2) Murayama, S. and Matsuoka, H.: A Microscopic Study on Shearing Mechanism of Soils, Proc. 8th Int. Conf. S.M.F.E., 1973, (to be published).
3) Matsuoka, H.: Stress-Strain Relationship of Soils under Three Different Principal Stresses, Annuals, Disaster Prevention Research Institute, Kyoto University, No.16B, 1973, (to be published in Japanese).
4) Taylor, D. W.: Fundamentals of Soil Mechanics, Modern Asia Edition, John Wiley & Sons, New York, 1948, pp.329–337.
5) Akai, K.: The Dilatancy Effect during Shear of Sands, Trans. of J.S.C.E., No.58, 1958, pp.76–81, (in Japanese).
6) Kirkpatrick, W. M.: Contribution to the Discussion, Proc. 5th Int. Conf. on S.M.F. E., Vol.3, 1961, pp.131–133.
7) Matsuoka, H. and Hashimoto, T.: A Newly Manufactured Multiaxial Apparatus and Analysis of its Measured Data, Proc., Annual Meeting of J.S.S.M.F.E. (8th), 1973, pp.231–234, (in Japanese).
8) Murayama, S.: A Theoretical Consideration on a Behaviour of Sand, Proc. of I.U.T.A.M. Symposium on Rheology and Soil Mechanics, Grenoble, 1964, Springer-Verlag, 1966, pp.146–159.
9) Karube, D. and Tamai T.: Stress-Strain Relations during Shear Test, Proc., Annual Meeting of J.S.C.E. (27th), III-41, 1972, pp.123–126, (in Japanese).
10) Murayama, S. and Matsuoka, H.: Shear Resistance and Particle Structure of Granular Soils, Proc., Annual Meeting of J.S.C.E. (25th), III-36, 1970, pp.105–108, (in Japanese).
11) Murayams, S. and Matsuoka, H.: The Mechanism of Shearing and its Similarity for Sands and Clays, Annuals, Disaster Prevention Research Institute, Kyoto University, No.14B, 1971, pp.551–563, (in Japanese).
12) Ichihara, M. and Matsuzawa, H.: Experiments on Shearing Characteristics of Dry Sand under Plane Strain Condition and Axial Symmetric Strain Condition, Proc., J.S.C.E., No.173, 1970, pp.47–59, (in Japanese).
13) Miyoshi, H. and Asai, K.: A Consideration on Stress-Deformation Characteristics

of Sand, Proc., Annual Meeting of Kansai Br., J.S.C.E., III-7, 1971, (in Japanese).
14) Tatsuoka, F.: Stress-Strain Characteristics of Sand in Triaxial Compression Test, Proc., Annual Meeting of J.S.S.M.F.E. (6th), 52, 1971, pp.205–208, (in Japanese).
15) Tatsuoka, F.: Stress-Strain Characteristics of Sand in Triaxial Compression Test (2nd report), Proc., Annual Meeting of J.S.C.E. (26th), III-21, 1971, pp.63–66, (in Japanese).
16) Tatsuoka, F. and Shiba, T.: Stress-Strain Characteristics of Sand in Triaxial Apparatus (3rd report), Proc., Annual Meeting of J.S.S.M.F.E. (7th), 42, 1972, pp.165–168, (in Japanese)
17) Rowe, P.W.: The Stress-dilatancy Relation for Static Equilibrium of an Assembly of Particles in Contact, Proc. Roy. Soc. London, Ser. A, Vol.269, 1962, pp.500–527.
18) Shibata, T.: On the Volume Changes of Normally-Consolidated Clays, Annuals, Disaster Prevention Research Institute, Kyoto University, No.6, 1963, pp.128–134, (in Japanese).
19) Shibata, T. and Karube, D.: Influence of the Variation of the Intermediate Principal Stress on the Mechanical Properties of Clays, Annuals, Disaster Prevention Research Institute, Kyoto University, No.7, 1964, pp.1–9, (in Japanese).
20) Shibata, T. and Karube, D.: Stress-Strain Relationship of the Normally Consolidated Clay, Annuals, Disaster Prevention Research Institute, Kyoto University, No.8, 1965, pp.515–523, (in Japanese).
21) Shibata, T. and Karube, D.: Influence of the Variation of the Intermediate Principal Stress on the Mechanical Properties of Normally Consolidated Clays, Proc. 6th Int. Conf. S.M.F.E., Vol.1, 1965, pp.359–363.
22) Karube, D. and Kurihara, N.: Dilatancy and Shear Strength of Saturated Remoulded Clay, Trans. of J.S.C.E., No.135, 1966, pp.16–24, (in Japanese).
23) Murayama, S. and Yagi, N.: On the Deformation Properties of Sands, Annuals, Disaster Prevention Research Institute, Kyoto University, No.7, 1964, pp.24–38, (in Japanese).
24) Murayama, S. and Yagi, N.: On the Deformation Characteristics of Sandy Soils, Tsuch-to-Kiso, J.S.S.M.F.E., Vol.13, No.2, 1965, pp.65–71, (in Japanese).
25) Yagi, N.: On Compression and Shearing Characteristics of Sand, Annuals, Disaster Prevention Research Institute, Kyoto University, No.10B, 1967, pp.375–381, (in Japanese).
26) Yagi, N.: On the Shearing Resistance of Sand, Annuals, Disaster Prevention Reseach Institute, Kyoto University, No.13B, 1970, pp.493–503, (in Japanese).
27) Hata, S. and Ohta, H.: A Consideration on the Pore Pressure in Clays under Undrained Shear, Trans. of J.S.C.E., No.155, 1968, pp.18–24, (in Japanese).
28) Ohta, H.: Analysis of Deformation of Soils Based on the Theory of Plasticity and its Application to Settlement of Embankments, Doctor Thesis, Kyoto Univ., 1971.

29) Ko, H. Y. and Scott, R. F.: A New Soil Testing Apparatus, Geotechnique, Vol.17, 1967, pp.40–57.

30) Ko, H. Y. and Scott, R. F.: Deformation of Sand in Shear, Proc. A.S.C.E., Vol. 93, No.SM5, 1967, pp.283–310.

31) Ko, H. Y. and Scott, R. F.: Deformation of Sand at Failure, Proc. A.S.C.E., Vol.94, No.SM4, 1968, pp.883–898.

32) Miyamori, T. and Shiraishi, T.: Deformation of Sand in Stress Condition $\sigma_2 \neq \sigma_3$, Proc., Annual Meeting of J.S.C.E. (27th), III-27, 1972, pp.72–82, (in Japanese).

33) Sugiuchi, Y.: Shear Characteristics of Compacted Clay during Simple Shear under Triaxial Stress Condition, Proc., Annual Meeting of J.S.C.E. (27th), III-49, 1972, pp.147–148, (in Japanese).

34) Ōmaki, S.: Deformation and Yield Value of Clays, Graduation Thesis, Kyoto Univ., 1968, (in Japanese).

35) Ishihara, K., Tatsuoka, F. and Yasuda, S.: Undrained Repeated Shear Characteristics of Saturated Sands, Proc., Annual Meeting of J.S.C.E. (27th), III-58, 1972, pp.177–180, (in Japanese).

36) Roscoe, K. H., Schofield, A. N. and Wroth, C. P.: On the Yielding of Soils, Geotechnique, Vol.8, 1958, pp.22–53.

37) Schofield, A. N. and Wroth, C. P.: Critical State Soil Mechanics, Mcgraw-Hill, London, 1968.

38) Bowden, F. P. and Tabor, D.: The Friction and Lubrication of Solids, Oxford, 1954.

CHAPTER 4

STRESS-STRAIN RELATIONSHIP OF CLAYEY SOIL[1),2),3),4)]

4.1 GENERAL DESCRIPTION

It is the generally accepted theory in soil mechanics that sand and clay are essentially different materials and, therefore, should be studied for their mechanical properties separately from each other. In fact, when one takes into account not merely the difference in grain size (4.76 to 0.074 mm for sand and less than 0.005 mm for clay) but also the properties of adsorbed water surrounding clay particles, the physico-chemical interaction between clay particle and pore fluid, the variety of structures formed by clay particles and so on, one naturally reaches the conclusion that the mechanical properties of sand and those of clay are different. For example, the time effects and temperature effects such as outstanding creep characteristics and stress relaxation characteristics manifested by clay are thought to have something to do with the aforementioned properties. In the present chapter, the author focusses his particular attention to the observation that sand and clay, which are regarded as apparently different materials as mentioned above, exhibit similarity in shear behavior as will be shown below.

Fig.1.4.1 represents the results of drained shear test on clay as published by

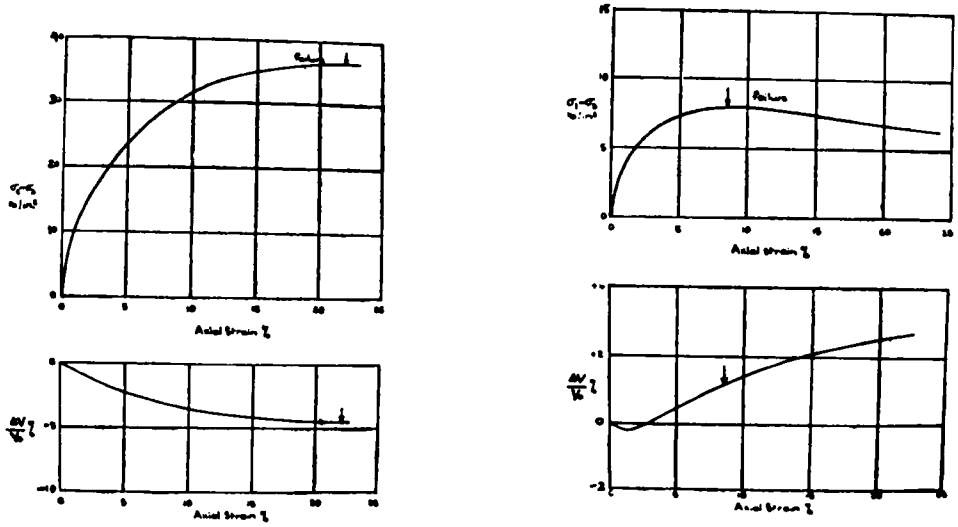

(a) Normally consolidated clay (b) Overconsolidated clay (O.C.R. = 24)

Fig.1.4.1 Relationship among $(\sigma_1 - \sigma_3)$, ϵ_1 and $\Delta V/V$ measured in drained triaxial compression test on normally consolidated and overconsolidated clay (after Henkel[5)]).

D. J. Henkel[5]. The diagram of (a) represents the data of normally consolidated clay and that of (b) the data of overconsolidated clay of which the overconsolidation ratio (O.C.R.) is 24. A look at these diagrams may possibly cause the reader to perceive the resemblance of the curves of (b) and (a) to those of stress-strain-volumetric change properties of dense sand and loose sand respectively. In fact, the measured values plotted on these diagrams, if rearranged in terms of the $\tau/\sigma_N \sim d\epsilon_N/d\gamma$ relationship on the mobilized plane as in the case of sand, seem to describe substantially straight lines (relevant data omitted). In the light of this observation, the author seeks in this chapter to apply to clay the various formulas of stress-strain relationships derived in Chapter 3 with respect to sand and, at the same time, consider related mechanisms.

4.2 SPECIMENS AND APPARATUS USED IN TEST

Clays known as Fujinomori clay, Umeda clay and Kaoline clay were used as test specimens.

Fujinomori clay is collected in the vicinity of Fujinomori, Fushimi of Kyoto and is sold in the form of dry powdered clay. For the test, this clay was kneaded with water and then subjected to preliminary consolidation (under a pressure of about 0.5 kg/cm^2) prior to use. The clay was found to have 44% of L.L., 26% of P.L. and 2.68 of specific gravity. In the classification with the ternary coordinates system, it fell in the category of silty clay loam. The distribution curve of its grain sizes is shown in Fig.1.4.2.

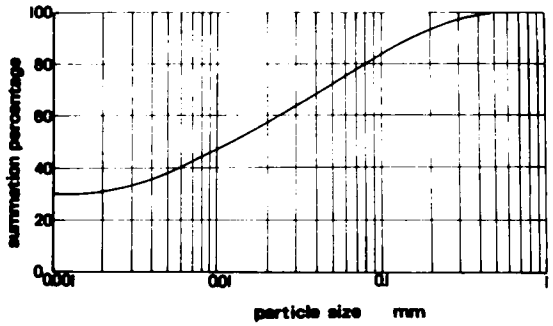

Fig.1.4.2 Grain size distribution curve of Fujinomori clay.

Umeda clay was a remolded, reconsolidated clay prepared from the alluvial clay occurring in Umeda of Osaka. It was found to have 77% of L.L., 32% of P.L. and 2.68 of specific gravity. In the classification with the ternary coordinates system, it fell in the category of clay. The distribution curve of its grain sizes is shown in Fig.1.4.3.

Kaoline clay was prepared by mixing kaoline and bentonite at a ratio of 40 : 1

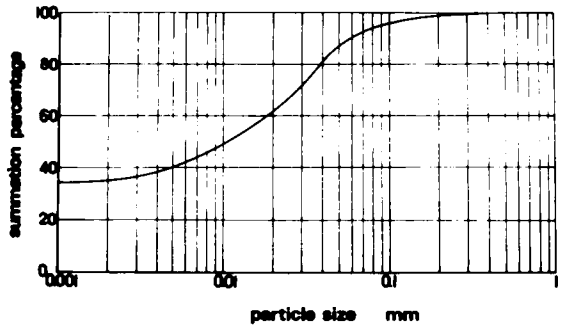

Fig.1.4.3 Grain size distribution curve of Umeda clay.

(by weight), rekneading the mixture with water and then subjected to preliminary consolidation (under a pressure of about 2 kg/cm^2). It was found to have 50% of L.L., 33% of P.L. and 2.72 of specific gravity. The distribution curve of its grain sizes is shown in Fig.1.4.4

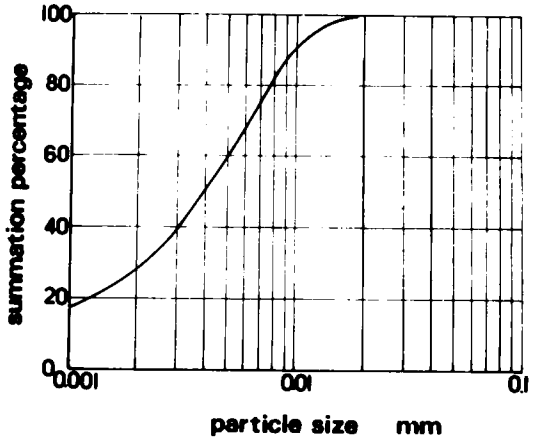

Fig.1.4.4 Grain size distribution curve of Kaoline clay.

Test specimens were formed in the shape of cylinders 3.5 cm in diameter and 8 cm in height. To lessen possible friction on the upper and lower end faces, a rubber membrane coated with silicone grease was inserted between the loading cap and the upper end of each test specimen and another rubber membrane similarly coated with silicone grease was placed to intervene between the lower end of the test specimen and an Araldite disc mounted on a porous stone. To provide drain path for the test piece, not only the lateral face of the test specimen but also that of porous stone were wrapped in filter paper of paper drain.

For the present test an ordinary triaxial apparatus (N.G.I. type made by Geonor) was used. The apparatus is too popular to call for any detailed description. In the drained traixial test, the shear speed was fixed at a sufficiently low level of 7200.01 min/10 mm.

4.3 VERIFICATION BY TEST DATA

4.3.1 Verification of Relationship between Shear-Normal Stress Ratio (τ/σ_N) and Normal-Shear Strain Increment Ratio ($d\epsilon_N/d\gamma$)

The formula of the $\tau/\sigma_N \sim d\epsilon_N/d\gamma$ relationship on the mobilized plane derived in Paragraph 2.7 of Chapter 2 is reinserted below:

$$\frac{\tau}{\sigma_N} = \lambda \cdot \left(-\frac{d\epsilon_N}{d\gamma}\right) + \mu \qquad (1.4.1)$$

where, μ denotes the coefficient of interparticle friction and λ a constant on the order of 1.1 to 1.5 to be determined by the value of μ. Here, the expression of (1.4.1) will be discussed with reference to the data of the drained triaxial test on clay. To begin with, Fig.1.4.5 represents the data of the drained triaxial compression test conduct-

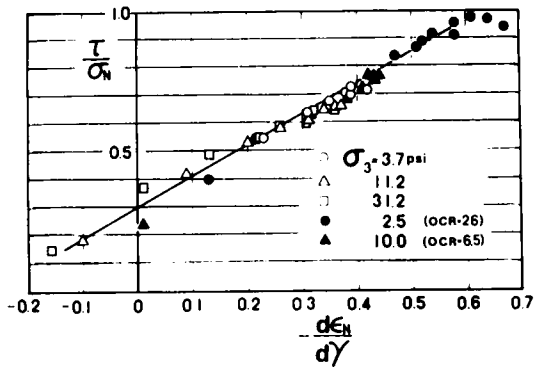

Fig.1.4.5 Relationship between τ/σ_N and $d\epsilon_N/d\gamma$ on one mobilized plane measured in drained triaxial compression test on normally consolidated and overconsolidated clay.

ed by B. Ladanyi et al[6] on clay, as rearranged in terms of the $\tau/\sigma_N \sim d\epsilon_N/d\gamma$ relationship on a single mobilized plane. The plot is seen to form a substantially straight line and found to give $\mu = 0.30$ and $\lambda = 1.1$. What is particularly interesting to note is the fact that the relevant coordinates substantially fall on one line for both normal consolidation (N.C.; indicated by white marks) and overconsolidation (O.C.; indicated by black marks). The data of the drained triaxial test of clay by D. J. Henkel[5] already introduced in Paragraph 4.1 and the data of the drained triaxial test on silt conducted by A.D.M. Penman[7] when arranged in the method mentioned above, seem to give substantially linear plots (relevant data omitted). The value of the ordinate intersection as obtained by the said arrangement of data appears to vary in an approximate range of from 0.2 to 0.5, depending on the kind of clay. As will be described in further detail afterward, it is considered to be equivalent to the physical constant corresponding to the interparticle friction of sand.

Strictly speaking, the shear test aimed at verification of the expression of (1.4.1)

ought to be performed under the conditions of a constant mean principal stress σ_m which is considered to produce strain exclusively ascribable to dilatancy. Fig.1.4.6

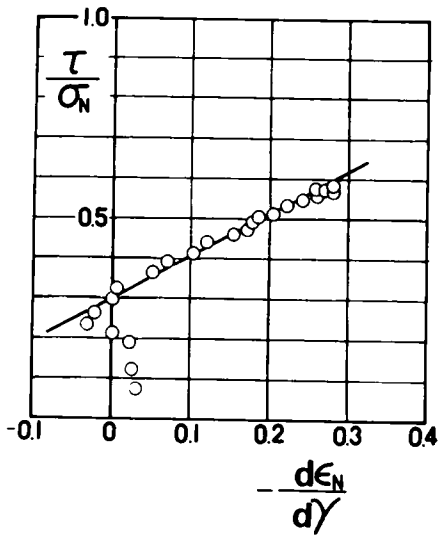

Fig.1.4.6 Relationship between τ/σ_N and $d\epsilon_N/d\gamma$ on one mobilized plane measured in drained triaxial compression test on normally consolidated Fujinomori clay.

represents the results of the drained triaxial test (N.C., initial water content $w_i = 33.2\%$) using Fujinomori clay as test specimen with the mean principal stress σ_m fixed at 1.0 kg/cm^2, rearranged in terms of the $\tau/\sigma_N \sim d\epsilon_N/d\gamma$ relationship on the mobilized plane similarly to the former case. From this diagram, it is seen that in the initial stage of shear, the plot tends to go up from below because of insufficient mobilization of ϕ_μ, that in the subsequent stage, the plot describes a substantially straight line and that the linear gradient λ is approximately 1.1 and the ordinate intersection μ seems to assume a value on the order of 0.30. Fig.1.4.7 represents the results of the drained triaxial test ($w_i = 30.7\%$) using an overconsolidated Fujinomori clay (O.C.R. = 1.5) and involving a fixed mean principal stress $\sigma_m = 1.0$ kg/cm^2, as rearranged in terms of the relationship mentioned above. The ordinate intersection if found from this diagram to assume a value in the neighborhood of 0.27. Comparison of this diagram with that of Fig.1.4.6 leads to a speculation that the data give substantially the same linear plot as those of normally consolidated clay. To seek the physical meaning of the value (about 0.27 to 0.30) of ordinate intersection for clay, the author carried out the following test. The simple shear test was conducted by using dry powder of Fujinomori clay as test specimen and the results were plotted in terms of the $\tau/\sigma_N \sim d\epsilon_N/d\gamma$ relationship on the true mobilized plane (see 3.5.8). Fig.1.4.8 shows the plot thus obtained. From this diagram, the linear gradient λ is found to be 1.2 - 1.3 in satisfactory agreement with

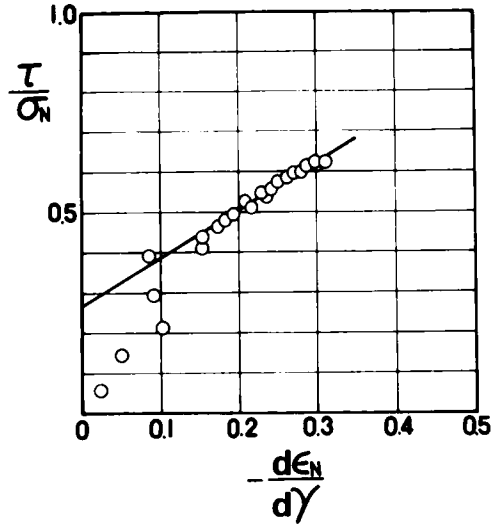

Fig.1.4.7 Relationship between τ/σ_N and $d\epsilon_N/d\gamma$ on one mobilized plane measured in drained triaxial compression test on overconsolidated Fujinomori clay.

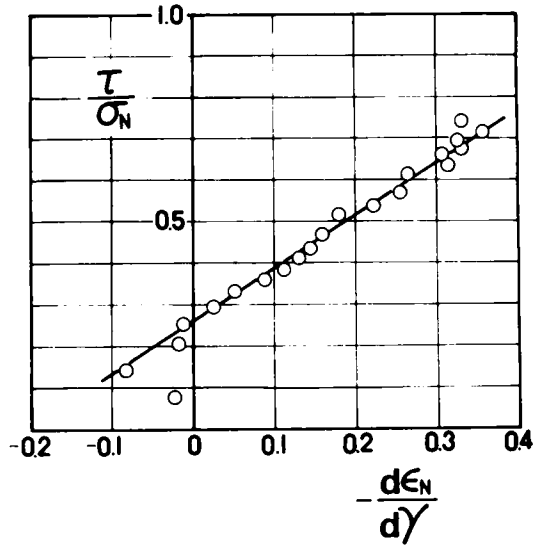

Fig.1.4.8 Relationship between τ/σ_N and $d\epsilon_N/d\gamma$ on mobilized plane measured in simple shear test on dry powder of Fujinomori clay.

the expression of (1.4.1). In this case, however, particular attention should be given to the value μ of ordinate intersection. The powdered Fujinomori clay, whether it is dried indoors or it is dried in an oven (110°C), shows the value of μ in the range of 0.25 to 0.30 which satisfactorily agrees with the range of 0.27 to 0.30 (see Fig.1.4.6 and Fig.1.4.7) for the value μ of ordinate intersection for a saturated test specimen of Fujinomori clay. This is an interesting experimental fact suggesting a possibility that the factor μ which is considered to correspond to the coefficient of friction of clay is not

appreciably affected by the pore fluid but is governed by the grain-to-grain contact.

Fig.1.4.9 represents the results of the drained triaxial test using Umeda clay of normal consolidation under a fixed value of $\sigma_3 = 1.0$ kg/cm^2, as rearranged in terms of the same relationship as mentioned above. From this diagram, the values of λ and μ are found to be 0.9 and 0.42 respectively. Fig.1.4.10 represents the values of the drained triaxial test conducted on Kaoline clay (O.C.R. = 1.5) under a fixed value $\sigma_3 = 4.0$ kg/cm^2, as rearranged in terms of the same relationship. The values of λ and μ are found from this diagram to assume the values of 1.2 and 0.29 respectively.

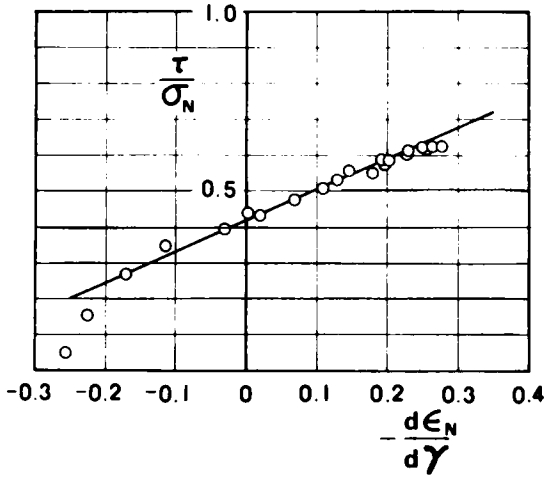

Fig.1.4.9 Relationship between τ/σ_N and $d\epsilon_N/d\gamma$ on one mobilized plane measured in drained triaxial compression test on normally consolidated Umeda clay.

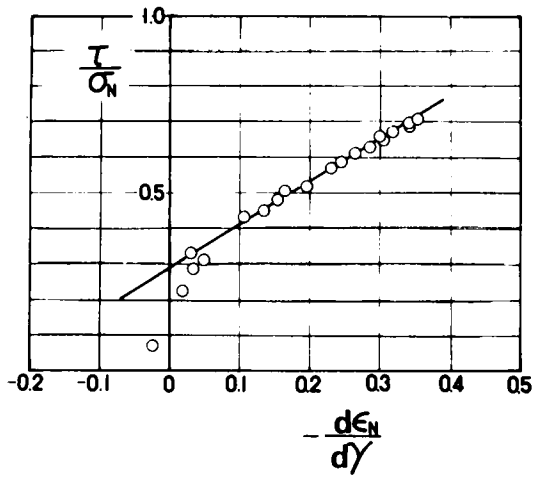

Fig.1.4.10 Relationship between τ/σ_N and $d\epsilon_N/d\gamma$ on one mobilized plane measured in drained triaxial compression test on overconsolidated Kaoline clay.

Now, the author proposes to consider the problem on why the equation of (1.4.1) (or, as formerly designated, Formula 1.2.36) derived with respect to such granular

soil as sand by assuming a mechanism depicted in Fig.1.2.11 of Paragraph 2.7, Chapter 2 is likewise applicable to clay. Fig.1.4.11 represents the structure of a quick clay

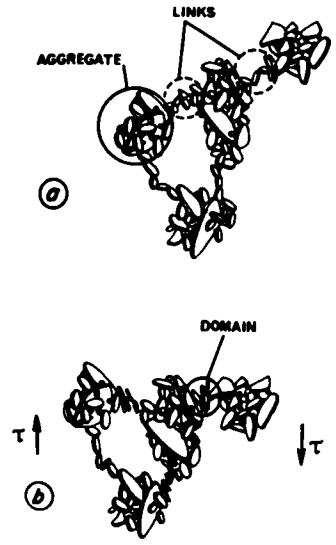

Fig.1.4.11 Microstructure of a quick clay (after Pusch[8]).

which R. Pusch[8] has sketched from many electron microscopic observations of the structure of clay. Pusch holds a position that, in clay, masses each composed of an assembly of several clay particles called aggregates are present in the form of secondary particles. If such aggragates behave as the unit of activity in shear similarly to the individual sand grains, then there may be a possibility that the aforementioned mechanism of shear with respect to sand will be applicable to clay. The question as to whether this is really the true mechanism of shear in clay is yet to be answered by ample effective use of the electron microscope, X-ray diffraction system and other instruments. For the purpose of the present study, the author wishes to proceed with analysis by assuming the aforementioned hypothesis as provisionally acceptable.

According to this concept, the phenomenon that Mohr's failure envelope as represented in Fig.1.4.12 gives rise to two linear (or curved) lines of different inclinations

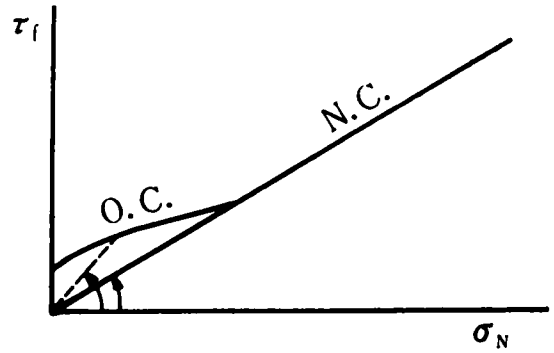

Fig.1.4.12 Mohr's failure envelope of normally consolidated and overconsolidated clay.

depending on normal consolidation and overconsolidation can easily be interpreted. In most cases, the failure envelope of normally consolidated clay gives a substantially straight line past the origin. A possible explanation for this may only require a postulation that, when subjected to shear, the normally consolidated clay shows a steady decline in volume and finally reaches the peak strength near the $d(\Delta V/V)/d\gamma = 0$ as is indicated by Fig.1.4.1 (a) and that, as is evident from the correspondence between $d(\Delta V/V)/d\gamma$ and $d\epsilon_N/d\gamma$, the stress ratio (τ_f/σ_N) at that point has a fixed value. By contrast, when the overconsolidated clay is subjected to shear, it appears to reach the peak strength (τ_f/σ_N) when the value of the ratio of $d(\Delta V/V)$ to $d\gamma$ assumes the maximum minus value (with the side of volumetric expansion taken as negative) as indicated in Fig.1.4.1 (b). However, since the maximum value of $d(\Delta V/V)/d\gamma$ tends to increase with increasing value of the overconsolidation ratio (O.C.R.), the ratio of τ_f/σ_N is likewise increased to give rise to a curve which rises above the failure envelope for normal consolidation as shown in Fig.1.4.12.

4.3.2 Verification of Relationship between Principal Stress Ratio (σ_1/σ_3) and Principal Strain Increment Ratio $(d\epsilon_3/d\epsilon_1)$

As already described in Chapter 3, the formula of the relationship between principal stress ratio (σ_1/σ_3) and principal strain increment ratio $(d\epsilon_3/d\epsilon_1)$ can be derived by converting the $\tau/\sigma_N \sim d\epsilon_N/d\gamma$ relationship existing on the mobilized plane into the relationship on the principal stress plane while assuming that the principal stresses and the principal strain increments agree in direction (see Formula (1.2.43) of Paragraph 2.7, Chapter 2). In the case of triaxial compression test, there is obtained the following equation as indicated by the formula of (1.3.16) of Sub-paragraph 3.5.2.

$$\frac{d\varepsilon_3}{d\varepsilon_1} = \frac{1}{2} \cdot \frac{\sigma_1/\sigma_3 - 2\mu \cdot \sqrt{\sigma_1/\sigma_3} + (\lambda - 1)}{(1-\lambda) \cdot \sigma_1/\sigma_3 - 2\mu \cdot \sqrt{\sigma_1/\sigma_3} - 1} \qquad (1.4.2)$$

For the verification of the equation given above, the results of the drained triaxial compression test using Fujinomori clay under a fixed mean principal stress $\sigma_m = 1.0$ kg/cm^2 were used. The plot thus obtained is shown in Fig.1.4.13. In this diagram, the solid line is a theoretical curve of the values calculated by using in Eq. (1.4.2) the values of $\mu = 0.30$, which is considered to be equivalent to the interparticle friction of Fujinomori clay, and $\lambda = 1.1$ (see Fig.1.4.6). In this diagram, the shear strain at the point at which the plot rising from the lower righthand side begins to overlap the said theoretical curve is found to be about 0.7%. Therefore, the principal portion up to the peak strength, it is believed, may be interpreted by Eq. (1.4.2).

To be definitely strict, the test conducted by using a fixed value of σ_m is considered to be appropriate for the purpose of verification of the formula of (1.4.2). It is considered, however, that this verification may approximately be accomplished by

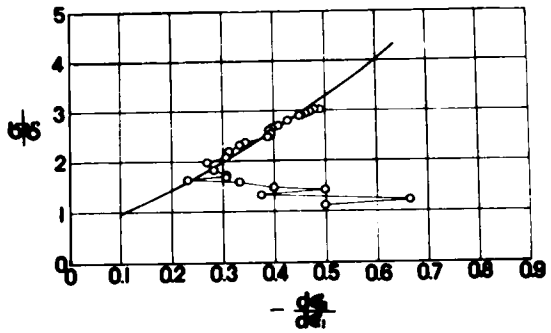

Fig.1.4.13 Relationship between σ_1/σ_3 and $d\epsilon_3/d\epsilon_1$ in drained triaxial compression test on Fujinomori clay.

use of the data of the drained triaxial test involving a fixed value of σ_3 which is easy to perform. In this respect, normally consolidated Umeda clay was subjected to drained triaxial compression test involving a fixed value of $\sigma_3 = 1.0$ kg/cm^2. Fig. 1.4.14 represents the results of this test, as rearranged in terms of the relationship be-

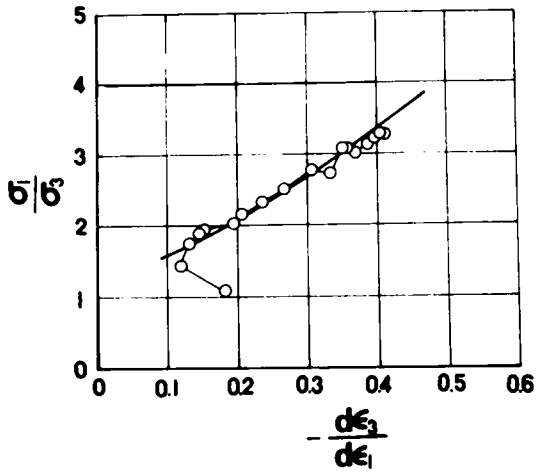

Fig.1.4.14 Relationship between σ_1/σ_3 and $d\epsilon_3/d\epsilon_1$ in drained triaxial compression test on Umeda clay.

tween σ_1/σ_3 and $d\epsilon_3/d\epsilon_1$. In the diagram, the solid line represents a theoretical curve of the values calculated by using in Eq. (1.4.2) the values of $\lambda = 0.9$ and $\mu = 0.42$ (see Fig.1.4.9). A possible reason for the relatively small value of λ is that Umeda clay has a high degree of compressibility and, therefore, reflects an influence not ascribable to the test conditions involving a constant σ_m. Fig.1.4.15 represents the results of the drained triaxial compression test using an overconsolidated Kaoline clay (O.C.R. = 1.5) under a fixed value of $\sigma_3 = 4.0$ kg/cm^2, as rearranged in terms of the same relationship as previously mentioned. In the diagram, the solid line represents the values calculated by using in Eq. (1.4.2) the values $\lambda = 1.2$ and $\mu = 0.29$

(see Fig.1.4.10). From all these diagrams, it is noted that the formula of (1.4.2) provides a satisfactory explanation to the measured values relating not only to sand but also to various kinds of clay.

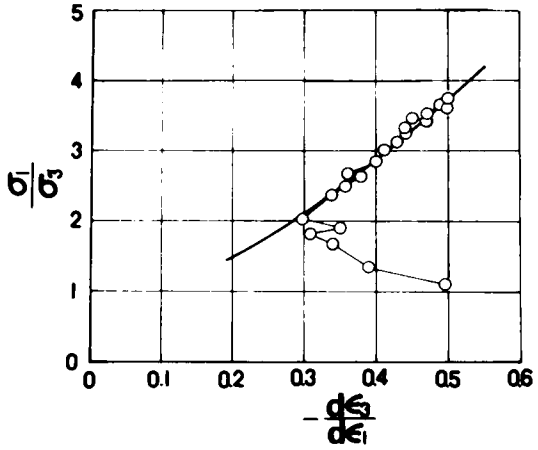

Fig.1.4.15 Relationship between σ_1/σ_3 and $d\epsilon_3/d\epsilon_1$ in drained triaxial compression test on Kaoline clay.

4.3.3 Verification of Relationship among Shear-Normal Stress Ratio (τ/σ_N), Shear Strain (γ) and Normal Strain (ϵ_N)

In Paragraph 3.3 of Chapter 3, the author derived the formula of the relationship between shear-normal stress ratio (τ/σ_N) and shear strain (γ) and that of the relationship between normal strain (ϵ_N) and shear strain (γ) existing on a single mobilized plane. They are restated below for the reader's convenience.

$$\frac{\tau}{\sigma_N} = (\mu' - \mu) \cdot \log_e \frac{\gamma}{\gamma_0} + \mu$$

$$= 2.3\,(\mu' - \mu) \cdot \log_{10} \frac{\gamma}{\gamma_0} + \mu \qquad (1.4.3)$$

$$\epsilon_N = \frac{\mu - \mu'}{\lambda} \cdot \gamma \cdot \left\{ \log_e \frac{\gamma}{\gamma_0} - 1 \right\}$$

$$= \frac{\mu - \mu'}{\lambda} \cdot \gamma \cdot \left\{ 2.3 \log_{10} \frac{\gamma}{\gamma_0} - 1 \right\} \qquad (1.4.4)$$

The plots of the measured data for the equation given above are shown in Fig.1.4.16 and Fig.1.4.17 respectively. Fig.1.4.16 represents the data of triaxial compression test on Fujinomori clay ($\sigma_m = 1.0$ kg/cm^2, N.C.) as plotted in terms of the relationship of $\tau/\sigma_N \sim \gamma \sim \epsilon_N$ existing on a single mobilized plane in conjunction with the curve of the

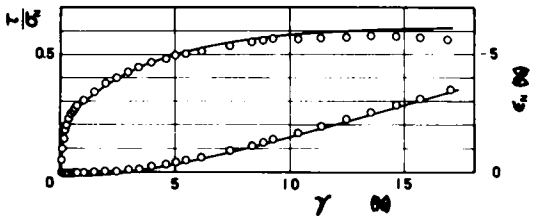

Fig.1.4.16 Relationship among τ/σ_N, γ and ϵ_N on one mobilized plane in drained triaxial compression test on Fujinomori clay.

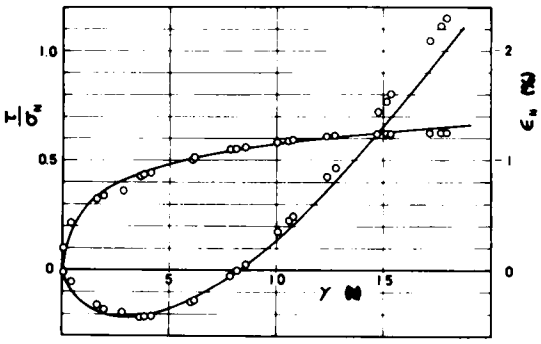

Fig.1.4.17 Relationship among τ/σ_N, γ and ϵ_N on one mobilized plane in drained triaxial compression test on Umeda clay.

values calculated in accordance with Eqs. (1.4.3) and (1.4.4). In the related calculations, the coefficients $\lambda = 1.1$, $\mu = 0.30$, $\mu' = 0.42$ proper to Fujinomori clay and $\gamma_0 = 1\%$ were used. Fig.1.4.17 represents the data of triaxial compression test (σ_3 = 1.0 kg/cm^2, N.C.) on Umeda clay as plotted in terms of the $\tau/\sigma_N \sim \gamma \sim \epsilon_N$ relationship existing on a single mobilized plane in conjunction with the curve of the values calculated in accordance with Eqs. (1.4.3) and (1.4.4). In the related calculations the coefficients $\lambda = 0.9$, $\mu = 0.42$, $\mu' = 0.55$ and $\gamma_0 = 3\%$ were used. The values of coefficients just mentioned were determined by the method described in Paragraph 3.7 of Chapter 3. It is observed from these diagrams that the curves of calculated values are in satisfactory agreement with the measured data also in the case of clay.

4.3.4 Verification of $\tau/\mu\cdot\sigma_N \sim \gamma/\gamma_0$ Relationship

The following equation is obtained by dividing both sides of the equation (1.4.3) by μ.

$$\frac{\tau}{\mu \cdot \sigma_N} = \left(\frac{\mu'}{\mu} - 1\right) \cdot \log_e \frac{\gamma}{\gamma_0} + 1$$

$$= 2.3 \left(\frac{\mu'}{\mu} - 1\right) \cdot \log_{10} \frac{\gamma}{\gamma_0} + 1 \qquad (1.4.5)$$

The formula given above may well be considered to be what is obtained by normalizing τ and γ respectively with $\mu \cdot \sigma_N$ ($\equiv \tau_0$) and γ_0. Further, this formula implies that the ratios $\tau/\mu \cdot \sigma_N$ and γ/γ_0 give rise to linear plots past the point (1, 1) on a semi-logarithmic section paper. It represents the results of plotting the measured values on the graphs of Fig.1.4.18 and Fig.1.4.19. Fig.1.4.18 represents the relationship of $\tau/\mu \cdot \sigma_N \sim \gamma/\gamma_0$ derived for Fujinomori clay and this graph indicates that the data, irrespectively of

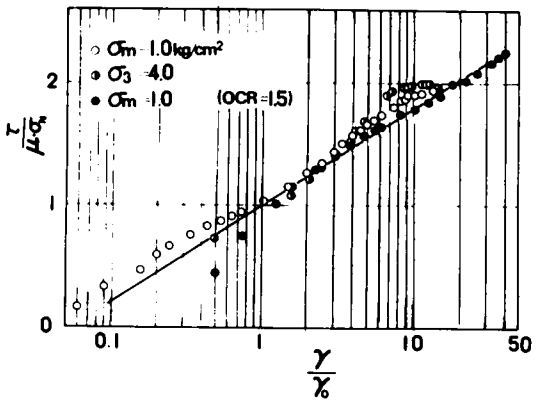

Fig.1.4.18 Relationship between $\tau/\mu \cdot \sigma_N$ and γ/γ_0 on one mobilized plane measured in drained triaxial compression tests on Fujinomori clay.

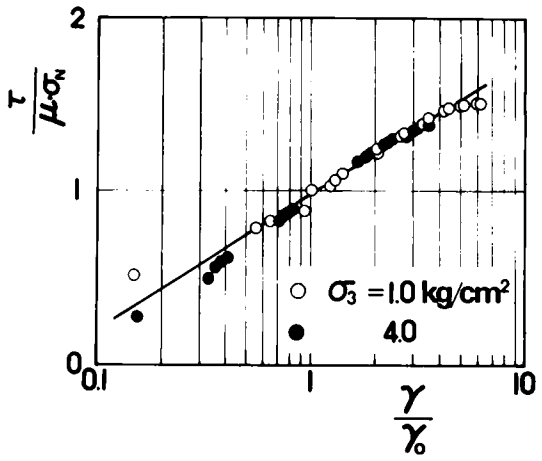

Fig.1.4.19 Relationship between $\tau/\mu \cdot \sigma_N$ and γ/γ_0 on one mobilized plane measured in drained triaxial compression tests on Umeda clay.

the magnitude of confining stress, describe linear plots substantially past the point (1, 1). The test conditions were $\sigma_m = 1.0$ kg/cm^2 for normally consolidated clay (ϕ marks), $\sigma_3 = 4.0$ kg/cm^2 for normally consolidated clay (o marks) and $\sigma_m = 1.0$ kg/cm^2 and an overconsolidation ratio 1.5 for overconsolidated clay (● marks) respectively. Fig.1.4.19 represents the results of plotting of the data obtained of Umeda clay. Again, the data

appear to describe linear plots substantially past the point (1, 1), irrespectively of the magnitude of confining stress. The test conditions in this case were $\sigma_3 = 1.0$ kg/cm^2 for normally consolidated clay (o marks) and $\sigma_3 = 4.0$ kg/cm^2 for normally consolidated clay (● marks) respectively. Although the data available are rather small in volume, they seem to justify a conclusion that the equation of (1.4.5) substantially holds good also for the case of clay.

4.3.5 Verification of Relationships between Principal Stress Ratio (σ_1/σ_3) and Principal Strains (ϵ_1 and ϵ_3) under Triaxial Compression and Extension Stress Conditions.

In Paragraph 3.4 of Chapter 3, the author derived the following formula as indicating the relationship between principal stress ratio (σ_1/σ_3) and principal strain (ϵ_1 and ϵ_3) under triaxial compression stress conditions ($\sigma_1 \geqq \sigma_2 = \sigma_3$):

$$\epsilon_1 = 2\,f\left(\frac{\sigma_1}{\sigma_3}\right), \quad \epsilon_2 = \epsilon_3 = g\left(\frac{\sigma_1}{\sigma_3}\right) \tag{1.4.6}$$

wherein, $X \equiv \sqrt{\sigma_1/\sigma_3} - \sqrt{\sigma_3/\sigma_1}$

$$f\left(\frac{\sigma_1}{\sigma_3}\right) = \frac{\gamma_0 \cdot \exp\left(-\frac{\mu}{\mu'-\mu}\right)}{2} \cdot \exp\left\{\frac{X}{2(\mu'-\mu)}\right\}$$

$$\cdot\left\{\frac{X^2}{8} + \left(\frac{1}{2} - \frac{1}{\lambda} - \frac{\mu'-\mu}{2}\right) \cdot X + (\mu'-\mu)^2 - (\mu'-\mu) + \frac{2\mu'}{\lambda} + 1\right\}$$

$$g\left(\frac{\sigma_1}{\sigma_3}\right) = \frac{\gamma_0 \cdot \exp\left(-\frac{\mu}{\mu'-\mu}\right)}{2} \cdot \exp\left\{\frac{X}{2(\mu'-\mu)}\right\}$$

$$\cdot\left\{-\frac{X^2}{8} + \left(\frac{1}{2} - \frac{1}{\lambda} + \frac{\mu'-\mu}{2}\right) \cdot X - (\mu'-\mu)^2 - (\mu'-\mu) + \frac{2\mu'}{\lambda} - 1\right\}$$

Therefore, the volumetric strain ($\Delta V/V$) can be expressed as a function of the principal stress ratio (σ_1/σ_3) by the following formula:

$$\Delta V/V = \epsilon_1 + 2\epsilon_3 = 2\,f\left(\frac{\sigma_1}{\sigma_3}\right) + 2g\left(\frac{\sigma_1}{\sigma_3}\right) \tag{1.4.7}$$

Fig.1.4.20 represents the data of triaxial compression test on Fujinomori clay ($\sigma_m = 1.0$ kg/cm^2, N.C.) as plotted in terms of the $\sigma_1/\sigma_3 \sim \epsilon_1 \sim \Delta V/V$ relationship in conjunction with the curves of the values calculated in accordance with the equations of (1.4.6) and (1.4.7). In the related calculations, the coefficients of $\lambda = 1.1$, $\mu = 0.30$, $\mu' = 0.42$ proper to Fujinomori clay and $\gamma_0 = 1\%$ were used. Fig.1.4.21 represents the data of triaxial compression test on Umeda clay ($\sigma_3 = 1.0$ kg/cm^2, N.C.) as plotted in terms of

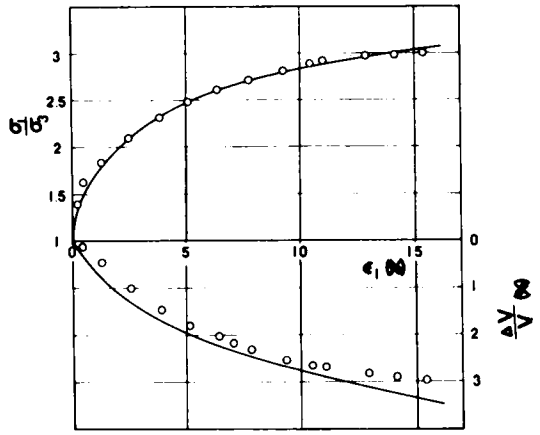

Fig.1.4.20 Relationship among σ_1/σ_3, ϵ_1 and $\Delta V/V$ in drained triaxial compression test on Fujinomori clay.

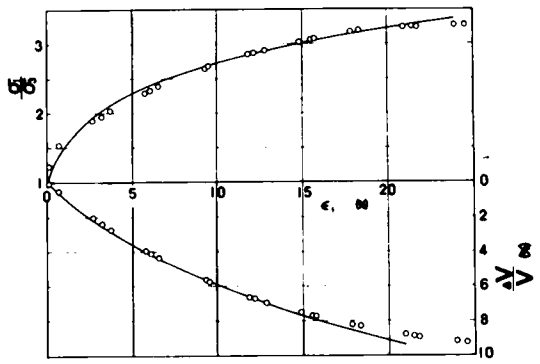

Fig.1.4.21 Relationship among σ_1/σ_3, ϵ_1 and $\Delta V/V$ in drained triaxial compression test on Umeda clay.

the $\sigma_1/\sigma_3 \sim \epsilon_1 \sim \Delta V/V$ relationship in conjunction with the curves of values calculated in accordance with Eqs. (1.4.6) and (1.4.7). In the related calculations the coefficients $\lambda = 0.9$, $\mu = 0.42$, $\mu' = 0.55$ proper to the used clay and $\gamma_0 = 3\%$ were used.

Fig.1.4.22 shows the data of triaxial compression and triaxial extension tests on normally consolidated Fujinomori clay ($\sigma_m = 1$, 2, 3 kg/cm^2) as plotted in terms of the relationship of $\Delta V/V \sim (\sigma_1 - \sigma_3)/\sigma_m$. The horizontal axis, $(\sigma_1 - \sigma_3)/\sigma_m$, of this graph is the scale of what Shibata, Karube et al.[9)10)] have proposed as a parameter capable of uniquely defining the amount of dilatancy of clay as previously treated of in Chapter 3. According to the concept underlying Eqs. (1.4.6) and (1.4.7) (for the details, see Paragraph 3.4 of Chapter 3), it is concluded that the dilatancy of soil is governed by the ratio σ_1/σ_3 or τ/σ_N. When the same data as those of Fig.1.4.22 are rearranged in terms of the relationship of $\Delta V/V \sim \tau/\sigma_N$, the results are as shown in Fig.1.4.23. In the diagram, the solid line represents the curve of values calculated in accordance with

the equation (1.4.7). It appears from these diagrams that dilatancy of clay is governed by τ/σ_N (or σ_1/σ_3) and not by the ratio of $(\sigma_1 - \sigma_3)/\sigma_m$ ($\equiv q/p$).

The diagrams discussed above indicate that the equations of (1.4.6) and (1.4.7) provide a satisfactory explanation to the measured values even in the case of clay.

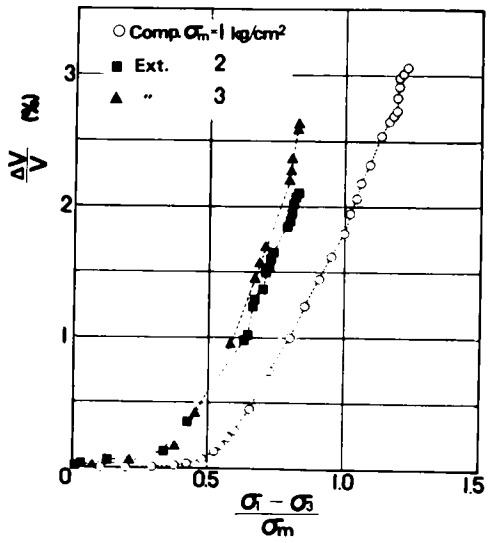

Fig.1.4.22 Relationship between $\Delta V/V$ and $(\sigma_1 - \sigma_3)/\sigma_m$ in triaxial compression and extension tests on Fujinomori clay.

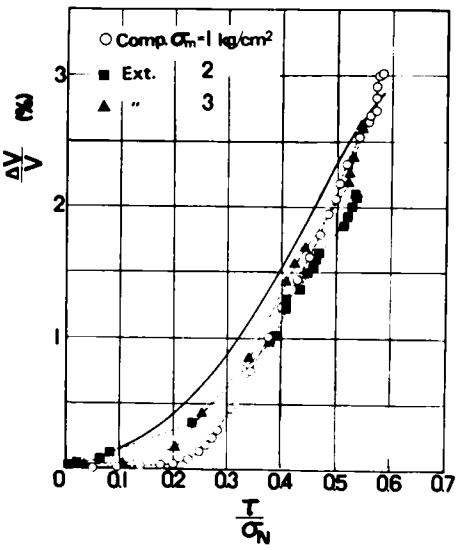

Fig.1.4.23 Relationship between $\Delta V/V$ and τ/σ_N in triaxial compression and extension tests on Fujinomori clay.

4.4 APPLICATION TO UNDRAINED SHEAR TEST, ETC.

As already pointed out in Paragraph 3.6 of Chapter 3, the following equations can be derived by assuming that the strain generally produced in the soil element is the combination of the strain ascribable to consolidation with the strain resulting from dilatancy.

$$\frac{\triangle V}{V} = \left(\frac{\triangle V}{V}\right)_c + \left(\frac{\triangle V}{V}\right)_d \qquad (1.4.8)$$

$$\epsilon_1 = (\epsilon_1)_c + (\epsilon_1)_d \qquad (1.4.9)$$

$$\epsilon_3 = (\epsilon_3)_c + (\epsilon_3)_d \qquad (1.4.10)$$

wherein, the suffix "c" stands for the strain due to consolidation and the suffix "d" for the strain caused by dilatancy (or shear).

The volumetric strain $(\Delta V/V)_c$ and the principal strains $(\epsilon_1)_c$, $(\epsilon_2)_c$ and $(\epsilon_3)_c$ caused by consolidation can be expressed by the following formulas, as is universally known. (See Paragraph 3.6 of Chapter 3 for further information.)

$$\left(\frac{\triangle V}{V}\right)_c = \frac{C_c}{1+e} \cdot \log_{10} \frac{\sigma_m}{\sigma_{mi}} \qquad (1.4.11)$$

$$(\epsilon_1)_c = (\epsilon_2)_c = (\epsilon_3)_c = \frac{1}{3} \cdot \frac{C_c}{1+e_i} \cdot \log_{10} \frac{\sigma_m}{\sigma_{mi}} \qquad (1.4.12)$$

wherein, C_c stands for compression (or expansion) index, e_i and σ_{mi} for the initial void ratio and the initial mean effective principal stress existing prior to consolidation. Generally, the volumetric strain $(\Delta V/V)_d$ and the principal strains $(\epsilon_1)_d$ and $(\epsilon_3)_d$ caused by dilatancy can be expressed by the equation of (1.3.9) and, in the case of triaxial compression test, by the equations of (1.4.6) and (1.4.7). This means that the relationship of principal stress ratio σ_1/σ_3, principal strain ϵ_1 and volumetric strain $\Delta V/V$ involving the phenomena of consolidation and shear can be found by calculation.

Since clay has a relatively large compressibility (expansibility), it is considered to be more subject to the effect of strain due to consolidation than the sand. Thus, the author compared the data of the test involving a fixed lateral pressure σ_3 considered to induce both phenomena of consolidation and dilatancy with the data of the test involving a fixed mean effective principal stress σ_m considered to induce only the phenomenon of dilatancy and, at the same time, compared these data with the values calculated in the method described above. Fig.1.4.24 represents the data of the drained triaxial compression test under $\sigma_m = 1.0$ kg/cm^2 and $\sigma_3 = 1.0$ kg/cm^2 as plotted in terms of the $\sigma_1/\sigma_3 \sim \epsilon_1 \sim \Delta V/V$ relationship in conjunction with the curves of values calculated accordingly. In the related calculations, the coefficients $\lambda = 1.1$, $\mu = 0.30$, $\mu' = 0.42$, $\gamma_0 =$

1.0%, $C_c = 0.24$ and $e_i = 0.897$ appropriate to the test specimen were used. From this diagram, it is noted that the relationship of $\sigma_1/\sigma_3 \sim \epsilon_1$ is not appreciably different under two sets of conditions. Fig.1.4.25 shows the measured values relative to the $\epsilon_3 \sim \epsilon_1$

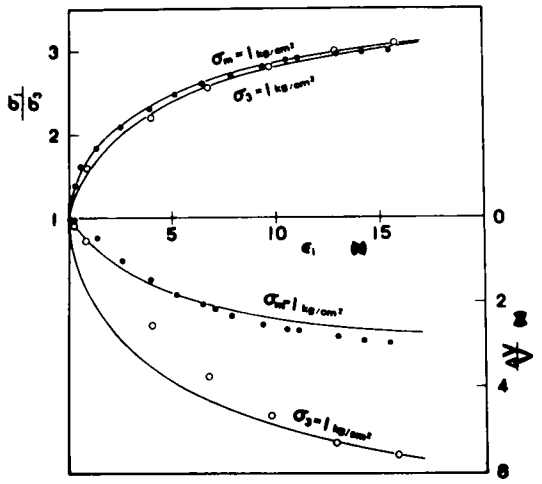

Fig.1.4.24 Relationship among σ_1/σ_3, ϵ_1 and $\Delta V/V$ for σ_m = const. and σ_3 = const. tests on Fujinomori clay.

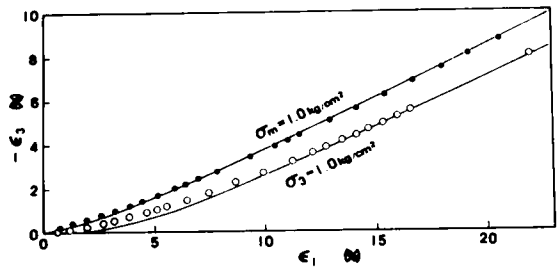

Fig.1.4.25 Relationship between ϵ_1 and ϵ_3 for σ_m = const. and σ_3 = const. tests on Fujinomori clay.

relationship and the curves of values obtained by calculations. These two diagrams seem to suggest a possibility that the values of calculation according to the said concept will approximately express the trend of the measured values of the test involving a fixed value of σ_m and the test involving a fixed value of σ_3.

In the case of the undrained test, necessary calculations can be carried out on condition that, as already described in Paragraph 3.6 of Chapter 3, the sum of the volumetric strain $(\Delta V/V)_c$ due to consolidation and the volumetric strain $(\Delta V/V)_d$ due to dilatancy is 0 (the lefthand member of the equation of (1.4.8) given as 0). Fig.1.4.26 represents the measured values[11] of the undrained triaxial compression test on Fujinomori clay in comparison with the curves (solid lines) of values obtained by calculation. It is

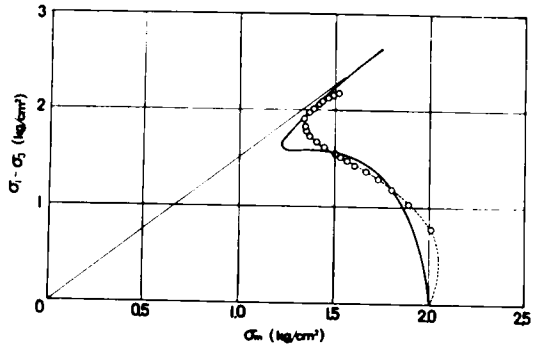

Fig.1.4.26 Relationship between $(\sigma_1 - \sigma_3)$ and σ_m in undrained triaxial compression test on Fujinomori clay.

noted from the graph that the trends of both plots are substantially in agreement. In the calculations mentioned above, there were used the coefficients of $\lambda = 1.1$, $\mu = 0.30$, $\mu' = 0.42$, $\gamma_0 = 0.7\%$, $C_c = 0.24$ and $e_i = 0.776$. Fig.1.4.27 shows a typical calculation of the stress path on the stress plane as proposed by Rendulic. The coefficients which were used in the calculation were $\lambda = 1.1$, $\mu = 0.30$, $\mu' = 0.42$, $\gamma_0 = 1.0\%$, $C_c = 0.24$ and $e_i = 0.897$, with σ_m taken as a variable. The resemblance between the curves

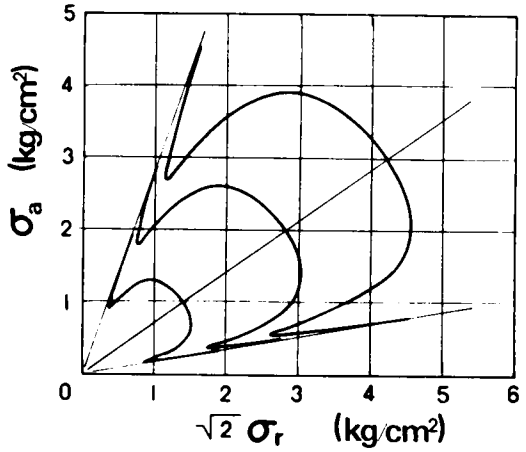

Fig.1.4.27 An example of calculated stress path on Rendulic's stress plane.

reminds us of Henkel's data[12]. It is also interesting to note that the stress path is inverted from left to right on the compression side as well as on the extension side.

What has been discussed to this point verifies that the stress-strain relationship under general conditions inducing the phenomena of consolidation and shear can substantially be explained adequately in accordance with the formulas of the stress-strain relationships due to shear which has been derived in the present work through the microscopic analysis of the mechanism of soil dilatancy and the formulas of the stress-strain relationships due to consolidation which has heretofore been adopted, on condition that

the strain is the combination of the strain resulting from shear with the strain caused by consolidation. It has further been confirmed that, as a special case, the stress path in undrained shear can be calculated on the precondition that the sum of volumetric strains due to the two phenomena is 0.

4.5 CONCLUSIONS

In the present chapter the author, taking special notice of the similarity of shear properties between sand and clay, sought to apply to clay the formulas of the stress-strain relationships which were derived in Chapter 2 from the microscopic analyses and which were experimentally verified with reference to sand and other granular test speciens. In the case of clay which is a mass of fine particles, the author proposes a view that secondary particles each formed as an assembly of several primary particles constitute the unit of activity rather than primary particles or individual clay particles move independently of one another. Even from the standpoint of the electron microscope observations[8),13),14),15)], this concept seems to be more concinving. In the case of clay, such secondary particles are frequently referred to as aggregates. Assuming that one aggregate corresponds with one sand particle, the shear mechanism ascertained with respect to sand is considered to be applicable also to clay. The task for thorough elucidation of the shear mechanism through the microscopic observation of the clay behavior will be reserved for a future study. In the present work, the author has pursued analysis in the light of the observation that sand and clay can be handled phenomenologically in the same way.

The results which have been ascertained in this chapter may be summarized as follows:

(1) It has been verified by triaxial compression test that the linear relationship between shear-normal stress ratio (τ/σ_N) and normal-shear strain increment ratio ($d\epsilon_N/d\gamma$) on the mobilized plane which was derived in Chapter 2 from the microscopic discussion holds good not only for sand but also for Fujinomori clay, Umeda clay and Kaoline clay. Although most test specimens used in the test were those of normally consolidated clay, there are indications that also overconsolidated clay will yield data which will give substantially linear plots. For a fixed test specimen of sand, the data give substantially linear plots, irrespectively of whether the test specimen is packed loosely or densely. It is interesting to note that the same formula of relationship can be applied to both normally consolidated clay and overconsolidated clay. In this connection, this concept can give a convincing explanation to the observation that Mohr's failure envelope describes two linear (or curved) lines of two different trends, depending on normal consolidation and overconsolidation.

(2) The relationship between principal stress ratio (σ_1/σ_3) and principal strain increment ratio ($d\epsilon_3/d\epsilon_1$) derived in Chapter 2 has been compared with the results of triaxial compression test on Fujinomori clay, Umeda clay and Kaoline clay. It has been verified that the values calculated show satisfactory correspondence with the measured values.

(3) The relationship among shear-normal stress ratio (τ/σ_N), shear strain (γ) and normal strain (ϵ_N) on the single mobilized plane derived in Chapter 3 has been verified with respect to the measured data of Fujinomori clay and Umeda clay. Satisfactory correspondence has been confirmed as a consequence.

(4) The values actually measured in accordance with the formula of $\tau/\mu\cdot\sigma_N - \log_{10}(\gamma/\gamma_0)$ relationship on the mobilized plane have been plotted on a semi-logarithmic section paper. Consequently, it has been learnt that under various conditions of confining stress, the data for Fujinomori clay and Umeda clay produce substantially linear plots respectively.

(5) The principal stress ratio (σ_1/σ_3) -principal strain (ϵ_1 and ϵ_3) relationship obtained by converting the formula of the stress-strain relationship on the mobilized plane in terms of the relationship on the principal stress plane has been verified with respect to the measured data of Fujinomori clay and Umeda clay. Satisfactory correspondence has been ascertained. The principal strain is thought to be a strain caused by dilatancy according to the fundamental concept underlying the derivation of the formula. The volumetric strain due to dilatancy has been calculated from the formula of the principal stress ratio to principal strain relationship mentioned above and then compared with the results of triaxial compression test on Fujinomori clay. The measured values and the calculated values have shown satisfactory correspondence. In this case, the formula proposed by the author suggests that the volumetric strain ascribable to dilatancy is governed by the principal stress ratio (σ_1/σ_3) or the shear-normal stress ratio (τ/σ_N) on the mobilized plane. This concept differs from the view advocated by Shibata, Karube et al.[9),10)] that the said volumetric strain is governed by the principal stress difference-mean effective principal stress ratio ($(\sigma_1-\sigma_3)/\sigma_m$) or the octahedral shear-normal stress ratio (τ_{oct}/σ_{oct}). Based on the data of triaxial compression and extension tests on normally consolidated Fujinomori clay, it is judged that dilatancy of clay may be governed uniquely by τ/σ_N (or σ_1/σ_3) and not by the ratio of $(\sigma_1-\sigma_3)/\sigma_{III}$ ($\equiv q/p$).

(6) It has been demonstrated that the relationship of stress and strain under general stress conditions inducing the two phenomena of consolidation and shear, for example, the relationship of stress and strain by the test involving a fixed lateral pressure (σ_3) can be calculated by assuming the combination of the strain due to dilatancy described in (5) above and the strain due to consolidation. It has been ascertained that the results of the calculation can substantially give a satisfactory

explanation to the measured values. Further, the stress path in the undrained test has been calculated by assuming the sum of the volumetric strain due to dilatancy and the volumetric strain caused by consolidation to be 0. When the results of this calculation are compared with the results of the undrained triaxial compression test on Fujinomori clay, the trends of the two are found to be in satisfactory correspondence.

(7) In some aspects, sand and clay are considered to be essentially different. The difference manifests itself in the form of time effects and temperature effects, for example. It is, however, quite interesting to note that in certain aspects, both sand and clay can be handled on the basis of the same principle. This seems to suggest that the shear of sand and that of clay occur in a fundamentally similar mechanism. It is also very interesting to know that the data for normally consolidated clay and those for overconsolidated clay can be handled on the same principle and that the same rule is applicable to drained shear and undrained shear alike. All the observations encourage the author to speculate that the stress-strain relationship, particularly the stress ratio-strain increment ratio relationship, under discussion may be one of the rules to govern the shear phenomenon of soil, i.e., both sand and clay.

References

1) Murayama, S. and Matsuoka, H.: The Mechanism of Shearing and its Similarity for Sands and Clays, Annuals, Disaster Prevention Research Institute, Kyoto University, No.14B, 1971, pp.551–563, (in Japanese).
2) Matsuoka, H.: The Stress-Strain Relation of Soils under Shearing derived from a Microscopic Consideration, Annuals, Disaster Prevention Research Institute, Kyoto University, No.15B, 1972, pp.499–511, (in Japanese).
3) Murayama, S. and Matsuoka, H.: A Microscopic Study on Shearing Mechanism of Soils, Proc. 8th Int. Conf. S.M.F.E., 1973, (to be published).
4) Matsuoka, H.: Stress-Strain Relationship of Soils under Three Different Principal Stresses, Annuals, Disaster Prevention Research Institute, Kyoto University, No.16B, 1973, (to be published in Japanese).
5) Henkel, D. J.: The Effect of Overconsolidation on the Behaviour of Clays during Shear, Géotechnique, Vol.6, 1956, pp.139–150.
6) Ladanyi, B., Larochelle, P. and Tanguay, L.: Some Factors Controlling the Predictability of Stress - Strain Behaviour of Clay, Canadian Geotech. J., Vol.2, No.2, 1965, pp.60–89.
7) Penman, A. D. M.: Shear Characteristics of a Saturated Silt measured in Triaxial Compression, Géotechnique, Vol.3, pp.312–328.

8) Pusch, R.: Micro-structural Changes in Soft Quick Clay of Failure, Canadian Geotech. J., Vol.7, No.1, 1970, pp.1–7.
9) Shibata, T.: On the Volume Changes of Normally-Consolidated Clays, Annuals, Disaster Prevention Research Institute, Kyoto University, No.6, 1963, pp.128–134, (in Japanese).
10) Shitata, T. and Karube, D.: Influence of the Variation of the Intermediate Principal Stress on the Mechanical Properties of Normally Consolidated Clays, Proc. 6th Int. Conf. S.M.F.E., Vol.1, 1965, pp.359–363.
11) Murayama, S., Sekiguchi, H. and Ueda, T.: On the Stress Relaxation Characteristics of Clays, Proc., Annual Meeting of Kansai Br. J.S.C.E., III-1, 1972, (in Japanese).
12) Henkel, D. J.: The Relationships between the Effective Stresses and Water Content in Saturated Clays, Géotechnique, Vol.10, 1960, pp.41–54.
13) Matsuo, S. and Kamon, M.: Study on the Structure of Clayey Soils by Scanning Electron Microscope, Proc., Annual Meeting of J.S.S.M.F.E. (7th), 27, 1972, pp.105–108, (in Japanese).
14) Matsuo, S. and Kamon, M.: Consideration on the Structure of Consolidated Clayey Soils by Scanning Electron Microscope, Proc., Annual Meeting of J.S.C.E. (27th), III-20, 1972, pp.55–58, (in Japanese).
15) Matsuo, S. and Kamon, M.: Microscopic Research on the Consolidated Samples of Clayey Soils, Int. Sym. of Soil Microstructure, 1973, (to be published).

CHAPTER 5

RELATION TO OTHER STUDIES

5.1 GENERAL DESCRIPTION

The author's study has as its building blocks the concept of the angle of the tangential plane at the individual contact points of particles (*angle of interparticle contact*) and the angle of interparticle friction adopted for the first time in Newland and Allely's study[1] and in Rowe's study[2], the concept of the probability distribution of angles of interparticle contact originated by Murayama[3], and the evaluation of the condition of transmission of interparticle force. The author attached special attention to the change of frequency distribution of angles of interparticle contact due to shear and studied the inter-relation of this frequency distribution with the stress-strain-dilatancy characteristics of soil. Based on his microscopic interpretation of the internal mechanism of the shear phenomenon in soil, the author sought to elucidate the basic stress-strain relationship for soil.

Here, the author expresses his view of the stress-dilatancy theory advocated by the Rowe school, the stress ratio-strain increment relationship in the energy theory proposed by the Roscoe school and the strength constant suggested by Hvorslev, which are all considered to have a close bearing on the shear-normal stress ratio $(\tau/\sigma_N) \sim$ normal-shear strain increment ratio $(d\epsilon_N/d\gamma)$ relationship constituting the very foundation of the author's study.

5.2 RELATION TO STUDY BY ROWE SCHOOL[4]

As described in Paragraph 2.2 of Chapter 2, Rowe's stress-dilatancy theory is developed to provide an extensive interpretation of the irregular arrangement of particles by using the minimum-energy ratio criterion in combination with the formula of the relationship existing in the regular arrangement of bars of an equal diameter and balls of equal dimensions. The theory is formulated by the following expression.[2].

$$\frac{\sigma_1}{\sigma_3 \cdot \left(1 - \dfrac{d(\Delta V/V)}{d\epsilon_1}\right)} = \tan^2\left(45^\circ + \frac{\phi_\mu}{2}\right) \qquad (1.5.1)$$

wherein, the volumetric strain $(\Delta V/V)$ satisfies the following equation in the case of triaxial compression test with the compression taken as a positive sign.

$$d(\Delta V/V) = d\epsilon_1 + 2d\epsilon_3$$

Therefore, the expression of (1.5.1) can be converted to the following formula.

$$\frac{\sigma_1 \cdot d\varepsilon_1}{-2\,\sigma_3 \cdot d\varepsilon_3} = \tan^2\left(45^\circ + \frac{\phi_\mu}{2}\right) \qquad (1.5.2)$$

Here, Rowe[5] holds the view that the lefthand side of the preceding equation can be regarded as indicating the ratio of the "*work in*" exerted on a test specimen to the "*work out*" issuing from the test specimen in a state of triaxial compression. By the same token, he has proposed the following formulas with respect to triaxial extension state and plane strain state respectively.

$$\frac{2\,\sigma_1 \cdot d\varepsilon_1}{-\sigma_3 \cdot d\varepsilon_3} = \tan^2\left(45^\circ + \frac{\phi_\mu}{2}\right) \qquad (1.5.3)$$

$$\frac{\sigma_1 \cdot d\varepsilon_1}{-\sigma_3 \cdot d\varepsilon_3} = \tan^2\left(45^\circ + \frac{\phi_\mu}{2}\right) \qquad (1.5.4)$$

From the equation of (1.5.2) through (1.5.4), the following equations indicating the principal stress ratio (σ_1/σ_3) - principal strain increment ratio $(d\varepsilon_3/d\varepsilon_1)$ relationship in the respective states of triaxial compression, triaxial extension and plane strain are derived.

$$\frac{\sigma_1}{\sigma_3} = 2K_\mu \cdot \left(-\frac{d\varepsilon_3}{d\varepsilon_1}\right) \qquad (1.5.5)$$

$$\frac{\sigma_1}{\sigma_3} = \frac{K_\mu}{2} \cdot \left(-\frac{d\varepsilon_3}{d\varepsilon_1}\right) \qquad (1.5.6)$$

$$\frac{\sigma_1}{\sigma_3} = K_\mu \cdot \left(-\frac{d\varepsilon_3}{d\varepsilon_1}\right) \qquad (1.5.7)$$

wherein, $K_\mu \equiv \tan^2(45^\circ + \phi_\mu/2)$. As briefly touched upon in Paragraph 3.3, Chapter 3, the relationship of $\sigma_1/\sigma_3 \sim d\varepsilon_3/d\varepsilon_1$ under any condition is expected, in view of Rowe's stress-dilatancy theory, to give plots of straight lines passing the origin. In the case of triaxial compression, for instance, the equation of (1.5.5) plotted by using $\mu = \tan\phi_\mu$ as a parameter will give a graph like the one shown in Fig.1.5.1.

According to the author's theory, the relationship of $\sigma_1/\sigma_3 \sim d\varepsilon_3/d\varepsilon_1$ in the triaxial compression, triaxial extension and plane strain conditions, as based on the stress-ratio - strain increment ratio relationship of the formula:

$$\frac{\tau}{\sigma_N} = \lambda \cdot \left(-\frac{d\varepsilon_N}{d\gamma}\right) + \mu \qquad (1.5.8)$$

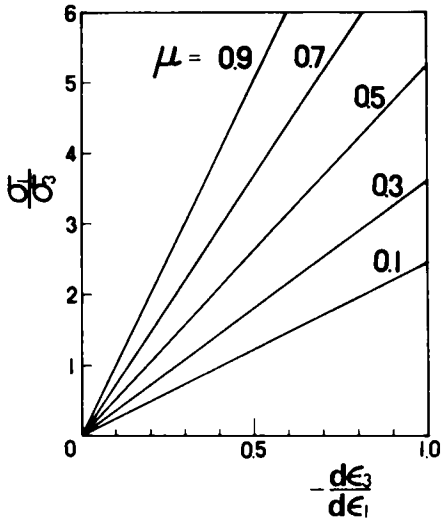

Fig.1.5.1 Relationship between σ_1/σ_3 and $d\epsilon_3/d\epsilon_1$ in triaxial compression stress condition by Rowe's stress-dilatancy theory.

for the mobilized plane, is given by the following equations (see Formulas (1.3.15) through (1.3.17) of Chapter 3).

$$\frac{d\epsilon_3}{d\epsilon_1} = \frac{1}{2} \cdot \frac{\sigma_1/\sigma_3 - 2\mu \cdot \sqrt{\sigma_1/\sigma_3} + (\lambda - 1)}{(1-\lambda) \cdot \sigma_1/\sigma_3 - 2\mu \cdot \sqrt{\sigma_1/\sigma_3} - 1} \tag{1.5.9}$$

$$\frac{d\epsilon_3}{d\epsilon_1} = 2 \cdot \frac{\sigma_1/\sigma_3 - 2\mu \cdot \sqrt{\sigma_1/\sigma_3} + (\lambda - 1)}{(1-\lambda) \cdot \sigma_1/\sigma_3 - 2\mu \cdot \sqrt{\sigma_1/\sigma_3} - 1} \tag{1.5.10}$$

$$\frac{d\epsilon_3}{d\epsilon_1} = \frac{\sigma_1/\sigma_3 - 2\mu \cdot \sqrt{\sigma_1/\sigma_3} + (\lambda - 1)}{(1-\lambda) \cdot \sigma_1/\sigma_3 - 2\mu \cdot \sqrt{\sigma_1/\sigma_3} - 1} \tag{1.5.11}$$

From the comparison of the equations (1.5.5) through (1.5.7) with those of (1.5.9) through (1.5.11), it is seen that, if correspondence is made with respect to any one of stress conditions, then the remaining conditions can be determined by deduction. With respect to the same triaxial compression condition as assumed above, the equation (1.5.9) plotted by using μ as a parameter will give a graph like the one shown in Fig.1.5.2. Comparison of the graphs of Fig.1.5.1 and Fig.1.5.2 shows that the one is a straight line and the other a curve of gentle curvature. In order for the plots, despite the said difference in shape, to occur at a substantially same position, it is seen that a considerably larger value of μ must be given to the graph of Fig.1.5.1 than to that of Fig.1.5.2. Something of this nature may be possible cause for which Rowe has been compelled to modify the equations (1.5.5) through (1.5.7) into those shown below by introducing a quantity "ϕ_f" larger in magnitude than ϕ_μ and ambiguous in

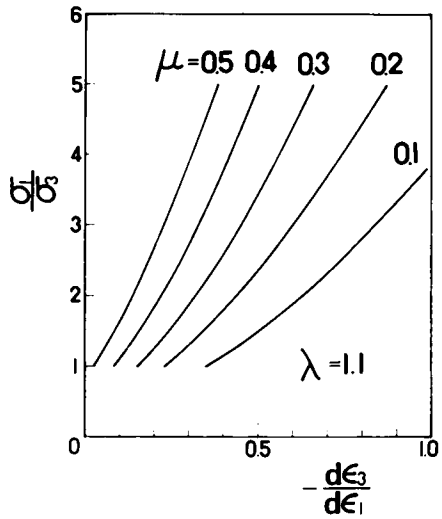

Fig.1.5.2 Relationship between σ_1/σ_3 and $d\epsilon_3/d\epsilon_1$ in triaxial compression stress condition by author's theory.

physical significance. Rowe has proposed the following equations for the states of triaxial compression, triaxial extension and plane strain.

$$\frac{\sigma_1}{\sigma_3} = 2K \cdot \left(-\frac{d\epsilon_3}{d\epsilon_1}\right) \qquad (1.5.12)$$

$$\frac{\sigma_1}{\sigma_3} = \frac{K}{2} \cdot \left(-\frac{d\epsilon_3}{d\epsilon_1}\right) \qquad (1.5.13)$$

$$\frac{\sigma_1}{\sigma_3} = K \cdot \left(-\frac{d\epsilon_3}{d\epsilon_1}\right) \qquad (1.5.14)$$

wherein, $K \equiv \tan^2(45^\circ + \phi_f/2)$ and ϕ_f is a value intermediate between ϕ_μ and ϕ_{cv} (ϕ in the critical void ratio state) and determined so as enables the equations (1.5.12) through (1.5.14) to fit actually measured values[6].

Despite such a modification, however, there seems to be a case in which measured values can hardly be recognized to describe a straight line passing through the origin or a case in which the value of ϕ_μ given by Rowe is considerably larger than the value of ϕ_μ actually measured by the author. For example, the frictional coefficient of glass beads as actually measured by the author is $\mu = 0.10 - 0.13$ ($\phi_\mu = 6^\circ$ to 8°) as already stated in Sub-paragraph 3.5.1 of Chapter 3, while the frictional coefficient of glass beads given by Rowe is $\mu = 0.31$ ($\phi_\mu = 17^\circ$). Apart from this question, Rowe's theory is open to criticisms[7] that his stress-dilatancy formulas are worked out on a modified mechanism in the regular arrangement of bars of an equal diameter and balls of equal dimensions, that the adequacy of the minimum-energy ratio criterion over the minimum energy

criterion requires substantiation and that the physical significance of ϕ_f is unclear. However, the values actually measured in connection with these formulas give interesting plots. This may possibly be explained by postulating that, if a slight modification is made as described above, the plots will assume a shape approximately corresponding to the plot of the equation (1.5.8) proposed by the author.

Finally, for the purpose of comparing the equations (1.5.12) through (1.5.14) with the equation (1.5.8) from which issue the equations (1.5.9) through (1.5.11), the formula (1.5.14) has been revised in terms of the relationship of τ/σ_N to $d\epsilon_N/d\gamma$ on a single mobilized plane using ϕ_f as a parameter. The graph consequently obtained is shown in Fig.1.5.3. From this diagram, it is seen that the formula (1.5.14)

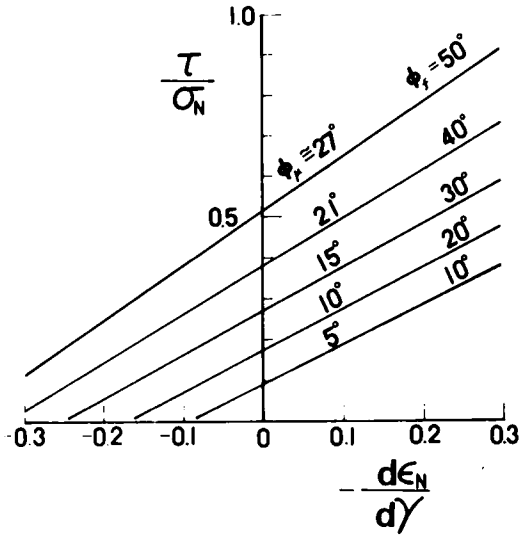

Fig.1.5.3 Rowe's stress-dilatancy theory plotted in terms of $\tau/\sigma_N \sim d\epsilon_N/d\gamma$ relationship on a single mobilized plane.

approximately gives a straight plot having practically the same inclination as that of the equation (1.5.8). When ϕ_μ is calculated by assuming the ordinate intersection in the graph of Fig.1.5.3 to be $\tan\phi_\mu$, the value is considerably smaller than the corresponding straight line of ϕ_f as is clear from the diagram. This indicates the same difference in the value of μ in the aforementioned comparison of Fig.1.5.1 with Fig.1.5.2.

5.3 RELATION TO STUDY BY ROSCOE SCHOOL

Roscoe et al. have developed the following theory on an assumed granular soil called Granta-gravel from the standpoint of energy principle[8]. The total amount of work, δE, done per unit volume on a triaxial test specimen is expressed in the respective states of triaxial compression and triaxial extension stress as follows.

$$\delta E = \sigma_a \cdot \delta\epsilon_a + 2\sigma_r \cdot \delta\epsilon_r = |\sigma_a - \sigma_r| \cdot \frac{2}{3} |\delta\epsilon_a - \delta\epsilon_r| + \frac{1}{3}(\sigma_a + 2\sigma_r) \cdot (\delta\epsilon_a + 2\delta_r) = q \cdot \delta\epsilon + p \cdot \delta v \quad (1.5.15)$$

wherein, the suffix "a" denotes the axial direction of triaxial test specimen and "r" indicates the radial direction and the equations, $q = |\sigma_a - \sigma_r|$, $p = (1/3)\cdot(\sigma_a + 2\sigma_r)$, $\delta\epsilon = (2/3)\cdot|\delta\epsilon_a - \delta\epsilon_r|$, and $\delta v = \delta\epsilon_a + 2\delta\epsilon_r$ (compression as positive), are established. The total amount of work, δE, is expressed as the sum of recoverable energy, δU, and energy, δW, consumed within the test specimen (thus, $\delta E = \delta U + \delta W$). Since the Granta-gravel is considered to be an ideal rigid-plastic model, it satisfies $\delta U = 0$. Then, the following equation is assumed.

$$\delta W = M \cdot p \cdot \delta\epsilon \quad (1.5.16)$$

In this equation, M (capital letter of μ) is considered to stand for the frictional constant. From the formulas (1.5.15) and (1.5.16), the following equation

$$q \cdot \delta\epsilon + p \cdot \delta v = \delta W = M \cdot p \cdot \delta\epsilon \quad (1.5.17)$$

and from the formula of (1.5.17), the following equation

$$\frac{q}{p} = M - \frac{\delta v}{\delta\epsilon} \quad (1.5.18)$$

are respectively derived to indicate the relationship between stress ratio (q/p) and strain increment ratio ($\delta v/\delta\epsilon$).

In the process of the derivation of the formula (1.5.18), the most important yet hardly admissible hypothesis is that of the formula (1.5.16). In pondering the underlying cause for the introduction of this formula (1.5.16), the following equations which are derived from the equation (1.5.15) and $\delta U = 0$ serve as helpful guideposts.

$$\frac{q}{p} = \frac{\delta W}{\delta\epsilon} \cdot \frac{1}{p} - \frac{\delta v}{\delta\epsilon} \quad (1.5.19)$$

or

$$q = \frac{\delta W}{\delta\epsilon} - p \cdot \frac{\delta v}{\delta\epsilon} \quad (1.5.20)$$

The equation (1.5.20) is identical with Ladanyi's formula[9] for energy correction. The assumption of the equation (1.5.16) can be interpreted to be such that M is substituted for the first term of the righthand member of the equation (1.5.19), i.e.,

the division of $\delta W/\delta\epsilon$ by p, which is thought to represent a term of frictional component. In a different way of modification, however, the equation (1.5.20) leads to Bishop's formula[10] for energy correction which is expressed by the following equation for the case of triaxial compression state.

$$q = \frac{\delta W}{\delta \epsilon_1} - \sigma_3 \cdot \frac{\delta v}{\delta \epsilon_1} \qquad (1.5.21)$$

In the equation (1.5.20), $\delta W/\delta\epsilon$ is assumed to represent the frictional component of principal stress difference q. In the equation (1.5.21), however, $\delta W/\delta\epsilon_1$ is taken to stand for the same component. Thus, uniformity of meaning is lacking with respect to the frictional component. Accordingly, there seems to be no positive theoretical ground for substituting the frictional constant M for the first term of the righthand side of the equation (1.5.19). Further, from the concept of the frictional constant (coefficient), it is thought appropriate to use the normal stress σ_N exerted on the relevant plane rather than to use the mean principal stress p as the divisor in the division. Thus, there is room for criticisms as mentioned above. Now, when the equation (1.5.18) is rewritten in terms of the relationship between τ/σ_N and $d\epsilon_N/d\gamma$ on a single mobilized plane with M as a parameter, there is obtained a graph like the one shown in Fig.1.5.4. In the diagram, the solid line represents the results of triaxial compression

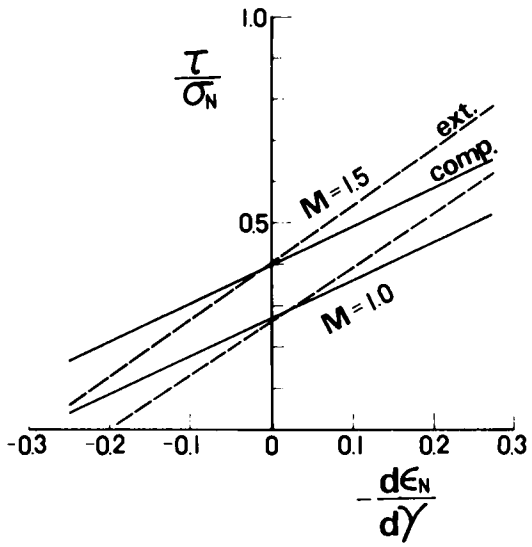

Fig.1.5.4 Roscoe et al's energy theory plotted in terms of $\tau/\sigma_N \sim d\epsilon_N/d\gamma$ relationship on a single mobilized plane.

and the dotted line those of triaxial extension respectively. When the equation (1.5.18) is converted to the relationship on a single mobilized plane, a discernible difference appears in the inclinations of plots for triaxial compression and triaxial extension.

Nevertheless, it is seen that the equation (1.5.18) represents a linear plot approximately corresponding to that of the equation (1.5.8). Fig.1.5.5 represents the data [11),12),13)] of triaxial compression tests (o marks; $\sigma_m = 3.0$ kg/cm^2, loose, Δ marks;

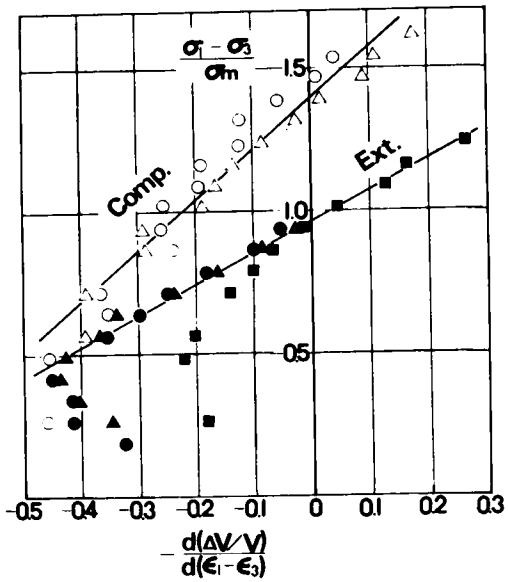

Fig.1.5.5 Relationship between $(\sigma_1 - \sigma_3)/\sigma_m$ and $d(\Delta V/V)/d(\epsilon_1 - \epsilon_3)$ in triaxial compression and triaxial extension tests on Sagami River sand.

$\sigma_m = 3.0$ kg/cm^2, medium) and triaxial extension test (● marks; $\sigma_m = 1.0$ kg/cm^2, loose, ▲ marks; $\sigma_m = 3.0$ kg/cm^2, loose, ■ marks; $\sigma_m = 1.0$ kg/cm^2, dense) on Sagami River sand as plotted in terms of the $(\sigma_1 - \sigma_3)/\sigma_m (\equiv q/p) \sim d(\Delta V/V)/d(\epsilon_1 - \epsilon_3)$ $(\equiv (2/3)\cdot(dv/d\epsilon))$ relationship. From this diagram, it is observed that the formula of the stress ratio (q/p) -strain increment ratio ($dv/d\epsilon$) relationship proposed by the Roscoe Scholl cannot uniquely define the stress-strain behavior of soil even for the cases of triaxial compression and triaxial extension stress conditions.

From such a point of view, one may note that Rowe's stress-dilatancy formula (1.5.1), Roscoe's formula (1.5.18) and the author's formula (1.5.8) which are established on totally different bases represent relationships which are fundamentally quite similar to one another. The study by the Rowe School and that by the Roscoe School seem to have a common point in this respect. In other words, what the present-day science of soil mechanics can offer as the stress-strain law of a fair degree of reliability for governing the behavior of soil may basically be the relationship of stress ratio to strain increment ratio.

5.4 RELATION TO STUDY BY HVORSLEV

A generalization that the shear strength of soil increases with the increasing compactness with which soil particles are held together and also with the increasing magnitude of the normal stress exerted on the contact points of soil particles is intuitively admissible. For example, the shear strength of soil, it is inferred, should be a function of the void ratio in the neighborhood of the sliding plane and the effective normal stress exerted on the said plane. Based on this principle, Hvorslev[14] has proposed the following formula as the failure criterion for soil.

$$\tau_f = c_e + \sigma_N \cdot \tan \phi_e \qquad (1.5.22)$$

where, c_e denotes teh effective cohesion which is a function of the void ratio existing in the neighborhood of the sliding plane at failure and ϕ_e denotes the effective angle of internal friction which is reported to be substantially constant against possible change in the void ratio. With respect to the effective cohesion c_e, Hvorslev proposes the following relationship.

$$c_e = \kappa \cdot \sigma_e \qquad (1.5.23)$$

wherein, κ denotes the coefficient of effective cohesion and σ_e the equivalent consolidation pressure respectively. By substituting the formula (1.5.23) in the formula (1.5.22) and dividing both sides of the resulting equation by σ_N, one obtains the following equation.

$$\frac{\tau_f}{\sigma_N} = \kappa \cdot \left(\frac{\sigma_e}{\sigma_N}\right) + \tan \phi_e \qquad (1.5.24)$$

According to the author's stress ratio - strain increment ratio relationship, the following equation holds even at failure.

$$\frac{\tau_f}{\sigma_N} = \lambda \cdot \left(-\frac{d\epsilon_N}{d\gamma}\right) + \tan \phi_\mu \qquad (1.5.25)$$

where, $(-d\epsilon_N/d\gamma)_f$ represents the normal-shear strain increment ratio at failure. Here, a study is made as to what correspondence there exists between the equation (1.5.24) and (1.5.25). The first term (σ_e/σ_N) of the righthand side of the equation (1.5.24) approximately corresponds to the overconsolidation ratio (O.C.R.) and it is thought that the value of the first term $(-d\epsilon_N/d\gamma)$ in the righthand side of the equation (1.5.25) will certainly increase in proportion to the increase in the value of the former first term. It has been demonstrated that tan ϕ_e in the equation (1.5.

24) and $\tan\phi_\mu$ in the equation (1.5.25) both assume constant values, irrespectively of the value of void ratio. In view of these factors, one may speculate that the equation (1.5.25) will provide a physical significance of the equation (1.5.22) and that ϕ_e will be equal to ϕ_μ. For example, there is a report[12] that $\phi_e \cong 27°$ was found for an alluvial clay from Umeda of Osaka. The value of ϕ_μ for Umeda clay used in Chapter 4 as calculated from the ordinate intersection $\tan\phi_\mu$ in the relationship of $\tau/\sigma_N \sim d\epsilon_N/d\gamma$ is about 23°. If more measured data are available in this respect, then interesting results may be obtained.

5.5 CONCLUSIONS

In the present chapter, the author has discussed the stress-dilatancy theory advocated by the Rowe School, the stress ratio (q/p) to strain increment ratio (dv/dε) relationship included in the energy theory proposed by the Roscoe School and the strength constants (c_e and ϕ_e) suggested by Hvorslev which are believed to have a close bearing upon the stress ratio (τ/σ_N) and strain increment ratio ($d\epsilon_N/d\gamma$) relationship, an important basic factor for the author's study. The interrelation among them has been explained and commented on. It is truly interesting to realize that these studies originating from totally different bases can unexpectedly be summarized into one relationship. This may suggest that the stress ratio-strain increment ratio relationship on the mobilized plane constitutes an important law for governing all possible stress-strain behaviors of soil.

The results obtained in this chapter may be summarized as follows:

(1) Rowe's stress-dilatancy formula clearly represents one relationship between stress ratio and strain increment ratio. It has been shown that this formula is in close correspondence with the author's stress ratio (τ/σ_N) - strain increment ratio ($d\epsilon_N/d\gamma$) relationship. In the process of derivation of Rowe's formula, however, a few points have been shown to be susceptible to criticism. They are thought to have compelled Rowe to introduce a quantity ϕ_f in the place of the angle of interparticle friction ϕ_μ for the purpose of necessary modification. The underlying cause for the introduction of such a quantity has been made clear through comparison with the author's formula.

(2) The theoretical foundation for the stress ratio (q/p) to strain increment ratio (dv/dε) included in the energy theory by the Roscoe School has been studied. Consequently, it has been demonstrated that this relationship, if revised in terms of the $\tau/\sigma_N \sim d\epsilon_N/d\gamma$ relationship on a single mobilized plane, gives rise to a relationship corresponding approximately to the author's formula. The study by the Rowe School appears to have a common point in this respect.

(3) A study of the failure criterion of soil proposed by Hvorslev has led to the discrovery that this criterion is in correspondence with the relationship of stress ratio (τ/σ_N) to strain increment ratio ($d\epsilon_N/d\gamma$) at failure as proposed by the author. Comparison of the two relationships suggests the possibility that the effective angle of internal friction ϕ_e proposed by Hvorslev will be equal to the angle of inter-particle friction ϕ_μ. In this connection, one example has been cited to compare actually measured data.

References

1) Newland, P. L. and Allely, B. H.: Volume Change in Drained Triaxial Tests on Granular Materials, Géotechnique, Vol.7, No.17, 1957, pp.17–34.
2) Rowe, P. W.: The Stress-dilatancy Relation for Static Equilibrium of an Assembly of Particles in Contact, Proc. Roy. Soc. London, Ser. A, Vol.269, 1962, pp.500–527.
3) Murayama, S.: A Theoretical Consideraion on a Behaviour of Sand, Proc. of I.U.T.A.M. Symposium on Rheology and Soil Mechanics, Grenoble, 1964, Springer-Verlag, 1966, pp.146–159.
4) Murayama, S. and Matsuoka, H.: The Mechanism of Shearing and its Similarity for Sands and Clays, Annuals, Disaster Prevention Research Institute, Kyoto University, No.14B, 1971, pp.551–563, (in Japanese).
5) Rowe, P. W.: Stress-Strain Behaviour of Soils, Session 2, Proc. of the Roscoe Memorial Symposium, Cambridge University, 1971, pp.143–194.
6) Rowe, P. W.: Stress-dilatancy, Earth Pressure and Slopes, Proc. A.S.C.E., Vol.89, SM3, 1963, pp.37–61.
7) Lee, I. K.: Soil Mechanics Selected Topics, Butterworths, London, 1968, p.228.
8) Schofield, A. N. and Wroth, C. P.: Critical State Soil Mechanics, Mcgraw-Hill, Longon, 1968.
9) Ladanyi, B.: Etude des relations entre les contraintes et les deformations lors du cisaillement des sols pulverulents, Annales des Travaux Publics de Belgique, 3, 1960, pp.241–270.
10) Bishop, A. W.: Correspondence, Géotechnique, Vol.4, 1954, pp.43–45.
11) Tatsuoka, F.: Stress-Strain Characteristics of Sand in Triaxial Compression Test, Proc., Annual Meeting of J.S.S.M.F.E. (6th), 52, 1971, pp.205–208, (in Japanese).
12) Tatsuoka, F.: Stress-Strain Characteristics of Sand in Triaxial Compression Test (2nd report), Proc., Annual Meeting of J.S.C.E. (26th), III-21, 1971, pp.63–66, (in Japanese).
13) Tatsuoka, F. and Shiba, T.: Stress-Strain Characteristics of Sand in Triaxial Apparatus (3rd report), Proc., Annual Meeting of J.S.S.M.F.E. (7th), 42, 1972, pp.165–168,

(in Japanese).

14) Hvorslev, M. J.: Physical Components of the Shear Strength of Saturated Clays, Research Conference on Shear Strength of Cohesive Soils, Colorado, 1960, pp.169–273.

15) Karube, D.: Creep Tests on Remolded Clay, Annuals, Disaster Prevention Research Institute, Kyoto University, No.11B, 1968, pp.523–528, (in Japanese).

CHAPTER 6

CONCLUSIONS

In the present part, the author has studied the change of soil structure in shear from a microscopic point of view and found basic rules governing the stress-strain relationships of soil with a view to determining a general stress-strain relationships of soil applicable under all conditions by using the basic soil parameters. To be specific, the basic formulas representing the stress-strain relationships on the mobilized plane have been derived from microscopic studies attaching emphasis to the behavior of sand particles and general formulas of stress-strain relationships existing under three different principal stresses have been derived by introducing the concept of the three compounded mobilized planes. These formulas have been verified, with satisfactory results, by using actually measured data from simple shear test, triaxial compression test, triaxial extension test, plane strain test and multiaxial test (universal triaxial test). These proposed formulas can be interpreted invariably by one principle without reference to method of test, void ratio of test specimen and magnitude of confining stress. All the coefficients involved have been explained in physical terms and can be predicted relatively easily. The author has also demonstrated that these formulas of relationships can be applied not only to sand but equally to clay, that they can explain not merely the results of drained test but also those of undrained test, and further that they permit the stress-strain properties in repeated shear to be analyzed from the same point of view. Particularly, the stress ratio - strain increment ratio relationship on the mobilized plane is such that it is considered to have a close bearing, in the underlying principle, upon the studies performed by the Rowe School, the Roscoe School and Hvorslev. There is a fair possibility that it constitutes one law that governs the shear phenomenon on soil, irrespectively of whether the soil is sand or clay.

The contents discussed in the present part may be summarized as follows. In Chapter 1, the author has expressed his attitude in the performance of the present study, given a general outline of the contents of his study as divided chapterwise, and clarified the position of his own study.

In Chapter 2, with a view to comprehending the internal mechanism of the shear phenomenon of sandy soil from a microscopic point of view, the author has discussed a direct shear box test and a simple shear test using not only actual soil but a piled mass of aluminum cylindrical bars of different diameters and a piled mass of cylindrical bars of a photoelastic material as two-dimensional models of sandy soil. Analysis of the test results has shown that the condition of the granular structure in the shear zone, particularly that of the granular structure on the mobilized plane, governs the shear pro-

perties of the soil. The interparticle force "f" on the mobilized plane, the angle of interparticle friction "ϕ_μ" and the angle of interparticle contact "θ" have been adopted as the microscopic factors governing the shear resistance directly. The shear resistance (τ/σ_N) and the dilatancy (ϵ_N) have been evaluated from a microscopic point of view by using these factors, to derive equations representing the relationship between shear-normal stress ratio (τ/σ_N) and normal-shear strain increment ratio ($d\epsilon_N/d\gamma$) existing on the mobilized plane, etc. In the process of this derivation, the concept of the frequency distribution of the angle of interparticle contact "θ" has been introduced to express the change of the angle of interparticle contact "θ" varying irregularly on the mobilized plane during shear, in the form of the variation in the frequency distribution. The frequency distribution is substantially symmetrical in the initial state prior to shearing. Near the peak strength of shear, the distribution is biassed to the positive region of "θ". The distribution again becomes symmetrical in the neighborhood of the residual strength. This frequency distribution is considered to constitute one index for evaluating the granular structure of soil. It has been shown that the frequency distribution has a close interrelation with the stress-strain-dilatancy relationship of soil. Further, the stress-strain relationship in repeated shear can clearly be explained by attaching special attention to the change of granular structure.

In Chapter 3, the formulas representing stress-strain relationships on the mobiblized plane have been derived from the various microscopic relationships of Chapter 2. On the basis of the basic formulas indicating the relationships existing on the mobilized plane, the concept of the compounded mobilized planes have been introduced to obtain general equations indicating the stress-strain relationships under three different principal stresses. These formulas on the stress-strain relationships have been verified with respect to measured data of triaxial compression test, triaxial extension test, plane strain test and multiaxial test involving the application of three different principal stresses which were conducted by using various kinds of sand and glass beads. At the same time, specific methods employed for the determination of coefficients included in these equations have been explained. It has also been demonstrated that the author's proposed formulas can explain the results of undrained shear test and those of repeated shear test as well.

In Chapter 4, the author has tried, by attaching special attention to the similarity of shear properties between sand and clay, to apply the various formulas on the stress-strain relationships derived from a microscopic point of view in the preceding chapters to the corresponding relationships of clay. Consequently, it has been established that these formulas are applicable not only to sand but equally to clay. It has also been shown that normally consolidated clay and overconsolidated clay may be explained in the same light, also that these formulas can silimarly be applicable to the undrained test on clay as well as on sand. Sand and clay are

thought of as being substantially different in certain aspects. It is, therefore, really interesting to realize that they can be analyzed similarly in some aspects as mentioned above. This seems to suggest that fundamentally the phenomenon of shear in sand and in clay proceeds in a similar manner. . The author has demonstrated that the similarity between the two can be explained by assuming the mechanism of shear involving the aggregate of clay particles as the unit of motion, with the electron microphotographs of clay structure in mind.

In Chapter 5, the author has discussed the stress-dilatancy theory advocated by the Rowe School, the stress ratio (q/p) to strain increment ratio ($dv/d\epsilon$) relationship included in the energy theory proposed by the Roscoe School and the strength constants (c_e and ϕ_e) suggested by Hvorslev which are believed to have a close bearing upon the stress ratio (τ/σ_N) and strain increment ratio ($d\epsilon_N/d\gamma$) relationship, an important basic factor in the author's study. The interrelation among them has been explained and commented on. It has been pointed out that, in the course of the author's study, these various studies originating from entirely different bases can be summarized into one relationship quite unexpectedly. The possibility of a conclusion that the effective angle of internal friction ϕ_e proposed by Hvorslev is equal to the angle of interparticle friction ϕ_μ has also been explained.

Here, the stress-strain properties displayed during application of sufficiently slow shear to soil has been the chief concern and possible time effects have been left out of study. Thoroughgoing elucidation of such time effects as creep and stress relaxation from the microscopic point of view as in the discussion of this part may be an interesting theme of study. The author wishes to preserve this subject for his future study. Determination of the general stress-strain-time-temperature-etc. relationships inclusive of such time effects and temperature effects is the most important subject that the workers in the science of soil mechanics should tackle with all their devotion. If general constitutive relations of soil are established on the basis of basic soil parameters, then they will become applicable to various soil engineering problems encountered in field work. Terzaghi's theory on consolidation is about the only theory that is currently used with respect to deformation of soil in field work. Little theoretical treatment is being given to soil deformations resulting from shear phenomenon. Such is the true status of affairs. Advancement of the long-lasting age of "*stability analysis*" of soil structure to the age of "*deformation analysis*" may be brought to realization by defining the deformation characteristics of soil in shear on the basis of the aforementioned concept and harmonizing the governing principle with the theory of consolidation[1),2),3)]. If the present study proves to be helpful at all in the task mentioned above, then the knowledge will certainly give the author an unexpected pleasure.

References

1) Murayama, S., Suematsu, T. and Matsuoka, H.: An Analysis of Sand Compaction Pile in Soft Cohesive Soil based on Stress-Strain Relationship of Soils (1st reprt), Proc., Annual Meeting of J.S.S.M.F.E. (7th), 1972, pp.399–402, (in Japanese).

2) Murayama, S., Matsuoka, H. and Kamo, I.: An Analysis of Sand Compaction Pile in Soft Cohesive Soil based on Stress-Strain Relationship of Soils (2nd reprt), Proc., Annual Meeting of J.S.S.M.F.E. (8th), 1973, pp.407–410, (in Japanese).

3) Sugano, Y., Hashimoto, T. and Matsuoka, H.: A Deformation Analysis of Soil Structure based on Stress-Strain Relationship of Soils, Proc., Annual Meeting of J.S.S.M.F.E. (8th), 1973, pp.403–406, (in Japanese).

PART II

SOME EXAMPLES OF DEFORMATION ANALYSIS OF GROUND

CHAPTER 1

INTRODUCTION

In the design of soil structures and grounds, it has been customary in soil mechanics to rely on "*stability analysis*" to investigate the stability of soil masses. This assumes that there exist arc slip surfaces and other forms of slip surfaces and that the shear strength of the soil manifests itself along these slip surfaces. Thus stability analysis allows us to judge whether or not a soil structure or ground is liable to failure. But, it does not help us in acquiring reliable information on the extent of soil deformation involved. Lack of adequate knowledge of the constitutive relation of soil applicable under various conditions has been solely responsible for the adoption of this incomplete methods of design. Once a general constitutive relation of soil has been formulated, it may then be analyzed with respect to the boundary conditions of a given plot of field to obtain data indicative of the presence or absence of possible soil failure as well as to determine the stress and strain conditions for all points in the soil. This allows the "*deformation analysis*" of grounds and soil structures. Even if constitutive equations of soil are complicated in form, current electronic computation methods permit such equations to be analyzed satisfactorily. Specifically, it is believed that the "*finite element method*" can be a highly advantageous means for this analysis.

In Chapter 2 of the present part, therefore, the author will develop the "*deformation analysis*" of sand pile-clay composite grounds in accordance with the general formulas of soil stress-strain relations. These have been derived from a microscopic point of view and have been verified with data of actual measurements in Part I. With regard to consolidation and shear in the soil, stress, strain, stress concentration ratio and settlement reduction rate occurring within grounds will be investigated, assuming that applied pressure, sand pile diameter and soil properties are variable. The author and his colleagues are employing "*deformation analysis*" to analyze slopes and grounds around holes using the "*finite element method*" in accordance with the given formulas of stress-strain relations[1),2)]. The outcome of this investigation will be published in a separate report.

As described above, grounds and soil structures should be analyzed strictly on the basis of general constitutive relations of soil. In some problems, however, deformation or settlement behavior may be analyzed by study of the mechanism underlying such phenomena. Concerning the settlement of ground caused by such a tunnel, for example, an analysis made by focusing special attention upon the mechanism of upward transfer of a void increasing zone due to dilatancy caused by local settlement provides a satisfactory explanation. In Chapter 3, such phenomena of local settlement within

grounds will be discussed by the analysis of relevant mechanisms to quantitatively explain surface and underground settlements caused, for example, by the excavation of tunnels.

Thus, in this part, the deformation of composite grounds will be analyzed from the standpoint of soil mechanics by the application of constitutive relations of soil and the problem of local settlement within grounds by the study of relevant mechanisms.

References

1) Sugano, Y., Hashimoto, T. and Matsuoka, H.: A Deformation Analysis of Soil Structure based on Stress-Strain Relationship of Soils, Proc., Annual Meeting of J.S.S.M.F.E. (8th), 1973, pp.403–406, (in Japanese).

2) Hashimoto, T. and Matsuoka, H.: A Deformation Analysis of Tunnel based on Stress-Strain Relationship of Soils, Proc., Annual Meeting of Kansai Br., J.S.C.E., III-32, 1973, (in Japanese).

CHAPTER 2

DEFORMATION ANALYSIS OF COMPOSITE GROUND[1),2)]

2.1 GENERAL DESCRIPTION

A sufficiently compacted sand pile is placed in a soft clay ground. The sand pile is expected to provide a pile effect and a consolidation drainage effect as well. This is the so-called sand compaction pile method. Various indoor tests and field tests have been conducted with respect to this method in an effort to clarify the behavior of the sand compaction pile. Some theoretical approaches[3)] have been also tried to study the mechanism which underlies the behavior of sand pile-clay system as a composite ground.

In this chapter, the author will analyze the behavior of sand pile-clay type composite ground which involves no lateral flow in accordance with the stress-strain relations of soil under the three different principal stresses determined in Part I, while taking into consideration the properties of consolidation and shear proper to sand and clay[4),5)]. By this, he is attempting to approach the problem not on the basis of elastoplastic analysis but rather on the basis of the analysis of the inherent characteristics of soil itself, with due regard paid to the spirit of soil mechanics. In numerical calculations, he will study stress, strain, stress concentration ratio and settlement reduction rate, on the conditions that applied pressure, sand pile diameter and soil properties are variable.

2.2 STRESS-STRAIN RELATIONS IN SAND PILE

As shown in Paragraph 3.4, Chapter 3 of Part I, the stress-strain relations of soil under three different principal stresses are generally given by the following equations.

$$\left.\begin{aligned}(\varepsilon_1)_d &= f\left(\frac{\sigma_1}{\sigma_3}\right) + f\left(\frac{\sigma_1}{\sigma_2}\right)\\ (\varepsilon_2)_d &= f\left(\frac{\sigma_2}{\sigma_3}\right) + g\left(\frac{\sigma_1}{\sigma_2}\right)\\ (\varepsilon_3)_d &= g\left(\frac{\sigma_1}{\sigma_3}\right) + g\left(\frac{\sigma_2}{\sigma_3}\right)\end{aligned}\right\} \qquad (2.2.1)$$

wherein, the following expressions are assumed on the conditon of $X \equiv \sqrt{\sigma_i/\sigma_j} - \sqrt{\sigma_j/\sigma_i}$ (i, j = 1, 2, 3, i ≦ j).

$$f\left(\frac{\sigma_i}{\sigma_j}\right) = \frac{\gamma_0 \cdot \exp\left(-\frac{\mu}{\mu'-\mu}\right)}{2} \cdot \exp\left\{\frac{X}{2(\mu'-\mu)}\right\}$$

$$\cdot \left\{\frac{X^2}{8} + \left(\frac{1}{2} - \frac{1}{\lambda} - \frac{\mu'-\mu}{2}\right) \cdot X + (\mu'-\mu)^2 - (\mu'-\mu) + \frac{2\mu'}{\lambda} + 1\right\} \quad (i < j)$$

$$g\left(\frac{\sigma_i}{\sigma_j}\right) = \frac{\gamma_0 \cdot \exp\left(-\frac{\mu}{\mu'-\mu}\right)}{2} \cdot \exp\left\{\frac{X}{2(\mu'-\mu)}\right\}$$

$$\cdot \left\{-\frac{X^2}{8} + \left(\frac{1}{2} - \frac{1}{\lambda} + \frac{\mu'-\mu}{2}\right) \cdot X - (\mu'-\mu)^2 - (\mu'-\mu) + \frac{2\mu'}{\lambda} - 1\right\} \quad (i < j)$$

$$f\left(\frac{\sigma_i}{\sigma_i}\right) = g\left(\frac{\sigma_i}{\sigma_i}\right) = 0 \qquad (i = j)$$

In the formulas given above, λ, μ, μ' and γ_0 are coefficients of which the numerical values are to be determined depending on the kind and condition of soil as described in detail in Chapter 3, Part I.

The strain caused by consolidation is given by the following equation.

$$(\varepsilon_1)_c = (\varepsilon_2)_c = (\varepsilon_3)_c = \frac{1}{3} \cdot \frac{C_c}{1+e_i} \cdot \log_{10}\frac{\sigma_m}{\sigma_{mi}} \qquad (2.2.2)$$

wherein, C_c, e_i, σ_{mi} denote compression index, initial void ratio and initial mean effective principal stress respectively.

Incidentally, the stresss exerted on a sand pile which is placed in a clay ground is considered to be composed of the triaxial compression stress due to the major principal stress σ_{zs} in the direction of depth and the minor principapl stress σ_{rs} in the radial direction (wherein, the suffix "s" signifies sand pile), as illustrated in Fig. 2.2.1. In the equation of (2.2.1) therefore, the conditions $\sigma_1 = \sigma_{zs}$ and $\sigma_2 = \sigma_3 = \sigma_{rs}$ are both satisfied. Assuming that the strain due to shear and the strain due to consolidation are superposed, the stress-strain relations of a sand pile can be expressed by the following equations (ϵ_{zs} and ϵ_{rs} stand for the principal strains respectively in the direction of depth and the radial direction):

$$\left.\begin{aligned}\epsilon_{zs} &= 2f\left(\frac{\sigma_{zs}}{\sigma_{rs}}\right) + \frac{1}{3} \cdot \frac{C_{cs}}{1+e_{is}} \cdot \log_{10}\frac{\sigma_{zs} + 2\sigma_{rs}}{3\sigma_{mi}} \\ \epsilon_{rs} &= g\left(\frac{\sigma_{zs}}{\sigma_{rs}}\right) + \frac{1}{3} \cdot \frac{C_{cs}}{1+e_{is}} \cdot \log_{10}\frac{\sigma_{zs} + 2\sigma_{rs}}{3\sigma_{mi}}\end{aligned}\right\} \qquad (2.2.3)$$

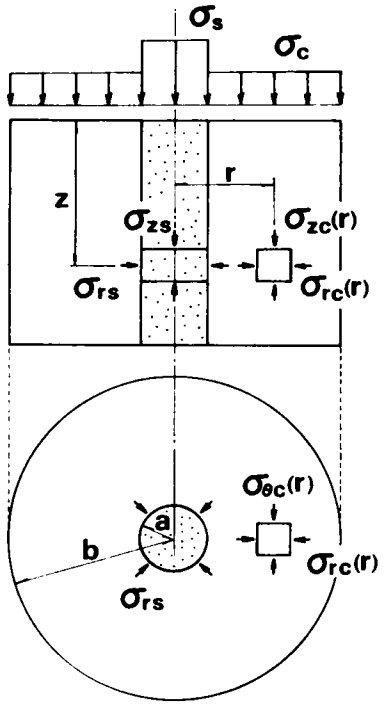

Fig.2.2.1 Stress states of sand pile-clay composite ground.

wherein, C_{cs}, e_{is} and σ_{mi} denote compression index, initial void ratio and initial mean effective principal stress prior to shear respectively.

2.3 STRESS-STRAIN RELATIONS IN CLAY GROUND

The stress consition of a clay ground exclusive of a sand pile corresponds to the K_0-consolidation state conditional on a uniform load to an infinite extent. It is considered, however, that on inclusion of a sand pile, the clay elements in the neighborhood of the boundary between the sand pile and the clay assume complicated stress conditions such as stress increases in the radial direction and stress decreases in the circumferential direction due both to dilatancy and other factors relating to the sand pile. Here, the author proposes to discuss clay elements at a depth of z in a radius of r within a clay ground, with the three principal stresses in the direction of depth, the radial direction and the circumferential direction denoted by σ_{zc} (r), σ_{rc} (r) and $\sigma_{\theta c}$ (r) (wherein, the suffix "c" signifies clay) respectively and the principal strains caused by the said three principal stresses denoted by ϵ_{zc} (r), ϵ_{rc} (r) and $\epsilon_{\theta c}$ (r) respectively. Since the elements of the clay are believed to be subjected simultaneously to shear and consolidation under the three different stresses, the following

equations are obtained which indicate the stress-strain relations in the clay ground, if the superposition of the strain due to shear and that due to consolidation is accepted. The following three equations are true where $\sigma_{zc}(r) \geqq \sigma_{rc}(r) \geqq \sigma_{\theta c}(r)$ is satisfied.

$$\left.\begin{aligned}
\varepsilon_{zc}(r) &= f\left(\frac{\sigma_{zc}(r)}{\sigma_{\theta c}(r)}\right) + f\left(\frac{\sigma_{zc}(r)}{\sigma_{rc}(r)}\right) + \frac{1}{3}\cdot\frac{C_{cc}}{1+e_{ic}}\cdot\log_{10}\frac{\sigma_{zc}(r)+\sigma_{rc}(r)+\sigma_{\theta c}(r)}{3\sigma_{mi}} \\
\varepsilon_{rc}(r) &= f\left(\frac{\sigma_{rc}(r)}{\sigma_{\theta c}(r)}\right) + g\left(\frac{\sigma_{zc}(r)}{\sigma_{rc}(r)}\right) + \frac{1}{3}\cdot\frac{C_{cc}}{1+e_{ic}}\cdot\log_{10}\frac{\sigma_{zc}(r)+\sigma_{rc}(r)+\sigma_{\theta c}(r)}{3\sigma_{mi}} \\
\varepsilon_{\theta c}(r) &= g\left(\frac{\sigma_{zc}(r)}{\sigma_{\theta c}(r)}\right) + g\left(\frac{\sigma_{rc}(r)}{\sigma_{\theta c}(r)}\right) + \frac{1}{3}\cdot\frac{C_{cc}}{1+e_{ic}}\cdot\log_{10}\frac{\sigma_{zc}(r)+\sigma_{rc}(r)+\sigma_{\theta c}(r)}{3\sigma_{mi}}
\end{aligned}\right\} \quad (2.2.4)$$

The following equations are true where $\sigma_{rc}(r) \geqq \sigma_{zc}(r) \geqq \sigma_{\theta c}(r)$ is satisfied.

$$\left.\begin{aligned}
\varepsilon_{rc}(r) &= f\left(\frac{\sigma_{rc}(r)}{\sigma_{\theta c}(r)}\right) + f\left(\frac{\sigma_{rc}(r)}{\sigma_{zc}(r)}\right) + \frac{1}{3}\cdot\frac{C_{cc}}{1+e_{ic}}\cdot\log_{10}\frac{\sigma_{rc}(r)+\sigma_{zc}(r)+\sigma_{\theta c}(r)}{3\sigma_{mi}} \\
\varepsilon_{zc}(r) &= f\left(\frac{\sigma_{zc}(r)}{\sigma_{\theta c}(r)}\right) + g\left(\frac{\sigma_{rc}(r)}{\sigma_{zc}(r)}\right) + \frac{1}{3}\cdot\frac{C_{cc}}{1+e_{ic}}\cdot\log_{10}\frac{\sigma_{rc}(r)+\sigma_{zc}(r)+\sigma_{\theta c}(r)}{3\sigma_{mi}} \\
\varepsilon_{\theta c}(r) &= g\left(\frac{\sigma_{rc}(r)}{\sigma_{\theta c}(r)}\right) + g\left(\frac{\sigma_{zc}(r)}{\sigma_{\theta c}(r)}\right) + \frac{1}{3}\cdot\frac{C_{cc}}{1+e_{ic}}\cdot\log_{10}\frac{\sigma_{rc}(r)+\sigma_{zc}(r)+\sigma_{\theta c}(r)}{3\sigma_{mi}}
\end{aligned}\right\} \quad (2.2.5)$$

wherein, $\sigma_{mi} = (1 + 2K_{oc})\, w_c z/3$ (in which, K_{oc} is the clay's coefficient of earth pressure at rest and w_c is the unit weight of the clay).

2.4 CONDITIONS FOR COMPOSITE GROUND

In the last two paragraphs 2.2 and 2.3, the stress-strain relations in the sand pile and the clay ground were determined. Here, the following conditions are assumed for the boundary in the composite ground. Let us now assume a case in which a uniform load is applied on a rigid loading plane.

(1) On the condition of the equal strain in the vertical direction, the following equation is obtained.

$$\varepsilon_{zs} = \varepsilon_{zc}(r) \qquad (a \leqq r \leqq b) \qquad (2.2.6)$$

(2) In the boundary (r = a) intervening between the sand pile and the clay ground, the following equations are satisfied.

$$\sigma_{rs} = \sigma_{rc}(a) \ , \qquad \varepsilon_{rs} = \varepsilon_{\theta c}(a) = -\frac{u(a)}{a} \qquad (2.2.7)$$

wherein, u(a) denotes the displacement in the radial direction of the position at a depth of z in a radius a in the ground.

(3) On the condition that the K_0-consolidation state exists in the outer boundary of a composite ground (r = b), the following equations are satisfied.

$$\varepsilon_{rc}(b) = \varepsilon_{\theta c}(b) = 0 \ , \qquad \sigma_{rc}(b) = \sigma_{\theta c}(b) = K_0 \cdot \sigma_{zc} \qquad (2.2.8)$$

(4) On the condition of the share of applied pressure on the surface of the composite ground, the following equation is satisfied.

$$p = \frac{a^2}{b^2} \cdot \sigma_s + \frac{b^2 - a^2}{b^2} \cdot \sigma_c \qquad (2.2.9)$$

wherein, p denotes the applied pressure, σ_s the shared stress on the open surface of the sand pile and σ_c the shared stress on the open surface of the clay ground respectively. Here, the distribution of stress in the radial direction is not considered for σ_s or σ_c as shown in Fig.2.2.1. Therefore, the equations $\sigma_s = \sigma_{zs} - w_s \cdot z$ and $\sigma_c = \sigma_{zc} - w_c \cdot z$ are satisfied (wherein, w_s and w_c stand for the unit weights of sand and clay respectively).

Theoretically, the values of stress, strain and stress concentration ratio (σ_s / σ_c) at various points in a composite ground can all be determined by considering the preceding equations of stress-strain relations in the sand pile and the clay ground, the equations of boundary conditions and the equations of the stress equilibrium.

2.5 EXAMPLES OF ANALYSIS AND DISCUSSION

Numerical calculations can now be carried out on the system described above, by fixing various coefficients of sand pile and clay ground. The following values are to be given to the coefficients which go to express the characteristics of soil:

Clay ground: The values of coefficients determined from the test data obtained of Fujinomori clay: They are $\lambda_c = 1.1$, $\mu_c = 0.30, \mu'_c = 0.42$, $\gamma_{oc} = 1.0\%$, $\sigma_{mi} = 0.5$ kg/cm^2 and $C_{cc} = 0.7$, $e_{ic} = 1.8$, $w_c = 1.6 \times 10^{-3}$ kg/cm^2 and $K_{oc} = 0.5$ (wherein, the suffix "c" signifies clay ground).

Sand pile: The values of coefficients determined from the test data obtained of Ishii River sand: They are $\lambda_s = 1.1$, $\mu_s = 0.40$, $\mu'_s = 0.62$, $\gamma_{os} = 1.3\%$, $e_{is} = 0.706$, $w_s = 1.98 \times 10^{-3}$ kg/cm^2 ($C_{cs} = 0$).

In addition, p (applied pressure) = 1 kg/cm^2 and b/a = 5 are given as standard values. The depth of ground is assumed to be such that the height of layer is 25 m and the calculations have been carried out at the center of the layer z = 12.5 m (below the level of underground water).

On the basis of the values described above, stress, stress ratio, stress concentration ratio, strain and settlement reduction rate (ratio of vertical strain occurring in the presence and absence of a sand pile in a clay ground) have been calculated for varied values of p, b/a, γ_{os}, C_{cs}, γ_{oc}, and C_{cc}. (Refer to Appendix B for a detailed discussion of the calculation.) Fig.2.2.2 shows the calcualted values of stress (σ_{zs} and σ_{zc}), stress ratio (σ_{zs}/σ_{rs}, $\sigma_{rc}(a)/\sigma_{\theta c}(a)$, $\sigma_{rc}(a)/\sigma_{zc}$ and $\sigma_{zc}/\sigma_{\theta c}(a)$), stress concentration ratio (σ_s/σ_c on the ground surface and σ_{zs}/σ_{zc} at depth of z = 12.5 m in ground) for varying applied pressure p. From the diagram, it is noted that the stress σ_{zs} of the sand pile and the stress σ_{zc} of the clay ground both increase with the increasing value of p. The results of the calculations seem to indicate that the stress concentration ratio on the ground surface has an approximate value of 9 and that within the ground is on the order of 3 ~ 7. In the diagrams following, plots of calcualted values

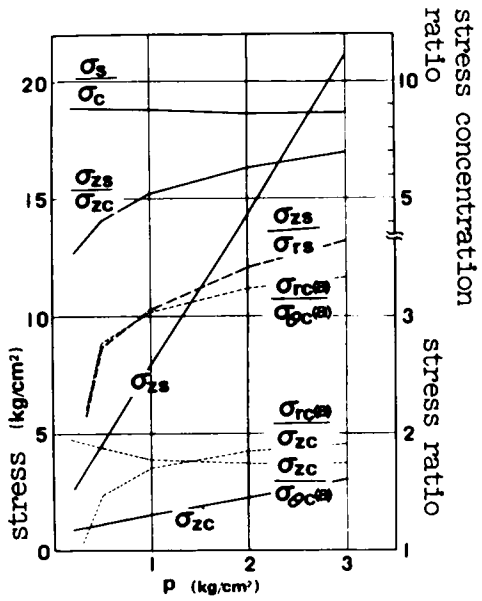

Fig.2.2.2 Effects of applied pressure p on stress, stress ratio and stress concentration ratio in composite ground.

are shown by broken lines for the purpose of clearly indicating points of calculated values. Fig.2.2.3 shows measured values obtained by Mogami et al.[6),7)] in a model test on composite ground composed of sand pile and oily clay. Since no information is

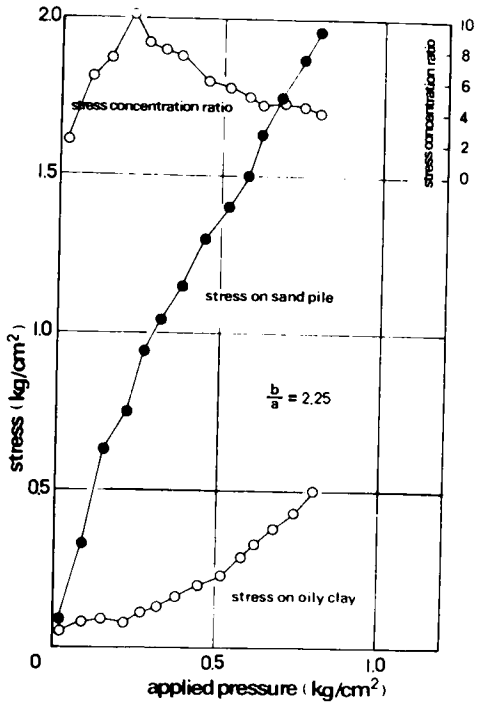

Fig.2.2.3 Results of model test on composite ground (after Mogami et al[6)]).

available to tell the numerical values of the coefficients for the sand and the oily caly used in this model test, the author is complelled to venture a rather qualitative discussion in this respect. It can be seen, however, that the trends of stress measured in the sand pile and stress measured in the oily clay as indicated in Fig.2.2.3 are in satisfactory agreement with those of σ_{zs} and σ_{zc} in Fig.2.2.2. The measured values $2 \sim 10$ of stress concentration ratio shown in Fig.2.2.3 are also in approximate agreement with the aforementioned values $3 \sim 9$. It is reported in literature[8)] that the values of stress concenration ratio of $4 \sim 4.5$ were obtained under ground (-6 m to -14 m under ground surface) in a field masurement. These values are also roughly in agreement with the calculated values of $3 \sim 7$ (refer to Fig.2.2.2) of stress concentration ratio under ground (σ_{zs}/σ_{zc}). Fig.2.2.4 shows the results obtained for varying sand pile diameter "a". The data presume the radius "b" of the outer circumference of composite ground to be 1 m. It is observed that σ_{zs} and σ_{zc} decrease and the ratio of σ_s/σ_c slightly increases with the increasing diameter "a". Fig.2.2.5 represents a case in which the value γ_{os} of sand pile was varied. In this case, γ_0 means the shear strain γ at the maximum compression point of the normal strain ϵ_N on the mobilized plane ($(\tau/\sigma_N)_{max}$ plane) as des-

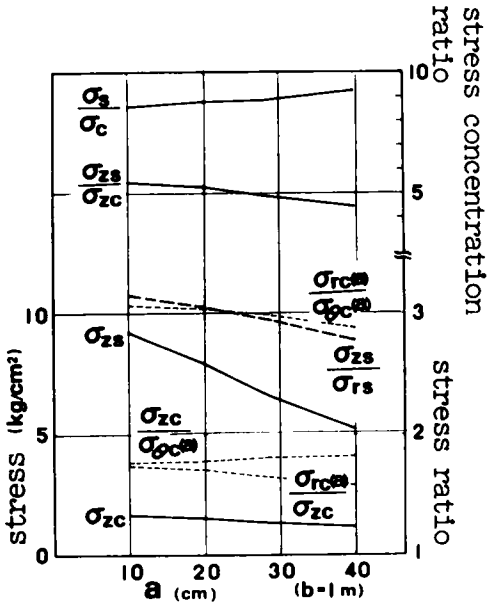

Fig.2.2.4 Effects of sand pile diameter a on stress, stress ratio and stress concentration ratio in composite ground.

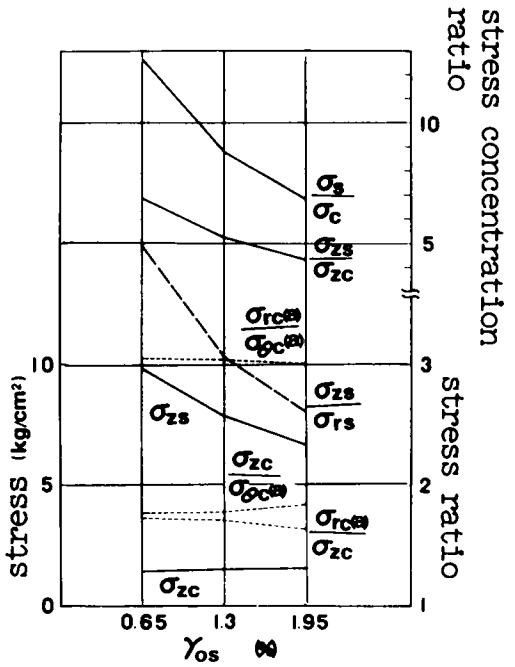

Fig.2.2.5 Effects of reference shear strain γ_{os} of sand on stress, stress ratio and stress concentration ratio in composite ground.

cribed in detail in Part I. It is thought to form a parameter for the evaluation of granular structure. The fact that γ_{os} is increased is equivalent to a statement that the sand pile is loosely packed. It is consequently seen that σ_{zs} decreases, σ_{zc} increases and σ_s/σ_c and σ_{zs}/σ_{zc} both decrease as γ_{os} is enlarged. In Fig.2.2.6, effects of compressibility of the sand pile are considered.

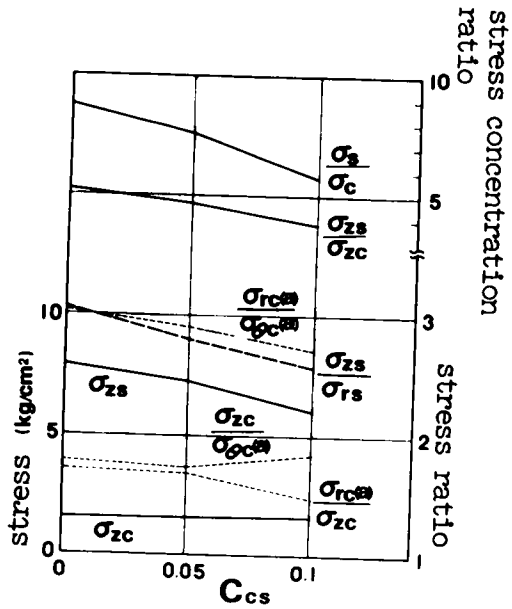

Fig.2.2.6 Effects of compression index C_{cs} of sand on stress, stress ratio and stress concentration ratio in composite ground.

As the compression index C_{cs} of the sand pile is increased, then σ_{zs} decreases, σ_{zc} increases and the ratios σ_s/σ_c and σ_{zs}/σ_{zc} both decrease similarly to Fig.2.2.5. When a sand compaction pile and a sand drain pile are compared as sand pile-clay composite ground, it is concluded that the stress concentration ratio (σ_s/σ_c) for the former is larger than that for the latter since "a" is larger and "γ_{os}" and "C_{cs}" are smaller for the former than for the latter.

Fig.2.2.7 shows the results of the calculations performed while varying the value of γ_{oc} of clay. Fig.2.2.8 shows the results obtained for varying value of C_{cc} of clay. If the increase of γ_{oc} corresponds to the decrease of compaction of clay with respect to the value γ_{os}, then the inclination of the calculated values of Fig. 2.2.7 is opposed to that of Fig.2.2.8 (except for σ_{zs}/σ_{rs}). Contrary to the intuition that σ_{zc} decreases with the increasing value of γ_{oc}, the relationship may be interpreted by postulating that the stress-strain relation changes to increase the strain and

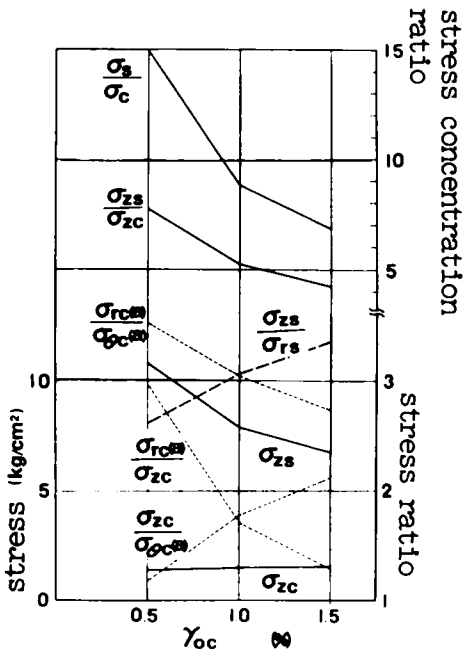

Fig.2.2.7 Effects of reference shear strain γ_{oc} of clay on stress, stress ratio and stress concentration ratio in composite ground.

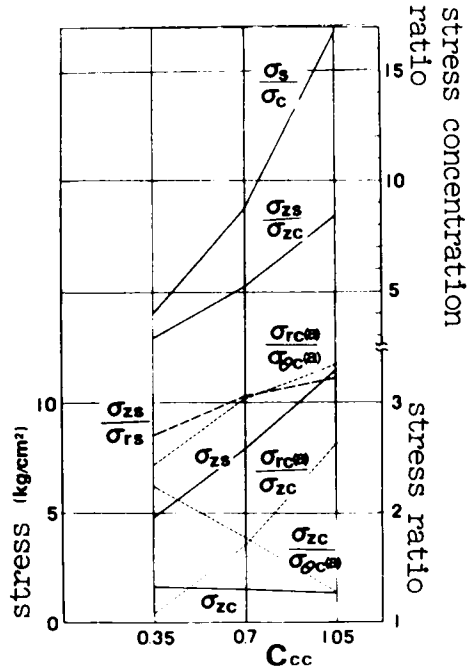

Fig.2.2.8 Effects of compression index C_{cc} of clay on stress, stress ratio and stress concentration ratio in composite ground.

consequently σ_{zc} as γ_{oc} is increased. This situation is depicted in Fig.2.2.9. Both γ_{oc} and C_{cc} serve as parameters to indicate characteristics of clay and are thought to be related in some way or other. Since they show opposite trends

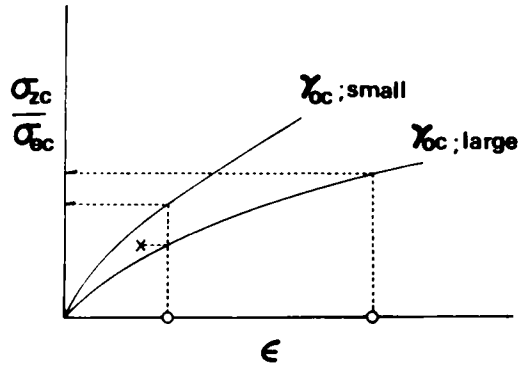

Fig.2.2.9 Explanation of the effect of parameter γ_{oc} on vertical stress σ_{zc} in clay ground.

with respect to stress concentration ratio, however, nothing definite may be said about the trend of the change in stress concentration ratio where the characteristics of clay ground are susceptible to variation.

Figs.2.2.10 through 2.2.15 show the results of the calculation of vertical strain ϵ_z ($z = 12.5$ m) for varying values of p, a, γ_{os}, C_{cs}, γ_{oc} and C_{cc} and the settlement reduction rate β ($\equiv \epsilon_z/\epsilon_{zo}$) indicating the ratio of ϵ_z to the vertical strain ϵ_{zo} (calculated for K_0-consolidation) existing in the clay ground excluding the sand pile. The graph of Fig.2.2.10 shows a trend which agrees with the trend of the measured values

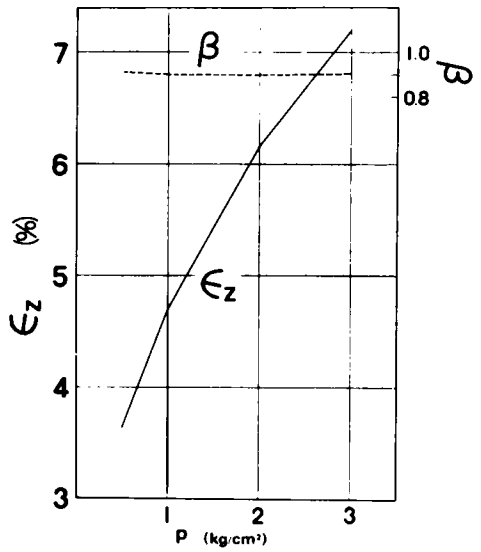

Fig.2.2.10 Effects of applied pressure p on vertical strain ϵ_z and settlement reduction rate β of composite ground.

of the load-settlement relation in a model test performed by Mogami et al.[6),7)] The graph of Fig.2.2.11 indicates that ϵ_z decreases with the increasing sand pile diameter, a trend which Matsuo et al.[9)] have deduced from test data. All these

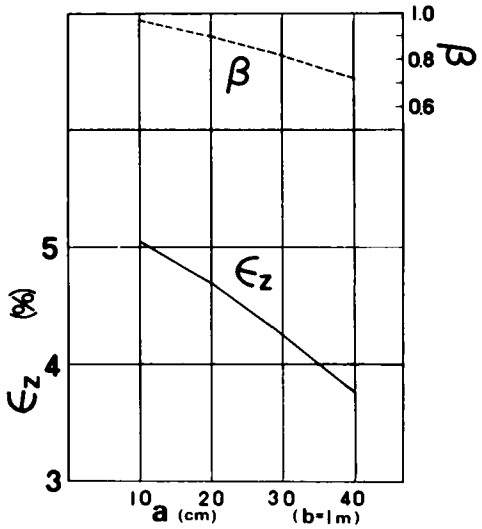

Fig.2.2.11 Effects of sand pile diameter a on vertical strain ϵ_z and settlement reduction rate β of composite ground.

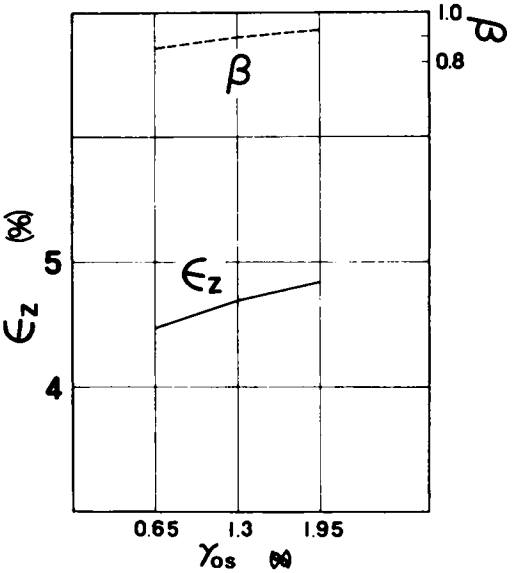

Fig.2.2.12 Effects of reference shear strain γ_{os} of sand on vertical strain ϵ_z and settlement reduction rate β of composite ground.

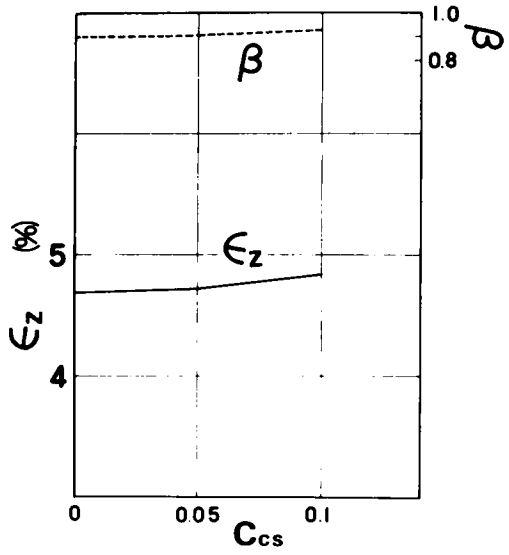

Fig.2.2.13 Effects of compression index C_{cs} of sand on vertical strain ϵ_z and settlement reduction rate β of composite ground.

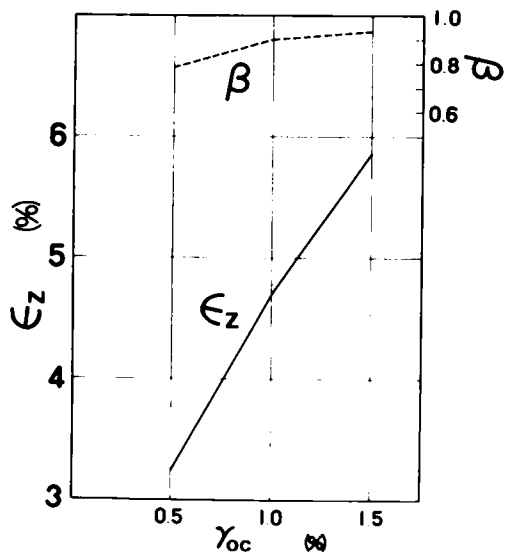

Fig.2.2.14 Effects of reference shear strain γ_{oc} of clay on vertical strain ϵ_z and settlement reduction rate β of composite ground.

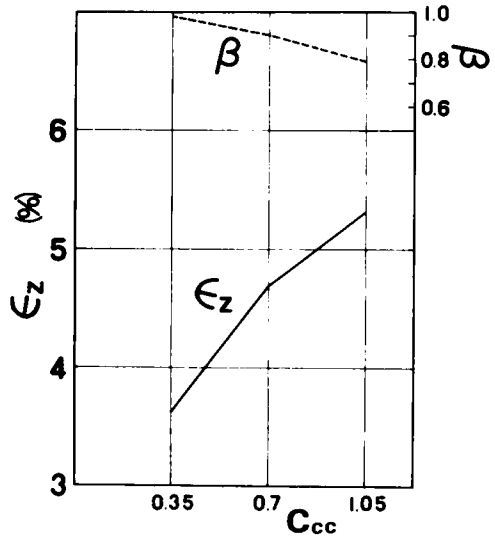

Fig.2.2.15 Effects of compression index C_{cc} of clay on vertical strain ϵ_z and settlement reduction rate β of composite ground.

graphs show trends whcih are intuitively obvious. However, Fig.2.2.10 in which β remains constant ($\beta \cong 0.9$) despite the increase of ϵ_z with increasing p and Fig.2.2.15 in which β decreases despite the increase of ϵ_z and C_{cc} deserve special attention.

2.6 CONCLUSIONS

The behavior of the sand pile-clay type composite ground has frequently been analyzed as a phenomenon of consolidation[6]. When the proportions of shear strain and consolidation strain which make up the strain in grounds are studied as shown above, results indicate that the shear strain is not negligibly small. In the present chapter, the author has, on the basis of the stress-strain equations given above, calculated stress, stress concentration raio, strain and settlement reduction rate within grounds for varying values of applied pressure, sand pile diameter and soil characteristics. Future problems may involve an experiment using sand and clay with known coefficients (λ, μ, μ', γ_0, C_c, e_i and w), verification through field experiment, establishment of method of analysis under conditions involving lateral flow due to applied pressure, and consideration of time-effect phenomenon due to consolidation and shear.

The results discussed in this chapter may be summarized as follows:

(1) The deformation of composite ground free from lateral flow can be analyzed by means of the stress-strain formulas for sand and clay, boundary conditions and stress equilibrium. That is, stress and strain at each point within the gound can be uniquely calculated.

(2) The results of the calculation of stress (σ_{zs}) exerted on sand pile, stress (σ_{zc}) exerted on clay ground and stress concentration ratio (σ_s/σ_c and σ_{zs}/σ_{zc}) for varying value of applied pressure (p) are found to be in satisfactory agreement with Mogami et al.[6),7)] and with the actual data of stress concentration ratio obtained in the field test[8)].

(3) The results of the calculation of stress (σ_{zs}) exerted on sand pile, stress (σ_{zc}) exerted on clay ground, stress concentration ratio (σ_s/σ_c and σ_{zs}/σ_{zc}), etc. for varying values of sand pile diameter (a), and soil characteristics (γ_{os}, C_{cs}, γ_{oc} and C_{cc}) of sand and clay are found to be reasonable. With respect to the reference shear strain γ_{oc} of clay, there have been obtained calculated values which apparently contradict intuition. Further study has brought out a plausible interpretation of these values.

(4) Variations in the vertical strain (ϵ_z) and in the settlement reduction rate (β) for various values of applied pressure (p), sand pile diameter (a) and soil characteristics (γ_{os}, C_{cs}, γ_{oc} and C_{cc}) have also been found calculable. The results of such calculation are found to be in satisfactory agreement with measured values[6),7),9)] obtained in several model tests as well as with intuition.

(5) The behavior of such composite ground has often been analyzed exclusively in terms of the phenomenon of consolidation. When the proportions of consolidation strain and shear strain which make up the total strain are thus considered, it is found that the shear strain is not negligibly small.

References

1) Murayama, S., Suematsu, C. and Matsuoka, H.: An Analysis of Sand Compaction Pile in Soft Cohesive Soil based on Stress-Strain Relationship of Soils (1st report), Proc., Annual Meeting of J.S.S.M.F.E, (7th), 1972, pp.399–402, (in Japanese).

2) Murayama, S., Matsuoka, H. and Kamo, I.: An Analysis of Sand Compaction Pile in Soft Cohesive Soil based on Stress-Strain Relationship of Soils (2nd report), Proc., Annual Meeting of J.S.S.M.F.E. (8th), 1973, pp.407–410, (in Japanese).

3) Murayama, S.: Consideration on Vibro-Compozer Method for Clayey Soils, Mechanization of Constructions, No.150, 1962, pp.10–15, (in Japanese).

4) Shibata, T.: On the Volume Changes of Normally-Consolidated Clays, Annuals, Disaster Prevention Research Institute, Kyoto University, No.6, 1963, pp.128–134, (in Japanese).

5) Mizuno, Y.: A Study on Stress Concentration Ratio of Composite Ground, Report for Disaster Prevention Research Institute of Kyoto University, 1970, (in Japanese).

6) Mogami, T., Nakayama, J., Ueda, S., Kuwata, H., Kamada, H. and Taguchi, S.: A Model Test on Composite Ground (1st report), Tsuchi-to-Kiso, J.S.S.M.F.E., Vol. l6, No.8, 1968, pp.9–17, (in Japanese).

7) Mogami, T., Nakayama, J., Ueda, S., Kuwata, H., Kamada, H. and Taguchi, S.: A Model Test on Composite Ground (2nd report), Tsuchi-to-Kiso, J.S.S.M.F.E., Vol. l6, No.11, 1968, pp.5–11, (in Japanese).

8) Aboshi, H., Yoshikuni, H., Ichimoto, E. and Harada, K.: On the Settlement Characteristics of Composite Ground, Symposium of Soil Engineering (6th), 1971, pp.73–80, (in Japanese).

9) Matsuo, M., Kuga, T. and Maegawa, I.: The Study on Consolidation and Shear Strength of Cohesive Soil containing Sand Pile, Trans. of J.S.C.E., No.141, 1967, pp.42–55, (in Japanese).

CHAPTER 3

ANALYSIS OF LOCAL SETTLEMENT WITHIN GROUND[1),2)]

3.1 GENERAL DESCRIPTION

When a portion of a given plot of ground undergoes local settlement, there arises a question as to how the effect of the local settlement is transmitted to the ground interior and to what extent the ground participates in the settlement. This problem is important in elucidating possible effects which the excavation of tunnels may have upon the settlement of ground surface. In the analysis of such settlement phenomenon occurring in a ground of sandy soil, an experiment is frequently performed in which dry sand is placed in a box and a portion of the bottom plate of the box is lowered[3),4),5),6)]. This experiment is called the "*lowering floor test*". When sand is used in a test, accurate observation of delicate movements of sand is difficult even if a glass plate is used in the front side of the box. Further, the friction between sand grains and the inner wall surface of the box causes an error which may lower the accuracy of that test. As a two-dimensional model, therefore, the author has employed a mass formed by having aluminum rods of various diameters mixed randomly and piled up sideways[7),8),9),10)] He has carefully studied the condition of the movement of individual rods within the mass due to removal of the lowering floor, the local change of voids distributed in the mass, the upward transfer of such local change of void distribution, the relation between the distance of the removal of the lowering floor and the amount of settlement of the mass, etc. Consequently, he has clarified the mechanism of local settlement of the ground of granular soil and, at the same time, derived formulas for the calculation of settlement amount of ground. He has also conducted a similar test with respect to a ground composed of sand and, consequently, verified that the theory developed with respect to a mass of aluminum rods is equally applicable to a ground of sand. For considertaion of settlement caused in the vicinal ground by excavation of tunnels, not only the analysis of settlement in the lateral direction but also the analysis of settlement in the longitudinal direction and consequently that of three-dimensional settlement are required. In the present study, the author has tried to analyze the phenomenon of ground settlement in the longitudinal direction of tunnel and in the three-dimensional aspect as well. He has examined actual field data of settlement collected on the site of tunnel excavation by comparing the data with results he obtained from a test.

How does a stratum of granular soil such as sand behave when a local settlement occurs within the stratum? This problem has been theoretically investigated by

Litwiniszyn[11]. Such investigation must be highly esteemed for the successful introduction of the concept of the stochastic process. However, the mechanical expression of the phenomenon of ground settlement is based on the assumption that soil particles move only in a downward vertical direction (i.e., the direction of gravitational attraction) and therefore, the model does not seem to be adequate in interpreting the complicated phenomena actually involved. For example, this theory does not consider arch action. In the present study, the author analyzes the condition of transfer of the effect of settlement on the basis of the zone of arch shape (called "*primary zone*") which follows the downward removal of the lowering floor.

3.2 OUTLINE OF TESTS

3.2.1 Material used in Tests

In the study of effects of local settlement occurring within a non-cohesive granular substance, a container in which dry sand is placed and in which a removable plate of a required width is used as part of the bottom plate has often been employed. A glass sheet is placed in the front side of the container, so that the movement of sand caused by gradual downward removal of the lowering plate can be observed. When such container is used, however, the sand moveing downward caused friction with the internal surface of the container wall. For this friction, the observed sand movement does not represent the true two-dimensional condition of the sand in actual ground. Further, in such test apparatus, it is difficult to place a reference point in the stratum of sand. This makes difficult accurate observation of the deformation in the sand stratum.

To eliminate such drawbacks, the author has conducted a test by using, as a model of ground, a mass formed by having cylindrical aluminum rods of a fixed length of 50 mm and various diameters mixed at a suitable ratio and piled up horizontally on their curved sides between two lateral partition walls. Chiefly mass formations have been used: (A) A mass formed by using a mixture of aluminum rods 1.6 mm and 3 mm in diameter and (B) a mass of a mixture of aluminum rods 3, 5 and 9 mm in diameter. The mixing weight ratio (3 : 2) of (A) and the mixing weight ratio (8 : 7 : 5) of (B) have been determined so as to correspond the grain size distribution curves of Toyoura standard sand. Adoption of such masses of aluminum rods is advantageous in that (1) the mass of rods can stand by itself and need not be supported on the front and rear sides with walls and, therefore, possible effects of friction which would otherwise occur between the test sample and the interior wall surface of contaniner are totally absent, (2) the displacement of individual rods simulates the two-dimensional stress-strain relation of a granular substance, (3) the condition of ground deformation can clearly be observed by directly placing reference points or reference lines on the end

planes of rods piled up in a mass, (4) the condition of the movement of individual rods can easily be photographed, (5) granular masses having various grain size distributions can be simulated by suitably changing the mixing ratio of aluminum rods of different diameters, (6) the specific gravity of aluminum rods (2.69) is similar to that of sand and gravel, and (7) the shear test conducted by using a mass of aluminum rods shows the internal friction angle to be approximately 30° which is closed to the internal friction angle observed with ordinary sand.

Then, with a view to studying whether the theory developed on the basis of data obtained of masses of aluminum rods is equally applicable to sand, the author has conducted a similar floor-lowering test on coarse sand (5.0 - 0.3 mm in grain size) and fine sand (1.0 - 0.1 mm in grain size) in their respective densely packed and loosely packed conditions. As the test material for the floor-lowering test (to be described afterwards) designed for the verification of the three-dimensional analysis of ground surface settlement, the author has used densely packed and loosely packed coarse sand.

3.2.2 Apparatus and Method used for Tests

The test apparatus incorporating a lowering floor and using a mass of cylindrical rods is illustrated in Photo.2.3.1. The handle on the lower side is designed to lower "*lowering floor*". When the handle connected via a chain to a motor is rotated one complete turn, the lowering floor moves downward 0.5mm. In ordinary runs of test, the lowering floor moves at the rate of about 1.0 mm/min. Although the earth pressure is excluded from the present study, the shaft serving to support the lowering plate is held in contact with the load cell so that the load exerted on the lowering plate can be measured as occasion demands. The width "B" of the lowering floor is variable. In the present test, a total of five widths, B = 3, 6, 9, 12 and 15 cm, were tried. Ordinarily, the two values of about 30 cm and 60 cm were used for soil depth (height of ground model material). The lateral partition walls in the apparatus were spaced at about 60 cm to provide ample space with respect to the width of lowering floor and the soil depth and to avoid producing undesired effects on the movement of ground material.

The test apparatus with a lowering floor adopted for the test on sand was an iron box having inside dimensions of 60 cm × 60 cm × 14 cm. A hard glass sheet was set on the front side. The box is provided with a lowering plate having a width of B = 10 cm.

In the test using a mass of aluminum rods, aluminum rods of different diameters mixed at a prescribed ratio were piled up in the space formed by the two lateral partition walls and reference lines (in the shape of squares) were drawn with ink on the end planes of the mass of rods. In the case of sand, the term "*dense packing*" is to refer to sand placed in a number of layers, with each layer of sand compacted by poking with a bar. Pigmented sand grains were laid horizontally between layers of sand to serve as a reference lines. To examine the condition of downward movement of

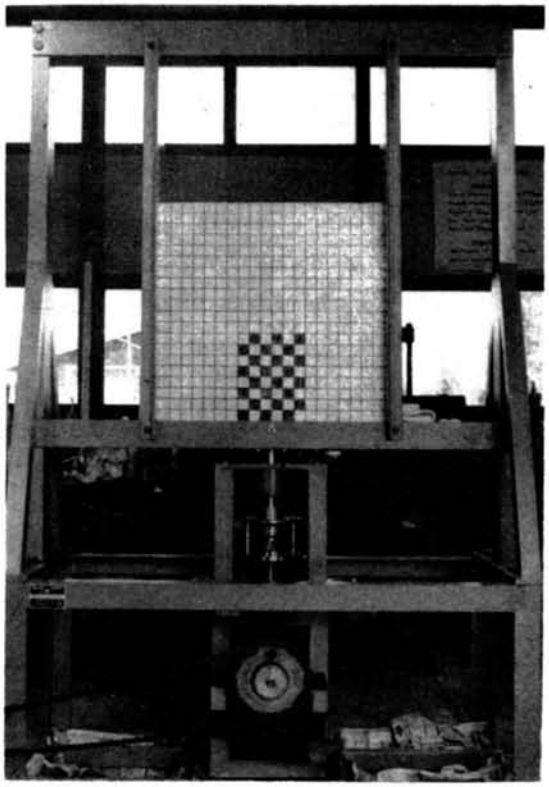

Photo2.3.1 Test apparatus with lowering floor for rod mass.

ground material in consequence of the removal of the lowering floor, the scenes of test were photographed in the following three ways.

Method-(a): A camera was fixed at a particular position of the ground. The ground profile was photographed each time the lowering floor moved a height of "δ". The photographs thus obtained enabled the author to tell the amount of settlement at various points of the ground and the condition of deformation of the ground profile.

Method-(b): A camera was fixed on the ground. The ground profile was photographed periodically on the same frame of film until the lowering floor was lowered to a fixed level. This film enabled the author to determine a flow line for the movement of ground material and to tell the conditions of ground movement.

Method-(c): A camera was fastened onto a stand joined directly to the lowering floor of the apparatus, so that the camera would move simultaneously with that floor section. The ground profile was photographed intermittently on one frame of film while the camera moved downward through a fixed distance. The photographs thus taken enabled the author to observe the range of ground which had fallen simultaneously with the lowering floor in the form of still images.

For accurate determination of settlement on the ground surface and within the ground interior, a dial gauge and a reading telescope were used. A shear test was per-

formed to find the internal friction angle ϕ of the ground materials (a mass of cylindrical aluminum rods and sand), the increment Δn_{max} of the porosity due to shear and the width "s" of the sliding zone. In the shear test performed on a mass of cylindrical aluminum rods, a special direct shear box apparatus (having the same design as described in Chapter 2 of Part I but measuring 6 cm in specimen width and 5 cm in height) was used which left the front and rear faces of rods unrestricted and permitted direct observation of the movement of the mass of rods. In the shear test performed on sand, an ordinary direct shear box apparatus was used.

The author further carried out floor-lowering tests for the analysis of ground settlement occurring in the longitudinal direction in consequence of tunnel excavation and also for the three-dimensional analysis of settlement of ground surface. These tests are discussed in later paragraphs.

3.3 CONDITION OF MOVEMENT OF GROUND MATERIAL

3.3.1 Width of Zone of Movement

To understand the condition of movement of the mass of aluminum rods and the strata of sand, the author photographed the ground profile on one frame of film while the lowering floor was lowered to a fixed level, using a camera which was fixed on the ground (refer to method-(b)). The photographs taken of the mass of aluminum rods and of the strata of sand are shown in Photo.2.3.2 - Photo2.3.4. An observation of these photographs reveals that the width of the zone of movement increases more than the width "B" of the lowering floor and that a regular flow line of movement

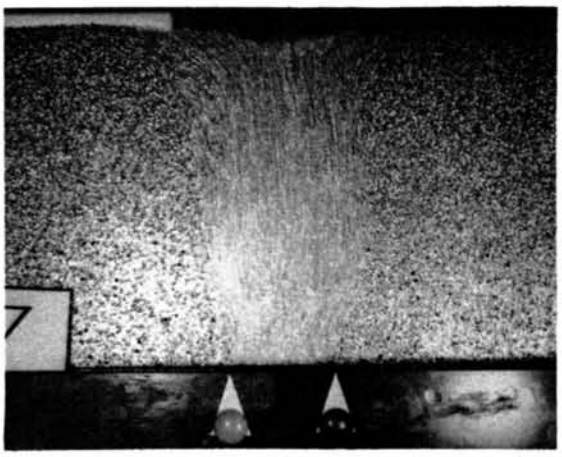

Photo.2.3.2 Movement of aluminum rod mass (ϕ 1.6mm and ϕ 3mm), B = 9cm, D = 30.7cm, δ = 46 ~ 70mm.

involving a certain width forms at a particular level when the amount of lowering "δ" exceeds a certain value. Determination of this range of the zone of movement is extremely important.

The author defines the width "B_c" of the zone of movement as the width at

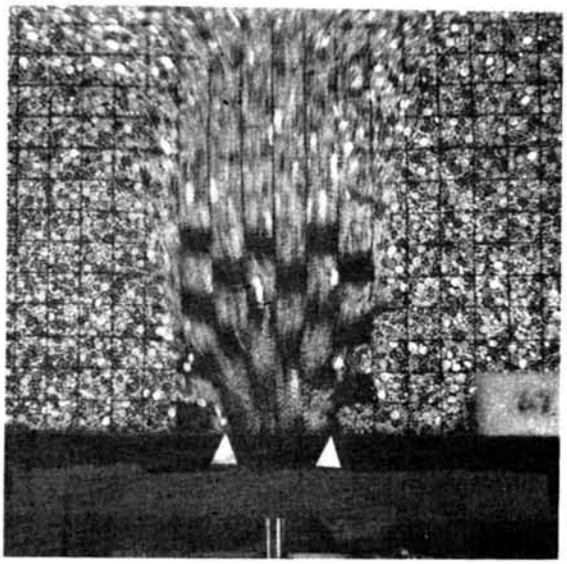

Photo.2.3.3 Movement of aluminum rod mass (φ 3mm, φ 5mm and φ 9mm), B = 10cm, D = 41.6cm, δ = 30～70mm.

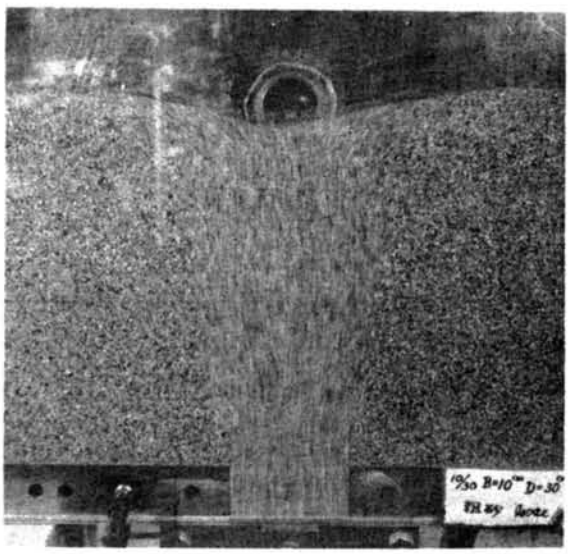

Photo.2.3.4 Movement of sand strata (loose coarse sand), B = 10cm, D = 30cm, δ = 52～64mm.

the point where the flow lines of movement are parallelized (see Fig.2.3.3). This width is variable with the soil height "D" and the width "B" of the lowering floor, the kind of ground material (mass of aluminum rods, coarse sand, fine sand) and also the condition of packing (dense packing and loose packing). When the width B_c of the zone of movement and the soil height D are plotted in terms of the $B_c/B \sim D/B$ relation deprived of dimensionality by the width B of the lowering floor, a linear relation is obtained as shown in Fig.2.3.1 which is determined by the kind and the

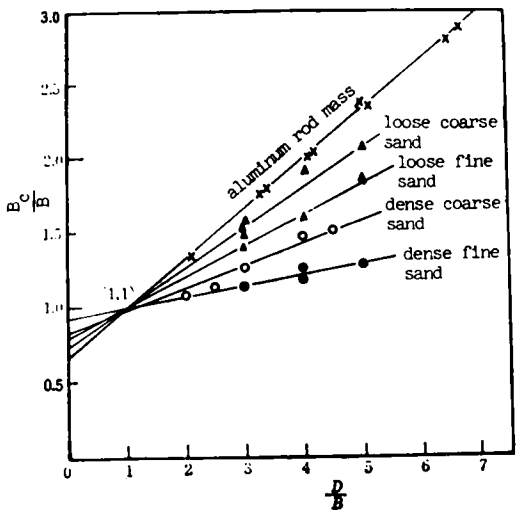

Fig.2.3.1 Relationship between B_c/B and D/B on aluminum rod mass, loose coarse sand, loose fine sand, dense coarse sand and dense fine sand.

condition of ground materials. This relation is expressed by the following equation.

$$\frac{B_c}{B} = C_1 \cdot \frac{D}{B} + C_2 \qquad (2.3.1)$$

wherein, C_1 and C_2 are constants fixed by the material and condition of packing. Although the relation (2.3.1) is empirical in nature, it can be proven for a fairly wide range of test conditions. The author, therefore, proposes to discuss this relation in its physical significance.

3.3.2 Primary Zone and Transfer Pattern of Settlement

Photo.2.3.5 through Photo.2.3.7 depict the mass of aluminum rods and the strata of sand photographed in a floor-lowering model test by using a camera so fixed as to move downward simultaneous with the lowering floor (refer to method-(c)). In the photographs, clearly photographed still areas show the zones of ground which fell simultaneously with the lowering floor. Such area is called hereinafter as "*primary zone*".

Since the shape of the primary zone was thought to be related to the grain sizes and grain distribution, the author decided to simulate the grain size distribution by

a mass of cylindrical aluminum rods with the two different diameters (1.6 mm and 3 mm). The author conducted a sampling of grains by following the method which Matsuo et al.[12] effected requiring sampling of sand having an ordinary grain size distribution

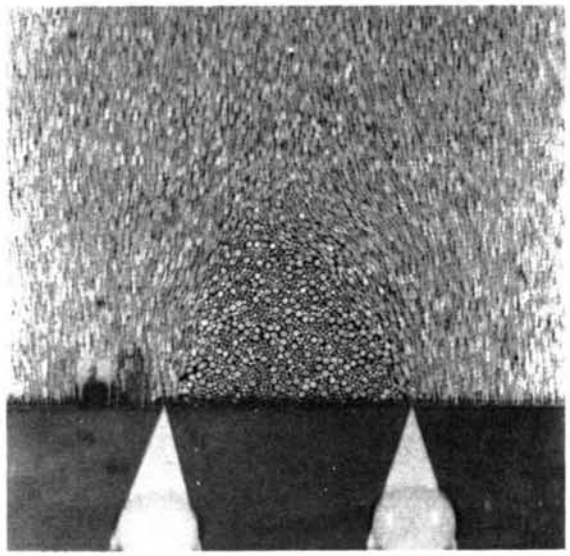

Photo.2.3.5 Movement of aluminum rod mass (ϕ 1.6mm and ϕ 3mm) photographed intermittently by the camera joined to lowering floor, B = 9cm, D = 30 cm, $\delta = 4 \sim 7$mm.

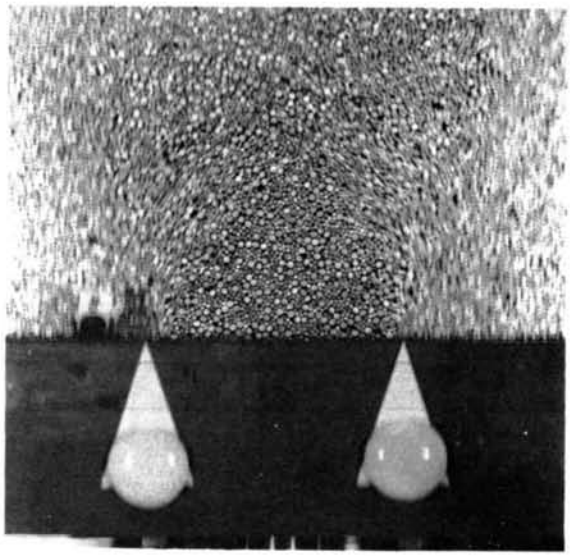

Photo.2.3.6 Movement of aluminum rod mass (ϕ 1.6mm and ϕ 3mm) photographed intermittently by the camera joined to lowering floor, B = 9cm, D = 30cm, $\delta = 28 \sim 31$mm.

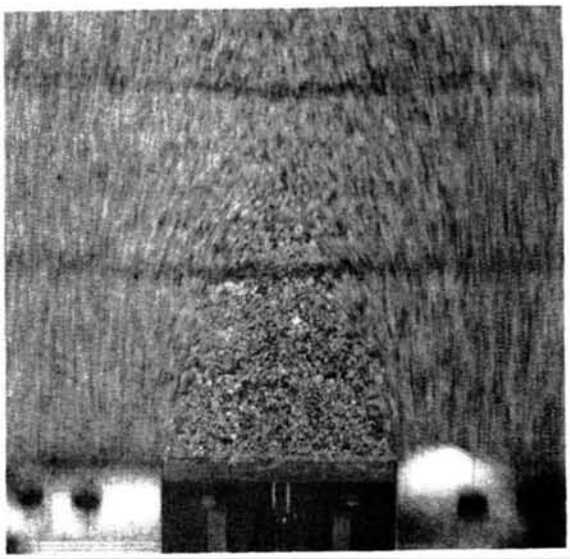

Photo.2.3.7 Movement of sand strata (loose coarse sand) photographed intermittently by the camera joined to lowering floor, B = 10cm, D = 49cm, $\delta = 0 \sim$ 10mm.

through a modified application of Monte Carlo method (cf. Paragraph 2.3 in Chapter 2 of Part I). The mixing ratio by weight (60 : 40) of the two rod diameters was converted to the ratio of numbers of rods (84 : 16) and the new ratio was tried by the uniform random number. When a number falling in the range of 01 — 84 was obtained, a grain 1.6 mm in diameter was sampled and when a number in the range of 85 — 00 was obtained, a grain having a diameter of 3 mm was sampled. The other grains were sampled out by repeating this procedure. Grains were placed side by side from left to right on the lowermost layer. On the second layer formed immediately above, grains were piled sequentially from left to right in their respective self-supporting positions. (The order "from left to right" was one rule for determining the order for arranging grains and, therefore, could have been reversed as "from right to left" to suit the occasion.) One example in which grains were sequentially piled up on the lowermost layer of grains in the manner just explained is illustrated in Fig.2.3.2. (The serial numbers found in the diagram show the order in which relevant grains were arranged.) The void ratio in this diagram was about 0.24, a value which satisfactorily agrees with the void ratio determined by an actual test. If, in this diagram, the width of the lowermost layer of grains is assumed to be the width of the lowering floor, then the zone of arch shape represents the portion which can move downwardly in a vertical direction in consequence of the downward removal of the lowering floor. This movement is considered to be the physical meaning of the primary zone. In fact, the shape shown in Fig.2.3.2 quite resembles the shapes of primary zones shown in Photos.2.3.5 and 2.3.6.

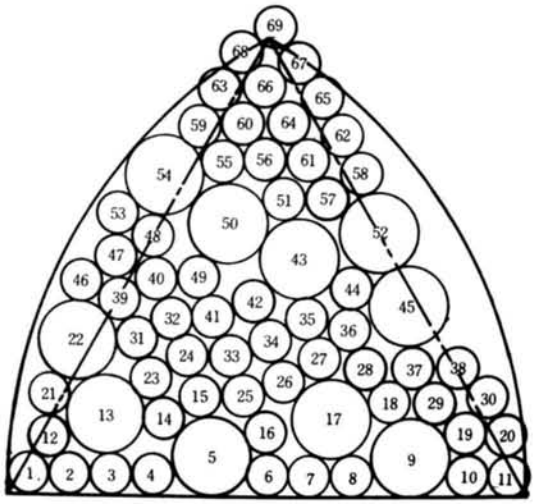

Fig.2.3.2 Simulation of two-dimensional particle arrangement obtained by applying Monte Carlo method and shape of primary zone.

As special cases, a structure having cylindrical aluminum rods of a uniform diameter (9 mm) packed to the densest possible extent (hexagonal arrangement) and a structure having the same rods packed to the loosest possible extent (square arrangement) are shown in Photo.2.3.8 and Photo.2.3.9 respectively. The photographs indicate that the primary zone is not necessarily fixed but is variable with the particle diameter and

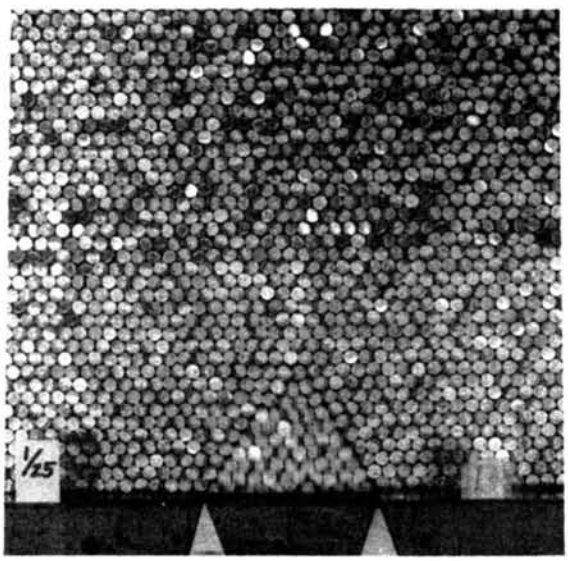

Photo.2.3.8 Movement of aluminum rod mass of a uniform diameter (9mm) packed in hexagonal arrangement, $\delta = 2 \sim 5$mm.

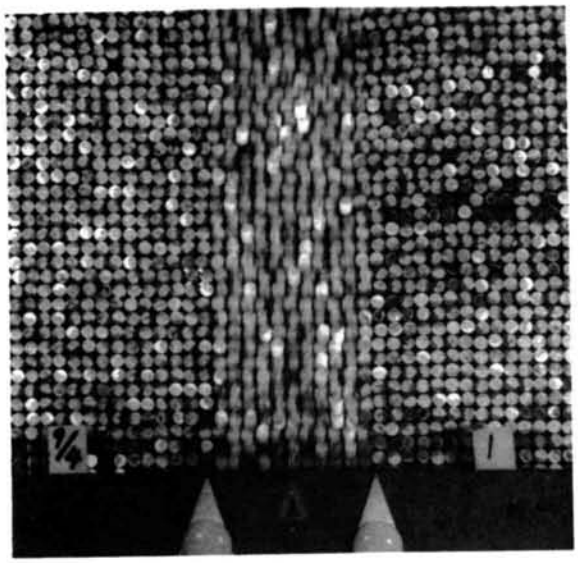

Photo.2.3.9 Movement of aluminum rod mass of a uniform diameter (9mm) packed in square arrangement, $\delta = 0 \sim 5$mm.

particle arrangement. The structure of the loosest possible packing (square arrangement) shown in Photo.2.3.9 represents an unstable particle arrangement and it is considered to exist only infrequently in actual grounds. The primary zone in the physical sense then means that zone of ground which can move downwardly in a vertical direction jointly with the lowering floor. This zone is thought to have the shape of an arch which approximately circumscribes an equilateral triangle, though it is variable with the particle size and the particle distribution.

As the lowering floor moved downward, loosening of the ground was transferred this primary zone and the transfer was seen to reach the ground surface shortly afterwards as shown in Photo.2.3.10 – Photo.2.3.13. The observation led the author to conceive of a transfer pattern of settlement as shown in Fig.2.3.3. This pattern is based on a hypothesis that a front line of loosening in the shape of an arch similar to the arched shape of the primary zone expands and at the same time transfers itself upwardly, and that when the forward end of the arch-shaped front reaches the ground surface, the width of the zone of movement no longer is increased. If the shape of the primary zone is assumed to be an arch approximately circumscribing an equilateral triangle, the width B_c of the zone of movement may be calculated from this transfer pattern of settlement as follows:

$$B_c = B + 2\left(D - \frac{\sqrt{3}}{2}B_c\right)\cdot\cot\theta$$

$$\therefore \frac{B_c}{B} = \frac{2}{\tan\theta + \sqrt{3}} \cdot \frac{D}{B} + \frac{\tan\theta}{\tan\theta + \sqrt{3}} \qquad (2.3.2)$$

wherein, θ is the angle of expansion of the zone of movement as shown in the diagram.

The formula (2.3.2) is similar in form to (2.3.1), satisfies $B_C/B \cong 1$ when $D/B = 1$ and does not contradict the fact that all straight lines approximately pass the coordinates (1, 1) as illustrated in Fig.2.3.1. So, the author seeks the meaning of the empirical formula of (2.3.1) in the formula of (2.3.2) and obtains the following relations:

$$C_1 = \frac{2}{\tan\theta + \sqrt{3}} \quad , \quad C_2 = \frac{\tan\theta}{\tan\theta + \sqrt{3}} \qquad (2.3.3)$$

The angle of expansion "θ" of the zone of movement will assume a practically fixed value when the kind of ground material and the condition of packing are determined from the floor-lowering test. This relation is entered in the fourth column of Table 2.3.1. In view of the values of θ thus indicated, the values of C_1 and C_2 calculated by Eq. (2.3.3) are in approximate agreement with those of C_1 and C_2 calculated on the basis of the gradients of corresponding straight lines and the intersections of relevant ordinates in Fig.2.3.1. Therefore, Eq. (2.3.1) may well be considered to have the physical meaning indicated by Eq. (2.3.2).

Since the width of expansion B_C of the zone of movement can be determined from Eq. (2.3.2) if the value of θ can be predicted, the author now considers the meaning of this angle θ. The boundary between the zone of movement and the stationary zone surrounding the zone of movement is unmistakably one slip plane. According to Mohr-Coulomb's failure criterion, the slip plane intersects the direction of the major principal stress with an angle of $(45^\circ - \phi/2)$ (wherein, ϕ is the internal friction angle). In the neighborhood of the lowering floor, an arch-shaped line of transfer of interparticle force like the one shown in Photo.2.3.14 or the line of major compressive principal stress is formed because of the arch action resulting from the downward removal of the lowering floor. Therefore, the slip planes which rise from both ends of the lowering floor are not straight lines. They are curved lines as shown in Photo.2.3.2 and Photo.2.3.3. In Fig.2.3.3, they are approximated by straight lines forming an angle of θ by averaging their curved portions. It follows that the average direction of the maximum principal stress near the ends of the lowering floor can be calculated by the above relation on the basis of the vaule of θ. The results of this calculation are shown in the sixth column of Table 2.3.1. The values invariably indicate that the directions are inclined by 16° outwardly from the vertical.

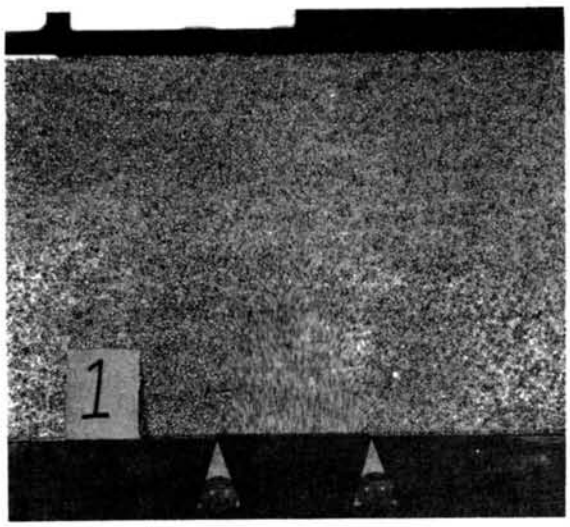

Photo.2.3.10 Transfer of movement of aluminum rod mass (ϕ 1.6mm and ϕ 3mm) No.1, $\delta = 0 \sim 5$mm, B = 12cm, D = 31.1cm.

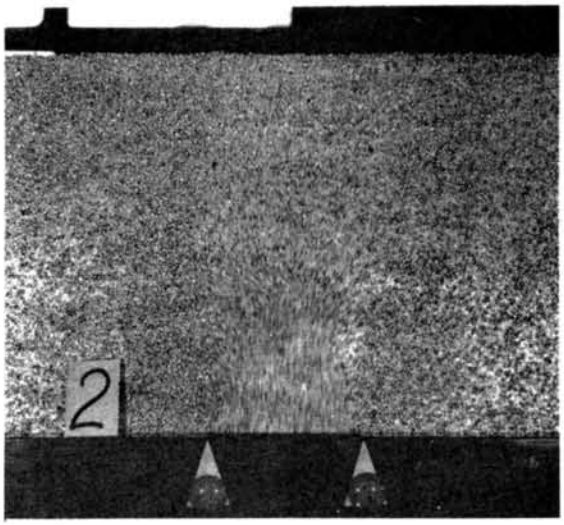

Photo.2.3.11 Transfer of movement of aluminum rod mass (ϕ 1.6mm and ϕ 3mm) No.2, $\delta = 5 \sim 10$mm.

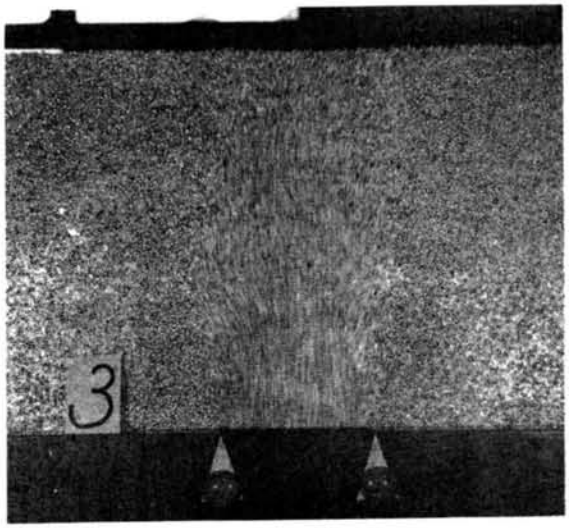

Photo.2.3.12 Transfer of movement of aluminum rod mass (ϕ 1.6mm and ϕ 3mm) No.3, $\delta = 10 \sim 20$mm.

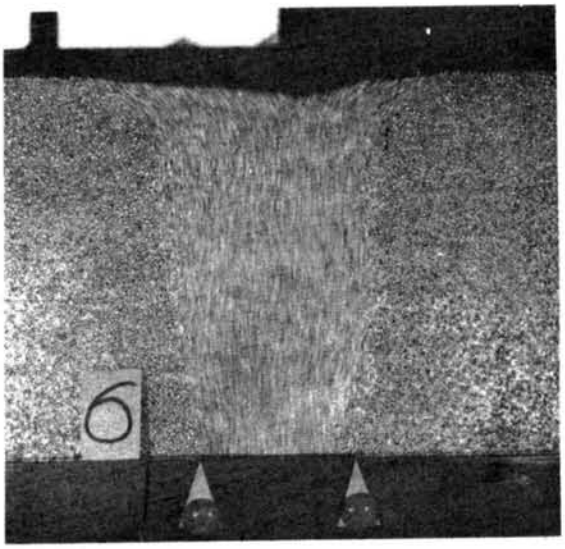

Photo.2.3.13 Transfer of movement of aluminum rod mass (ϕ 1.6mm and ϕ 3mm) No.4, $\delta = 40 \sim 50$mm.

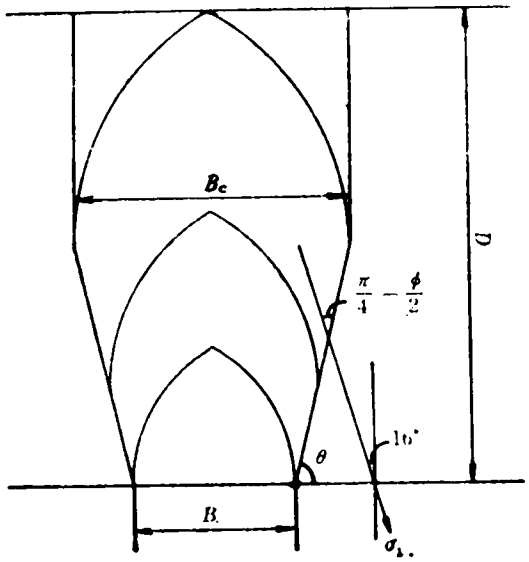

Fig.2.3.3 Transfer pattern of settlement and rotation of principal stress direction.

Table 2.3.1 Relationship among ground materials, angle of expansion θ of zone of movement, internal friction angle ϕ and direction of principal stress.

Ground materials		Grain size (mm)	Void ratio e	θ	Internal friction angle ϕ	$\theta - \frac{\phi}{2} - 45^\circ$
Aluminum rod mass		ϕ 1.6, ϕ 3.0	0.23 ~ 0.27	76°	30°	16°
Coarse sand	Loose	0.3 ~ 5.0	0.74 ~ 0.81	80°	37°	16°
	Dense		0.65 ~ 0.69	85°	48°	16°
Fine sand	Loose	0.1 ~ 1.0	0.88 ~ 0.94	83°	43°	16°
	Dense		0.72 ~ 0.76	88°	54°	16°

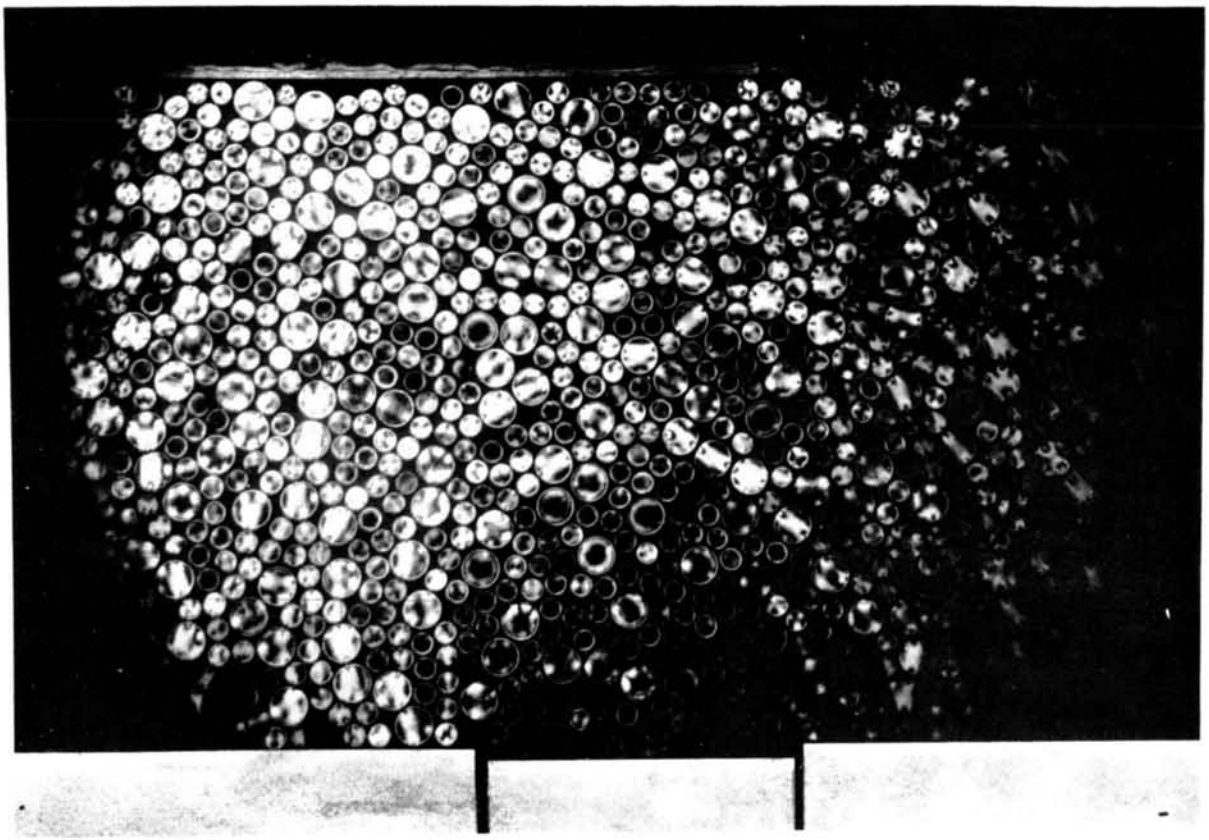

Photo.2.3.14 Arch-shaped line of transfer of interparticle force in photoelastic rod mass (ϕ 6.2mm and ϕ 10mm), B = 7.5cm, δ = 4mm.

It should be noted that the values of ϕ (fifth column of Table 2.3.1) used in this calculation are those which have been determined by the direct shear box test which was performed by adjusting the test material and its stress condition to the relevant floor-lowering test condition. In other words, it is considered that the direction of the major principal stress which is substantially vertical prior to the start of the downward removal of the lowering floor is turned 16° outwardly from the vertical after the downward removal is started. In the floor-lowering test described above, the direction of the major principal stresses were invariably turned 16° from the vertical direction. If the direction of principal stress during the local settlement can be estimated under other conditions, then it is possible to determine the value of θ by calculating the value of ϕ through the shear test of a given ground material. Consequently, the coefficients in the formula of (2.3.2) can be determined emprically.

3.4 ANALYSIS OF GROUND SURFACE SETTLEMENT

In the preceding section, the range of the zone of movement and the physical meaning of the zone of movement have been discussed. The mechanism of settlement of the ground of a granular soil has been analyzed on the basis of this formulation in an effort to derive the formula for calculating the amount of ground surface settlement, ρ_{SO}, along the central line of the lowering floor.

A void of the amount of $B \cdot \Delta\delta$ per unit depth occurs when the lowering floor completes a downward movement of the amount of $\Delta\delta$. This void is immediately filled up by the portion of ground material situated directly above, with the result that the void is transferred upwardly throughout the depth of the ground. In the case of a liquid, such void (bubbles) invariably reach the free surface and cause the surface level to fall. In the case of granular materials, the void is not invariably transferred as far as the surface even though the ground surface may sink as a result. Part of such void is believed to remain in the form of an increased porosity in the ground interior. With this in mind, the author has proceeded with an analysis on the basis of the following two observations.

(1) The increase in porosity has limits. That is, there exists a critical porosity under stress conditions.

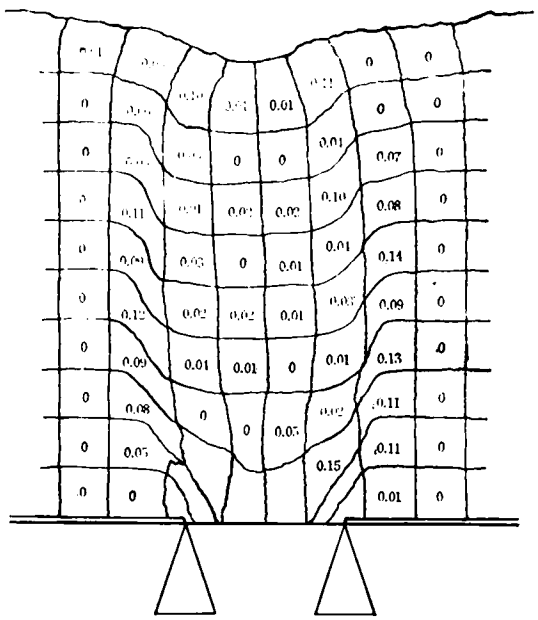

Fig.2.3.4 Change of reference lines of aluminum rod mass (ϕ 1.6mm and ϕ 3mm) and amount of increase of porosity in the mass due to downward movement of lowering floor (δ = 7cm), B = 9cm, D = 30.7cm.

(2) The void is not uniformly dispersed throughout the ground interior. The increase of porosity is observed to occur concentrically in a certain area.

Fig.2.3.4 shows how the reference lines drawn horizontally and vertically on the end planes of cylindrical aluminum rods were disturbed after the lowering floor completed a downward movement of the amount of 7 cm ($=\delta$). The increase in the porosity due to the downward movement of the lowering floor (from $\delta = 0$ cm to $\delta = 7$ cm) was calculated by determining, by a planimeter, the change in the area enclosed within perpendicularly crossing reference lines, with the calculated increase amount indicated in each relevant area. Referring first to the observation (2), it is clearly seen from the diagram that the porosity increases conspicuously along the left and right slip planes (called "*outer boundary planes*") which form boundary planes between the zone of movement and the vicinal stationary zones. This volumetric increase in consequence of the relative displacement of grains known as dilatancy, it is believed, contributes largely to the increase in porosity. A slight increase of the porosity is also observed to occur in the neighborhood of the boundary plane (called "*inner boundary plane*") between the primary zone and the secondary zone (the zone formed above the primary zone and moved to follow the primary zone). For the convenience of the present discussion, only the increase in the void along the outer boundary planes will be considered. This exclusion of the inner boundary plane represents an assumption on the safe side which admits the possibility of the amount of settlement being overestimated. As concerns (1), it is inferred from the data of Fig.2.3.4 that even within the area along the outer boundary planes which shows a heavy increase of void, the void does not infinitely increase but there exists a substantially fixed ultimate value Δn_{max} to the increase in the porosity. It has further been ascertained that this ultimate value does not appreciably change even when the lowering floor is further moved downward. From this, it may be concluded that the portion of the ground is in the state of "*critical void ratio*" under the relevant stress conditon.

On the basis of these two observations, the author has analyzed settlement by simplifying the phenomenon as illustrated in Fig.2.3.5. It is assumed that a downward movement of the lowering floor by an amount δ causes the occurrence of a clear slip plane over a length of l along the left and right outer boundary planes; that the maximum increase Δn_{max} of porosity occurs within the slip planes; and that the ground surface settles by ρ_{so} on the central line of the lowering floor. This assumption was made for the convenience of calculation, although the maximum increase of Δn_{max} is not limited to the length of l along the outer boundary planes but extends to some degree beyond that length. It is further assumed that an additional downward movement of the lowering floor by $\Delta\delta$ causes an upward transfer of the slip planes by Δl and a settlement of the ground surface by $\Delta\rho_{so}$ along the central line of the lowering floor. Thus, the following relation is established:

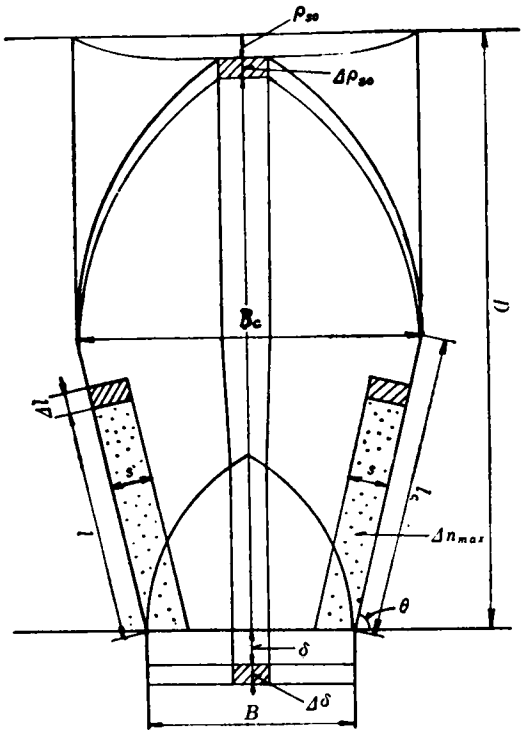

Fig.2.3.5 Ground surface settlement and increase of void in ground.

$$B \cdot \triangle\delta = B_c \cdot \triangle\rho_{so} + 2\,(\triangle l \cdot s \cdot \triangle n_{max}) \qquad (2.3.4)$$

In this formula, s stands for the width of the slip zone. From the formula (2.3.4), the following equation is derived.

$$\triangle\rho_{so} = \alpha \cdot \triangle\delta - \beta \cdot \triangle l \qquad (2.3.5)$$

wherein,

$$\alpha = B/B_c,\quad \beta = (2 \cdot s \cdot \triangle n_{max})/B_c$$

By dividing both sides of the general formula (2.3.5) by $\Delta\delta$, one obtains the following equation.

$$\frac{\triangle\rho_{so}}{\triangle\delta} = \alpha - \beta \cdot \frac{\triangle l}{\triangle\delta} \qquad (2.3.6)$$

With a dial gauge placed on the surface of the ground, the amount of surface settlement, ρ_{SO}, along the central line of the lowering floor was measured. The results obtained were plotted with respect to the relation between $\Delta\rho_{SO}/\Delta\delta$ and δ. These plots are given in Fig.2.3.6, Fig.2.3.7 and Fig.2.3.8. The data of Fig.2.3.6 are those of a ground simulated by a mass of aluminum rods; those of Fig.2.3.7, of a ground

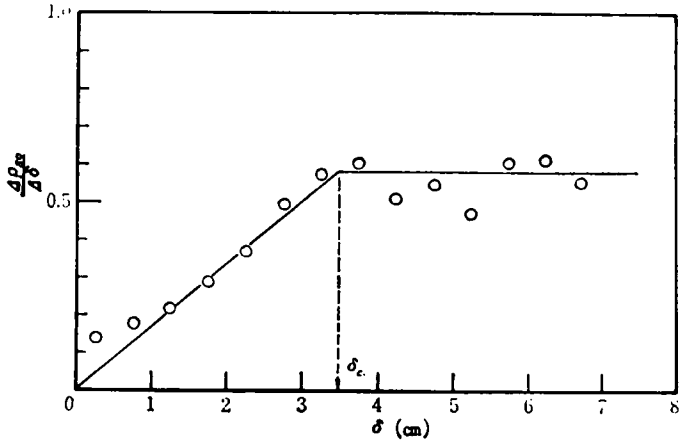

Fig.2.3.6 Relationship between $\Delta\rho_{SO}/\Delta\delta$ and δ on aluminum rod mass (ϕ 1.6mm and ϕ 3mm), B = 9cm, D = 30.1cm.

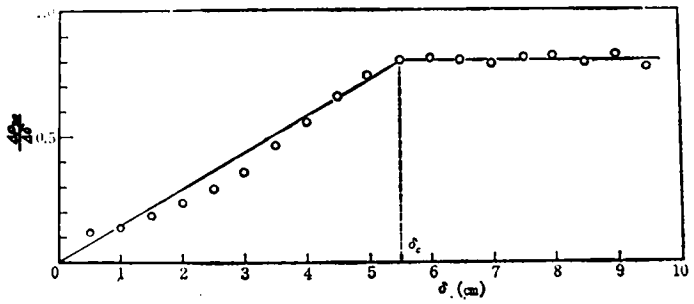

Fig.2.3.7 Relationship between $\Delta\rho_{SO}/\Delta\delta$ and δ on dense coarse sand (e_i = 0.66), B = 10cm, D = 30cm.

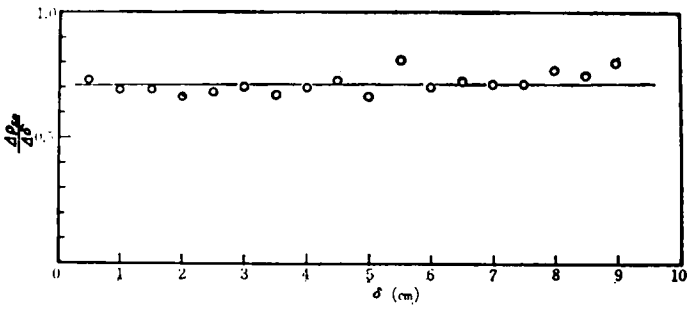

Fig.2.3.8 Relationship between $\Delta\rho_{SO}/\Delta\delta$ and δ on loose fine sand (e_i = 0.91), B = 10cm, D = 30cm.

simulated by a densely packed mass of coarse sand; and those of Fig.2.3.8, of a ground simulated by a loosely packed mass of find sand.

In the case of a ground of loosely packed fine sand, the value of $\Delta\rho_{so}/\Delta\delta$ is large initially and remains substantially at a fixed level as is evident from Fig.2.3.8. It is noted that this fixed value approximately equals the value of $\alpha \equiv B/B_c$. Thus we can postulate that the stratum of sand is the critical void ratio (i.e., the void ratio no longer occurs in consequence of the phenomenon of shear). The substitution of $\Delta n_{max} = 0$ in the formula (2.3.6) eliminates the second term of the right-hand member of the equation. Thus $\Delta\rho_{so}/\Delta\delta = \alpha$. When a direct shear box test was carried out on this sand under an estimated normal stress on the outer boundary planes as calculated by the application of Terzaghi's arching theory[13] to the slip planes or outer boundary planes, the void ratio in the sand stratum was found to be approximately equal to the critical void ratio.

In the case of a ground simulated by a mass of aluminum rods or a densely packed coarse sand, it is seen from Fig.2.3.6 and Fig.2.3.7 that the value of $\Delta\rho_{so}/\Delta\delta$ increases linearly with δ, reaching a fixed level when $\delta = \delta_c$ and remaining essentially unchanged after that. It has been found that this fixed value of $\Delta\rho_{so}/\Delta\delta$ approximately equals the value of α which can be calculated. This can be understood by the following interpretation. As shown in Fig.2.3.5, the length l of the portion in which the maximum increase Δn_{max} occurs along the left and right outer boundary planes increases with δ; and the forward end of the arch-shaped transfer pattern of settlement which stands on the planes reaches the ground surface when $l = l_c$ is satisfied. With regard to the system enclosed by the pair of slip planes (each of a length of l_c along the outer boundary planes) and the periphery of the arch-shaped transfer pattern of settlement standing on these boundary planes, we conclude that no further increase occurs in the void. Then, $\Delta\rho_{so}/\Delta\delta = \alpha$ is satisfied by Eq. (2.3.6). In fact, it is observed from photographed test results that slip planes are clearly extended as far as the point of $l = l_c$ when $\delta = \delta_c$.

In the case of a ground of ordinarily packed mass, the relation of $\Delta\rho_{so}/\Delta\delta \sim \delta$ is characteristic of dense packing, suggesting that even natural grounds show characteristics of dense packing in most cases. Since Fig.2.3.8 is thought to apply to the case where $\delta_c = 0$, the author proceeds to consider cases as represented in Fig.2.3.6 and Fig. 2.3.7. It is assumed, in these cases, that the value of $\Delta\rho_{so}/\Delta\delta$ increases linearly with δ until $\delta = \delta_c$ equals α when $\delta = \delta_c$ is satisfied. Then, the following relations are established.

$$0 \leqq \delta \leqq \delta_c \; ; \quad \frac{\alpha \rho_{so}}{\alpha \delta} = \frac{\alpha}{\delta_c} \cdot \delta \qquad (2.3.7)$$

$$\delta \geqq \delta_c \; ; \quad \frac{\alpha \rho_{so}}{\alpha \delta} = \alpha \qquad (2.3.8)$$

By integrating Eq. (2.3.7) and assuming the condition $\rho_{so} = 0$ for $\delta = 0$, we derive the following relation.

$$\rho_{so} = \frac{\alpha}{\delta_c} \cdot \frac{\delta^2}{2}, \quad (0 \leqq \delta \leqq \delta_c) \qquad (2.3.9)$$

By integrating Eq. (2.3.8) and introducing the condition permitting consistancy with Eq. (2.3.9) when $\delta = \delta_c$, we obtain the following relation.

$$\rho_{so} = \alpha \cdot (\delta - \frac{\delta_c}{2}), \quad (\delta \geqq \delta_c) \qquad (2.3.10)$$

If the value of δ_c can be found, therefore, the amount of ground surface settlement ρ_{so} can be calculated as a function of the downward movement δ.

The length l of the slip planes within the aforementioned system equals l_c when $\delta \geqq \delta_c$. By integrating Eq. (2.3.5) and substituting $l = l_c$, we obtain the following.

$$\rho_{so} = \alpha \cdot \delta - \beta \cdot l_c \quad (\delta \geqq \delta_c) \qquad (2.3.11)$$

Equating the right members of Eqs. (2.3.10) and (2.3.11),

$$\delta_c = \frac{2\beta}{\alpha} \cdot l_c \qquad (2.3.12)$$

Substitution of

$$\alpha = B/B_c, \quad \beta = (2 \cdot s \cdot \triangle n_{max})/B_c, \quad l_c = (D - \frac{\sqrt{3}}{2} B_c) \cdot \mathrm{cosec}\theta$$

in Eq. (2.3.12) produces the following:

$$\delta_c = (4 \cdot s \cdot \triangle n_{max}) \cdot \mathrm{cosec}\theta \cdot (\frac{D}{B} - \frac{\sqrt{3}}{2} \frac{B_c}{B}) \qquad (2.3.13)$$

By substituting Eq. (2.3.2) in Eq. (2.3.13) and rearranging the results, one obtains the following formula.

$$\delta_c = \frac{4 \cdot s \cdot \triangle n_{max}}{\sin\theta + \sqrt{3} \cdot \cos\theta} \cdot (\frac{D}{B} - \frac{\sqrt{3}}{2}) \qquad (2.3.14)$$

Fig.2.3.9 shows plots of δ_c vs. D/B obtained from a mass of cylindrical aluminum rods, densely packed masses of coarse and fine sand respectively. We conclude that δ_c increases substantially linearly with D/B and that all these lines intersect the horizontal axis at approximately $\sqrt{3}/2 \cong 0.87$, which does not contradict Eq. (2.3.14). The

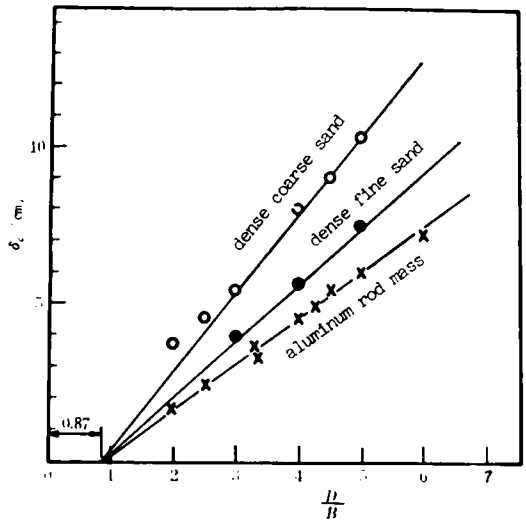

Fig.2.3.9 Relationship between δ_c and D/B on dense coarse sand, dense fine sand and aluminum rod mass.

Table 2.3.2 Comparison of coefficient $(4 \cdot s \cdot \Delta n_{max})$

Ground materials	$(4 \cdot s \cdot \Delta n_{max})$ obtained from the gradient of Fig.2.3.9	① s (cm)	② Δn_{max}	$(4 \cdot s \cdot \Delta n_{max})$ calculated by $4 \times ① \times ②$
Aluminum rod mass	2.02	3 ~ 4	0.10 ~ 0.15	1.20 ~ 2.40 (mean value: 1.80)
Dense coarse sand	2.83	4 ~ 4.5	0.13 ~ 0.18	2.08 ~ 3.24 (mean value: 2.66)
Dense fine sand	1.88	2 ~ 3	0.13 ~ 0.19	1.04 ~ 2.28 (mean value: 1.66)

value of $(4 \cdot s \cdot \Delta n_{max})$ has also been calculated on the basis of "s" actually found from the deformation of horizontal reference lines in the test ground and the value of Δn_{max} obtained by a direct shear box test conducted by conforming the stress condition and the initial void ratio to the ground under test. The two sets of values thus obtained are compared in Table 2.3.2. In the case of a direct shear box test which involves an ordinary thickness of test material, the shear zone may not extend through the entire thickness of material. In the shear test for sand, therefore, the thickness of test material was reduced. Where a mass of cylindrical aluminum rods was used, the

width of the slip zone was determined from the deformation in the reference lines drawn on the end planes of the rods (which was found to be 3 ~ 4 cm similar to the test ground) and the value of Δn_{max} calculated by the volumetric increase relative to the width of the slip zone. The average values of $(4 \cdot s \cdot \Delta n_{max})$ calcualted (enumerated in the fifth column of Table 2.3.2) are found to be in relative agreement with the values calculated from the gradient of Fig.2.3.9. This suggests that δ_c has the physical meaning indicated by Eq. (2.3.14).

That the average values of $(4 \cdot s \cdot \Delta n_{max})$ shown in the fifth column of the table are slightly larger may be explained by considering a possible effect of the assumption (see Fig.2.3.5) that when δ has a certain value the increase of void occurs only along the outer boundary planes and that the maximum increase of void occurs only to the length of l along the outer boundary planes on both sides. We have assumed that shear within the ground is caused by the movement of soil particles due to gravitational attraction and, therefore, represents a phenomenon of progressive failure gradually expanding from the portions juxtaposed to the lowering floor along the outer boundary planes. In the direct shear box test, however, the grains on the shear plane are simultaneously subjected to shear displacement. As previously described, however, the width of the slip zone, s = 3 to 4 cm, obtained with the model test of ground is similar to that obtained by the direct shear box test on the mass of aluminum rods. Also the increase in porosity shown in Fig.2.3.4 suggests that the values, $\Delta n_{max} = 0.10$ to 0.15 (in the fourth column of Table 2.3.2), obtained by the direct shear box test are substantially reasonable ones. From this, we may conclude that shear within the ground interior corresponds, in principle, to the phenomenon of shear within the shear test apparatus though not completely and that the width "s" of the slip zone and that Δn_{max} can approximately be estimated by considering stress and the material condition. If s and Δn_{max} can be estimated, then δ_c can be calculated by Eq. (2.3.14). ρ_{SO}, the ground surface settlement on the central line of the lowering floor can then be calculated as a function of the downward movement δ of the lowering floor by substituting the calculated value of δ_c in Eqs. (2.3.9) and (2.3.10).

(Example 1) A ground simulated by a mass of cylindrical aluminum rods (having diameters of 1.6 mm and 3 mm) is tested, with the width of the lowering floor B = 9 cm and the soil depth D = 30 cm. In this case, we obtain the following equation from Fig.2.3.1 or by substituting $\theta = 76^\circ$ in Eq. (2.3.2).

$$\frac{B_c}{B} = 0.34 \times \frac{30}{9} + 0.70 = 1.83 \qquad \therefore B_c = 16.5 \text{ (cm)}$$

Therefore, $\alpha = B/B_c = 9/16.5 = 0.55$ is obtained.

By substituting s = 4 cm, $\Delta n_{max} = 0.13$ and $\theta = 76^\circ$ in Eq. (2.3.14), or from Fig.2.3.9 the following value is obtained.

$$\delta_c = 1.5 \times \left(\frac{30}{9} - \frac{\sqrt{3}}{2}\right) = 3.7\ (\mathrm{cm})$$

Accordingly, ρ_{so} can be calculated as a function of δ by substituting α and δ_c in Eqs. (2.3.9) and (2.3.10). Where δ = 7.0 cm, for example, the value of ρ_{so} is calculated by Eq. (2.3.10) as follows:

$$\rho_{so} = 0.55 \times \left(7.0 - \frac{3.7}{2}\right) = 2.8\ (\mathrm{cm})$$

The value determined by means of a dial gauge placed on the ground surface was 2.83 cm.

3.5 ANALYSIS OF SETTLEMENT OF GROUND INTERIOR

ρ_o, the amount of settlement of points in the ground interior along the central line of the lowering floor was measured with the aid of a reading telescope and was plotted in terms of the $\Delta\rho_o/\Delta\delta \sim \delta$ relation. The plot thus obtained is shown in Fig.2.3.10. This graph has the same trend as Fig.2.3.6 and Fig.2.3.7. This suggests

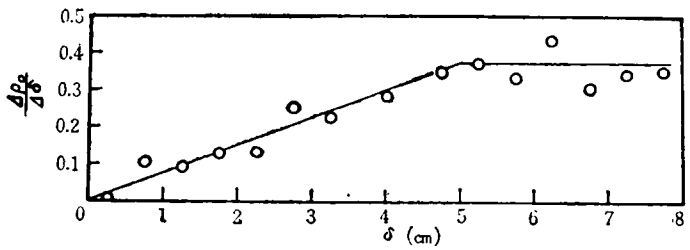

Fig.2.3.10 Relationship between $\Delta\rho_o/\Delta\delta$ and δ on aluminum rod mass (ϕ 1.6mm and ϕ 3mm), B = 6cm, D = 36cm, z = 25.5cm.

that Paragraph 3.4 can be expanded to include the settlement of the ground interior at a given depth of ground. Specifically with respect to a given point within the ground interior, the left and right slip planes rise and the arch-shaped transfer pattern of settlement front which stands on the slip planes rises to reach the critical point, at which time the void existing within that system remains unchanged and the grains move so as to satisfy continuity.

In considering the phenomenon of settlement within the ground interior, α and δ_c which were constants in Paragraph 3.4 are now functions of the position "z" within the ground interior (the position "z" is measured vertically from the position of the lowering floor prior to the start of its downward motion). Therefore, ρ_o is a function of not only δ but also z. As a first step, the author considers $\alpha(z)$. Assume a flow

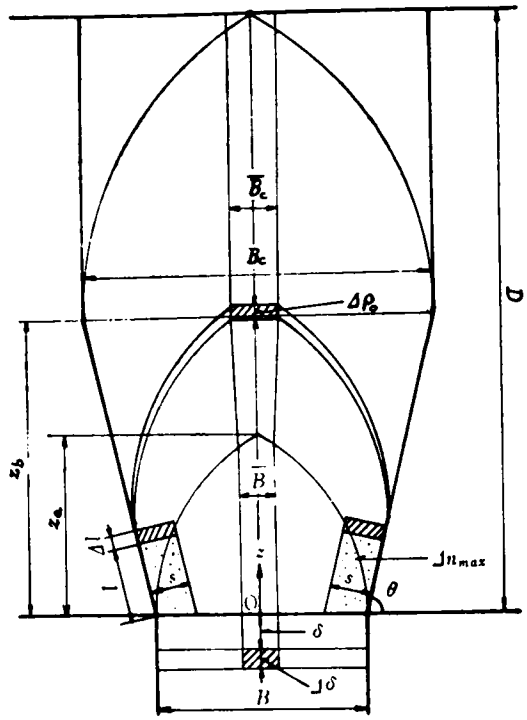

Fig.2.3.11 Underground settlement and increase of void in ground.

pipe formed when the width $\overline{B}$ illustrated in Fig.2.3.11 is expanded to $\overline{B}_c$. Then $\overline{B} = B/n$ and $\overline{B}_c = B_c/n$, wherein n is a suitable divisor. The primary zone falls simultaneously with the downward movement of the lowering floor as if it were mounted on the lowering floor. Consequently, the width $\overline{B}$ remains unchanged and α is 1 by the formula of its definition. Since parallel flow lines are formed with an expanded width of B_c where $z \geqq z_b$, $\alpha = \Delta\rho_0/\Delta\delta = B/B_c$ is obtained from continuity. Where $z_a \leqq z \leqq z_b$, it is assumed that the width increases linearly from $\overline{B}$ for $z = z_a$ to $\overline{B}_c$ for $z = z_b$. In this case, $\overline{B}_c(z)$ for $z_c \leqq z \leqq z_b$ can be expressed by the following.

$$\overline{B}_c(z) = \frac{\overline{B}_c - \overline{B}}{z_b - z_a} \cdot (z - z_a) + \overline{B} \qquad (2.3.15)$$

Here, it is assumed that $z_a = (\sqrt{3}/2)\cdot B$ and $z_b = D - (\sqrt{3}/2)\cdot B_c$ as described in Paragraph 3.3. Therefore $\alpha = \overline{B}/\overline{B}_c(z)$ holds well. Summarizing the above, one obtains the following.

$$\alpha(z) = \begin{cases} 1 & (0 \leqq z \leqq z_a) \\ \overline{B}/\overline{B}_c(z) & (z_a \leqq z \leqq z_b) \\ \overline{B}/\overline{B}_c = B/B_c & (z \geqq z_b) \end{cases} \qquad (2.3.16)$$

Then, $\delta_c(z)$ is expressed in the same form as Eq. (2.3.14) and can be found by substituting the soil depth D of Eq. (2.3.14) by z. Thus, we obtain the following.

$$\delta_c(z) = \frac{4 \cdot s \cdot \Delta n_{max}}{\sin\theta + \sqrt{3} \cdot \cos\theta} \left(\frac{z}{B} - \frac{\sqrt{3}}{2} \right) \qquad (2.3.17)$$

The amount of settlement of ground interior is also expressed in the same form as Eqs. (2.3.9) and (2.3.10). It can be expressed as a function of z and δ as follows.

$$\rho_o(z, \delta) = \begin{cases} \dfrac{\alpha(z)}{\delta_c(z)} \cdot \dfrac{\delta^2}{2} & (0 \leqq \delta \leqq \delta_c(z)) \\ \alpha(z) \cdot \left(\delta - \dfrac{\delta_c(z)}{2} \right) & (\delta \geqq \delta_c(z)) \end{cases} \qquad (2.3.18)$$

When the test conditions are specified, ρ_o can be calculated from knowledge of δ at the point under consideration.

(Example 2) A mixed mass of cylindrical aluminum rods (1.6 mm and 3 mm in diameter) was tested in an apparatus in which B = 6 cm and D = 30 cm. Similar to Example 1, the following relations are derived from Eq. (2.3.2).

$$B_c / B = 0.34 \times \frac{30}{6} + 0.70 = 2.40 \qquad \therefore B_c = 14.4 \text{ (cm)}$$

Substitution of the relations $z_a = (\sqrt{3}/2) \cdot B = 5.2$ cm and $z_b = D - (\sqrt{3}/2) \cdot B_c = 17.5$ cm in Eq. (2.3.15) yields the following.

$$\overline{B}_c(z) = \frac{1}{n} \left\{ \frac{14.4 - 6}{17.5 - 5.2} \times (z - 5.2) + 6 \right\} = \frac{1}{n} (0.68z - 2.45)$$

Therefore, $\alpha(z)$ can be derived from Eq. (2.3.16) as shown below.

$$\alpha(z) = \begin{cases} 1 & (0 \leqq z \leqq 5.2 \text{ cm}) \\ \dfrac{6}{0.68z - 2.45} = \dfrac{1}{0.11z - 0.41} & (5.2 \text{ cm} \leqq z \leqq 17.5 \text{ cm}) \\ 0.42 & (z \geqq 17.5 \text{ cm}) \end{cases}$$

And $\delta_c(z)$ is obtained, as in Example 1, from Eq. (2.3.17) as follows.

$$\delta_c(z) = \begin{cases} 1.5 \times \left(\dfrac{z}{6} - 0.87 \right) = 0.25z - 1.30 & (z \geqq 5.2 \text{ cm}) \\ 0 & (0 \leqq z \leqq 5.2 \text{ cm}) \end{cases}$$

Now that the forms of $\alpha(z)$ and $\delta_c(z)$ have been determined, $\rho_o(z, \delta)$ can be calculated from Eq. (2.3.18). Here, ρ_o where δ = 7 cm and δ = 3 cm is calculated as a function z.

(i) In case of δ = 7 cm: The value of z which satisfies $\delta_c(z)$ = 7 cm is 33.2 cm. Since this value is larger than the soil depth D = 30 cm, we note that $\delta \geqq \delta_c(z)$. Accordingly, the following relations are obtained from the second equation of Eq. (2.3.18).

$$\rho_o(z,\ \delta = 7\,\text{cm}) = \begin{cases} 7 & (0 \leqq z \leqq 5.2\,\text{cm}) \\ \dfrac{7.65 - 0.13z}{0.11z - 0.41} & (5.2\,\text{cm} \leqq z \leqq 17.5\,\text{cm}) \\ 3.21 - 0.05z & (z \geqq 17.5\,\text{cm}) \end{cases}$$

The values involved in the preceding formulas have the dimension of cm.

(ii) In case of δ = 3 cm: The value of z which satisfied $\delta_c(z)$ = 3 cm is 17.2 cm. Therefore, $\delta \geqq \delta_c(z)$ for $0 \leqq z \leqq 17.2$ cm and $\delta \leqq \delta_c(z)$ for $z \geqq 17.2$ cm. When $\rho_o(z, \delta = 3\,\text{cm})$ is calculated by Eq. (2.3.18), we obtain the following.

$$\rho_o(z,\ \delta = 3\,\text{cm}) = \begin{cases} 3 & (0 \leqq z \leqq 5.2\,\text{cm}) \\ \dfrac{3.65 - 0.13z}{0.11z - 0.41} & (5.2\,\text{cm} \leqq z \leqq 17.2\,\text{cm}) \\ \dfrac{4.5}{(0.11z - 0.41)(0.25z - 1.30)} & (17.2\,\text{cm} \leqq z \leqq 17.5\,\text{cm}) \\ \dfrac{1.89}{0.25z - 1.30} & (z \geqq 17.5\,\text{cm}) \end{cases}$$

The curves of the values of settlement calcualted above are compared with the values actually measured from the reference lines drawn within the ground interior in Fig. 2.3.12. In this diagram, satisfactory agreement is observed between the calculated values (solid line) and the measured values (o marks). Ito[14] performed measurements on underground settlement of sand and treated the results of the measurement in the same manner shown in Fig.2.3.12. The trend of the measured values shows a satisfactory agreement with that of the calculated values.

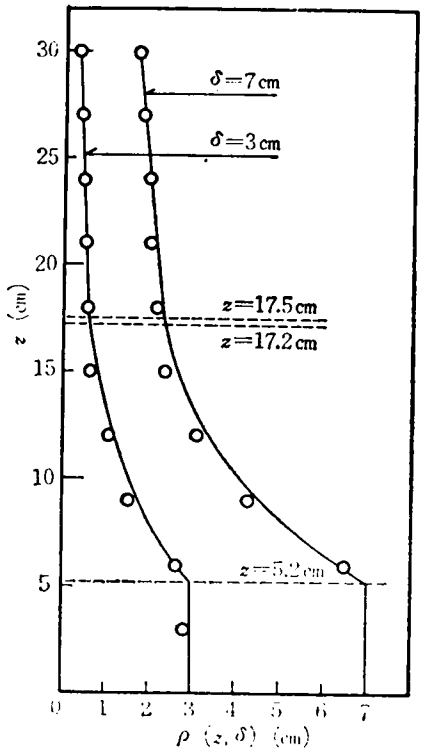

Fig.2.3.12 Comparison of calculated values and measured values of underground settlement along the central line of the lowering floor.

3.6 CURVE OF GROUND SURFACE SETTLEMENT IN LATERAL DIRECTION

In Paragraph 3.4 and Paragraph 3.5, the author has derived the formulas for calculating the surface settlement ρ_{so} and the underground settlement $\rho_o(z)$ along the central line of the lowring floor. He has not discussed what form of settlement occurs at varying distances from the central line of the lowering floor. Here, the author proceeds to calculate the curve of ground surface settlement with respect to the lateral direction of the lowering floor.

As the first step, the curve $\rho_s(x)$ of ground surface settlement is assumed to be a normal probability distribution curve in view of the photographs of the floor-lowering test and the field data[6]. On the basis of this assumption, the following formula is proposed.

$$\rho_s(x) = \rho_{so} \cdot \exp(-hx^2) \qquad (2.3.19)$$

wherein, ρ_{so} denotes the amount of ground surface settlement along the central line of the lowering floor and h is a coefficient relating to the shape of the curve of settle-

ment. Incidentally, the void Bδ produced directly above the lowering floor owing to the downward removal of the lowering floor is expressed by the sum of the increase in the void within the ground interior and the area A of the ground surface settlement as follows:

$$A = B \cdot \delta - 2 (l \cdot s \cdot \triangle n_{max}) \qquad (2.3.20)$$

wherein, l denotes the length of the slip plane (outer boundary plane) on each side, s the width of the slip zone and Δn_{max} the maximum increment of the porosity in the zone just mentioned. After the left and right slip planes are extended to l_c, they rise in a substantially vertical direction and diverge sharply toward the ground surface. For the convenience of analysis, however, they are assumed to rise vertically to the ground surface as shown in Fig.2.3.13. When $0 \leqq \delta \leqq \delta_c, 0 \leqq l \leqq l_c$ and no increase of void is observed in the interval of l_c to l'_c (see Fig.2.3.13). By taking into account Eq. (2.3.9), therefore, one obtains the following.

$$A = B_c \cdot \rho_{so} = \frac{B}{\delta_c} \cdot \frac{\delta^2}{2} = \frac{1}{2} \cdot \frac{(B\delta)^2}{B\delta_c} \qquad (0 \leqq \delta \leqq \delta_c) \qquad (2.3.21)$$

Now assume that δ equals δ'_c where $l = l'_c$. Since no further increase of void occurs within the ground interior when $\delta \geqq \delta'_c$, the following results.

$$A = B \cdot \delta - 2 (l'_c \cdot s \cdot \triangle n_{max}) \qquad (\delta \geqq \delta'_c) \qquad (2.3.22)$$

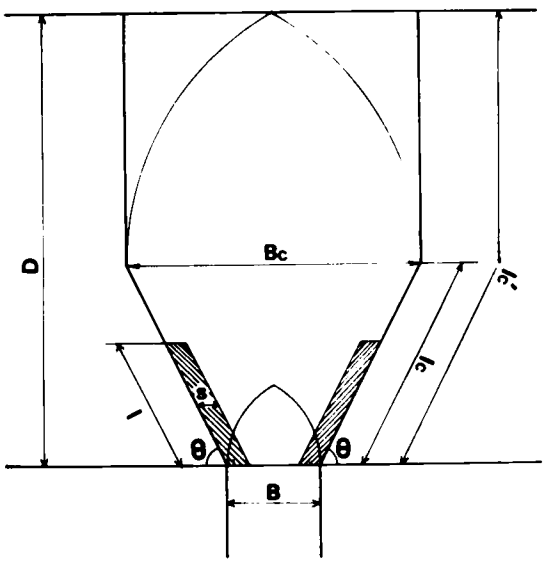

Fig.2.3.13 Transfer pattern of settlement and increase of void in ground.

The equation $A = B\ \delta_c/2$ is derived from Eq. (2.3.21) when $\delta = \delta_c$. This implies that the void produced in consequence of the downward removal of the lowering floor is divided equally into the increase in the void within the ground interior and the area of ground surface settlement. Fig.2.3.14 shows a plot of the area A of ground surface settlement vs. the void Bδ immediately above the lowering floor actually detemined from the results of floor-lowering test conducted on a mass of cylindirical

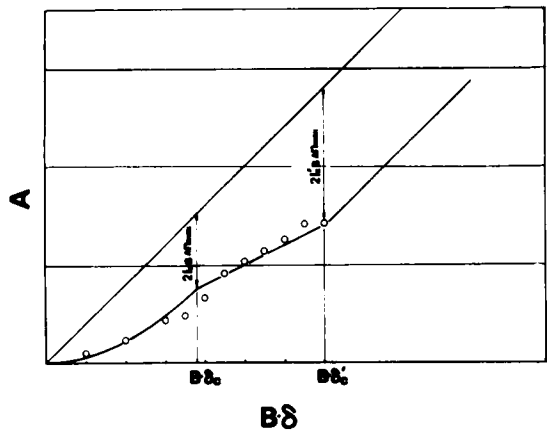

Fig.2.3.14 Relationship between void Bδ immediately above lowering floor and area A of ground surface settlement.

aluminum rods. Referring to this diagram, it is assumed that Bδ in the range between $B\delta_c$ and $B\delta'_c$ is equally divided into the increase of the void within the ground interior and the area of ground surface settlement.

$$A = \frac{1}{2} \cdot B \cdot \delta \qquad (\delta_c \leqq \delta \leqq \delta'_c) \qquad (2.3.23)$$

Since Eqs. (2.3.22) and (2.3.23) should conform to each other where $\delta = \delta'_c$, Eq. (2.3.22) can be converted as follows.

$$A = B \cdot \left(\delta - \frac{\delta'_c}{2}\right) \qquad (\delta \geqq \delta'_c) \qquad (2.3.24)$$

In this connection, the relation between δ'_c and l'_c can be expressed by the following.

$$\delta'_c = \frac{4 \cdot s \cdot \triangle n_{max}}{B} \cdot l'_c \qquad (2.3.25)$$

Assuming that $\rho_s(x)$ can be given by Eq. (2.3.19), the area of ground surface settlement can be expressed as follows.

$$A = \int_{-\infty}^{\infty} \rho_s(x)\,dx = \rho_{so} \int_{-\infty}^{\infty} \exp(-hx^2)\,dx$$

$$= \frac{\sqrt{\pi}}{\sqrt{h}}\,\rho_{so}\,\frac{1}{\sqrt{\pi}}\int_{-\infty}^{\infty} \exp(-u^2)\,du = \frac{\sqrt{\pi}}{\sqrt{h}}\rho_{so} \qquad (2.3.26)$$

wherein, $\frac{1}{\sqrt{\pi}}\int_{-\infty}^{\infty} \exp(-u^2)\,du = 1$ and $u^2 = hx^2$.

Therefore, the unknown coefficient h can be expressed by the following by equating Eqs. (2.3.21), (2.3.23) and (2.3.24) with Eq. (2.3.26).

$$\sqrt{h} = \begin{cases} \dfrac{\sqrt{\pi}}{B_c}, & (0 \leqq \delta \leqq \delta_c) \\ \dfrac{\sqrt{\pi}}{B_c} \cdot \dfrac{\delta - \delta_c/2}{\delta/2} & (\delta_c \leqq \delta \leqq \delta_c') \\ \dfrac{\sqrt{\pi}}{B_c} \cdot \dfrac{\delta - \delta_c/2}{\delta - \delta_c'/2} & (\delta \geqq \delta_c') \end{cases} \qquad (2.3.27)$$

From the above, ρ_{so} can be calculated from Eqs. (2.3.9) and (2.3.10) of Paragraph 3.4 and h from Eq. (2.3.27). Therefore, the curve of ground surface settlement, $\rho_s(x)$, which is given by Eq. (2.3.19) can be calcualted as function of δ. Fig.2.3.15 and

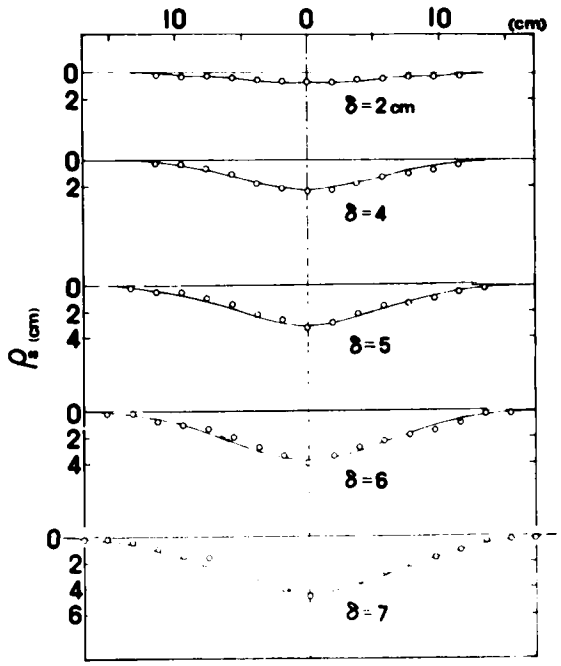

Fig.2.3.15 Calculated curves and measured values of ground surface settlement of aluminum rod mass (ϕ 1.6mm and ϕ 3mm) in lateral direction, B = 15cm, D = 30.8cm.

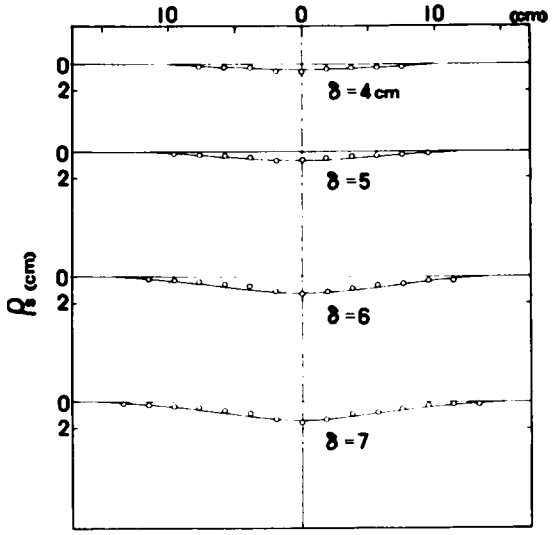

Fig.2.3.16 Claculated curves and measured values of ground surface settlement of aluminum rod mass (ϕ 1.6mm and ϕ 3mm) in lateral direction, B = 6cm, D = 30.8cm.

Fig.2.3.16 compare the value (solid lines) calculated by using the amout δ of lowering as a parameter and the values of actual measurement obtained in the floor-lowering test using a mass of cylindrical aluminum rods (1.6 mm and 3 mm in diameter). Both sets of data satisfactorily agree. The test conditions were B = 15 cm and D = 30.8 cm for the data of Fig.2.3.15 and B = 6 cm and D = 30.8 cm for the data of Fig.2.3.16.

3.7 ANALYSIS OF GROUND SURFACE SETTLEMENT IN LONGITUDINAL DIRECTION

In the preceding paragraphs, phenomena of two-dimensional settlement in the lateral direction of the underground excavation have been studied. In the actual excavation of tunnels, there are involved phenomena of settlement in the longitudinal direction as working faces advance with the progress of works. Elucidation of such phenomena, therefore, is believed to constitute an equally important task. The author, using an apparatus having lowering floors of a width, L = 3 cm, laid side by side as illustrated in Photo.2.3.15 and employing a mass of cylindrical aluminum rods as ground material, simulated the phenomenon of settlement occurring in the longitudinal direction as a consequence of tunnel excavation. It is seen from this photograph that the width-expanding angle θ_1 of the zone of movement on the front side of the lowering floors

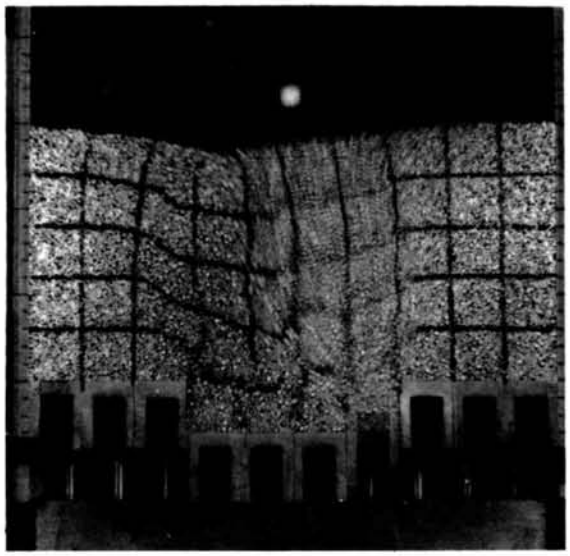

Photo.2.3.15 Movement of aluminum rod mass (ϕ 1.6mm and ϕ 3mm) in longitudinal direction.

(on the righthand side in the photograph) is substantially equal to that of the settlement in the lateral direction but that the width-expanding angle θ_2 on the rear side is about 60° and smaller than θ_1 (see Fig.2.3.17). A possible cause for this is the arch-shaped interparticle force formed in consequence of the downward removal of each preceding lowering floor (see Photo.2.3.14). In view of the observation made in the test, the author has conceived of a transfer pattern of settle-

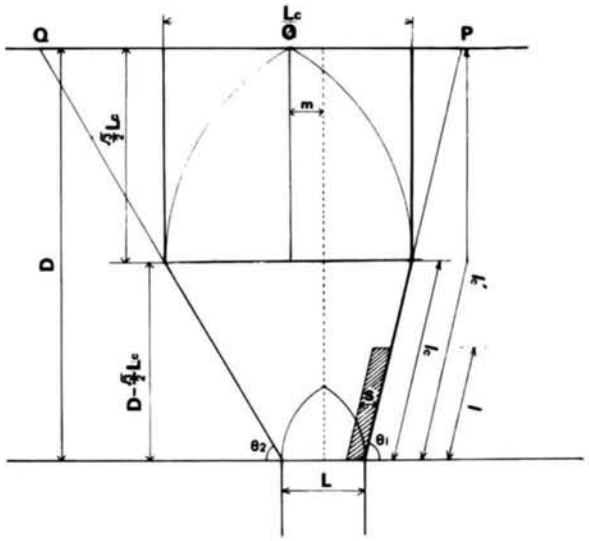

Fig.2.3.17 Transfer pattern of settlement and increase of void in ground in longitudinal direction.

ment shown in Fig.2.3.17 with respect to the downward removal of each lowering floor. The width, L_c, of the zone of movement is expressed by the following (see Eq. (2.3.2) of Paragraph 3.3).

$$\frac{L_c}{L} = \frac{2(\cot\theta_1 + \cot\theta_2)}{2+\sqrt{3}(\cot\theta_1 + \cot\theta_2)} \cdot \frac{D}{L} + \frac{2}{2+\sqrt{3}(\cot\theta_1 + \cot\theta_2)} \qquad (2.3.28)$$

The point 0 at which the forward end of the transfer pattern of settlement reaches the ground surface falls to the rear from the central line of the lowering floor. The length m with which the point 0 deviates from the central line is calculated by the following.

$$m = \frac{L_c - L}{2} - \left(D - \frac{\sqrt{3}}{2} L_c\right) \cdot \cot\theta_1 \qquad (2.3.29)$$

In this connection, the author has assumed that the increase in the void within the ground interior due to the downward removal of the lowering floors in the longitudinal sequence occurs along the slip plane on the front side because the increase of the void on the rear side has already reached its critical condition (critical void ratio) in consequence of the downward removal of the preceding lowering floor. ρ_{SO}, the amount of settlement at 0 is expressed in the same form as Eqs. (2.3.9) and (2.3.10). In this case,

$$\alpha = \frac{L}{L_c} \qquad (2.3.30)$$

$$\delta_c = \frac{2 \cdot s \cdot \triangle n_{max}}{L} \cdot l_c \qquad (2.3.31)$$

There are indications that the curve of ground surface settlement in the longitudinal direction differs before and behind the point 0 and that the rate of decline is smaller on the rear side. The author, therefore, has derived the following formulas to express the curve of ground surface settlement.

For the front side:

$$\rho_{s1}(y) = \rho_{so} \cdot \exp(-h_1 y^2)$$

For the rear side:

$$\rho_{s2}(y) = \rho_{so} \cdot \exp(-h_2 y^2) \qquad (2.3.32)$$

wherein, h_1 and h_2 are coefficients relating to the shape of the curves of ground surface settlement in the longitudinal direction and y is a distance in the longitudinal direction measured from the point 0 of Fig.2.3.17. The area A of ground surface settlement is expressed, as in the case of the ground surface settlement in the lateral direction considered in the preceding paragraph, by the following formulas.

$$A = \begin{cases} \dfrac{L}{\delta_c} \cdot \dfrac{\delta^2}{2} & (0 \leqq \delta \leqq \delta_c) \\ \dfrac{1}{2} \cdot L \cdot \delta & (\delta_c \leqq \delta \leqq \delta_c') \\ L \cdot (\delta - \dfrac{\delta_c'}{2}) & (\delta \geqq \delta_c') \end{cases} \qquad (2.3.33)$$

In this case, the following equation is established.

$$\delta_c' = \frac{2 \cdot s \cdot \triangle n_{max}}{L} \therefore l_c' \qquad (2.3.34)$$

On the other hand, when the curve $\rho_S(y)$ is found by Eq. (2.3.32), the area A is calculated as follows.

$$A = \int_0^\infty \rho_{s_1}(y)\, dy + \int_0^\infty \rho_{s_2}(y)\, dy$$

$$= \rho_{so} \int_0^\infty \exp(-h_1 y^2)\, dy + \rho_{so} \int_0^\infty \exp(-h_2 y^2)\, dy$$

$$= (\frac{\sqrt{\pi}}{\sqrt{h_1}} + \frac{\sqrt{\pi}}{\sqrt{h_2}}) \cdot \frac{\rho_{so}}{2} \qquad (2.3.35)$$

If $\rho_{S_2}(y)$ is assumed to be obtained by extending $\rho_{S1}(y)$ to a length "k" times as great in the horizontal direction, then we obtain the following.

$$k = \frac{\sqrt{h_1}}{\sqrt{h_2}} \qquad (2.3.36)$$

From Fig.2.3.17, the following equation is assumed.

$$k = \frac{\overline{OQ}}{\overline{OP}} = \frac{1 + \sqrt{3} \cot\theta_2}{1 + \sqrt{3} \cot\theta_1} \qquad (2.3.37)$$

Then, in accordance with Eq. (2.3.35), A can be expressed by the following.

$$A = \frac{(1 + k) \sqrt{\pi}}{2 \sqrt{h_1}} \cdot \rho_{so} \qquad (2.3.38)$$

Accordingly, by equating Eq. (2.3.33) with Eq. (2.3.38), the coefficient h_1 can be expressed as follows.

$$\sqrt{h_1} = \begin{cases} \dfrac{(1+k)\sqrt{\pi}}{2L_c} & (0 \leqq \delta \leqq \delta_c) \\ \dfrac{(1+k)\sqrt{\pi}}{2L_c} \cdot \dfrac{\delta - \delta_c/2}{\delta/2} & (\delta_c \leqq \delta \leqq \delta_c') \\ \dfrac{(1+k)\sqrt{\pi}}{2L_c} \cdot \dfrac{\delta - \delta_c/2}{\delta - \delta_c'/2} & (\delta \geqq \delta_c') \end{cases} \qquad (2.3.39)$$

It has thus been ascertained that the curve of settlement $\rho_s(y)$ due to the downward removal of one of the series of lowering floors can be calculated as a function of δ. By repeating the calculation for each of the succeeding floors, the overall curve of settlement in the longitudinal direction can be obtained. Fig.2.3.18 is a graph of the calculated values (solid line) of the curves of ground surface settlement obtained in the manner mentioned above and the values actually measured in a floor-lowering test using a mass of

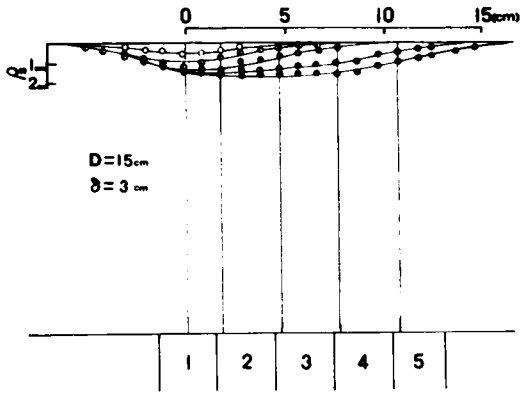

Fig.2.3.18 Calculated curves and measured values of ground surface settlement in longitudinal direction.

cylindrical aluminum rods shown in Phot.2.3.15. (In this graph, the curve of o marks represents the downward movement of the lowering floor 1; that of ⊙ marks, the lowering floors 1 and 2; that of ⊕ marks, the lowering floors 1 through 3; that of ◑ marks, the lowering floors 1 through 4; and that of ● marks, the lowering floors 1 through 5 respectively). The calcualted values and measured values are in satisfactory agreement.

In the preceding analysis, the two-dimensional behavior of a mass of cylindrical rods shown in Photo.2.3.15 has been used as a model for settlement in the longitudinal direction involving no plane strain condition. The author believes that such model is acceptable as an approximation.

3.8 THREE-DIMENSIONAL ANALYSIS OF GROUND SURFACE SETTLEMENT

Consideration of the three-dimensioanl settlement caused by the downward movement of one lowering floor has led the author to postulate of a transfer pattern of settlement like the one shown in Fig.2.3.19. In the diagram, B denotes the width of

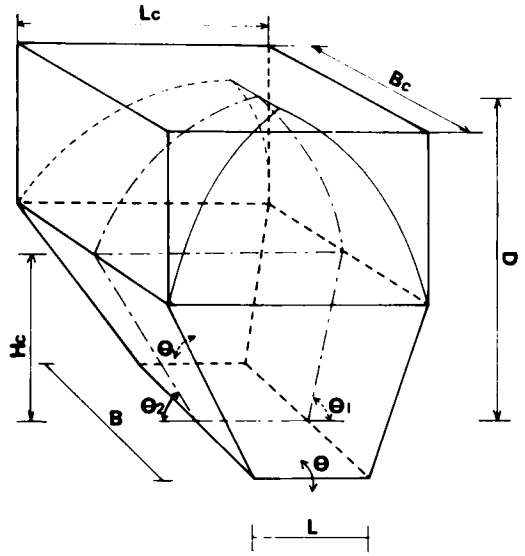

Fig.2.3.19 Three-dimensional transfer pattern of settlement and slip planes.

the lowering floor, L the length of the floor and suffixes 1 and 2 the front and rear sides respectively. Let H_c stand for the height which exists when the width increases such that $B = B_c$ and $L = L_c$, and H_c can be expressed as follows.

$$H_c = \frac{2D - \sqrt{3}L}{2 + \sqrt{3}(\cot\theta_1 + \cot\theta_2)} \qquad (2.3.40)$$

B_c and L_c can be expressed as functions of H_c, as follows.

$$B_c = B + 2H_c \cdot \cot\theta \qquad (2.3.41)$$

$$L_c = L + H_c \cdot (\cot\theta_1 + \cot\theta_2) \qquad (2.3.42)$$

It is also assumed that the increase of the void occurs in the zone indicated by slanted lines in Fig.2.3.20. As an analogue to the variable l used in the two-dimensional analysis, a quantity S representing the area in which the void increases is introduced. If $S = S_c$ and $\delta = \delta_c$ when the height H of the area involving the increase of void equals H_c, then Eqs. (2.3.9) and (2.3.10) which permit calculation of ρ_{so} become applicable similarly to the two-dimensional case. In this case,

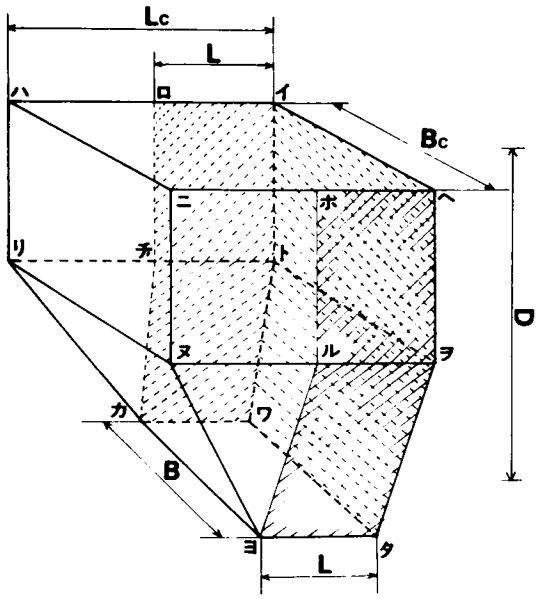

Fig.2.3.20 Zone that new increase of void occurs and slip planes in three-dimensional settlement.

$$\alpha = \frac{B \cdot L}{B_c \cdot L_c} \qquad (2.3.43)$$

$$\delta_c = \frac{2 \cdot s \cdot \triangle n_{max}}{B \cdot L} \cdot S_c \qquad (2.3.44)$$

At the same time, the following expression also holds.

$$S_c = (B + H \cdot \cot\theta) H_c \cdot \mathrm{cosec}\theta + 2 L H_c \cdot \mathrm{cosec}\theta \qquad (2.3.45)$$

The shape of ground surface settlement is then assumed to be as shown in Fig.2.3.21 and expressible by the following.

On the front side:

$$\rho_{s1}(x, y) = \rho_{so} \cdot \exp(-h x^2) \cdot \exp(-h_1 y^2)$$

On the rear side:

$$\rho_{s2}(x, y) = \rho_{so} \cdot \exp(-h x^2) \cdot \exp(-h_2 y^2) \qquad (2.3.46)$$

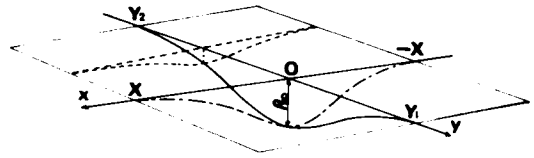

Fig.2.3.21 Shape of three-dimensional ground surface settlement.

x represents the distance in the lateral direction and y the distance in the longitudinal direction. Then, the void BLδ produced when a lowering floor having a width of B and a length of L completes a downward movement of δ can be expressed as the sum of the increase of void within the ground interior and the volume V of ground surface settlement as follows.

$$V = B \cdot L \cdot \delta - S \cdot s \cdot \triangle n_{max} \qquad (2.3.47)$$

The volume V can be expressed, as in the two-dimensional analysis, by the following.

$$V = \begin{cases} \dfrac{BL}{\delta_c} \cdot \dfrac{\delta^2}{2} & (0 \leqq \delta \leqq \delta_c) \\ \dfrac{1}{2} BL\delta & (\delta_c \leqq \delta \leqq \delta_c') \\ BL\left(\delta - \dfrac{\delta_c'}{2}\right) & (\delta \geqq \delta_c') \end{cases} \qquad (2.3.48)$$

wherein, the following relation is established.

$$\delta_c' = \frac{2 \cdot s \cdot \triangle n_{max}}{BL} \cdot S_c' \qquad (2.3.49)$$

Here, S'_c represents the area indicated by slanted lines in Fig.2.3.20 and, therefore, satisfies the following equation.

$$S'_c = S_c + (L + B + 2H_c \cot\theta) \cdot (D - H_c) \qquad (2.3.50)$$

If $\rho_S(x, y)$ is found by Eq. (2.3.46), then the volume V can be calculated by the following.

$$V = \iint \rho_{s1}(x, y)\,dx\,dy + \iint \rho_{s2}(x, y)\,dx\,dy$$

$$= \rho_{so} \int_0^\infty 2\exp(-hx^2)\,dx \cdot \int_0^\infty \exp(-h_1 y^2)\,dy$$

$$+ \rho_{so} \int_0^\infty 2\exp(-hx^2)\,dx \cdot \int_0^\infty \exp(-h_2 y^2)\,dy$$

$$= \frac{\sqrt{\pi}}{\sqrt{h}}\left(\frac{\sqrt{\pi}}{\sqrt{h_1}} + \frac{\sqrt{\pi}}{\sqrt{h_2}}\right) \cdot \frac{\rho_{so}}{2} \qquad (2.3.51)$$

Here, the following relation is introduced by expressing the ratio of h_1 to h_2 by Eqs. (2.3.36) and (2.3.37) and considering the ratio of h and h_1 similarly while directing special attention to the relation of $\theta = \theta_1$.

$$\frac{\sqrt{h}}{\sqrt{h_1}} = \frac{L_c}{B_c} \qquad (2.3.52)$$

In this case, V is given by the following formula.

$$V = \frac{(1+h)\pi}{2\left(\frac{L_c}{B_c}\right) h_1} \cdot \rho_{so} \qquad (2.3.53)$$

Accordingly, by equating Eq. (2.3.48) with Eq. (2.3.53), h_1 can be expressed by the following.

$$h_1 = \begin{cases} \dfrac{(1+k)\pi}{2L^2_c} & (0 \leqq \delta \leqq \delta_c) \\ \dfrac{(1+k)\pi}{2L^2_c} \cdot \dfrac{\delta - \delta_c/2}{\delta/2} & (\delta_c \leqq \delta \leqq \delta_c') \\ \dfrac{(1+k)\pi}{2L^2_c} \cdot \dfrac{\delta - \delta_c/2}{\delta - \delta_c'/2} & (\delta \geqq \delta_c') \end{cases} \qquad (2.3.54)$$

It has been ascertained that the curve, $\rho_s(x, y)$, of three-dimensional settlement caused by the downward removal of one lowering floor can be calculated as a function of δ. By repeating this calculation for each of the succeeding lowering floors, the overall shape of settlement can be determined.

The author, with a view to simulating the tunnel excavation, carried out a floor-lowering test on dry sand. The test apparatus had ten lowering floors, 10 cm in lateral dimension and 3 cm in longitudinal dimension, laid continuously the center of the bottom of a box 50 cm in width, 70 cm in length and 20 cm in height (see Photo. 2.3.16). A longitudinal cross section of this apparatus is illustrated in Fig.2.3.22. Fig.

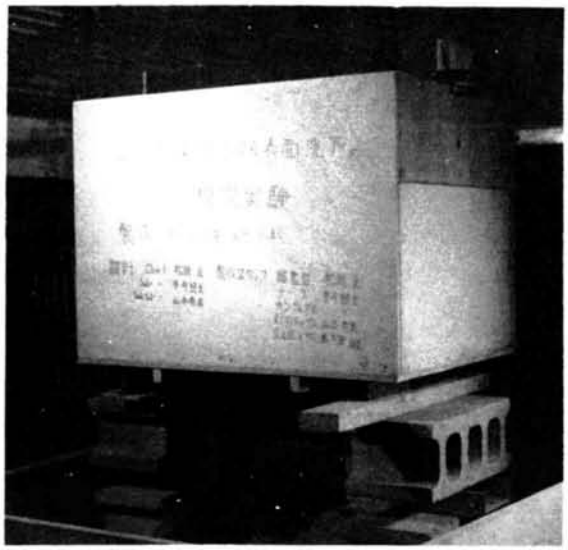

(a) Complete view.

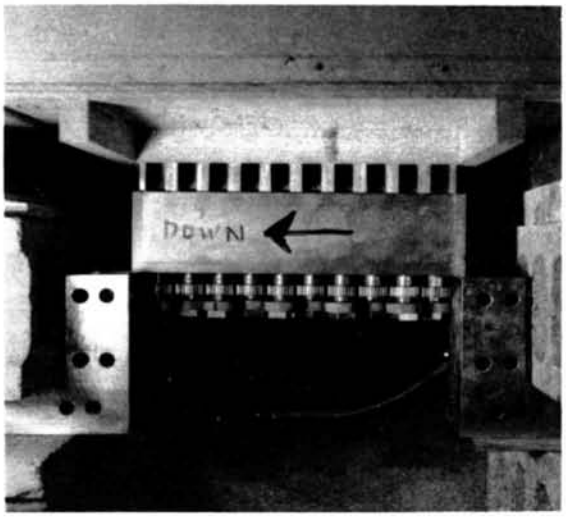

(b) Part of apparatus to remove downwardly the lowering floors.

Photo.2.3.16 Test apparatus for three-dimensional settlement of ground.

2.3.23, Fig.2.3.24 and Fig.2.3.25 compare the values of settlement measured by two dial gauges placed on the ground surface along the central line of the lowering floors (indicated by ○ and ● marks) with the curves of the values calculated by the method mentioned above. In the graphs, the abscissa is the distance from the forward end (corresponding to the working face in the tunnel excavation site) of the lowering floor in a lowered position to the point at which the dial gauge is positioned, with negativity of value indicating that the working face has not reached the vertical line containing the dial gauge. While the data given in Fig.2.3.23 and Fig.2.3.25 are for densely packed sand ($e = 0.67$), the coefficient $\Delta n_{max} = 0.07$ has been used in the calculation. This value was determined by a simple shear test (N.G.I. type) performed by adjusting test conditions such that the magnitudes of void ratio and confining stress would conform to those of model test. The data of Fig.2.3.24 are those for loosely packed sand ($e = 0.85$). In this case, it was assumed that $\Delta n_{max} = 0$. All the values indicated in the graphs represent the results of measurement made for $\delta = 3$ cm.

In this chapter, analysis of settlement has been made for a ground of sandy soil having a small degree of compressibility and excluded consideration of the phenomenon of compressive (consolidation) settlement due to changes in stress resulting from tunnel excavation or other similar work. In other words, the author has considered the balance of void and derived formulas for calculation by taking into account only the volumetric change occurring within the ground interior because of shear, i.e., the phenomenon of dilatancy.

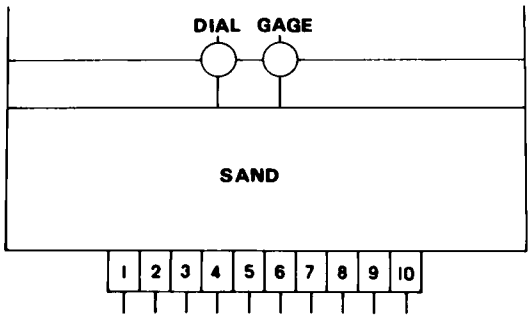

Fig.2.3.22 Longitudinal cross section of test apparatus for three-dimensional settlement of ground.

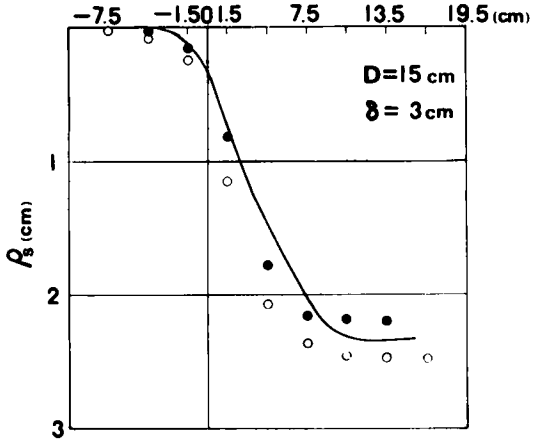

Fig.2.3.23 Measured values and calculated curve of ground surface settlement on dense sand, D = 15cm, δ = 3cm.

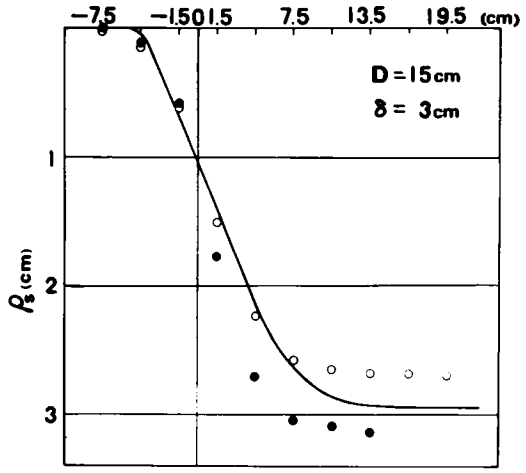

Fig.2.3.24 Measured values and calculated curve of ground surface settlement on loose sand, D = 15cm, δ = 3cm.

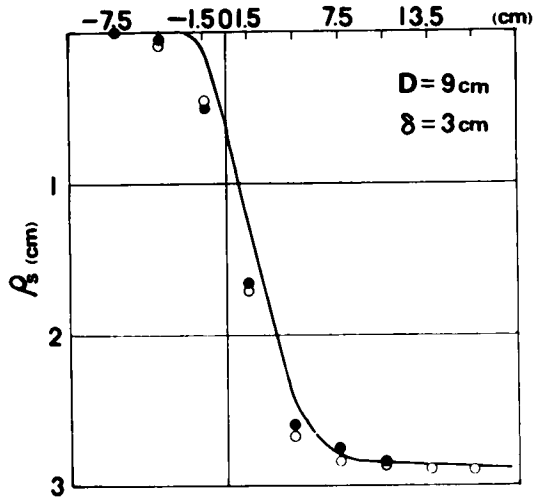

Fig.2.3.25 Measured values and calculated curve of ground surface settlement on dense sand, D = 9cm, δ = 3cm.

3.9 REVIEW OF FIELD DATA ON GROUND SURFACE SETTLEMENT DUE TO TUNNEL EXCAVATION

Fig.2.3.26[15] gives curves of settlement measured in the lateral direction of a tunnel (indicated as plots (a) and (b) in the graph) and time-course curves of settlement measured along the central line of a tunnel (indicated as plots (c) and (d)). It is noted that the curves in this graph have trends similar to those shown in Fig.2.3.15, Fig.2.3.16, Fig.2.3.23, Fig.2.3.24 and Fig.2.3.25. The author has, therefore, proceeded with an analysis based on the these formulas by assuming that the manner of ground loosening in a floor-lowering test and that in a tunnel excavation correspond. In considering the condition in the neighborhood of the working face in an actual tuunel excavation, the analysis of three-dimensional settlement discussed in the preceding paragraph may be necessitated. Since the factor corresponding to the length (lateral depth) L of the lowering floor (which may be regarded as the distance of excavation effected by one explosion or the length of excavation made per day) is difficult to estimation, the possible increase of void due to the sliding of ground at the front side of the working face has been disregarded. Analysis has therefore been based on the two-dimensional model. We will now describe the results of analysis of settlement occurring in the lateral direction in a selected ground of rather sandy soil.

The author has given two interpretations in Fig.2.3.27 to support the assumed correspondence bwtween ground loosening in the floor-lowering test and ground loosening

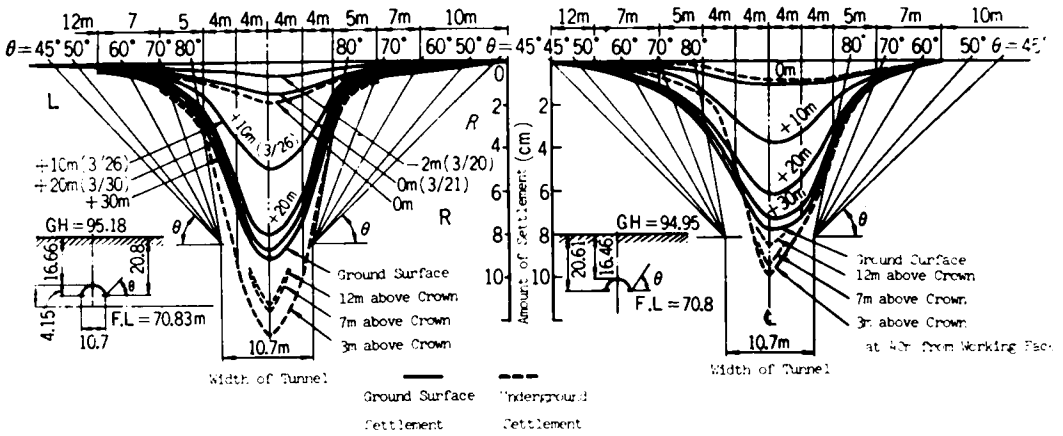

(a) Ground surface settlement and underground settlement in the lateral direction of a tunnel at measuring line A, with the distance from the working face as a parameter.

(b) Ground surface settlement and underground settlement in the lateral direction of a tunnel at measuring line B, with the distance from the working face as a parameter.

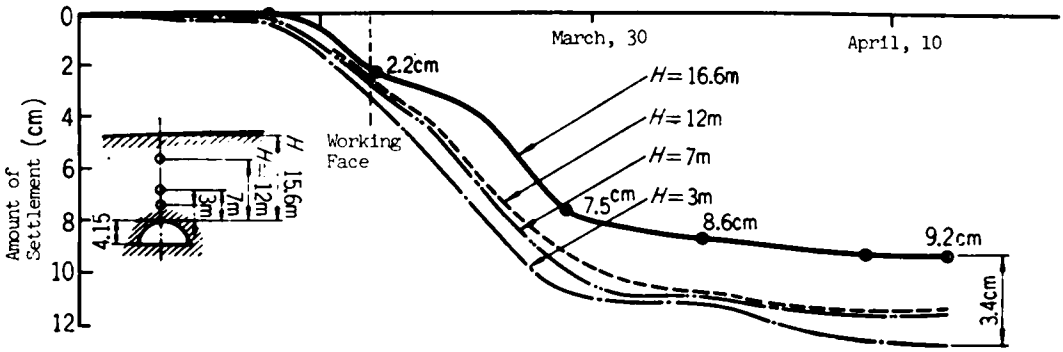

(c) Time-course curves of settlement measured at the central line of the tunnel at measuring line A.

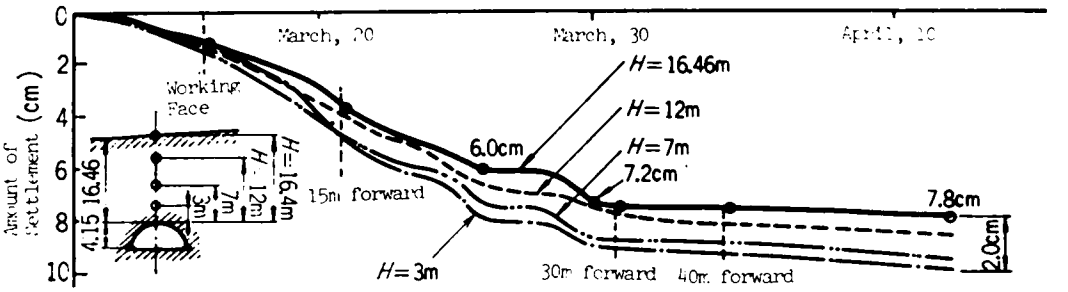

(d) Time-course curves of settlement measured at the central line of the tunnel at measuring line B.

Fig.2.3.26 Results of measurement of ground surface settlement and underground settlement in TS tunnel (after Shimada and Iizuka[15]).

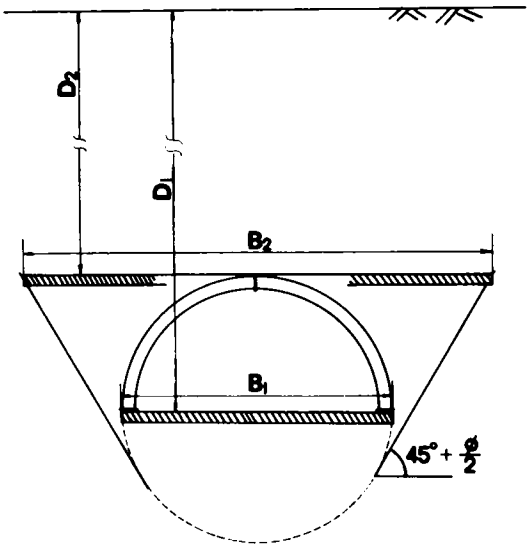

Fig.2.3.27 Assumed correspondence between ground loosing in floor-lowering test and ground loosing in actual tunnel excavation.

in actual tunnel excavation. He has assumed that the width B of the lowering floor is equal to the width B_1 of the tunnel excavation and that in the case of a tunnel of circular cross section, B is equal to the width B_2 between the left and right slip planes which rise with an angle $(45^\circ + \phi/2)$ (ϕ: internal friction angle) as illustrated. In this case, the soil depth D will be D_1 or D_2 (see Fig.2.3.27).

In Fig.2.3.26, the curves (a) and (b) represent values actually measured of ground surface settlement (solid line) and underground settlement (dotted line) along the measuring lines A and B drawn in a tunnel called TS. The plurality of curves results from the use of the distance from the points of measurement to the working face as a parameter. In this report, the width-increasing angle θ of the zone of flow is described to fall in the range of 75° to 85°. We note that this value satisfactorily agrees with the value of θ given in Table 2.3.1 of Paragraph 3.3. The soil involved in the test was a sandy soil (SHIRASU soil and tuffy andesite).

The width of tunnel excavation at the measuring line A was 10.7 m and the soil depth from the tunnel crown was 16.6 m. The underground settlement at a point 3 m above the tunnel crown was also measured. Since this point was considered to have fallen within the primary zone, the author used the measured value of 12.6 cm for the underground settlement as an equivalent to the amount δ of downward removal of an analogous lowering floor. If such a measured value was not avaibale, then δ would have to be assumed otherwise. As a boundary condition, it should be given. Considering that the soil involved was a sandy soil, the author has adopted 85° (densely packed coarse sand) as the value of θ from Table 2.3.1 of Paragraph 3.3 and 2.83

(densely packed coarse sand) as the value of $4 \cdot s \cdot \Delta n_{max}$ (s: width of the slip zone, Δn_{max}: maximum increment of void ratio) from Table 2.3.2 of Paragraph 3.4. Now, ρ_{so}, the amount of ground surface settlement along the central line of tunnel and the curve of ground surface settlement can be calculated. The results of a calculation performed by assuming $B = B_1$ and $B = B_2$ are indicated with solid lines in Fig.2.3.28. The plots given in this graph represent actually measured values. It is seen by the comparison that the measured values are closer to the curve where B was assumed equal to B_1.

Along the measuring line B, the width of tunnel excavation was 10.7 m and the soil depth from the tunnel crown was 16.4 m. Similarly to the measuring line A, the measured value of underground settlement, 9.8 cm, at the point 3 m from the tunnel crown has been adopted as equivalent to the amount of the downward removal of the lowering floor δ. Since the soil is thought to be practically the same as along the measuring line A, $\theta = 85°$ and $4 \cdot s \cdot \Delta n_{max} = 2.83$ have been used. The curves of

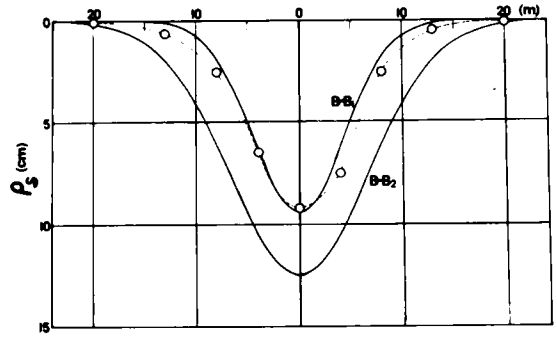

Fig.2.3.28 Measured values and calculated curve of ground surface settlement along the lateral measuring line A in TS tunnel.

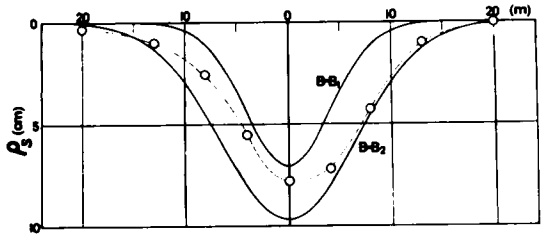

Fig.2.3.29 Measured values and calculated curve of ground surface settlement along the lateral measuring line B in TS tunnel.

ground surface settlement have thus been calcualted. These results are shown in Fig. 2.3.29. The graph indicates that the measured values describe plots which may fall between the two curves of settlement calculated.

Finally, data obtained in the construction of shield tunnels at Nishi-kanda along the Metropolitan Rapid Transit Route 6 are discussed as another example for comparison

Table 2.3.3 Comparison between measured values and calculated values of ground settlement along the central lines of shield tunnels (after Endo et al.[16]).

Measuring points	Above preceding tunnel			Above following tunnel		
Depth (m)	0.5	6	12	0.5	6	12
Calculated values of elastic settlement (mm)	29	32	53	40	47	83
Calculated values of settlement due to ground loosening (mm)	119	121	125	124	125	202
Measured ultimate values of settlement (mm)	123	133	195	151	158	241

of calcualted values with values actually measured in the filed. According to Endo et al.[16] values calcualted by the above formulas and referred to as "*amount of settlement due to ground loosening*" show a satisfactory agreement with values actually measured. The values of the so-called elastic settlement calcualted by the finite element method assuming the ground as an elastic mass (see Table 2.3.3) seem to be excessively small compared with measured values. Endo et al.'s report does not touch upon detailed calcualtion conditions.

In this connection, one may consider the problem of similarity between the floor-lowering test and the actual tunnel. As previously dicussed in Paragraph 2.3, analysis based on the phenomenon of compression or shear of soil element may be similarly applicable to an actual tunnel. The applicability of results obtained where the width of the lowering floor is extremely small compared with the particle size and the difference in the applied stress level between the floor-lowering test and the actual tunnel excavation as well as other factors may require special attention.

3.10 CONCLUSIONS

In this chapter, the author has experimentally and theoretically analyzed the phenomenon of local settlement of ground composed of granular soil by conducting a floor-lowering test. In the floor-lowering test, two-dimensional masses of cylindrical

aluminum rods having different diameters were used besides dry sand. The mass of aluminum rods permits easy observaton. The author has clarified the various characteristics of settlement by carrying out accurate measurement on the movement of rods, the local change of void in the mass, the condition of upward transfer of void, the relation between the amount of the downward movement of the lowering floor and the amount of settlement of the mass, etc. Based on the characteristics thus determined, the author has considered the movement of component particles of ground as a form of fluidity and, consequently, derived formulas for the calculation of ground surface settlement and underground settlement along the central line of the lowering floor. The coefficients involved in these formulas can be estimated by an easy shear test of the relevant ground material. The theory developed with respect to the mass of cylindrical aluminum rods has been shown applicable to sand. As is evident from the cited examples, calcualted values of settlement show a satisfactory agreement with measured values. Methods of calculation have been proposed not only for the amount of settlement along the central line of the lowering floor but also for the curves of ground surface settlement in the lateral cross section of the lowering floor. By analyzing settlement in the longitudinal direction of tunnel excavation and combining settlement in the lateral and longitudinal directions, the author has expanded the analysis to a three-dimensional analysis of ground surface settlement. The curves calculated through such analysis show a satisfactory agreement with the results of the floor-lowering test conducted on a mass of cylindrical aluminum rods and on sand. By assuming correspondence between ground loosening in the floor-lowering test and ground loosening due to the tunnel excavation, the author has attempted to analyze the measured values of ground settlement by use of the above theory.

The results obtained may be summarized as follows.

(1) The zone of movement of ground due to the downward removal of the lowering floor can be determined by assuming a transfer pattern having the primary zone as its basis. This has been verified by the floor-lowering test using a mass of cylindrical aluminum rods, using coarse sand (loosely packed and densely packed), and using fine sand (loosely packed and densely packed).

(2) It has been inferred that the void produced in consequence of the downward removal of the lowering floor partly transfers itself to reach the ground surface and induces the phenomenon of ground surface settlement; and that part of the void remains in the form of an increase in porosity within the ground. This increase in the void has a limit. In other words, there exists a critical void ratio which can maintain itself under the stress condition. Also the void is not uniformly distributed throughout the ground interior. The increase in void ratio is conspicuously observed along the left and right slip planes (outer boundary planes) which constitute boundary planes between the zone of movement and the surrounding stationary zone. This increase of void due to dilatancy makes a remarkable contribution.

(3) As a result of accurate measurement of the relation between the downward movement of the lowering floor and the amount of ground settlement, it has been ascertained that the ratio of the increment of settlement to the increment of downward movement of the lowering floor ($d\rho_{SO}/d\delta$) increases substantially linearly with the increase of the amount of downward movement of the floor and levels off at a certain value of δ ($=\delta_c$). Further, this fixed value agrees with the ratio α ($= B/B_c$) between the width B of the lowering floor and the width B_c of the zone of movement. A logical explanation of this results from assuming that, with the system under review, no further increase of void occurs.

(4) By taking into account the various characteristics introduced above, the author has derived formulas for calculation of the amount of ground surface settlement and the amount of underground settlement along the central line of the lowering floor. The coefficients involved in these formulas can be estimated by a shear test of the relevant ground material. The values calculated show a satisfactory agreement with the measured values.

(5) With a view to calculating the amount of settlement along the central line of the lowering floor and the curves of ground surface settlement in the lateral cross section of the lowering floor as well, the author has assumed the curve of settlement as a normal probability distribution and performed analysis accordingly. The curves of ground surface settlement thus obtained give a satisfactory correlation with values actually measured by a floor-lowering test.

(6) For the purpose of analyzing the phenomenon of settlement occurring in the longitudinal direction of tunnel excavation, the author has observed the condition of ground movement by using a test apparatus having a plurality of small lowering floors laid continuously. Consequently, he has made clear the difference between the phenomenon of settlement in the lateral direction and that in the longitudinal direction and, at the same time, derived formulas for the calculation of the curves of ground surface settlement in the longitudinal direction. These calculations show a satisfactory agreement with values measured in a floor-lowering test.

(7) By combining the phenomenon of settlement in the lateral direction with that in the longitudinal direction, the author has tried to analyze the settlement of ground surface from the three-dimensional point of view. As a result, he has derived formulas for the calculation of ground surface settlement and verified them by the three-dimensional floor-lowering test using dry sand, with satisfactory resutls.

(8) For the convenience of analysis, the author has introduced two interpretations to support the assumed correspondence between the manner of ground loosening in floor-lowering tests and the manner of ground loosening in tunnel excavations. When ground settlement measured on a tunnel construction site is analyzed by the

theory mentioned, above results indicate a satisfactory agreement between calculated values and measured values.

References

1) Murayama, S. and Matsuoka, H.: On the Settlement of Granular Media caused by the Local Yielding in the Media, Proc. of J.S.C.E., No.172, 1969, pp.31–41, (in Japanese).
2) Murayama, S., Matsuoka, H. and Nakai, T.: Analysis of Ground Surface Settlement due to Tunnel Excavation, Proc., Annual Meeting of J.S.C.E. (27th), III-149, 1972, pp.471–474, (in Japanese).
3) Ono, R. and Manai, K.: On the Vertical Pressure in Dry Sand, Journal of J.S.C.E., Vol.24, No.5, 1938, pp.437–495, (in Japanese).
4) Mizuno, T.: On the Vertical Stress in Sand, Memories of Faculty of Eng., Kyushu Univ., Vol.17, No.1, 1942, pp.31–45, (in Japanese).
5) Ito, T.: Calculation of Sand Pressure on Horizontal Top Surface of the Tunnel Heading, Technical Report of Osaka Univ., 10–374, 1960, pp.109–111.
6) Getzler, Z., Komornik, A. and Mazurik, A.: Model Study on Arching buried Structures, Proc. A.S.C.E., SM5, 1968, pp.1123–1141.
7) Murayama, S.: Earth Pressure on Vertically Yielding Section in Sand Layer, Annuals, Disaster Prevention Research Institute, Kyoto University, No.11B, 1968, pp.549–565, (in Japanese).
8) Ladanyi, B. and Hoyaux, B.: A Study of Trap-door Problem in a Granular Mass, Canadian Geotechnical Journal, Vol.6, No.1, 1969, pp.1–15.
9) Murayama, S.: The Time-dependency Character of Earth Pressure in Tunnel, Proc. of 6th National Tunnel Symposium, 1970, pp.4–1 ~ 4–23.
10) Murayama, S. and Matsuoka, H.: Earth Pressure on Tunnels in Sandy Ground, Proc. of J.S.C.E., No.187, 1971, pp.95–108, (in Japanese).
11) Litwiniszyn, J.: An Application of the Random Walk Argument to the Mechanics of Granular Media, Proc., I.U.T.A.M. Symposium on Rheology and Soil Mechanics, Grenoble, 1964, Springer-verlag, 1966, pp.82–89.
12) Matsuo, M., Komada, T. and Takahashi, M.: A Study on Deformation of Sand Layer by Monte Carlo Method, Proc., Annual Meeting of J.S.C.E. (21st), III-52, 1966, (in Japanese).
13) Terzaghi, K.: Theoretical Soil Mechanics, John Wiley & Sons, New York, 1943, pp.66–76.
14) Ito, T.: Mechanical Study on Design of Tunnel Construction, Doctor Thesis, Osaka Univ., 1958, (in Japanese).
15) Shimada, T. and Iizuka, Z.: On Case Study of Measurement of Ground Surface Settlement due to Tunnel Excavation, Proc. of 5th National Tunnel Symposium,

1969, pp.15–34, (in Japanese).

16) Endo, K., Murata, H., Kawasaki, T., Miyazaki, H. and Arizono, T.: Behaviors of Ground due to Subway Shield Tunnel Excavation, Proc., Annual Meeting of J.S.C.E. (27th), III-147, 1972, pp.465–466, (in Japanese).

CHAPTER 4

CONCLUSIONS

In the design of ground and soil structures, stability analysis which directs its attention to the elimination of shear failure still prevails. Today, various theories have been proposed for the stress-strain relation of soil and the practical application of that relation. The time is ripe for stability analysis of soil to be advanced to the stage of the deformation analysis. There are indications that, in view of the course of the history of soil mechanics, we are now in a transient period from "*stability analysis*" to "*deformation analysis*".

In the present part, the author has considered the problem of a composite ground composed of sand pile and clay and analyzed this ground by the various formulas indicative of general stress-strain relations derived from a microscopic point of view in Part I. It is the author's position that an orthodox solution resides in an analysis which relates formulas of boundary condition and stress equilibrium to the constitutive equations of soil. Yet, the problem of generalizing the stress-strain formulas on the principal stress plane found based on the stress-strain relations on the mobilized plane, the problem of analytically solving the constitutive relations because of the fact that the relations, having the law of friction reflected, are expressed as functions of stress ratios, and other similar problems remain yet to be solved. At present, these problems can be attacked to some extent through electronic computation methods. Yet, this method can hardly be called a convenient approach. As another method for analysis of ground, amounts of deformation may ingeniously be calculated through elucidation of phenomenon involved. In this case, however, there must be found particular methods to suit the phenomenon under consideration which can prove to be more difficult than the aforementioned orthodox method. The phenomenon of settlement of peripheral ground due to occurrence of a cavity within the ground interior has been discussed as an example in which the amount of settlement could be calculated by basic analysis of the mechanism of settlement.

The contents of the present part may be summarized as follows. Chapter I outlined the circumstances in which stability analysis prevails for the design of ground and soil structures, the conditions which must be met for materializing the defomation analysis, and the methods of analysis and study to be used in this work.

Chapter 2 discussed composite ground of the pile-clay system as an example of deformation analysis of ground based on the constitutive relation of soil and analyzed this problem on the basis of the basic principles of soil mechanics. Formulas indicative of the stress-strain relations of sand pile and clay ground have been derived from the

stress-strain relations of soil under three different principal stresses which were derived by the microscopic analysis of the behavior of soil grains during shear in Part I and those of the stress-strain relations of soil during consolidation. Then, stress, strain, stress concentration ratio, settlement reduction ratio, etc. within the ground interior have been calculated by incorporating boundary conditions for composite ground into the constitutive equations described above. These factors have been calculated for varying sand pile diameters and soil properties and the results have been compared with measured values obtained in model tests and field tests. It has been ascertained that the calculated values substantially correspond to the measured values.

Chapter 3 considered the phenomenon of settlement due to a cavity within the ground interior as an example of analysis of deformation characteristics through consideration of the mechanism involved instead of directly analyzing such characteristics with respect to constitutive relations of soil. This has bearing upon possible effects which tunnel excavation may have upon ground surface settlement and underground settlement. The floor-lowering test was carried out by using not only dry sand but a mass of cylindrical aluminum rods with various diameters as ground materials. Since a mass of aluminum rods permits easy observation of phenomena, the test has enabled the author to clarify the pattern of ground movement due to downward removal of the lowering floor, to view the local change of the void within the ground interior as well as the condition of upward transfer of void, and the relation between the amount of the downward movement of the lowering floor and the amount of ground settlement. Consequently, formulas for the calculation of the ground surface settlement and the underground settlement along the central line of the lowering floor have been derived. The curves of ground surface settlement in the lateral direction of the lowering floor as well as the amount of settlement along the central line of the lowering floor have been assumed to be given by the normal probability distribution and calculated as such. At the same time, the phenomenon of settlement in the longitudinal direction of tunnel due to advancement of the working face of tunnel excavation has been analyzed. By combining considerations of ground settlement in the lateral plane and that in the longitudinal plane, the ground surface settlement has been analyzed three-dimensionally. It has been verified that the values calculated through these analyses show a satisfactory agreement with the results of the floor-lowering test performed by using a mass of cylindrical aluminum rods and using sand. Finally, with the manner of ground loosening in the floor-lowering test adjusted to conform to the manner of ground loosening due to tunnel excavation, the values of ground settlement actually measured in the tunnel excavation have been analyzed by the application of the above theory. The calculated values show a satisfactory agreement with the measured values.

As a future task, we look forward to the establishment of a general method of analysis permitting deformation analysis of ground and soil structures by the use of constitutive relations of soil. In other words, there must be established means of

deformation analysis which serves by determining the stress-strain relations of soil and reflecting boundary conditions and stress equilibrium formulas, whether the object of analysis may be a slope, a footing or a retaining wall. It is thus necessary to further generalize and simplify the stress-strain relation formulas of soil to make effective use of relation formulas expressed in terms of stress ratios, and to develop an effective and convenient way of utilizing the finite element method. Introduction of the time-effect characteristics of soil into constitutive relations and application of these characteristics to design are important tasks. The fundamental evaluation of the time-effect characteristics of soils during consolidation and during shear, represented by creep characteristics and stress relaxation characteristics, and the introduction of these characteristics to constitutive relations of soils will prove to be very important.

ACKNOWLEDGEMENTS

The author sincerely acknowledges his indebtedness to Professor Sakuro Murayama of Kyoto University, for his continual guidance and encouragement given throughout the present study. A grateful acknowledgement is made to Professor Toru Shibata of Kyoto University, Assistant Professor Norio Yagi of Kanazawa University and Assistant Professor Daizo Karube of Kobe University, for their helpful advice, criticisms and encouragement. It is a pleasure to acknowledge valuable discussions and support given by Messrs. Yoshiharu Ishii and Norio Kurihara, who were Assistants of Kyoto University.

The author would like to emphasize that this study has also been greatly promoted by many others through extensive discussions in daily academic activities. In this respect he wishes to extend his gratitude to Assistant Professor Hideki Ohta of Kyoto University, Messrs. Seiki Ohmaki, Tadashi Hashimoto and Yasuo Sugano, Assistants of Kyoto University, and Messrs. Hideo Sekiguchi, Hiroshi Bando, Ei Yoshida, Iwaki Hattori, Ryosuke Kitamura, Teruo Nakai and others, who are graduate students at the Professor Murayama's laboratory of Kyoto University, for their discussions and support. The author is also grateful to Messrs. Chokkan Suematsu and Ichiro Kamo, Research Workers of Kyoto University, who kindly offered their assistance in doing the calculations involved. The author would like to express his appreciation to Dr. Fumio Tatsuoka, who was a graduate student of Tokyo University, for his kind discussion and the offer of his published experimental data.

The author is also indebted to Professor Ahmet Cakmak of Princeton University for his kind correction of this English manuscript.

APPENDIXES

APPENDIX A

CALCULATION TO CONVERT THE STRESS RATIO-STRAIN RELATIONSHIPS ON THE MOBILIZED PLANE INTO THE PRINCIPAL STRESS RATIO-PRINCIPAL STRAIN RELATIONSHIPS.

The relationships among the shear-normal stress ratio (τ/σ_N), shear strain (γ) and normal strain (ϵ_N) on the mobilized plane were derived in Paragraph 3.3 of Chapter 3 as follows:

$$\frac{\tau}{\sigma_N} = (\mu' - \mu) \cdot \log_e \frac{\gamma}{\gamma_0} + \mu \qquad (A.1)$$

$$\epsilon_N = \frac{\mu - \mu'}{\lambda} \cdot \gamma \cdot \{ \log_e \frac{\gamma}{\gamma_0} - 1 \} \qquad (A.2)$$

The following relationship is also given as shown in Eq. (1.2.40) of Chapter 2.

$$\frac{\tau}{\sigma_N} = \tan\phi_{m0} = \frac{\sigma_1 - \sigma_3}{2\sqrt{\sigma_1\sigma_3}} = \frac{1}{2}(\sqrt{\sigma_1/\sigma_3} - \sqrt{\sigma_3/\sigma_1}) = \frac{1}{2} \cdot X \qquad (A.3)$$

wherein, $X \equiv \sqrt{\sigma_1/\sigma_3} - \sqrt{\sigma_3/\sigma_1}$.

By substituting Eq. (A.3) in Eq. (A.1), the following expression is obtained.

$$\gamma = \gamma_0 \cdot \exp\left(\frac{\frac{1}{2}X - \mu}{\mu' - \mu}\right) \qquad (A.4)$$

$$\therefore d\gamma = \frac{\gamma_0}{2(\mu' - \mu)} \cdot \exp\left(\frac{\frac{1}{2}X - \mu}{\mu' - \mu}\right) \cdot dX \qquad (A.5)$$

By substituting Eq. (A.4) in Eq. (A.2), the following expression is obtained similarly.

$$\epsilon_N = \gamma_0 \cdot \frac{\mu' - \frac{1}{2}X}{\lambda} \cdot \exp\left(\frac{\frac{1}{2}X - \mu}{\mu' - \mu}\right) \qquad (A.6)$$

$$\therefore d\epsilon_N = \frac{\gamma_0}{2\lambda} \cdot \frac{\mu - \frac{1}{2}X}{\mu' - \mu} \cdot \exp\left(\frac{\frac{1}{2}X - \mu}{\mu' - \mu}\right) \cdot dX \qquad (A.7)$$

The following equations are given by assuming that the principal stress and the principal strain increment coincide in direction.

$$\frac{d\gamma}{2} = (d\epsilon_1 - d\epsilon_3) \cdot \cos\phi_{m0} \qquad (A.8)$$

$$d\epsilon_N = \frac{d\epsilon_1 + d\epsilon_3}{2} - \frac{d\epsilon_1 - d\epsilon_3}{2} \cdot \sin\phi_{m0} \qquad (A.9)$$

where, $\phi_{mo} = \arctan(\tau/\sigma_N)$ as shown in Eq. (A.3). The following equations are obtained from Eqs. (A.8) and (A.9).

$$d\epsilon_1 = d\epsilon_N + \frac{1+\sin\phi_{m0}}{2\sin\phi_{m0}} \cdot d\gamma \tag{A.10}$$

$$d\epsilon_3 = d\epsilon_N - \frac{1-\sin\phi_{m0}}{2\cos\phi_{m0}} \cdot d\gamma \tag{A.11}$$

Because of the following relationships,

$$\sin\phi_{m0} = \frac{\sigma_1 - \sigma_3}{\sigma_1 + \sigma_3} = \frac{X}{\sqrt{X^2+4}} \tag{A.12}$$

$$\cos\phi_{m0} = \frac{2\sqrt{\sigma_1\sigma_3}}{\sigma_1 + \sigma_3} = \frac{2}{\sqrt{X^2+4}} \tag{A.13}$$

the following expressions are derived by substituting Eqs. (A.5) and (A.7) in Eqs. (A.10) and (A.11).

$$d\epsilon_1 = \frac{\gamma_0}{2} \cdot \exp\left(-\frac{\mu}{\mu'-\mu}\right) \cdot \exp\left\{\frac{X}{2(\mu'-\mu)}\right\} \cdot \left\{\frac{\mu}{\lambda(\mu'-\mu)} - \frac{X}{2\lambda(\mu'-\mu)} + \frac{1}{4(\mu'-\mu)} \cdot \left(\sqrt{X^2+4}+X\right)\right\} \cdot dX \tag{A.14}$$

$$d\epsilon_3 = \frac{\gamma_0}{2} \cdot \exp\left(-\frac{\mu}{\mu'-\mu}\right) \cdot \exp\left\{\frac{X}{2(\mu'-\mu)}\right\} \cdot \left\{\frac{\mu}{\lambda(\mu'-\mu)} - \frac{X}{2\lambda(\mu'-\mu)} - \frac{1}{4(\mu'-\mu)} \cdot \left(\sqrt{X^2+4}-X\right)\right\} \cdot dX \tag{A.15}$$

By integrating Eqs. (A.14) and (A.15), the relationships between the principal stress ratio (σ_1/σ_3) and the principal strains (ϵ_1, ϵ_3) can be derived. The results of the integration of each term in the righthand members of Eqs. (A.14) and (A.15) are shown as follows:

$$\frac{\mu}{\lambda(\mu'-\mu)} \cdot \int \exp\left\{\frac{X}{2(\mu'-\mu)}\right\} \cdot dX = \frac{2\mu}{\lambda} \cdot \exp\left\{\frac{X}{2(\mu'-\mu)}\right\} \tag{A.16}$$

$$\frac{1}{2\lambda(\mu'-\mu)} \cdot \int X \cdot \exp\left\{\frac{X}{2(\mu'-\mu)}\right\} \cdot dX = \frac{1}{\lambda}\left\{X - 2(\mu'-\mu)\right\} \cdot \exp\left\{\frac{X}{2(\mu'-\mu)}\right\} \tag{A.17}$$

$$\frac{1}{4(\mu'-\mu)} \cdot \int \sqrt{X^2+4} \cdot \exp\left\{\frac{X}{2(\mu'-\mu)}\right\} \cdot dX$$

$$= \frac{1}{4(\mu'-\mu)} \cdot \int \left(2 + \frac{1}{4}x^2 - \frac{3}{64}x^4 + \cdots\right) \cdot \exp\left\{\frac{X}{2(\mu'-\mu)}\right\} \cdot dX$$

$$\cong \frac{1}{4(\mu'-\mu)} \cdot \int \left(2 + \frac{1}{4}x^2\right) \cdot \exp\left\{\frac{X}{2(\mu'-\mu)}\right\} \cdot dX$$

$$= \exp\left\{\frac{X}{2(\mu'-\mu)}\right\}\cdot\left[1+\frac{1}{8}\left\{X^2-4(\mu'-\mu)\cdot X+8(\mu'-\mu)^2\right\}\right] \qquad (A.18)$$

$$\frac{1}{4(\mu'-\mu)}\cdot\int X\cdot\exp\left\{\frac{X}{2(\mu'-\mu)}\right\}\cdot dX=\left\{\frac{X}{2}-(\mu'-\mu)\right\}\cdot\exp\left\{\frac{X}{2(\mu'-\mu)}\right\} \qquad (A.19)$$

The principal stress ratio (σ_1/σ_3) – principal strain (ϵ_1, ϵ_3) relationships can be derived as follows from the results of the intergration shown in the above four equations.

$$\epsilon_1=\frac{\gamma_0}{2}\cdot\exp\left(-\frac{\mu}{\mu'-\mu}\right)\cdot\exp\left\{\frac{X}{2(\mu'-\mu)}\right\}$$
$$\cdot\left\{\frac{X^2}{8}+\left(\frac{1}{2}-\frac{1}{\lambda}-\frac{\mu'-\mu}{2}\right)\cdot X+(\mu'-\mu)^2-(\mu'-\mu)+\frac{2\mu'}{\lambda}+1\right\} \qquad (A.20)$$

$$\epsilon_3=\frac{\gamma_0}{2}\cdot\exp\left(-\frac{\mu}{\mu'-\mu}\right)\cdot\exp\left\{\frac{X}{2(\mu'-\mu)}\right\}$$
$$\cdot\left\{-\frac{X^2}{8}+\left(\frac{1}{2}-\frac{1}{\lambda}+\frac{\mu'-\mu}{2}\right)\cdot X-(\mu'-\mu)^2-(\mu'-\mu)+\frac{2\mu'}{\lambda}-1\right\} \qquad (A.21)$$

APPENDIX B

A METHOD OF CALCULATION ON STRESS AND STRAIN STATES IN COMPOSITE GROUND

(1) Coefficients of soils are determined by conducting the consolidation test and the drained triaxial compression test on the clay used for clay ground and the sand used for sand pile.

Clay ground: $\lambda_c = 1.1$, $\mu_c = 0.30$, $\mu_c' = 0.42$, $\gamma_{oc} = 1.0\%$,

$C_{cc} = 0.7$, $e_{ic} = 1.80$, $w_c = (1.6 - 1) \times 10^{-3}\ kg/cm^3$,

$(K_{oc} = 0.5,\ \sigma_{mi} = 0.5\ kg/cm^2)$.

Sand pile: $\lambda_s = 1.1$, $\mu_s = 0.40$, $\mu_s' = 0.62$, $\gamma_{os} = 1.3\%$,

$e_{is} = 0.706$, $w_s = (1.98 - 1) \times 10^{-3}\ kg/cm^3$, $(C_{cs} = 0)$.

(2) Stress-strain relationships are determined by using the above coefficients.

(i) Consolidation term of clay:

$$(\varepsilon_1)_c = (\varepsilon_2)_c = (\varepsilon_3)_c = \frac{1}{3} \cdot \frac{C_{cc}}{1 + e_{ic}} \cdot \log_{10} \frac{\sigma_m(r)}{\sigma_{mi}}$$

$$= 8.33 \cdot \log_{10} \{ \frac{1}{1.5} (\sigma_{zc} + \sigma_{rc}(r) + \sigma_{\theta c}(r)) \} \qquad (B.1)$$

(ii) Shear terms of clay:

$$f_c \left(\frac{\sigma_i}{\sigma_j}\right) = 0.041 \cdot \exp(4.167X) \{ 0.125X^2 - 0.47X + 1.658 \} (\%) \qquad (B.2)$$

$$g_c \left(\frac{\sigma_i}{\sigma_j}\right) = 0.041 \cdot \exp(4.167X) \{ -0.125X^2 - 0.35X - 0.37 \} (\%) \qquad (B.3)$$

wherein, $X \equiv \sqrt{\sigma_i / \sigma_j} - \sqrt{\sigma_j / \sigma_i}$ $(i \leqq j)$.

(iii) Shear terms of sand:

$$f_s \left(\frac{\sigma_i}{\sigma_j}\right) = 0.105 \cdot \exp(2.273X) \{ 0.125X^2 - 0.52X + 1.955 \} (\%) \qquad (B.4)$$

$$g_s \left(\frac{\sigma_i}{\sigma_j}\right) = 0.105 \cdot \exp(2.273X) \{ -0.125X^2 - 0.30X - 0.141 \} (\%) \qquad (B.5)$$

(3) Assuming the vertical strains of sand pile and clay ground are equal at $r = b$, the relationship between $(\sigma_{ZS}/\sigma_{rS})$ and σ_{ZC} is derived as follows.

The vertical strain of sand pile is represented by

$$\varepsilon_{zs} = 2 f_s \left(\frac{\sigma_{zs}}{\sigma_{rs}}\right) \qquad (B.6)$$

Stress states in the clay element at $r = b$ are assumed to be

$$\sigma_{mi} = \frac{1}{3} (1 + 2K_{oc}) \cdot w_c \cdot z, \quad \sigma_m = \frac{1}{3} (1 + K_{oc}) \cdot \sigma_{zc}$$

and $\sigma_1 / \sigma_3 = 1/K_{oc}$.

Then the vertical strain of clay ground at $r = b$ is represented as follows by considering strains due to consolidation and shear.

$$\epsilon_{zc}(b) = \frac{1}{3} \cdot \frac{C_{cc}}{1+e_{ic}} \cdot \log_{10} \frac{\sigma_m}{\sigma_{mi}} + 2 f_c \left(\frac{\sigma_1}{\sigma_3}\right)$$

$$= \frac{1}{3} \cdot \frac{C_{cc}}{1+e_{ic}} \cdot \log_{10} \frac{\sigma_{zc}}{w_c \cdot Z} + 2 f_c \left(\frac{\sigma_1}{\sigma_3}\right)$$

$$= 8.33 \cdot \log_{10} \frac{\sigma_{zc}}{0.75} + 2.14 \quad (\%) \qquad (B.7)$$

Therefore, the following relationship is obtained assuming $\epsilon_{ZS} = \epsilon_{ZC}$ (b).

$$2 f_s \left(\frac{\sigma_{zs}}{\sigma_{rs}}\right) = 8.33 \cdot \log_{10} \frac{\sigma_{zc}}{0.75} + 2.14 \qquad (B.8)$$

(4) Considering share of applied apressure on the surface of the composite ground, the following equation is satisfied.

$$p = \frac{a^2}{b^2} \cdot (\sigma_{zs} - w_s \cdot z) + \frac{b^2 - a^2}{b^2} \cdot (\sigma_{zc} - w_c \cdot z) \qquad (B.9)$$

By substituting $p = 1.0\ kg/cm^2$, $b/a = 5$, $w_S \cdot z = 1.2225\ kg/cm^2$ and $w_C \cdot z = 0.75\ kg/cm^2$ ($z = 12.5$ m) in Eq. (B 9), the relationship between σ_{ZS} and σ_{ZC} is obtained.

$$\sigma_{zs} + 24 \sigma_{zc} = 94.225 \qquad (B.10)$$

(5) The relationship between σ_{ZC} and σ_{rS} is derived from Eqs. (B·8) and (B·10). On the condition $\sigma_{rS} = \sigma_{rC}(a)$ the relationship between σ_{ZC} and $\sigma_{rC}(a)$ is also obtained. This is then considered for $\sigma_{ZC} \geqq \sigma_{rC}(a)$ and for $\sigma_{ZC} \leqq \sigma_{rC}(a)$.

(6) If $\epsilon_{rS} = \epsilon_{\theta C}(a)$ at the boundary between sand pile and clay ground ($r = a$), the relationship between σ_{ZC} and $\sigma_{\theta C}(c)$ can be derived. Then to eliminate the consolidation term, the following relation is obtained by utilizing the condition of the equal vertical strain $\epsilon_{ZS} = \epsilon_{ZC}$.

$$\epsilon_{zs} - \epsilon_{rs} = \epsilon_{zc} - \epsilon_{\theta c}(a) \qquad (B.11)$$

For $\sigma_{ZC} \geqq \sigma_{rC}(a)$;

$$2 f_s \left(\frac{\sigma_{zs}}{\sigma_{rs}}\right) - g_s \left(\frac{\sigma_{zs}}{\sigma_{rs}}\right)$$

$$= f_c \left(\frac{\sigma_{zc}}{\sigma_{\theta c}(a)}\right) + f_c \left(\frac{\sigma_{zc}}{\sigma_{rc}(a)}\right) - g_c \left(\frac{\sigma_{zc}}{\sigma_{\theta c}(a)}\right) - g_c \left(\frac{\sigma_{rc}(a)}{\sigma_{\theta c}(a)}\right) \qquad (B.12)$$

For $\sigma_{ZC} \leqq \sigma_{rC}(a)$;

$$2 f_s \left(\frac{\sigma_{zs}}{\sigma_{rs}}\right) - g_s \left(\frac{\sigma_{zs}}{\sigma_{rs}}\right)$$

$$= f_c \left(\frac{\sigma_{zc}}{\sigma_{\theta c}(a)}\right) + g_c \left(\frac{\sigma_{rc}(a)}{\sigma_{zc}}\right) - g_c \left(\frac{\sigma_{rc}(a)}{\sigma_{\theta c}(a)}\right) - g_c \left(\frac{\sigma_{zc}}{\sigma_{\theta c}(a)}\right) \qquad (B.13)$$

Since the $\sigma_{ZC} \sim \sigma_{ZS}/\sigma_{rS}$ relation (cf. Eq. (B·8) and the $\sigma_{ZC} \sim \sigma_{rc}(a)$ relation (cf. (5)) have been already known in Eqs. (B·12) and (B·13), the relationship between σ_{ZC} and $\sigma_{\theta c}(a)$ can be obtained.

(7) On the condition of the equal vertical strain of sand pile and clay ground at r = a, the value of σ_{ZC} can be calculated.

The vertical strain of sand pile is represented by

$$\epsilon_{zs} = 2 f_s \left(\frac{\sigma_{zs}}{\sigma_{rs}}\right) \qquad (B.14)$$

The vertical strain of clay ground at r = a is represented as follows.

For $\sigma_{ZC} \geqq \sigma_{rc}(a)$;

$$\epsilon_{zc}(a) = \frac{1}{3} \cdot \frac{C_{cc}}{1+e_{ic}} \cdot \log_{10} \frac{\sigma_m(a)}{\sigma_{mi}} + f_c \left(\frac{\sigma_{zc}}{\sigma_{\theta c}(a)}\right) + f_c \left(\frac{\sigma_{zc}}{\sigma_{rc}(a)}\right)$$

$$= 8.33 \cdot \log_{10} \left\{\frac{1}{1.5}(\sigma_{zc} + \sigma_{rc}(a) + \sigma_{\theta c}(a))\right\} + f_c \left(\frac{\sigma_{zc}}{\sigma_{\theta c}(a)}\right) + f_c \left(\frac{\sigma_{zc}}{\sigma_{rc}(a)}\right)$$

For $\sigma_{ZC} \leqq \sigma_{rc}(a)$; (B.15)

$$\epsilon_{zc}(a) = \frac{1}{3} \cdot \frac{C_{cc}}{1+e_{ic}} \cdot \log_{10} \frac{\sigma_m(a)}{\sigma_{mi}} + f_c \left(\frac{\sigma_{zc}}{\sigma_{\theta c}(a)}\right) + g_c \left(\frac{\sigma_{rc}(a)}{\sigma_{zc}}\right)$$

$$= 8.33 \cdot \log_{10} \left\{\frac{1}{1.5}(\sigma_{zc} + \sigma_{rc}(a) + \sigma_{\theta c}(a))\right\} + f_c \left(\frac{\sigma_{zc}}{\sigma_{\theta c}(a)}\right) + g_c \left(\frac{\sigma_{rc}(a)}{\sigma_{zc}}\right) \qquad (B.16)$$

Since the $\sigma_{ZC} \sim \sigma_{ZS}/\sigma_{rS}$ relation (cf. Eq. (B·8)) is known, the $\epsilon_{ZS} \sim \sigma_{ZC}$ relationship is obtained by Eq. (B·14). The $\epsilon_{ZC}(a) \sim \sigma_{ZC}$ relationship is also derived from Eqs. (B·15) and (B·16) because the $\sigma_{rc}(a) \sim \sigma_{ZC}$ relation (cf. (5)), and the $\sigma_{\theta c}(a) \sim \sigma_{ZC}$ relation (cf. (6)) have been already known. Therefore the value of σ_{ZC} can be calculated since $\epsilon_{ZS} = \epsilon_{ZC}(a)$ as follows.

$$\sigma_{zc} = 1.51 \quad kg/cm^2.$$

(8) Once the vaule of σ_{ZC} is obtained, all other values of stresses, strains, stress ratios, stress concentration ratio and settlement reduction rate can be calculated as follows.

From Eq. (B·10), $\sigma_{ZS} = 7.90\ kg/cm^2$.

From Eq. (B·8), $\sigma_{rS} = \sigma_{rc}(a) = 2.58\ kg/cm^2$.

From the $\sigma_{ZC} \sim \sigma_{\theta c}(a)$ relationship obtained in (6),

$\sigma_{\theta c}(a) = 0.85\ kg/cm^2$.

From Eq. (B·14), $\epsilon_{ZS} = \epsilon_{ZC} = 4.69\ \%$.

From the equation $\sigma_c = \sigma_{ZS} - w_S \cdot z$,

$\sigma_S = 7.90 - 1.225 = 6.68\ kg/cm^2$.

From the equation $\sigma_c = \sigma_{zc} - w_c \cdot z$,

$$\sigma_c = 1.51 - 0.75 = 0.76 \text{ kg/cm}^2.$$

Stress concentrain ratio at the ground surface;

$$\frac{\sigma_s}{\sigma_c} = 8.79$$

Stress concentration ratio within the ground (z = 12.5 m);

$$\frac{\sigma_{zs}}{\sigma_{zc}} = 5.23$$

Various stress ratios;

$$\frac{\sigma_{zs}}{\sigma_{rs}} = 3.06, \quad \frac{\sigma_{rc}(a)}{\sigma_{\theta c}(a)} = 3.04, \quad \frac{\sigma_{zc}}{\sigma_{\theta c}(a)} = 1.78,$$

$$\frac{\sigma_{rc}(a)}{\sigma_{zc}} = 1.71 .$$

If ϵ_{zo} denotes the vertical strain of the clay ground without including the sand pile, ϵ_{zo} can be calculated by substituting $\sigma_{zc} = p + w_c \cdot z = 1.75$ kg/cm^2 in Eq. (B·7).

$$\therefore \quad \epsilon_{zo} = 5.21 \ \%$$

Therefore the settlement reduction rate β due to the sand pile is obtained as follows.

$$\beta = \frac{\epsilon_z}{\epsilon_{zo}} = \frac{4.69}{5.21} = 0.90$$